NASA Contractor Report 177626

Aerodynamic Control of NASP-Type Vehicles Through Vortex Manipulation

Volume IV

Simulation

Brooke C. Smith, Carlos J. Suárez, William M. Porada, and Gerald N. Malcolm

CONTRACT NAS2-13196
September 1993

National Aeronautics and Space Administration

NASA Contractor Report 177626

Aerodynamic Control of NASP-Type Vehicles Through Vortex Manipulation

Volume IV

Simulation

Brooke C. Smith, Carlos J. Suárez, William M. Porada, and Gerald N. Malcolm

Eidetics International, Inc.
3415 Lomita Blvd.
Torrance, CA 90505

Prepared for
Ames Research Center
CONTRACT NAS2-13196
September 1993

National Aeronautics and
Space Administration

Ames Research Center
Moffett Field, California 94035-1000

TABLE OF CONTENTS

NOMENCLATURE

A_{ref}	reference wing area
b	wing span
c	wing chord
L	reference length = total length of the model
$C\mu$	momentum coefficient of blowing = $\dot{m}j\ Vj / q\ A_{ref}$
$\dot{m}_j$	mass flow rate of the blowing jet
q	free-stream dynamic pressure
V	free-stream velocity
V_j	average exit velocity of the blowing jet
α, AOA	angle of attack
β	sideslip angle
ϕ	roll angle
μ	velocity vector roll angle
Φ	azimuth angle (from the windward meridian)
Phidot, p	roll rate, body axis
Phiddot	roll acceleration, body axis
P	period of wing rock oscillation
δe	elevator deflection (+ down)
δr	rudder deflection (+ right)
$\delta e,l$	left elevon deflection
$\delta e,r$	right elevon deflection
Ixx	Moment of inertia
CN	normal force coefficient
Cm	pitching moment coefficient
Cn	yawing moment coefficient
Cl	rolling moment coefficient
Cy	side force coefficient
CL	stability axis lift coefficient
ΔCn	yawing moment increment
ΔCl	rolling moment increment
Cp	pressure coefficient
$Cn\beta$	directional stability derivative
$Cl\beta$	lateral stability derivative
Clp	roll moment rate derivative = $\frac{\partial Cl}{\partial(pb/2V)}$

LIST OF FIGURES

SUMMARY

Forebody Vortex Control (FVC) is an emerging technology that has received widespread and concentrated attention by many researchers for application on fighter aircraft to enhance aerodynamic controllability at high angles of attack. This technology has also been explored in this research program for potential application to a NASP-type configuration. The configuration investigated is characterized by a slender, circular cross-section forebody and a 78° swept delta wing. A man-in-the-loop, six-degree-of-freedom, high-fidelity simulation has been developed that demonstrates the implementation and advantages of pneumatic forebody vortex control. Static wind tunnel tests were used as the basis for the aerodynamic characteristics modeled in the simulation. Dynamic free-to-roll wing rock wind tunnel tests were analyzed and the wing rock motion investigated. A non-linear model of the dynamic effects of the bare airframe and the forebody vortex control system were developed that closely represented the observed behavior in the wind tunnel. Multiple state-of-the-art digital flight control systems were developed that included different utilizations of pneumatic vortex control. These were taken to manned simulation and evaluated. In addition, data were collected regarding the use of blowing and the quantities and rates of mass flow consumption required during realistic flight maneuvers. Based on these data, the most important conceptual design parameters for a pneumatic forebody vortex control system were discussed.

AERODYNAMIC CONTROL OF NASP-TYPE VEHICLES THROUGH VORTEX MANIPULATION

VOLUME IV: SIMULATION

1.0 PURPOSE

The purpose of the simulation task is to demonstrate the feasibility and implementation of pneumatic forebody vortex control on an advanced aircraft configuration. The aircraft is geometrically similar to the configuration tested in water tunnel and low-speed wind tunnel tests. The flight regime to be explored is high angle of attack (i.e., low speed) where other similar designs have difficulty due to reduced stability and control power (e.g., max gross weight return to landing and cross wind take-off).

Water tunnel and wind tunnel static tests are discussed in Volumes I and II, respectively. Volume III summarizes the results of the wing rock experiments performed first in the Eidetics water tunnel and later in the NASA Ames Research Center 7 x 10 ft wind tunnel. This volume of the Final Report presents the development of a man-in-the-loop simulation that includes the static and dynamic aerodynamic behavior presented in the preceding volumes.

2.0 REVIEW OF PNEUMATIC VORTEX CONTROL

One of the most significant and ambitious programs of the aerospace industry in the near future will be the development and eventual flight test of the National Aero-Space Plane (NASP, X-30). Much of the technological research now being conducted to support the development of a NASP concentrates on the hypersonic regime. In addition to excellent hypersonic performance, however, high-quality low-speed flight must also be achieved. Conceivably, configurations optimized for hypersonic flight may experience adverse low-speed aerodynamic phenomena dominated by separated and vortex flows, such as wing rock or non-zero yawing moments at zero sideslip, which could complicate the effort of attaining good handling qualities during the takeoff and the approach and landing phases. Using conventional control effectors such as rudder or aileron to overcome the effects of these adverse phenomena and satisfy low-speed flight quality criteria may result in excess weight over that if hypersonic flight quality was the only concern. Use of non-conventional vortex control effectors, on the other hand, may potentially satisfy low-speed flight quality criteria with a substantially lower weight penalty. The principal mechanism to accomplish a saving in weight is with fluid amplification, where a small fluidic input, such as surface blowing in the forebody region, results in large output control forces and moments to the airframe by influencing the vortex flow field.

Powerful forebody vortices are a principal cause of aircraft instabilities at high angles of attack. An effective means of suppressing the instabilities in this flight regime is, therefore, to directly control these vortices. Recent research efforts on

fighter-type aircraft indicate that some of the most promising methods for Forebody Vortex Control (FVC) are movable forebody strakes, rotatable nose-tip and nose-boom devices, and blowing on the forebody surface. The use of symmetrically deployed forebody strakes has been shown to be effective in forcing naturally occurring asymmetric vortices at high angles of attack to be symmetric. The large forebody side forces and resulting yawing moments at zero sideslip are therefore reduced or eliminated. The use of asymmetrically deployed forebody strakes has been investigated for the possible application of controlling the yawing moment[1,2]. Rotatable nose-tip devices have also been found to be effective in controlling the forebody flow. These devices are in the forms of a small cylinder attached to the tip[3], machined flats[3], elliptic tips[4], and small vortex generators[5]. Miniature, rotatable strakes attached to the nose-boom of an F-16 also influence the forebody vortex flow field, creating forces and moments that can be used for additional control[6]. Due in part to the concern about strakes and mechanical surfaces interfering with forebody radar operation, various forebody blowing techniques to control the forebody vortex orientations have also been investigated as alternatives to mechanical devices. Two main forms of blowing have been studied: (1) blowing from a localized jet[2,7,8], and (2) blowing from a tangential slot[2,8-12]. In both forms, blowing was highly effective in controlling the vortex orientation.

The Phase I technical results[13] show that it is potentially feasible to utilize vortex manipulation with blowing to provide the necessary control forces for a NASP-type configuration, as well as fighter configurations, at low speeds and high angles of attack. The mass flow requirements for blowing scaled to a full-size NASP based on sub-scale experiments appear to be low, well within practical limits of acquiring the required mass flow through engine bleed or similar sources. The resulting control moments, based on wind tunnel studies of fighter configurations, can be greater than those generated by a typical rudder. The vertical tail area and structural weight may be reduced, and thus, potentially lead to an improvement in the hypersonic drag performance. Preliminary tests in this Phase II investigation also show that blowing can produce sizable forces and moments at angles of attack between 20° and 30°.

3.0 FULL SCALE AIRCRAFT DESCRIPTION

It is important to note that at the time the research contract with NASA was awarded, a specific design for the NASP had not been selected. The models used in the Phase I study and in this investigation are based on drawings of a generic, preliminary NASP configuration provided by the duPont Aerospace Co., Inc. The configuration that now appears from the consolidated NASP design team, however, is significantly different. Even though it still has highly swept wings, the fuselage has a blunt forebody, so the lateral-directional stability problems will be different. This by no means diminishes the value of this research program; the general results obtained in this study may be applicable to similar configurations, such as the High Speed Civil Transport (HSCT) or any other supersonic/hypersonic advanced configuration. Also, the basic fluid mechanics associated with blowing will be better understood from this study. Despite the dissimilarity between the current NASP and the configurations

used in this investigation, the models will still be referred to as NASP-type configurations.

3.1 Characteristic Dimensions

Despite not representing the current design for NASP, the model tested in the wind tunnel is similar to other aircraft concepts under consideration, such as a hypersonic interceptor. The manned simulation study and the pneumatic system sizing and preliminary design were based partly on the geometry of one of these configurations. The overall length of the conceptual interceptor is 75 feet and the gross weight is 100,000 pounds. Conveniently, the wind tunnel model is a 1/15 scale of this size vehicle.

4.0 OBJECTIVES

Many different forebody vortex control schemes have been examined in wind tunnel tests and have demonstrated their potentials as additional sources of control power. The next step in the process of advancing forebody vortex control methodology out of the laboratory and into flight is exploration of the implementation and use of the system in an aircraft. The objectives of the present tasks were to perform manned simulation and define some of the requirements for developing a conceptual forebody blowing system. This required the development of an aerodynamic model of a vehicle that could employ pneumatic forebody vortex control and to demonstrate the implementation, use, and potential benefits.

5.0 APPROACH

The approach was to develop a simple control system that captured the significant aspects of pneumatic vortex control and allowed the behavior of the control system to be examined. Simple flight tasks were developed to allow the evaluation of the benefits of blowing and to determine some of the system requirements, such as duty cycles, blowing capacity and rates required, tolerable lag time in the response, etc.

6.0 TASKS

6.1 Static Aero Model From Wind Tunnel Tests

The baseline static aerodynamic model was developed from the static wind tunnel test described in Volume II of this report. Effects of the vertical tail were included as separate increments to the basic data so that the tail effectiveness could be easily varied.

6.2 Conventional and Pneumatic Control Modeling

Conventional control effects were determined directly from the static wind tunnel tests. The pneumatic control characteristics were improved from those demonstrated in the current wind tunnel test and were based partially on the results of additional,

more extensive, test programs where the full potential of pneumatic forebody vortex control was developed. This "optimization" of the pneumatic control data was acceptable, realizing that incorporation of the "first-cut" system from the test was premature.

6.3 Develop Simple Control Laws With and Without Pneumatic Controls

A number of different control schemes incorporating different forms of blowing control were evaluated and compared. In addition to the baseline conventional control system, five alternatives for pneumatic forebody vortex control were examined. These implementations ranged in sophistication from simple open-loop steady blowing for wing rock suppression to a fully active complementary filtered frequency mix of conventional and pneumatic controls. Three control schemes were selected for further evaluation with the manned simulation. The controls were integrated with two distinct flight control systems, one representative of a modern fully augmented fly-by-wire aircraft, and the other modeling a simplified, partially augmented system that highlights the differences between the control techniques.

6.4 Pilot-In-The-Loop Simulation And Evaluation

Manned simulations evaluated the relative performance benefits of the different control schemes. Evaluation tasks were developed to explore regions of the flight envelope where pneumatic controls are effective, namely at high angles of attack during the landing approach and during maneuvering flight. High angles of attack are also attained during take-off. The application of pneumatic control during take-off was evaluated.

7.0 WIND TUNNEL MODEL DESCRIPTION

The model used in the wind tunnel test can be seen in Figs. 1 and 2. The forebody has a length-to-base diameter ratio of 6, and is circular in cross-section. The wing is a sharp-edge delta with a 78° sweep. This NASP-type configuration possesses characteristics that are similar to certain forebody/leading-edge extension (LEX) and missile forebody/canard combinations. Surface mounted transducers monitored the pressure changes produced by blowing and provided useful time lag data. An internal 6-component sting balance was used to acquire force and moment data.

The experiments were conducted in the NASA Ames Research Center 7 x 10 Foot Wind Tunnel. Most of the static wind tunnel tests, reported in Volume II, were performed at a dynamic pressure q = 1915 Pa (40 psf), which corresponds to a free stream velocity of 55 m/sec (180 ft/sec), and a Reynolds number of 570,000 based on the body diameter. The tests were performed for an angle of attack range from 0° to 30° and for a sideslip angle range from -10° to 10°.

The blowing ports were located at two longitudinal positions and at $\Phi = 150°$ radially, as seen in Fig. 2b. The total pressure and temperature at the nozzle exits were measured to determine the mass flow rate and the blowing coefficient $C\mu$. The

flow was choked at the nozzle exit for all test conditions. The different blowing techniques investigated, which are illustrated in Fig. 3, include aft blowing from the forward location, aft blowing at an angle, forward blowing from the aft and forward locations, and combined blowing. Aft blowing jets were selected as the configuration for the simulator study.

8.0 STATIC AERODYNAMIC MODEL

The static aerodynamic model was developed directly from the results of the static wind tunnel tests described in Volume II. Only low-speed aerodynamic characteristics are included. Aerodynamic asymmetries discovered in the bare airframe were retained as representative of those expected in a full size aircraft. Conventional control effectiveness increments were broken out separately to facilitate sizing studies. The static effects of pneumatic controls were modified to represent the behavior expected of a "developed" system.

8.1 Static Aerodynamics

The longitudinal and lateral-directional aerodynamic models, with the exception of the drag component, were developed directly from the experimental data. The matrix of angles of attack and sideslip tested in the wind tunnel were extrapolated slightly to range from -4° to 34° AOA and sideslip angles to ±10°. The wind tunnel data were fitted with smooth curves in both angle of attack and sideslip and interpolated at 2° increments. The moment reference center for these plots is the same as was used during the static wind tunnel test, namely at 67% of the body length or 30% mean aerodynamic chord. The aerodynamic math model is expressed in body axes coefficients.

8.1.1 Longitudinal Aerodynamics

Plots of C_N and C_m are shown in Figs. 4a and 4b for $\beta = 0°$. Sideslip variation up to 10° had little effect on the normal force and pitching moment. Static stability and static margin are shown as functions of angle of attack in Figs. 5a and 5b. Included in these plots are the effects of full up and down elevator deflections.

The basic drag polar shown in Fig. 6 was determined from DATCOM[14] for the clean configuration. The drag increment due to the landing gear extension was scaled from data of a similar configuration[15] and is plotted in Fig. 7.

8.1.2 Lateral - Directional Aerodynamics

Typically, configurations with high fineness ratio fuselages and forebodies exhibit asymmetric aerodynamic behavior at high angles of attack. Over some range of AOA, many wind tunnel tests of these configurations have shown significant yawing and rolling moments developed at zero sideslip. Many studies attribute this behavior to small, unavoidable imperfections of the forebody, which trigger the highly sensitive forebody vortices to assume an asymmetric orientation. The wind tunnel test results from this research were no exception.

It is assumed that these asymmetries will exist in any full size aircraft of this configuration and the flight control system will be required to compensate for them. The asymmetric behavior was represented by an additional component build-up parameter with a separate scaling factor. The factor allows the amount of asymmetry present in the aerodynamic model to be easily varied.

The static lateral-directional aerodynamic coefficients are modeled in a build-up form where the individual contributions of the vertical tail, control deflections and asymmetries are tabulated separately. The mathematical form of the yaw moment build-up equation is shown for illustration below:

$$Cn = Cn(\alpha,\beta)|_{tailoff} + k_1 \Delta Cn(\alpha,\beta)|_{\Delta tail} + k_0 \Delta Cn_0(\alpha)|_{tailoff} + k_0 k_1 \Delta Cn_0(\alpha)|_{\Delta tail}$$

This allows maximum flexibility in modifying the data base to represent different configurations. For example, if the effects of smaller vertical tails were to be explored, the factor k_1 would be set to a value smaller than 1. Similarly, values of k_0 less than 1 include smaller amounts of the asymmetric moments.

8.2 Conventional Controls

The NASP configuration in this study has three independent conventional control surfaces. A single rudder is the primary yaw control surface. Full span control surfaces at the trailing edge of the wing (elevons) are deflected together for pitch control and differentially for roll control.

The conventional control effects are added onto the basic static aerodynamic build-up equations in a similar manner as described above. Continuing with the yaw moment build-up equation as an illustration, two additional terms are added on to represent the contributions of the aileron and rudder deflections.

$$Cn = Cn(\alpha,\beta)|_{tailoff} + k_1 \Delta Cn(\alpha,\beta)|_{\Delta tail} + k_0 \Delta Cn_0(\alpha)|_{tailoff} + k_0 k_1 \Delta Cn_0(\alpha)|_{\Delta tail} + \Delta Cn(\alpha,\delta a) + k_1 \Delta Cn(\alpha,\delta r)$$

Plots of the individual components used in the build-up equations of the lateral-directional aerodynamic coefficients are shown in Figs. 8a through 8e for yaw moment and Figs 9a through 9d for roll moment. In general, rudder deflections produced yaw moment without causing a roll moment. Aileron deflections, i.e., differential elevon deflection, caused a significant amount of yaw moment along with the desired roll moment.

8.3 Pneumatic Controls, Static Effects

The static wind tunnel tests revealed that pneumatic forebody vortex control was effectively uncoupled from the longitudinal aerodynamics and did not significantly alter the pitch moment or lift characteristics of the aircraft. The pneumatic control did exhibit large effects in yaw and roll moments at high angles of attack. The side force effect was small and not modeled for the simulation.

8.3.1 Yaw Moment Effects

The concepts tested in the wind tunnel established the ability of pneumatic techniques to provide yaw moment control. However, the particular configurations were not as well behaved as other nozzle configurations[7,8] that have been more fully developed. Since the purpose of the simulation exercise was to provide a preliminary look at how pneumatic control might be integrated into an aircraft flight control system, the results from the wind tunnel were modified to represent an "optimized" blowing system. The pneumatic yaw control characteristics were based on a combination of X-29[7], F-16C[8], and generic fighter test results[16], tempered by the behavior observed in the wind tunnel.

8.3.2 Computer Model Formulation

The yaw moment control effectiveness of forebody vortex control by pneumatic jets is a function of mass flow rate and the aerodynamic angles, α and β. When a sideslip condition exists, the effectiveness also depends on whether the blowing jet is on the windward or leeward side of the forebody. The following equation was developed to include these effects individually:

$$\Delta Cn|_{Right\ Side\ Blowing} = k_\alpha(\alpha)k_\beta(\beta)Cn(C\mu|_{Right\ Side})$$

$$\Delta Cn|_{Left\ Side\ Blowing} = -k_\alpha(\alpha)k_\beta(-\beta)Cn(C\mu|_{Left\ Side})$$

The terms in the equation are non-linear functions and are evaluated by table look-up. Figure 10 shows plots of each term in the yawing moment increment due to pneumatic control equation. The k_α term shows that the pneumatic control does not become effective until the angle of attack is greater than 10°, at which point the effectiveness rapidly grows. The beta term shows the observed trend that blowing on the windward side provides a larger restoring moment than is produced by blowing on the leeward side. Interestingly, this characteristic results in an increase in the static yaw stability with steady blowing simultaneously on both sides. The change in sign of $k\beta$ indicates that at a sideslip angle greater than 7° the effect of lee side blowing becomes stabilizing and provides a restoring moment. The C_μ term shows a deadband until the mass flow coefficient increases above 0.001, followed by a leveling of the curve at high flow rates.

8.3.3 Roll Moment Effects

The computer formulation of the roll control due to forebody blowing is similar to that used for the yaw control. The static effects of pneumatic control on the roll moment at small blowing rates were determined from the static wind tunnel test results. The behavior at larger blowing rates was determined from the wing rock tests and will be discussed later. The static roll moment effects of pneumatic control are presented in Fig. 11. The characteristics of the dependencies are similar to the yaw moment effects discussed above with the exception of the angle of attack term. This term includes the reversal in effectiveness that was consistently observed during the NASP wind tunnel test series.

In addition to the static control effects, the pneumatic control has a large influence on the dynamic behavior of the roll aerodynamics. These effects will be established through the use of a simple one-degree-of-freedom simulation that is described in a later section of this report.

8.3.4 Pneumatic Control Time Lag

Time histories of the surface pressures shown in Volume II show that the time lag after the onset of blowing and before the response is seen is nearly equal to the time required for the freestream flow to travel the same distance. Based on this observation, the time constant for the yaw and roll moment effects were nominally set as a fraction of the body length divided by the freestream velocity. The distance from the pneumatic control nozzle exit to the wing aerodynamic center (48.31 feet for the full-scale aircraft) was used as the characteristic length.

The manned simulation used a first order lag to model the time delay as sketched in the block diagram below:

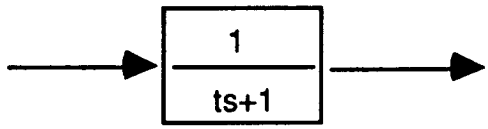

9.0 DYNAMIC AERODYNAMICS

With the exception of the large amplitude lateral aerodynamics, the rate dependent aerodynamic characteristics were estimated by handbook methods and comparison with similar configurations. Handbook methods, such as DATCOM[14], are based on compilations of a large number of aircraft and generally do a poor job estimating specific characteristics of unconventional configurations. Published studies of two recent high-speed aircraft configurations[15,17-20] were also used as a basis for estimations of the NASP dynamic derivatives. It is recognized that an active "fly-by-wire" flight control system will be needed for this class of aircraft, and, given sufficient control power, the bare airframe stability and damping characteristics will be completely overshadowed by the artificial effects of the flight control system. Consequently, only approximate values for the aerodynamic rate derivatives are required to meet the objectives of this study.

The primary aerodynamic dynamic derivatives that are included in the simulation model are:

$$Cm_{\dot{\alpha}}(\alpha),\ Cm_q(\alpha)$$

$$Cn_p(\alpha),\ Cn_r(\alpha)$$

$$Cl_p(\alpha,\beta), Cl_r(\alpha)$$

The roll moment due to roll rate was established through the use of a one-degree-of-freedom simulation of the wing rock motion observed in the wind tunnel. The process of determining the non-linear behavior of the roll damping is described in the following sections.

10.0 WIND TUNNEL WING ROCK RESPONSE

The wing rock phenomena experienced during the wind tunnel test has been thoroughly documented in Volume III of this report. Some examples of the wing rock limit cycle behavior will be presented in this section along with a brief summary of the significant results.

10.1 Time Histories

In general, the wing rock behavior began at $\alpha = 22°$; for angles of attack below 22°, the model either rolled to a static and dynamically stable position, or experienced a very irregular motion. Roll angle histories at various angles of attack are shown in Fig. 12. The oscillatory behavior was established within the first cycle, but it took 4 to 6 cycles for the motion to reach its maximum amplitude. The wing rock frequency was approximately 3 Hz at the wind tunnel test conditions, or $\left(\frac{pb}{2V}\right) = 0.1$.

10.2 Phase Plane Plots

The high quality of the recorded values of roll angle during the wing rock experiments allows them to be numerically differentiated twice to determine the roll angular accelerations. The simple one-degree-of-freedom equation of motion shows that the total aerodynamic rolling moment is proportional to the angular acceleration. Plots of $\ddot{\phi}$ vs. ϕ reveal the energy balance of the limit cycle behavior as discussed in Volume III.

Phase plane plots for a single cycle of wing rock at $\alpha = 25°$ are shown in Fig. 13. The cycle begins at $\phi = 0°$ with the model moving right-wing down at the maximum angular velocity. The model decelerates until the velocity is zero and the roll angle is a maximum. The motion then reverses direction and the velocity increases negatively as the model approaches the zero roll position. The second half of the cycle continues in a similar fashion. The roll acceleration, $\ddot{\phi}$, produces typical wing rock hystersis loops[21,22] when plotted as a function of roll angle. In this graph, a clockwise loop denotes an area where energy is being added to the system, i.e., the oscillations are being driven and are growing in amplitude. Counter-clockwise loops near the maximum roll angles represent areas where the system is consuming energy and therefore the motion is damped. In Fig. 13, the areas enclosed by the two destabilizing loops and the single stabilizing loop are roughly equal, indicating an energy balance which yields the stable limit cycle motion of wing rock. The crossing points of the loops indicate the points in the cycle where the damping changes sign from undamped to damped.

10.3 Summary Behavior And Dominant Trends

The reduced frequency of the limit cycle oscillation shows a slight increase with angle of attack as shown in Fig. 14. As discussed below, the wing rock frequency largely depends upon the static roll moment due to sideslip, which displays a similar variation with angle of attack. Figure 15 shows that the maximum peak-to-peak amplitude of the oscillation increases rapidly once the motion becomes well established above 22° angle of attack. Between 24° and 28°, the amplitude increases more slowly, reaching a maximum of ±42°. The limit cycle amplitude decreased slightly at 30° angle of attack. These characteristics will be reproduced in the manned simulation, but in preparation, a simple one-degree-of-freedom (1DOF) simulation will be presented.

11.0 ONE-DEGREE-OF-FREEDOM WING ROCK SIMULATION

A simple one degree of freedom simulation was created to develop the wing rock aerodynamic model. The purpose was to isolate and identify the contributions of the various aerodynamic inputs to the wing rock behavior. The wing rock response of various aerodynamic models was compared to the behavior witnessed in the wind tunnel to evaluate the adequacy of the mathematical model to capture the significant aspects of the aerodynamics.

The specific objectives of the 1-DOF simulation exercise were:

1. Develop an aerodynamic model and simulation that closely reproduces the observed behavior from the free-to-roll wing rock wind tunnel test.

2. Identify the significant parameters of the aerodynamic model by comparison of the simulation with the experimental results.

3. Determine the dynamic effects of the pneumatic forebody vortex control and develop a model for the manned simulation.

Reference 23 presents the results of a non-linear simulation using values of Clp determined from rotary balance and forced oscillation wind tunnel tests. The purpose of this investigation was to determine the significant characteristics of Clp from comparison of a simple simulation with the observed behavior from the free-to-roll wing rock wind tunnel test.

12.0 WING ROCK LATERAL AERODYNAMICS

12.1 Wind Tunnel Model Mass Moment of Inertia Estimation

Crucial to the successful simulation of any dynamic motion is an accurate estimation of the system's mass and inertia. Due to its prominent role in the wing rock equations of motion, the roll moment of inertia of the wind tunnel model needed to be estimated. Two methods were used to estimate the roll inertia. First, the roll inertia

was directly estimated from the weights of individual components of the model along with the geometry and relative positioning of the components. This value of Ixx for the wind tunnel model was 0.0312 slug-ft^2. The second method was used to validate the estimation. As will be discussed below, the frequency of the wing rock oscillation is strongly dependent upon the model's roll moment due to sideslip, Cl_β, and the roll moment of inertia, Ixx. Independently, Cl_β can be determined from the static wind tunnel test results. Together, the values of Cl_β/Ixx from each test condition where the model wing rocked and the values of Cl_β from the static test give multiple estimations of Ixx. These estimates verified the accuracy of the moment of inertia value.

12.2 Wing Rock Aerodynamic Models

Nguyen, et. al.[23] express the equation of motion for the one-degree-of-freedom simulation as:

$$\ddot{\phi} = \frac{q\ Aref\ b}{Ixx} Cl$$

where $Cl = fcn(\alpha, \beta, \phi, p, etc.)$

Note: The aerodynamic angles, α and β, and the wind tunnel sting pitch and roll angles, θ and ϕ, are related by the following equations:

$$\tan\alpha = \tan\theta \cos\phi \qquad \cos\theta = \cos\alpha \cos\beta$$
$$\sin\beta = \sin\theta \sin\phi \qquad \tan\phi = \tan\beta / \sin\alpha$$

Nguyen et al. compared the results of their non-linear simulation with an approximate analytic solution based on small angle assumptions and a simplified model of the roll moment behavior. Their simplified model is presented as:

$$Cl = Cl_\beta \beta + (Clp_o + Clp_\beta |\beta|) \frac{pb}{2V}$$

or using the small roll angle assumption $\beta \approx \sin(\theta)\ \phi$,

$$Cl = Cl_\beta \sin(\theta)\ \phi + (Clp_o + Clp_\beta \sin(\theta) |\phi|) \frac{pb}{2V}$$

After substituting this form into the equation of motion, they present the following approximate solution for the limit-cycle amplitude and period of oscillation:

$$\Delta\phi = \frac{-3\pi}{4\sin(\theta)} \frac{Clp_o}{Clp_\beta}$$

$$P = \frac{2\pi}{\sqrt{-Cl\beta \frac{q\ Aref\ b}{Ixx} \sin(\theta)}}$$

Reference 23 reports good agreement between the nonlinear simulation, the approximate solution and the experimentally observed wing rock amplitude and period.

12.2.1 Absolute Value Model (First Order)

12.2.1.1 Development of Model

Following the lead of Nguyen, et al., the damping terms were represented by a linear relation expressed in terms of the absolute value of the roll angle:

$$Clp = Clp_O + Clp_\phi |\phi|$$

This relation is shown schematically in Fig. 16 as a solid line. It can be seen that the point where the damping is zero is at the roll angle, ϕ_i, the intersection of the linear curve with the $|\phi|$ axis. Solving the damping expression for this roll angle yields:

$$\phi_i = \frac{-Clp_O}{Clp_\phi}$$

Thus, the approximate solution for the wing rock amplitude shown by Nguyen can be written as:

$$\Delta\phi = \frac{3\pi}{4} \phi_i$$

This expression shows the relation between the roll angle at which the damping changes sign and the amplitude of the limit-cycle motion, using the linear damping model. Consequently, from observations of maximum amplitude and frequency of the wing rock, the only remaining unspecified term in the first order aerodynamic model is Clp_O, the roll damping value at zero roll angle.

Increasing the value of Clp_O increases the slope of the Clp line (which is constrained to pass through ϕ_i) and increases the "stiffness" of the system, causing the wing rock motion to more rapidly develop into the steady-state limit-cycle. Observation of the wing rock motion build-up, such as shown in Fig. 17, and comparison with the simulation can lead to a value for the system stiffness through a trial and error approach.

The first order aerodynamic damping model is more conveniently expressed using ϕ_i, as:

$$Clp = Clp_o \left(1 - \frac{|\phi|}{\phi_i}\right)$$

12.2.1.2 Evaluation of First Order Model Results

As an example of the first order model, the wing rock behavior at a sting angle $\theta = 30°$ will be simulated. Figure 18 shows a time history and phase plot after the wing rock motion has reached the limit-cycle. Comparison of these plots with the experimental results shown in Figs. 19 and 20, show the strengths and weaknesses of the first order model. As expected, the frequency, maximum amplitude, and maximum angular accelerations of the simulated motion agree quite well with the experiment. However, the character of the value of $\ddot{\phi}$ variation with roll is not reproduced well. Since $\ddot{\phi}$ is proportional to the aerodynamic moment (see the equation of motion), this means the damping model is not an accurate representation of the actual behavior. Specifically, the abrupt slope change at zero roll angle shown by the simulation correlates directly to the slope change in Clp as the roll angle changes sign.

In addition, the roll angle where the curve crosses over itself does not agree with the experiment. This angle is the point where the damping changes sign, ϕ_i in the notation above. According to the development of the first order model, the ratio of $\phi_i/\Delta\phi$ is $4/3\pi$ (or 0.424). The experimental results of Fig. 19 show this ratio to be approximately 0.544.

12.2.2 Parabolic Model (Second Order)

Observation of the behavior of the first order model and comparisons with the experimental results led to the development of a second order model for the aerodynamic damping. This model is formulated below.

$$Clp = \frac{Clp_o}{2}\left(1 - \left(\frac{|\phi - \phi bias|}{\phi_i}\right)^2\right)$$

The second order model is depicted in Fig. 16 as a dotted line. The additional $\phi bias$ term in this model is an adjustment to reproduce the asymmetric behavior of the ϕ_i points seen in the experimental results.

The frequency behavior of this model is the same as the first order model discussed above, so the value used for Cl_β is also the same. Also, the value of Clp, used to set the growth rate, is the same for the two models.

12.2.2.1 Evaluation of Second Order Model Results

Figure 21a shows the limit-cycle behavior of the second order model at a 30° pitch angle corresponding to the experimental results shown in Figs. 19 and 20. Again, just as with the first order model, the maximum amplitude and frequency of the oscillation agree closely with the experiments. The general shape of the phase plot

(Fig. 21b) agrees more closely with the experiment, showing the improvement in the damping model around zero roll angle. The ratio of $\phi_i/\Delta\phi$ for the second order model is 0.5, which also is closer to the experimental observations.

As a further example of the second order model, the build-up of the wing rock behavior at $\theta = 25°$ will be simulated. Figure 22a shows the time history of roll angle when the simulation is started with an initial roll angle of 6°. Figure 22b shows the next 2 seconds of wing rock as the limit-cycle is reached. These plots show good agreement with the build-up shown previously in Fig. 17. Figure 23 shows the phase plots corresponding to the final 2 seconds shown in the previous figure.

12.2.3 Higher Order Model (nth Order)

To further increase the accuracy of the simulation, the order of the model was allowed to vary to match the experimental observation of the $\phi_i/\Delta\phi$ ratio. The n^{th} order model was formulated as:

$$Clp = \frac{Clp_o}{n}\left(1 - \left(\frac{|\phi - \phi bias|}{\phi_i}\right)^n\right)$$

It was found that a value of n equal to 2.84 produced a $\phi_i/\Delta\phi$ ratio equal to the 0.544 value observed in the wind tunnel. The resulting phase plot is shown in Fig. 24. Again, the frequency, amplitude, and maximum angular acceleration all matched the experimental results closely.

12.2.4 Remarks

First, second and n^{th} order models for the aerodynamic damping were developed and examined with a one degree of freedom simulation. Very good agreement with the observed behavior from the wind tunnel tests was obtained. The wing rock growth rate, the maximum amplitude, frequency and maximum angular acceleration of the limit-cycle behavior were all closely reproduced by the simulation.

12.3 Pneumatic Controls, Dynamic Effects

The one-degree-of-freedom simulation was also used to explore the dynamic effects of pneumatic forebody vortex control. Comparison of the time histories obtained in the wing rock wind tunnel test with the output of the simulation program allowed different modeling schemes to be tested. The final aerodynamic model for pneumatic forebody vortex control closely reproduced the observed behavior in the wind tunnel.

The static wind tunnel test revealed that blowing from a jet located on the forebody generated roll and yaw moments by affecting the formation and interaction of the forebody vortices with the wing and LEX vortices. In addition, the wing rock tests

show the dynamic effects on the vehicle's lateral aerodynamics. The major effects of blowing from forebody jets are:

- a yaw moment increment
- a roll moment increment
- an increase in roll damping

The different pneumatic control schemes tested during the wing rock tests were: steady blowing on one side, combined blowing simultaneously on both sides, and pulsed blowing rapidly alternating between sides. The overall effects of the different methods will be presented below along with the results of modeling the effects in the one-degree-of-freedom simulation. More detailed discussion of the pneumatic control effects on the wing rock behavior can be found in Volume III of this report.

12.3.1 One Side Blowing

Initiation of blowing from a jet located on one side of the forebody during an established wing rock oscillation caused the motion to damp out, provided the blowing mass flow rate was sufficient. When the motion stopped, the model was not in a wings-level attitude. This creates a trimmed condition with a non-zero sideslip angle, or in other words, the blowing caused an increment in the zero β roll moment (ΔClo). This is consistent with the observations from the static wind tunnel test.

12.3.1.1 Clo Effect

The roll moment model was presented earlier when the static yaw control effectiveness was discussed. However, at that time, the determination of the roll moment characteristics at large blowing rates was not explained.

The maximum value of the blowing momentum coefficient examined during the static wind tunnel tests was $C\mu = 0.0015$. Subsequently, this level of blowing was found to be ineffective in alleviating the wing rock. Blowing levels of $C\mu = 0.0028$ and 0.0037 were used during the dynamic wind tunnel tests. Due to the lack of overlap between the two test series, ΔClo effect of the higher momentum rates had to be estimated from the final trim roll angle of the model after the wing rock had been damped.

The equation for the one-degree-of-freedom roll moment developed in an earlier section, when solved for trimmed, static conditions appears as:

$$Cl = Cl_\beta \sin(\theta)\, \phi_{ss} = 0 \quad \text{for trim conditions}$$

From this relation, the value of Cl_β can be determined easily for the different sting pitch angles and blowing rates tested. These values were then appended to the results of the static wind tunnel test to provide an aerodynamic model valid over the entire range of blowing coefficients.

12.3.1.2 Damping Effect, Clp

Time histories of the wing rock oscillation and the blowing pressure signal are shown in Fig. 25. At the larger blowing rate of $C\mu = 0.0037$, blowing on the left or right sides caused a shift in the mean value of the oscillation (the ΔClo effect), and smoothly damped the oscillation. The slight differences observed in the damping due to blowing with the left or right jets is related to the natural asymmetry of the vortex flow pattern as explained in Volume III of this report. For the purpose of the simulation model, the asymmetric damping effect is of lesser importance and will not be modeled.

Figure 26 compares the responses at two different blowing rates, $C\mu = 0.0028$ and 0.0037, at an angle of attack of 25°. The small blowing rate was not as effective in damping the wing rock oscillation; rather, it only reduced the amplitude. Blowing rates less than 0.0028 were unable to eliminate the oscillation. The blowing effectiveness was approximately the same at $\alpha = 25°$ and 30° for the same value of $C\mu$. In general, the damping contribution of pneumatic forebody vortex control jets appears to be proportional to the blowing rate and shows angle of attack sensitivity similar to the static control effectiveness.

12.3.2 Model Description

The computer formulation of the static roll moment control effectiveness due to pneumatic forebody vortex control was identical in form to the yaw control model and was presented earlier in Section 8.3.3 covering static aerodynamic controls. The roll control system similarly included a first order lag, but with provisions for a longer characteristic length yielding a greater time delay in response.

Pneumatic forebody vortex control has a major effect on the dynamic aerodynamic characteristics. The additional roll damping provided by forebody jets blowing on one side individually was modeled in the computer simulations by the following equation:

$$\Delta Clp|_{Blowing} = -Clp_O(\alpha)\left(\frac{Cl|_{Blowing}}{Cl|_{C\mu=0.0028}}\right)$$

This formulation keys the additional damping contribution to the amount of dynamic instability present in the bare airframe at the current flight condition, yielding a consistent damped response with the activation of forebody blowing. The magnitude of the damping increment is also scaled with the static roll control power provided by the blowing system, thus including the effects of varying blowing rates.

12.3.2.1 Model Validation Via Comparison With Wind Tunnel Tests

Proof of the appropriateness of the dynamic blowing model was obtained through comparison of the experimentally observed response to the predictions of the one-degree-of-freedom simulation. Results of the experiment at an angle of attack of $\alpha = 30°$ were presented earlier in Fig. 25. The results of the simulation at the same conditions are shown in Fig 27. The wing rock limit cycle was fully established at the

beginning of the plot (time = 0). Steady blowing on the right side was initiated at 0.1 seconds at $C\mu = 0.0037$. The wing rock damped in approximately 5 oscillations, establishing a steady trimmed roll offset of 10°. The agreement demonstrated by this example is typical of comparisons made over the entire range tested in the wind tunnel. Differences noted in specific comparisons fell well within the run-to-run variations observed during the wind tunnel tests, and therefore the computer formulation is judged to be an adequate representation of the static and dynamic aerodynamic behavior of pneumatic forebody vortex control.

12.3.3 Combined Blowing

Combined blowing simultaneously on both sides of the forebody was tested in the wind tunnel. This was very effective in damping the wing rock oscillation and produced very little residual roll moment compared to blowing on one side alone. The computer modeling of combined blowing was a simple addition of the left and right blowing models. The result is a canceling of the static roll moment effect at zero sideslip, though a net roll moment exists at non-zero sideslip due to the differing effectiveness of blowing on the windward and leeward sides. The damping increment of the two sides sum to produce a larger damping effect than that from single side blowing. The justification for this simple summation of the single effects can be seen by again referring to Fig. 25. The experiment clearly showed a more rapid damping to a steady state roll angle closer to zero than in the case of single side blowing.

12.3.4 Pulsed Blowing

As discussed earlier, concern for the mass flow required for simultaneous combined blowing led to the testing of rapidly pulsed blowing alternating between the left and right sides. The computer model of this technique is a combination of the two single side blowing models. The frequency and duty cycle of the pulses could be varied. At a sufficiently high pulsing frequency, the airframe does not respond to the roll and yaw moment perturbations due to the blowing, yielding a time-averaged moment cancellation and symmetry. However, the additional roll damping produced by blowing on each side is of the same sign, so the time-averaged response is an increase in the level of damping similar to that obtained from blowing steadily on one side. The experimentally observed behavior will be reproduced by this computer formulation.

13.0 FULL SCALE MASS PROPERTIES

13.1 Estimation Techniques

Basic aircraft design handbooks[15,24] were consulted for methods to estimate the component weights, cg's, and moments of inertia. Not surprisingly, due to the unconventional nature of this configuration, the different empirical methods gave widely varying estimates for the mass properties. Based on the geometry of the various components and comparison of weight fractions of similar aircraft, the following weight build-up was estimated:

Structural Section	Weight (lbs)
Wing	8,500
Vertical Stab	1,000
Fuselage + Payload	28,000
Engines	8,000
Fuel	54,500
Total	**100,000**

Recognizing the difficulty of accurately estimating mass moments of inertia, the values obtained from the empirical methods were compared with those of other aircraft of similar design and flight regime. Of course, there are not too many of those in existence, but using scaling techniques suggested by Raymer[24], the principal moments of inertia for the XB-70, A-12 (SR-71), and the paper study aircraft designated AST-105-1 were reduced to a non-dimensional form and compared. The final values for the mass properties used in this study are based on the average of the non-dimensional mass properties of these three aircraft.

Bar charts comparing the non-dimensional inertias of these 3 example aircraft and the average value used for the NASP configuration are shown in Fig. 28 for the full fuel gross weight condition and the empty fuel condition. The mass properties used in the full-scale control system development and manned simulation are shown in the table below.

	Full Fuel Condition	Empty Fuel Condition
Weight (lbs)	100,000	45,000
Ixx (slug-ft^2)	26,554	15,367
Iyy (slug-ft^2)	669,415	378,697
Izz (slug-ft^2)	540,904	308,466
Ixy (slug-ft^2)	0	0

14.0 1DOF SIMULATION, SCALE EFFECTS

The one-degree-of-freedom simulation closely reproduced the limit cycle motion as observed during the wing rock wind tunnel test. In preparation for the man-in-the-loop simulation, the full scale aircraft dimensions and mass properties were input into the one-degree-of-freedom simulation. The model scale conditions were those of the wind tunnel test. The full scale conditions were set at 30% fuel weight, 200 KIAS at sea level, standard day conditions. These are tabulated below.

	Model Scale	Full Scale
q (psf)	21.0	135.59
V (ft/s)	132.84	337.56
b (ft)	17.3/12	259.5/12
S (ft^2)	335/144	75375/144
Ixx (slug-ft^2)	0.0312	18723.

Figure 29 compares the two simulation results at an angle of attack $\alpha = 30°$. The plots are presented in pairs, with the model scale and full scale results at similar conditions shown together. Note that the time scales are different. The series of plots begin with the roll time histories during the build-up of the oscillation after being released from an initial roll angle of $\phi = 6°$, followed by the phase plane plots covering the same period. The next set, Fig. 30, continues from the final conditions of the previous set and shows the development of the limit cycle. The final set, Fig. 31, shows the effects of initiating steady forebody blowing on the right side at a rate of $C\mu = 0.0037$. The blowing begins 0.2 seconds into the simulation of the model scale and at 1.0 seconds for the full scale example.

It is apparent from the comparisons that the overall character of the wing rock behavior is similar between the model scale and the full scale with the exception of the time scale. The frequency of the oscillations were 2.91 Hz for the model scale and 0.554 Hz for the full scale aircraft at these conditions. The amplitude of both oscillations grew at approximately the same percentage each cycle and the maximum amplitude of limit cycle was the same. Moreover, the response to forebody blowing was similar for both configurations.

14.1 Nondimensional Inertias, Dynamic Similitude

The reduced frequencies of the wing rock limit cycles are shown in the table below. The similarity of the values shows that the wind tunnel model and test conditions were close to being dynamically scaled for the assumed full scale flight conditions. Had this wind tunnel test been intended as a proper dynamic test of a specific aircraft, the non-dimensional mass moment of inertias would have been matched to those of the full scale aircraft and flight conditions[25]. The relative mass moment of inertia values for the wind tunnel test and flight conditions are shown in the table:

		Model Scale	Full Scale
Reduced Frequency	$\left(\frac{\pi\ f\ b}{V}\right)$	0.0992	0.1115
Reduced Inertia	$\left(\frac{2\ Ixx}{\rho\ Aref\ b^3}\right)$	3.766	2.976

The dynamic scaling is significant because it indicates that the aerodynamic phenomena observed in the wind tunnel correspond to conditions likely to be seen in full scale flight. In fact, variations of the assumed full scale parameters can create conditions where exact dynamic similitude with the wind tunnel test exists. For example, if the altitude were increased to 7800 ft or the fuel load increased to 74% of maximum, then the reduced inertia values for the full scale aircraft would exactly match those of the wind tunnel test model.

15.0 FULL SCALE CONTROL SYSTEM DEVELOPMENT

15.1 Methodology and Approach

The basic requirements for the flight control system are to provide adequate handling qualities such that the aircraft becomes flyable. The bare airframe as tested in the wind tunnel has severe cross-coupling of the control effects and inadequate damping in all axes. The longitudinal flight control system combines an angle of attack command system (at low speeds) with a load factor, n_z, command system (at high speed). The lateral-directional control system will consist of roll rate and sideslip commands. Lateral movement of the pilot's control stick commands the flight control system to execute a pure, uncoupled velocity-vector roll. Similarly, depressing the rudder pedals produces a stability axis yaw command resulting in a pure, uncoupled sideslip maneuver.

Each axis has available feedbacks of aerodynamic and flight path angles and rates. A fully augmented flight control system will be implemented that is similar to that found in a state-of-the-art high performance aircraft. This design is representative of a system that would be expected, or even required, for a flight vehicle of this class. In addition, a partial-augmentation flight control system will be modeled. This system has the rate feedback paths in the lateral and directional axes disconnected, resulting in no artificial damping supplementing the bare airframe in these axes. The purpose of including this unrealistic flight control system is to highlight the effects of various pneumatic forebody vortex control schemes.

15.2 Design Flight Condition

The flight control system synthesis was done for low speed and high speed flight conditions; however, a great part of the development concentrated on the approach to landing configuration. The landing configuration studied was 30% fuel weight, 200 to 300 knots airspeed, and altitudes from sea level to 10,000 feet. Full fuel weights and inertias were used to represent the take-off condition.

15.3 Design Criteria

The criteria chosen for the flight control system (FCS) was per MIL-F-8785C. Longitudinal short period characteristics were augmented so as to be within the ω_{sp} vs. n_z boundaries for Class IV airplanes. Lateral-directional modes were also augmented so as to meet the frequency and damping requirements of the specification.

Attention was also given to handling qualities. Longitudinal motion was tuned so as to meet Gibson's criteria[28] (i.e., pitch angle dropback for pitch pulse inputs). Lateral motion was tuned to have zero sideslip and sideslip rate during roll maneuvers. The control system also provided a "pure decoupling" between each axis.

15.4 Longitudinal Flight Control System

Figure 32 shows the block diagram of the longitudinal flight control system. The longitudinal FCS combines an AOA command system with an n_z load factor control system. At low speeds, the pilot's stick inputs command angle of attack. The command path is scaled for +30° AOA for full aft stick displacement and -5° AOA for full forward stick. At high speed, the stick commands a load factor at the pilot station (about 25 ft forward of the reference cg). The command path is scaled for +5g's for full aft stick and -2g's for full forward. The system fades between AOA and n_z modes at the airspeed where an AOA of 30° produces a 5g load factor. This airspeed is a function of weight, altitude, and ambient temperature. For the landing approach configuration, the airspeed for the mode change occurs around 300 knots.

Figure 32 also shows that the forward path makes use of a proportional plus integral signal. The feedback quantities through the forward path are α (at low speed) and n_z (at high speed). The AOA bias used in the AOA command system is the estimated AOA to hold a given flight path angle and flight path bank with zero pitch rate, as calculated below:

$$p = \frac{-g}{V_T}\cos\gamma\cos\mu + \frac{1}{V_T}\frac{\bar{q}S}{m}(C_{L\alpha}\alpha + C_{L0}) = 0$$

$$\alpha_{bias} = \left(\frac{mg}{\bar{q}S}\cos\gamma\cos\mu - C_{L0}\right)\frac{1}{C_{L\alpha}}$$

As a result, for neutral stick the forward loop proportional integral pathway holds angle of attack at the α_{bias} value. Any slight error is taken out by the pilot with the trim button on the stick.

In n_z mode, the n_z feedback is biased with $\cos\theta\cos\phi$. This is so that for a neutral stick position, the load factor at the pilot's station will be equal to the amount of gravity projected on the z-axis of the aircraft. The n_z bias helps hold the same attitude for neutral stick.

The command path is shaped and filtered so as to provide fine control and reduced sensitivity around the neutral stick position but to still provide maximum capability for large amplitude displacements.

Pitch rate feedback is used downstream of the forward loop integrator to provide artificial damping. Pitch rate is biased with the amount of pitch rate required to hold

zero $\dot{\alpha}$. This helps eliminate angle of attack excursions due to kinematic coupling and changes in projected gravity during rolls and/or sideslips. The Q_{bias} value is given by:

$$Q_{bias} = \tan\beta(P\cos\alpha + R\sin\alpha) - \frac{g}{V_T}\cos\gamma\cos\mu$$

Pitch rate feedback is also filtered through a lead-lag to provide good pitch responses and proper frequency and damping characteristics.

A lead term is incorporated downstream of the forward loop integrator labeled $\dot{n}$ in the block diagram. This accounts for the pitching moment produced by the time rate of change of the projection of the gravity vector and the time rate of change of the kinematic coupling terms in the $\dot{\alpha}$ equation. The value of $\dot{n}$ is given by:

$$\dot{n} = \tan\beta(\dot{P}\cos\alpha + \dot{R}\sin\alpha) + \dot{\alpha}(R\cos\alpha - P\sin\alpha)$$
$$- \dot{\beta}(P\cos\alpha + R\sin\alpha)\frac{1}{\cos^2\beta}$$
$$+ g\left(\dot{\beta}\tan\beta\cos\gamma\cos\mu - P_{wind}\cos\gamma\sin\mu - Q_{wind}\sin\gamma\right)\frac{1}{V_T\cos\beta}$$

This feedback also helps in reducing angle of attack excursions during rolls and sideslips. The "dumbbell effect" during high AOA velocity vector rolls is eliminated by the use of P·R inertial coupling as shown in the block diagram.

The gains in the pitch axis FCS were obtained at every point in the flight envelope. The gains are scheduled as a function of Mach number and static pressure levels. Synthesis and analysis of the FCS was accomplished using the Boeing control system analysis program EASY5.

15.5 Lateral - Directional Flight Control System

Figures 33a to 33c represent the lateral-directional control system design. Lateral movement of the pilot's control stick commands the stability axis roll rate. This command is then transformed into body axis roll and yaw rates through $\cos\alpha$ and $\sin\alpha$. Sideslip is commanded by rudder pedal deflections and its error signal goes through a proportional-integral path. The output from the proportional-integral path commands stability axis yaw rate, and it also goes through the $\cos\alpha$ and $\sin\alpha$ transformation to get body axis roll and yaw rates. The rate commands from both command channels are summed to get the total body axes rate commands.

The roll axis command path is scheduled as a function of dynamic pressure and angle of attack. The roll rate command is set by computing the maximum available control power at each flight condition assuming a stability axis roll. The control power computation takes into account inertial coupling, airframe roll/yaw damping, and control power for stability augmentation. Approximately 15% of the maximum available control power is reserved for transients. The roll axis is shaped and filtered

in the command channel as well. This provides fine roll control around neutral stick and reduces sensitivity.

The yaw axis command path is also scheduled as a function of dynamic pressure and angle of attack. The command value is set in much the same way as the roll axis.

The lateral-directional flight control system is designed to provide zero sideslip and sideslip rate during rolls. It is also capable of eliminating stability axis roll rate while commanding sideslip. The two axes are decoupled by designing to the following criteria:

1. Closed loop roll rate and yaw rate responses must have the same rise time for roll stick inputs. This is done by augmentation so that $L_P = N_R = \frac{-1}{T_R}$.

2. Augmented L_R and N_P must be zero.

3. Dutch roll frequency and damping is fixed by the relationship: $2\zeta\omega = \frac{-1}{T_R}$, provided (1) and (2) are true.

The derivation of the above relationships for decoupled modes is easy but is beyond the scope of this discussion.

The block diagrams in Figs. 33a to 33c show how the lateral-directional FCS satisfies the above criteria. The bare airframe stability derivatives are essentially taken out with the controls. These derivatives are then replaced with the desired quantities. Augmented L_P and N_R are set by the $\frac{-1}{T_R}$ functions in the block diagrams. Dutch roll frequency is set in the yaw axis forward loop gain. This gain, k_β, is the augmented frequency, ω_d^2.

Gravity compensation is also used to help eliminate β excursions during roll maneuvers. This is shown in the stability axis yaw rate channel as:

$$R_{S_{gravity}} = \frac{g}{V_T}\cos\gamma\sin\mu$$

Compensation for the time rate of change of the projection of gravity into the wind axis is also done by the $\dot{m}$ term in Fig. 33b of the block diagram. This term is given by:

$$\dot{m} = \dot{\alpha}(P\cos\alpha + R\sin\alpha) + g\left(P_{wind}\cos\gamma\cos\mu + R_{wind}\sin\gamma\right)\frac{1}{V_T}$$

Inertial coupling is also accounted for in both the roll and yaw channels.

15.6 Control Mixing Methodology

The NASP configuration uses elevons at the trailing edge of the wing as primary control surfaces for both pitch and roll control. The lateral-directional flight control system produces a set of moment commands that are passed through a mixing algorithm and results in a differential elevon command, δ_A, and rudder command, δ_R. A collective elevon command, δ_E, is computed by the pitch axis FCS. The collective and differential elevon commands are combined to determine the individual left and right elevon deflections by the following relations:

$$\delta_{E,L} = (\delta_E - \delta_A) \qquad \delta_{E,R} = (\delta_E + \delta_A)$$

Due to the use of this mixing, one elevon will generally reach its deflection limit before the other one. At that point, any additional deflection commanded by the flight control system can no longer be delivered and a compromise must be made. Because this investigation primarily involves a landing task and maneuvering in close proximity to the ground, the control limiting scheme gives preference to the pitch command. That is, if both a large elevator and a large aileron deflection are commanded by the flight control system, the elevons will deflect to give the full commanded value of elevator deflection at the expense of aileron.

15.7 Static Trim Requirements

As a simple example of the benefits of pneumatic forebody vortex control, the control deflections required for a trim flight condition will be presented. The flight condition is 5,000 ft altitude, standard day, Mach = 0.365 (400 ft/s). The aircraft is trimmed, wings level, in a 15° glide at its empty fuel weight. Trim is defined in this case as a condition of zero angular and linear accelerations. Airframe asymmetries, as measured in the wind tunnel, are included in the basic aerodynamics, producing trimmed flight with a steady state sideslip.

The aircraft trims under these conditions at an angle of attack α = 17.455° and sideslip β = 3.855°. The use of forebody blowing relieves the conventional control system of some of the burden of supplying trimming moments as shown in the following table of required control deflections:

Cμ used	Trim δ_R	Trim $\delta_{E,L}$	Trim $\delta_{E,R}$
0	-13.898	-3.129	-28.818
0.00155	-7.015	-3.129	-28.818
0.00185	-2.732	-3.129	-28.818
0.00216	-0.425	-3.129	-28.818

Large differential elevon deflections are required to trim the roll moment due to sideslip and the basic airframe asymmetries. At this angle of attack, the blowing system does not contribute to the rolling moment, so variation of the blowing rate does not effect the elevator or aileron deflection requirements. The rudder trim results clearly illustrates the ability of pneumatic forebody vortex control to provide significant control moments to supplement the conventional control system.

15.8 Pneumatic Control Implementation Schemes

The wind tunnel tests show that pneumatic forebody vortex manipulation offers some potential for use as a supplemental control system. In general, pneumatic techniques have the following major strengths that could be advantageously incorporated into an aircraft's control system:

- Large yaw moment generation at high AOA
- Increased roll damping

Five schemes for implementation of the pneumatic control will be discussed below in order of increasing sophistication. Two of the methods are "non-active," meaning the implementation is not a primary control method but rather is a simple on/off device. The last three discussed use the pneumatic control in concert with the conventional control system.

15.8.1 Non-Active Controls: Wing Rock Suppression

The first two control schemes utilize the demonstrated ability of pneumatic forebody vortex control to increase the natural roll damping of the aircraft. The major advantage of using forebody vortex control to provide roll damping is that it frees the primary flight control surfaces for their primary task, i.e., controlling the aircraft. This has the benefits of increasing the available control power, simplifying the primary control system, and reducing the overall system requirements.

The pneumatic systems are basically simple on/off implementations that are automatically activated by the aircraft angle of attack. The implementations are classified as non-active controls because the systems are not used in the direct control of the aircraft and do not use feedback of the aircraft state (except for angle of attack) to regulate the amount of control.

15.8.1.1 Steady Simultaneous Blowing

The simplest use of pneumatic control is simultaneous blowing on both sides of the forebody. As discussed in Volume III of this report, this was found to be an effective means of reducing the wing rock oscillation. The system would begin blowing as the angle of attack increased into the range where the bare airframe lacks roll damping. Steady blowing reduces the de-stabilizing interaction of the forebody and wing vortex systems, thereby increasing the roll damping.

However, there are some drawbacks to this implementation. The airframe's natural asymmetric yaw and roll moments at zero sideslip are still present, and in some cases are reinforced by the blowing. The mass flow requirements are the largest of any of the implementations, and other pneumatic control techniques showed greater increases in roll damping.

15.8.1.2 Pulsed Alternating Blowing

A non-active pneumatic forebody vortex control implementation that does not share the undesirable side effects of steady simultaneous blowing is pulsed blowing. In this implementation, the blowing is rapidly alternated between the left and right sides. The wind tunnel test demonstrated that if the switching frequency is approximately twice the wing rock frequency, the beneficial supplement to roll damping is retained without the accompanying asymmetric moments. The natural frequency of the airframe is low enough that the airframe cannot respond significantly to the alternating moments. As a result, it appears to the airframe as if the time-averaged yaw and roll moment due to the pneumatic control is zero and the forebody vortex flow is stabilized into an effectively symmetric configuration. Additionally, the total mass flow requirements of this control system should be roughly half of that for the implementation of steady simultaneous blowing on both sides, if the blowing alternates sides with no overlap or pause between pulses.

15.8.2 Active Controls

Three methods of incorporating pneumatic forebody vortex control into the primary flight control system will be discussed. The pneumatic control is treated as another source of yaw moment, similar to the conventional rudder control, but with different characteristics. In each of these concepts, the use of the pneumatic control increases with angle of attack as the pneumatic control power increases and the conventional control loses effectiveness. The three techniques generally increase in sophistication in the order presented, but each method has specific characteristics that would be advantageous in different conditions.

15.8.2.1 Dithered Control

As shown in an earlier section, the yaw moment due to blowing is not a linear function of $C\mu$; rather, there is a deadband below which blowing has little effect, followed by a rapid increase in yaw moment increment, then a leveling of the curve showing the effectiveness is reducing. A highly nonlinear control gradient causes an aircraft to have poor handling qualities and to be difficult (or impossible) to fly. A technique to create linear behavior from a nonlinear control response is through control dithering. The degree of nonlinearity exhibited by this configuration was not severe, but would require compensation from the control system and would cause more difficulty in implementation.

Dithering can be thought of as an extension of the pulsed alternating blowing previously described. The blowing will switch rapidly back and forth between the left and right sides at a frequency greater than the airframe natural frequency. However, the duty cycle, that is, the relative time spent blowing on each side, will be varied in proportion to the commanded yaw moment. In this manner, the resultant net control gradient is linear and the effects of the deadband and the nonlinear response to $C\mu$ are reduced or eliminated.

The advantages and disadvantages of the dithered control system are similar to the pulsed blowing. Roll damping is automatically increased whenever the pneumatic system is operating. Undesirable asymmetric forebody vortex flow is eliminated in a time-average sense. Also, the same drawback of dithered control is that, like the pulsed blowing, the mass flow requirements are high because the system is continuously blowing on one side or the other at high angles of attack.

15.8.2.2 Scheduled Proportion of Commanded Control

This approach treats the pneumatic controls as just another source for yaw moment. In response to a requirement for control moment, the control logic divides the requirement between all available controls by a specified mix. For example, the flight control system interprets a pedal input as a yaw rate command requiring yaw moment. The flight control system divides the requirement between the yaw moment sources, in this case the rudder and forebody vortex control. Each control provides a percentage of the total requirement. An early version of this control scheme used a fixed ratio splitting the work between the conventional and pneumatic control systems. A more sophisticated version, used in the manned simulation, divided the demand according to the ratio of maximum control power available from each system. At low angles of attack the rudder provided 100% of the yaw moment. As the angle of attack was increased above 20°, the pneumatic control system became active and satisfied larger amounts of the yaw requirement.

This control implementation has smaller total mass flow requirements than the previous schemes because blowing is only active when needed. While the jet blowing is actually taking place, the level of roll damping will be increased; however, during other times, the damping will have to be artificially augmented by the conventional controls.

15.8.2.3 High Frequency / Low Frequency Mix

Some configurations of forebody vortex control may exhibit significant time lags between a control actuation and the resultant force or moment generation. A control implementation that addresses this problem would use complementary filtering to produce a high-frequency / low-frequency control mix. The rudder, the high frequency control, would deflect to satisfy the yaw rate requirement onset and then wash-out as the pneumatic system, the low frequency system, becomes effective. This then returns the rudder to a neutral position, restoring its full control capacity. Another way to look at this implementation is the pneumatic system as the coarse control with the conventional controls functioning as the fine tuning (providing that the convential control is still effective at that flight condition).

The response time of the aerodynamics after the initiation of blowing was estimated from the pressure measurement time histories from the wind tunnel test described in Volume II. The delay in pressure rise was determined to be only the time required for the freestream flow to transverse from the blowing jet location to the pressure sensor. The distance from the nose to the wing reference center is 48 feet on the full scale aircraft. At a minimum flight speed of 200 knots, the control power would take only 0.14 seconds to fully develop. The control system as implemented for this

study runs at 20 Hz, or in other words, with a time between updates of 0.05 seconds. The control lag for this configuration was not a critical issue.

15.8.3 Implementations for Further Study

In addition to the conventional control baseline, two pneumatic control systems were selected for further development and study. The first is the non-active pulsed blowing to explore the advantages of a simple implementation. The wind tunnel test indicated that the time lags of the pneumatic control effectiveness were small enough not to be an issue in this configuration, so the proportional technique was chosen as the active control implementation.

15.8.4 Demonstration Testbeds

The three control concepts (one conventional and two pneumatic) were each incorporated into two distinct system architectures. The first system, a partial-augmentation system, handles control system mixing logic and produces uncoupled responses to control commands. This minimal system does not use rate feedbacks in the lateral-directional axes so the airframe damping is not artificially enhanced. The second system, a fully augmented system, is representative of a modern digital fly-by-wire system with full augmentation in all axes. This control system has position, state and rate feedbacks available and schedules gains such that good flying qualities are produced. The minimal system highlights the differences in the aircraft behavior with the different control systems, i.e., without blowing, with pulsed blowing, and with proportional blowing. The three control systems in the fully augmented aircraft appear similar to the pilot, unless maximum performance maneuvers are performed. In total, five different control systems were evaluated in the manned simulation. (The combination of pulsed blowing and a fully augmented flight control system was deemed of little value.)

16.0 MANNED SIMULATION

The static and dynamic aerodynamic model and control systems were incorporated into a manned simulation for the purpose of evaluating the use and benefits of pneumatic forebody vortex control in a flight vehicle. The flight tests were performed with a high-fidelity six-degree-of-freedom simulator. The evaluation pilot was qualified and regularly flies high performance, supersonic fighter aircraft. Evaluation tasks were designed to require a high degree of piloting skill and aircraft performance in the flight regimes where forebody vortex control is effective.

16.1 ARENA Description

The ARENA simulator[26] is a low-cost, man-in-the-loop, real time air combat simulator that provides high-fidelity flight mechanics, avionics and controls. It has been successfully used in studies of close-in air combat and in ground attack scenarios. The fixed base (non-motion) simulator has a large rear projection screen

providing out-the-window views forward. It features a glass cockpit that is easily reconfigured to represent other aircraft or different avionics. A battle manager station controls test set-up and real-time monitoring of the simulation, in addition to collecting data for post-flight analysis. A sketch of the ARENA hardware configuration is shown in Fig. 34.

16.2 Implementation

Adaptation of the ARENA manned simulation cockpit to the NASP configuration was relatively straight-forward. The aerodynamic model described above was supplemented with generic models of engine performance (suitably scaled), speed brakes, and landing gear. The cockpit layout is typical of a modern fighter aircraft using the HOTAS (hands on throttle and stick) philosophy. Existing switches on the control stick were reprogrammed to function as pitch trim control.

16.2.1 Winds, Turbulence

Provisions were added to allow for atmospheric disturbances to affect the aircraft. Steady horizontal inertial winds were input with an altitude variation representative of the Earth's boundary layer profile as described by Etkin[27]. The middle profile shown in Fig. 35 corresponds to a surface roughness expected in open country and is assumed to be appropriate for the regions surrounding an airport.

Atmospheric disturbances were incorporated in the simulation following the guidelines of MIL-STD-1797 "Flying Qualities of Piloted Vehicles" (Ref. 28). The Dryden form of turbulent velocity spectra with a low-altitude disturbance model was used. The Dryden model is a convenient spectral form based on an exponential autocorrelation function for the axial component. The other components of turbulence intensity are based on the axial component. Turbulence intensity was variable on a scale of 1 to 10 with 1 corresponding to light turbulence and 10 representing severe turbulence. In the simulated landing tasks a turbulence level of 5 (moderate) was used.

16.2.2 Instrumentation

The ARENA cockpit used in the manned simulation incorporates a Head Up Display (HUD) and out-of-window displays, but due to the aircraft attitude during the high angle of attack approach and the inability of the pilot to see anything but sky, they were of limited utility. The primary instruments used during the simulation tasks were: an attitude indicator with glideslope and localizer bars, angle of attack meter, airspeed indicator, vertical velocity indicator, and horizontal situation display including gyro compass and DME (distance measuring equipment). No special instrumentation beyond what is found in a typical state-of-the-art cockpit was used.

16.3 Evaluation Tasks

Evaluation tasks were identified that would explore the use of pneumatic forebody vortex control. As suggested earlier, the principal advantages of this control system are increased roll and yaw control power and greater roll damping at high angles of attack. Three maneuvers were selected that involve high angle of attack maneuvering:

- Landing Approach. A low-speed precision tracking task that requires good handling qualities and smooth control response.
- Loaded Roll. A high agility maneuver that requires maximum control power and response.
- Cross Wind Take-Off. Requires control power in sideslip and crossed control conditions.

These maneuvers are described individually in the following paragraphs.

16.3.1 Glideslope and Localizer Tracking

A standard FAR landing approach scenario was designed to test the pilot's ability to execute a precision tracking task. The standard 3° glideslope was used. The piloting task began at a trimmed flight condition at 0.6 Mach, 5,000 ft altitude, 100,000 ft uprange from the runway center, and offset 8,000 ft to the side of the runway centerline. The pilot was asked to fly a 30° course to the localizer and turn to smoothly intersect the runway heading, while simultaneously transitioning to the glideslope.

The pilot was instructed to maintain a constant airspeed and aircraft configuration once established on the glideslope. The approach airspeed was fixed at 200 kts which required 25° angle of attack to maintain a trimmed flight condition. The pilot's workload at this condition was extremely high due to: poor handling qualities of the aircraft, the extreme body attitude which did not allow "out-the-window" sight of the ground, and the large effect of thrust on the flight path and trim. Adding to the pilot's workload was the presence of atmospheric turbulence which precluded the establishment of a steady trimmed descent attitude.

16.3.2 Bank-to-Bank Loaded Rolls

To illustrate the maneuverability advantages of pneumatic forebody vortex control, a series of loaded rolls were performed. A loaded roll is a roll about the velocity vector performed with a constant angle of attack or load factor. Aerodynamically, this maneuver is very similar to a departure and spin but control is retained throughout. This requires good handling qualities and a large amount of control power in roll and yaw.

The evaluation maneuvers each began at the same altitude and airspeed (5,000 ft and 300 knots). The pilot rolled to approximately ϕ = -90°, stabilized the roll angle, increased angle of attack to a prescribed value, and rolled 180° to ϕ = +90°

while trying to maintain a constant angle of attack and airspeed. He was not required to hold sideslip to zero. The pilot was allowed to use any combination of control inputs to minimize the time required to complete the roll maneuver.

16.3.3 Cross Wind Takeoff

An inherent characteristic of this class of long slender aircraft with highly swept wings and high wing loadings is a limitation in allowable cross-wind capability during take-off[16]. This is due to the low speed and high gross weight conditions, requiring high angles of attack after rotation. In the high angle of attack regime, many of these configurations suffer from low directional stability and reduced directional control power.

16.4 Evaluation Matrix

The implementation of the aerodynamic and control system models in the manned simulation includes provisions for exploring the effects of varying turbulence levels, inertial winds including shear layers, reduced control size control surfaces, airframe asymmetries, reduced longitudinal and lateral-directional stability, pneumatic control time lag effects, etc. With the limited resources available in this contract, the evaluation matrix was limited to the five control systems described above in the landing approach task and the two fully augmented control systems in the bank-to-bank loaded roll. The landing tasks were performed with a single turbulence level and no wind. The loaded rolls included no atmospheric disturbances.

16.5 Results and Discussion

The following section shows comparisons between various flight parameters for the five different flight control system schemes described above. The flights selected for analysis represent typical simulation results obtained from multiple tests with each configuration. The purpose is to compare the appropriate flight parameters and draw some conclusions regarding the advantages and disadvantages of using forebody blowing with flight control systems using partial or full augmentation to contribute to the overall improvements in the flying qualities for the different flight tasks.

Results from the manned simulation will be shown and evaluated. As stated earlier, the purpose of the manned simulation was to fly the vehicle with several different control systems performing specific flight tasks. The primary flight tasks were a Landing Approach and a Loaded Roll at high angles of attack. The control systems consisted of five different combinations of conventional and forebody vortex controls. These are categorized as:

1) Partial augmentation, no blowing: conventional control surfaces only are used for stability and control. Pitch damping and pitch controls to compensate for pitch/roll/yaw coupling are included and are automatic. There are no artificial lateral/directional damping inputs from the control system.

2) Partial augmentation with pulsed blowing: the control system is the same as No. 1 except that pulsed blowing is automatically activated (open loop, no feedback except angle of attack) on the forebody to suppress wing rock above a specified angle of attack, set here at 20°.

3) Partial augmentation with proportional blowing: the control system is the same as No. 1 except that the flight control system chooses the proportional mix of forebody blowing control input and the conventional aft-body control surface input to meet the control input demand from the pilot. The proportionality is based on the angle of attack and the respective control power that is available from the forebody and the conventional surface at that angle of attack. The proportionality scheme was described earlier in Section 15.8.2.2.

4) Full augmentation, no blowing: the control system is configured to provide artificial damping in all axes, including lateral/directional, by utilizing whatever control surfaces are required. The full augmentation means full utilization of all control surfaces as needed to maintain good handling qualities throughout the flight regime, to the extent possible with the available control power from the conventional surfaces. No inputs from forebody blowing are available.

5) Full augmentation with proportional blowing: the control system is the same as No. 4 except that forebody blowing is also available to contribute control forces and moments. The integration of the forebody blowing with the conventional surfaces is accomplished through proportional control logic as in No. 3. The principal difference from No. 4 is that the blowing system can also be used along with conventional surfaces for full augmentation to provide good handling qualities through artificial damping, etc.

16.5.1 Pilot Control Inputs

Control inputs from the pilot with a fully augmented flight control system produce commands to the control effectors, where the proportion of conventional and blowing contributions are determined by the flight control system based on a prescribed proportionality scheme.

16.5.1.1 Conventional Control Surfaces

Longitudinal stick - pure pitch (Nz command at speeds above "corner" speed, angle of attack command at speeds below corner speed), requires simultaneous movement of elevons

Lateral stick - velocity vector roll rate, requires rudder (for yaw) and differential elevons (for roll), simultaneous elevons (nose-down for pitch coupling) to produce a pure velocity vector roll

Rudder petals - sideslip angle command, similar to lateral stick input, i.e., rudder and simultaneous elevons for roll/pitch control to produce a pure stability-axis yaw motion

16.5.1.2 Forebody Blowing

Longitudinal stick - no forebody input

Lateral stick - blowing from one jet only, determined by stick deflection and at a level determined by proportionality formula for required static moment, and to provide sufficient roll/yaw damping with feedback from velocity vector roll rate and roll direction

Rudder pedals - similar to lateral stick except blowing on left/right sides as required to produce a pure stability-axis yaw motion

16.5.2 Landing Approach

The landing approach task was described earlier in Section 16.3.1. The landing approach originates 100,000 ft in the -X-direction from the center point of the runway and 8000 ft in the -Y-direction from the airport runway centerline. The desired flight path is from the starting point at a 30° angle to the intersection with the approach path (extended vertical plane running through the center of the runway) and then turns 30° for final approach. Desired touchdown is on the centerline of the runway 4000 ft prior to the reference center point of the runway. This results in the starting point being 96,000 ft in the -X-direction from the touchdown point. With a 3° glideslope to the touchdown point the altitude at a distance of 96,000 ft would be 5031 ft. Since the initial altitude is 5000 ft, the pilot is to fly at constant altitude until he intersects the plane for the 3° glideslope to the touchdown point (a distance of 591 ft for an altitude difference of 31 ft). A perfect landing would touch down on the center line of the runway at a distance of -4000 ft from the center point of the runway.

The following five groups of figures (Figs. 36 through 40) show comparisons between several flight parameters that have been chosen to illustrate the relative merits of the various flight control schemes. Parameters that have been chosen (where appropriate) for comparison include the following:

a) Variation in altitude (-Z) and horizontal excursions (Y) from an extended vertical plane through the centerline of the runway along the ground track, X
b) Cross-track and altitude errors, (horizontally, ΔY and vertically, ΔZ), deviation (desired minus actual) of the aircraft cg from the desired approach flight path along the ground track, X
c) Angle of attack vs. time
d) Angle of sideslip vs. time
e) Roll angle vs. time
f) Roll rate vs. time
g) Flight velocity vs. time
h) Dynamic pressure vs. time
i) Rudder deflection angle vs. time
j) Aileron deflection, (left elevon - right elevon)/2 vs. time
k) Blowing coefficient (left and right nozzles) vs. time
l) Mass flow rate (left and right nozzles) vs. time

Discussion of the results of the five test cases are intended primarily to illustrate the benefits of forebody blowing, where appropriate, to both the partially augmented

flight control system and the fully augmented flight control system. The evaluation of the relative merits will be based on examining some of the flight parameters in Figs. 36 through 40.

16.5.2.1 Partially Augmented, No Blowing

Figure 36 represents the case for a partially augmented flight control system with no forebody blowing available. Figure 36a shows the flight path leading to an attempted touchdown point (X=-4000, Z=0, Y=0). The obvious result is that the target was not reached, i.e., Z=0 at X=-30,000 ft (crashed). The deviation of the actual flight path from the desired flight path is shown in Fig. 36b. The obvious errors are a descent in altitude that is much too steep, and some difficulty in holding lateral flight path. The variations in angles of attack, sideslip and roll angle are much more revealing in terms of the difficulty in flying this configuration. These are shown in Figs. 36c and 36d. In order to hold the velocity to 200 KIAS and to keep from dropping altitude too rapidly, a high angle of attack must be flown in order to provide adequate lift and drag.

These curves show angles of attack consistently in the range of 20° to 27°, angles where there are severe directional stability deficiencies and wing rock (lateral dynamic instability). The large oscillations in roll (phi) and sideslip (beta) are evidence of the difficulty of maintaining control in these modes. These instabilities are ultimately what led to the "crash". The angular excursions become uncontrollable after about 120 seconds into the flight. Figures 36e-36h show an expanded scale to illustrate the detailed time history of angle of attack, roll and roll rate. The buildup in roll angle oscillations and rate to a limit cycle motion are significant and the motion cannot be overcome by the pilot. The wing rock frequency is approximately 0.5 Hz.

Figures 36i and 36j show the time history of the velocity, Mach number, and dynamic pressure. The task was to decrease the initial velocity from M=0.6 to M=0.33 (approximately 200 KIAS) and hold this velocity until touchdown. This was virtually impossible to accomplish, as can be seen. Figures 36k and 36l show the time history of the rudder and aileron (differential elevon) deflections. Both of these are commanded by the pilot in an open loop fashion, i.e., there are no automatic or closed-loop rudder and aileron inputs from the flight control system to improve the handling qualities. The difficulty for the pilot is that since the stability is so poor in both roll and yaw axes, it is difficult to coordinate all the proper control movements to counteract the large amplitude motions at the frequencies that are being experienced.

16.5.2.2 Partially Augmented With Pulsed Blowing

Figure 37 has the same control system but with the addition of an open loop blowing system that acts as an automatic wing rock suppression system at high angles of attack. The pulsed blowing system is initiated at angles of attack greater than 20° with the mass flow increasing linearly with angle of attack until reaching a specified maximum level. The period of the pulsing was set equal to the pneumatic control time constant. This represents a greater frequency than was possible in the wind tunnel due to experimental limitations and produces smaller roll and yaw disturbances to the airframe. The pulsing frequency is approximately 6Hz, or approximately 12 times the natural wing rock frequency (the pulsing nozzle flow suppresses the roll moment

inputs by interfering with the natural periodic communication between the forebody vortices and the wing vortices.) The net result of the automatic wing rock suppression is that the roll oscillation time histories are much improved, but the ability to fly the vehicle is not significantly better. The cross-track error in Fig. 37b is actually worse than the one in Fig. 36. Angle of attack excursions are still quite large (up to 30°) where the airframe directional stability is very poor: thus the large excursions in β. The roll angle is still significant, but the limit cycle roll oscillations observed in Fig. 36d beginning at 120 sec are not present in Fig. 37d. There are no other significant differences in the use of the control surfaces. The pilot is still struggling to keep the aircraft under control and finally loses control and crashes approximately 20,000 ft from the runway center.

It should also be noted that with this particular blowing scheme, i.e., a pulsing frequency of approximately 6Hz (variant depending on the velocity), and at a maximum blowing coefficient of 0.0032, the consumption of pressurized gas with a fairly high mass flow rate over a long period of time is approximately 400 lbm per side. This accumulation is charted in Figs. 37k and 37l. A pulsed system that pauses or has a deadband between pulses might still be effective in reducing the interactions of the vortices and would require less total blowing mass.

16.5.2.3 Partially Augmented With Proportional Blowing

Figure 38 demonstrates the behavior of the simulated flight test vehicle with a partially augmented flight control system as before, but with the addition of a blowing system that is used in a proportional manner with the conventional flight control surfaces as described in Section 15.8.2. The flight control system control laws decide how much of the control input should come from the forebody system and how much from other control surfaces. There still is no provision for automatic damping in this system.

The addition of the added control power via forebody vortex control means that a control input at high angles of attack will result in a more robust response of the airframe to control inputs. It does not make the aircraft easier to fly with respect to proper timing of these control inputs. This must still be done by the pilot, especially in the lateral and directional modes where the largest instabilities occur. The flight profile in Fig. 38a and the deviations from the target flight path in Fig. 38b are not substantially different from the no-blowing cases of Figs. 36a and 36b. The exception is that the airplane came closer to being able to land successfully (crashed at approximately X=-14,000 ft) and showed somewhat less error in the cross-track and altitude errors.

The largest difference between this case and the case with no blowing is that the roll angle excursions are less with blowing than without, and the use of blowing in a proportional system is much more efficient than in an open loop pulsed system as shown in Fig. 37. The amount of time the blowing is on and the levels required for sufficient control are substantially less than in the pulsed blowing case. The other difference is that with a proportional blowing system to enhance the directional and roll control, the demand on the rudder is substantially less as can be seen by comparing Fig. 38g to Fig. 36k. The advantage, of course, is that the rudder is not the sole yaw

control, and there is a substantial amount of control power remaining for control purposes, if so demanded.

It is interesting to note that there is not much difference in the use of the ailerons with and without blowing, comparing Fig. 36l to Fig. 38h. In both control systems the pilot is attempting to counteract the wing rock motion with well-timed rudder and aileron inputs (phasing is critical). But since the wing rock is suppressed only with the system that has blowing, the rudder and aileron inputs do not have much benefit. Aileron inputs are only effective in the wing rock suppression mode if they are timed precisely with the motion that needs to be suppressed. If the timing is off, the inputs can substantially enhance the motion (pilot-induced-oscillations). The blowing provides roll damping (wing-rock suppression) simply by being on, even without proper phasing with the motion. Effectiveness is improved if the blowing is in the proper phase relationship with the wing rock motion, but it is not essential. Blowing on one side does have the effect of creating a small offset in roll angle which must be taken out by the pilot or the flight control system with ailerons and possibly some rudder. The aileron usage is only slightly increased compared to Fig. 36, which perhaps reflects this. The variation in blowing coefficient on left and right nozzles and the corresponding mass flow requirements are shown in Figs. 38i-38n. The usage is substantially less than that for the pulsed system in Fig. 37.

16.5.2.4 Fully Augmented, No Blowing

Figure 39 illustrates the case for a fully augmented conventional flight control system with no blowing inputs from the forebody. If the flight path and the displacement errors from the flight path (Figs. 39a and 39b) are compared to the partially augmented without blowing case in Figs. 36a and 36b, there is an obvious improvement in the ability to track the desired flight path for the fully augmented system, as one would expect. The aircraft has small deviations from the target flight path, and the pilot was able to land the aircraft at the proper location. In Fig. 39c the excursions in sideslip angle are significantly less in than in Fig. 36c. The angle of attack still varies over the entire range of 0 to 30° in order to maintain the proper altitude and velocity, but the aircraft is controllable. The rudder is very active (Fig. 39g) in order to maintain small sideslip angles due to the weak natural airframe directional stability at high angles of attack. But with the automatic control system, the pilot work load is significantly less.

Aileron deflections are not significantly different between these two cases, despite the fact that the partially augmented system experienced uncontrollable wing rock motions and the fully augmented case shows virtually no wing rock. The conclusion might be that the aileron deflection that was commanded was much more effective in the fully augmented case because it was timed much better with the motion it was trying to damp compared to what the pilot can do on his own. It may also be that the pilot simply did not choose or was unable to command aileron to suppress the roll oscillation and relied more heavily on the rudder to try to maintain control laterally as well as directionally. Even with the flight control system in command in the fully augmented case, the ailerons were used much less than the rudder. There are some significant excursions in roll angle (Fig. 39d), but no evidence of wing rock. The ability to maintain small sideslip by proper use of the rudder has undoubtedly benefited the

stability in the lateral mode as well because of the coupling between the directional and lateral modes of motion.

A comparison of Fig. 39 with Fig. 38 will provide some insight into the relative merits of the fully augmented conventional system with the partially augmented system with blowing available in an open-loop but proportionally-controlled mode. Comparing the flight path displacement errors would suggest that the fully augmented system is somewhat better than the partially augmented system, even though more control power is available at the higher angles of attack for the blowing case. The improvements gained from the full augmentation can also be seen by comparing the variations in roll and sideslip angles between the two cases. The partially augmented control system cannot effectively dampen the wing rock tendency as well as the fully augmented system. The control power is available with blowing, but without an intelligent flight control system to provide the blowing command based on feedback of roll and roll rate, it is difficult to use it properly.

It is also interesting to note the differences in the usage of the rudder. With partial augmentation, the rudder is not being utilized much when blowing is available. This is undoubtedly due to the proportional control system that provides a blend of rudder and forebody blowing for directional control. The pilot is working hard to maintain low sideslip angles, and a rudder command will result in more forebody control input at high angles of attack than rudder, thus a reduction in the rudder deflections. This graphically demonstrates the advantage of having the blowing available, but it also demonstrates that the use of the blowing must be carefully integrated into the flight control system with the benefits of motion feedback to use it to best advantage.

16.5.2.5 Fully Augmented With Proportional Blowing

Having shown that the fully augmented system with conventional control surfaces only is superior to the partially augmented system with blowing available, an obvious question is: what are the advantages of having blowing available in a fully augmented system? Figure 40 illustrates the flight parameters for this particular case and is best evaluated by comparison to Fig. 39 for the fully augmented case without blowing. A comparison of the performance in terms of the flight path deviation (Figs. 39b and 40b) show no significant difference. The pilot was able to maintain the desired flight path and land successfully in both cases. There is some improvement for the blowing case in the early part of the flight in cross-track error but it is not of major importance.

The time histories of roll angle and sideslip angle are similar in terms of maximum amplitude and the suppression of wing rock. This indicates that the conventional control system has enough control power through the use of the rudder and the ailerons to suppress wing rock without having to resort to forebody blowing, provided that there is a flight control system that can use it intelligently, as discussed in the previous section. The primary advantage in the use of forebody blowing for this particular aircraft is in the difference in the duty cycle of the rudder. Because of the capability to derive control power from the forebody and blend it properly with the rudder, there is a significant reduction in the use of the rudder to maintain good lateral-directional stability. This can be seen by comparing Figs. 39g and 40g. The benefit is

that the rudder is not operating near saturation just to maintain stability and is, therefore, available for more robust control inputs. The additional control power of the forebody may also allow the vertical tail and rudder area to be reduced, saving weight and reducing drag. There will also be cases where the basic airframe cannot provide adequate directional and lateral stability, and the addition of blowing that is well-controlled by the flight control system will be essential to fly the aircraft.

16.5.2.6 Advantages of Forebody Blowing With And Without Full FCS Augmentation

Although the comparison of the partially augmented system with blowing to the fully augmented system with blowing (Figs. 38 and 40) can be made by comparing each with the fully augmented system without blowing (Fig. 39), a direct comparison is useful to highlight the differences and explain what they mean.

In both cases, blowing is available as a proportional control input. That is, it is blended in a prescribed manner with the rudder and ailerons, depending on angle of attack, in order to maximize the control forces that are available. The key difference is the ability of the flight control system to use it properly, primarily in terms of when to use it with respect to the aircraft motion. With the partially augmented system, the pilot is deciding when to input the controls to maintain directional and lateral stability, a difficult task with an aircraft that is directionally unstable and is prone to violent wing rock at medium to high angles of attack. In order to fly the desired landing approach profile, high angles of attack are a necessity, meaning that the pilot needs as much help as possible to provide acceptable handling qualities.

For this aircraft, it is virtually impossible to fly with acceptable excursions in sideslip and roll without the use of an automatic and fully augmented flight control system. This can be seen clearly by comparing Figs. 38c and 38d with Figs. 40c and 40d, where the excursions in sideslip and roll angle are significantly less for the fully augmented system. An automatic flight control system with full augmentation for all axes will be even more important in an aircraft where the conventional control surfaces are inadequate on their own and are supplemented from other sources such as forebody blowing. This blending must be managed effectively and efficiently by the flight control system.

16.5.3 Loaded Roll

In addition to the landing approach task, a maneuvering task was also evaluated. Forebody vortex control has been promoted as an effective method of providing robust yaw/roll control for fighter aircraft at high angles of attack where the conventional aft-fuselage control surfaces such as rudder and differential tail have been shown to be severely reduced in effectiveness because of the immersion of these surfaces in the wakes of the wing, fuselage, etc. In particular, for a velocity vector roll, which is an important capability for an enhanced-agility fighter, the forebody can produce significant forces to provide the required moment around the velocity vector, essentially a yawing moment with coordinated roll moment. Although this aircraft configuration is not specifically designed for high maneuverability, it is judged worthwhile to evaluate the capability for performing such a maneuver.

The description of the loaded roll maneuver for this simulation task was provided in Section 16.3.2. The pilot is attempting to roll around the velocity vector as rapidly as possible at 300 knots starting at 5000 feet altitude for a total of 180° (from -90° to +90°) at a fixed angle of attack. He was allowed to use any combination of control inputs he desired to maintain angle of attack and minimize the time required to perform the 180° roll. The maneuver was performed with two of the five designated flight control systems described earlier for the landing approach task. The two systems are (1) Fully augmented without blowing and (2) Fully augmented with proportional blowing. Each was evaluated at three conditions, i.e., trying to hold angles of attack of 20°, 25° and 30°. Five trials were run for each condition.

The first example to be discussed is the fully augmented case with no blowing and trying to hold 25° AOA. Figure 41 illustrates this case. The time history of the velocity vector roll angle, mu (μ), is shown in Fig. 41a. The motion starts at μ = -90° and progresses to μ = + 90° and stops shortly thereafter (or the simulation run was terminated). The run numbers represent the five trials. The important parameter to observe is the time to roll the 180°, or the slope of the curve between μ = -90° and +90°. The first run (41) was the slowest and the remaining were fairly equal. The exception to the pattern is run 47 which starts very slowly at first and then builds rapidly to a rate nearly equal to the other three runs (44, 50, and 53). Note the loss in altitude (-Z) in Fig. 41c, which is a result of losing the lift vector in the vertical plane because of the roll.

Angle of attack (Fig. 41d) is held reasonably close to 25° for the duration of the roll (from approximately t=10 to t=20 seconds), although there is wide variation approaching and departing from 25° AOA with time. Recall that the fully augmented flight control system is supposed to produce a velocity vector roll with only a lateral stick input by using whatever surfaces are available, including rudder, elevons and ailerons (differential elevons). The test pilot did not fly the maneuver with "feet on the floor" causing the resulting maneuver to deviate from a zero-sideslip velocity vector roll. Referring to Figs. 41e and 41f, the roll is produced primarily from a rudder deflection, with only a small input from the ailerons to help stabilize the aircraft. Figures 41g and 41h show the response of the aircraft in terms of body-axis roll (p) and yaw (r) rates.

For comparison, the same maneuver is performed with full augmentation including proportional blowing, again attempting to hold 25° AOA. This case is documented in Fig. 42. The variation of the velocity vector roll angle μ with time in Fig. 42a shows more consistency than in the previous case, very linear and all nearly equal in slope. The roll rate also appears to be higher than the case where blowing was not available (rates are compared later). There is still approximately the same loss in altitude during the maneuver (Fig. 42c) but less variation from run to run. The ability to hold 25° AOA does not appear to be substantially better for the blowing case. This capability depends primarily on the ability of the control surfaces to provide pitch control to counteract the inertial pitchup effects of rolling at angle of attack. Since there is no control power in pitch provided by forebody blowing, it is not surprising to see little difference between the two cases.

The rudder deflection is substantially less for the blowing case (Fig. 42e) than for the non-blowing case (Fig. 41e), primarily because the forebody blowing provides a substantial portion of the yawing moment (or velocity vector roll moment) to produce the commanded velocity vector roll rate. Interestingly, when blowing is contributing to velocity vector roll through a body-axis yaw moment, one nozzle is blowing on the side in the direction in which the nose is moving, causing a body-axis rolling moment that must be countered with the ailerons in order to maintain the commanded roll and yaw rates.

The aileron activity was increased because of the need to provide an adequate roll input to complement the roll moment produced by the blowing forebody. This does not detract from the advantages of using blowing. It shows clearly that the proper balance between the conventional and forebody blowing control inputs chosen by appropriate flight control system laws can result in an improved flight vehicle.

Similar runs were made for angles of attack at 20° and 30°, and comparisons were made between the achievable velocity vector roll rates with and without proportional forebody blowing. A summary of these data is shown in Fig. 43. This comparison was developed by averaging the observed velocity vector roll rates between $\mu = \pm 90°$ for each of the cases (3 angles of attack and blowing vs. no blowing). The highest and lowest roll rates were eliminated from each set of runs before the average was calculated. The average roll rates are shown for the three angles of attack investigated with and without blowing.

There is a clear advantage in the cases with blowing, as one would expect, because the blowing adds additional control power at the higher angles of attack. It appears that, if used properly in an automatic flight control system, blowing not only provides the control power, but also provides it in a manner that can be used to enhance loaded roll agility performance.

16.5.4 Cross Wind Capability

The additional cross-wind take-off capability afforded by the use of pneumatic forebody vortex control has been estimated by examining the steady state trim capabilities of the aircraft. Generally, aircraft of this class suffer from a low value of maximum trimmable sideslip which limits the cross-wind take-off capability. An additional source of yaw moment control would increase the level of cross-wind that could be tolerated. However, the configuration investigated in this study does not show this advantage for two reasons. First, the rudder area was scaled for a conventionally controlled aircraft and is quite large. As discussed earlier, one of the benefits of forebody vortex control is the potential for reducing the tail size. The large rudder remained very effective throughout the angle of attack range, allowing large sideslip angles to be trimmed with conventional controls alone. The second unusual feature of the current configuration is the reversal in leeside blowing effectiveness beyond 7° sideslip. In other words, at sideslip greater than 7°, blowing on either side produces a restoring moment that decreases the sideslip. (See Section 8.3.2 and Fig. 10.) This characteristic increases the stability level of the airframe, but limits the level of trimmable sideslip to 7°.

16.5.5 Handling Qualities

As evidenced by the ground tracks and by the evaluation pilot's comments, the three configurations with only partially augmented flight control systems were virtually unflyable. However, the use of pneumatic controls did improve the handling qualities somewhat due to the added damping provided when the pneumatic control was activated. The two configurations with full-augmentation flight control systems appeared quite similar to the pilot with a slight preference expressed for the aircraft with the pneumatic control system due to its increased maneuver performance.

17.0 JET BLOWING SYSTEM REQUIREMENTS

17.1 Blowing Coefficient And Blowing Sources

The parameter typically used to quantify jet blowing in a forebody vortex control system is a non-dimensional "momentum coefficient" expressed as:

$$C\mu = \frac{\dot{m} v_j}{q_\infty A_{ref}}$$

where the numerator is equivalent to a force or "thrust" produced by the momentum of the jet, and the denominator has the usual terms to non-dimensionalize aerodynamic forces for coefficients, i.e.:

$\dot{m}$	=	mass flow rate from the jet
v_j	=	velocity of the jet stream
q_∞	=	flight or freestream dynamic pressure
A_{ref}	=	configuration reference area, usually wing area

A mass flow rate corresponding to $C\mu$ of practical effectiveness for forebody jet blowing usually requires a nozzle pressure ratio resulting in choked flow (i.e., $P_o/P_j > 1.893$), thereby establishing v_j equal to the speed of sound at the exit. The jet velocity is therefore a function of only the temperature of the jet at the exit and will be constant regardless of the pressure. The mass flow rate then is increased by increasing the density of the jet flow or by increasing the pressure. For a typical example the temperature can be assumed to be near ambient conditions unless the source of the jet air supply is heated or cooled.

Since $\dot{m} = \rho_j v_j A_j$ where

ρ_j	=	density of the jet flow
v_j	=	sonic velocity
A_j	=	area of the jet

then $\dot{m}$ is a function of the local total temperature (T_o) and pressure (P_o) of the supply air source for the blowing system. Therefore, for a specific temperature, T_o, the requirements for $\dot{m}$ are dictated by the area (or diameter, d_j) of the jet nozzle and the level of the supply pressure, P_o.

The following derivation will illustrate the appropriate equations to define the relationships between d_j and P_o, and $\dot{m}$, P_o, and d_j. These are the perfect gas relations for a compressible, isentropic, adiabatic gas.

$$C\mu = \frac{\dot{m}\, v_j}{q_\infty A_{ref}}$$

$$v_j = v^* = a^*$$

$$\dot{m} = \rho^* v^* A_j$$

where

$$\rho^* = \left(1 + \frac{\gamma-1}{2}\right)^{-1/\gamma-1} \rho_o = \left(\frac{2}{\gamma+1}\right)^{1/\gamma-1} \rho_o = \left(\frac{2}{\gamma+1}\right)^{1/\gamma-1} \frac{P_o}{RT_o}$$

$$v^* = a^* = (\gamma R)^{1/2} (T^*)^{1/2} = (\gamma R)^{1/2} \left(1 + \frac{\gamma-1}{2}\right)^{-1/2} T_o^{1/2}$$

$$= (\gamma R)^{1/2} \left(\frac{2}{\gamma+1}\right)^{1/2} T_o^{1/2}$$

so then from $\dot{m} = \rho^* v^* A_j$

$$\dot{m} = \frac{P_o}{\sqrt{T_o}} \sqrt{\frac{\gamma}{R}} \sqrt{\left(\frac{2}{\gamma+1}\right)^{\gamma+1/\gamma-1}} A_j$$

$$\dot{m} = \left[\left(\frac{\gamma}{T_o R}\right) \left(\frac{2}{\gamma+1}\right)^{\gamma+1/\gamma-1} \right]^{1/2} A_j P_o$$

$$C\mu = \frac{\dot{m}^2}{(\rho^* A_j) q_\infty A_{ref}}$$

$$C\mu = \frac{\frac{P_o^2}{T_o}\left(\frac{\gamma}{R}\right)\left(\frac{2}{\gamma+1}\right)^{\gamma+1/\gamma-1} A_j^2}{\frac{P_o}{RT_o}\left(\frac{2}{\gamma+1}\right)^{1/\gamma-1} A_j \; q_\infty A_{ref}}$$

$$= (\gamma)\left(\frac{2}{\gamma+1}\right)^{\gamma/\gamma-1} \frac{P_o}{q_\infty} \frac{A_j}{A_{ref}}$$

$$= (\gamma)\left(\frac{2}{\gamma+1}\right)^{\gamma/\gamma-1} \frac{P_o}{q_\infty A_{ref}} \frac{\pi d_j^2}{4}$$

$$C\mu = \frac{\pi\gamma}{4}\left(\frac{2}{\gamma+1}\right)^{\gamma/\gamma-1} \frac{P_o}{q_\infty A_{ref}} d_j^2$$

Therefore:

$$d_j = \left[\frac{4}{\pi\gamma}\left(\frac{2}{\gamma+1}\right)^{-\gamma/\gamma-1} \frac{q_\infty}{P_o} A_{ref}\, C\mu\right]^{1/2}$$

$$\dot{m} = \left[\left(\frac{\gamma}{T_o R}\right)\left(\frac{2}{\gamma+1}\right)^{\gamma+1/\gamma-1}\right]^{1/2} \frac{\pi d_j^2}{4} P_o$$

For air :

$\gamma = 1.4$

$R = 1716\ ft^2/sec^2{}^\circ R.$

With the following units for the various parameters,

d_j = ft, P_o = lbs/ft^2, T_o = °R, q_∞ =lbs/ft^2, A_{ref} = ft^2

then

$C\mu = 0.5806\ P_o\ d_j^2 / q_\infty\ A_{ref}$

$P_o = 1.7214\ q_\infty\ A_{ref}\ C\mu / d_j^2$

$$d_j = 1.312 \left[\frac{q_\infty}{P_o} A_{ref} \right]^{1/2} C\mu^{1/2}$$

$$\dot{m} = 0.01298\, d_j^2\, P_o/T_o^{1/2}$$

With the establishment of a typical flight envelope and performance requirements for a specific vehicle and with knowledge of the maximum level of $C\mu$ for a desired level of aerodynamic control power, A_{ref}, q_{max}, and $C\mu_{max}$ can be chosen. Once chosen, the designer's choice for a blowing system requires an evaluation of the trade-off between nozzle size and the pressure available from various potential sources. The size of the nozzle will be influenced by a desire to keep the nozzles small and to integrate them into the upper surface of the forebody as much as possible, minimizing the projection above the surface. However, as the equation shows, smaller jets require higher supply pressure to obtain an equivalent $C\mu$ level.

17.2 Potential Sources For High-Pressure Gas

The blowing can be provided by a number of potential sources:

1) Engine bleed air
2) Stored pressurized gas
3) Regenerative stored gas supply
4) Combustible or reactant gas system
5) Non-engine related high pressure gas source

The choice of potential sources for supplying adequate gas (air) supply for the blowing system will depend on several parameters. The primary ones are:

1) Duty cycle requirements
   a) Frequency of jet-on commands
   b) Mass flow rate required during jet-on state
   c) Maximum length of time for each jet-on condition
   d) Maximum total time for jet-on condition for typical flight mission
2) Capacity for high pressure gas storage or generation
   a) Engine bleed capacity
   b) Capacity for on-board high-pressure canisters
   c) Regeneration of high pressure gas with power take-off from engine
   d) Chemical reactant or combustion source

3) Plumbing constraints

   a) Volume required for stored gas containers
   b) Volume for piping hot gas from engine to forebody
   c) Problems associated with high temperatures and pressures (safety, etc.)

The demand for blowing for any given time in a flight mission in terms of mass flow rate and the duration of the jet-on state will play a significant role in determining whether the rate and duration must be met by a continuous supply of high pressure gas, as from engine bleed, or whether the demand can be met by a stored gas supply, which can be regenerated at times in the flight mission when blowing is not required. The requirement for a specific pressure level to acquire the desired mass flow rate will also influence the choice of pressure sources. Using engine bleed, one also must consider the plumbing requirements to move hot air from the rear of the aircraft to the front, etc. If adequate on-board storage can be provided, it may be possible to pressurize high pressure bottles on the ground prior to flight and to replenish them on landing, provided that the storage capacity is sufficient for an entire flight mission. It may also be possible to regenerate the high pressure reservoir in flight if a power take-off from the engine can drive a compressor at a time when the forebody blowing system is not needed. If the system is needed only for approach and landing, the storage capacity could be renewed on the ground before each flight. If the system is needed throughout the flight envelope, then a regenerative system, or a continuous supply of gas from engine bleed would be required.

17.3 Design Guidelines For Blowing System

The following discussion of design guidelines is based on a configuration and an example approach and landing task discussed earlier in this report in Section 16.5.2.5. The configuration has a fully augmented flight control system and proportional forebody blowing.

The plot in Fig. 44 illustrates the relationship between the jet diameter and the supply pressure required for a maximum $C\mu$ of 0.002, and a maximum q associated with the example landing task of $q_{max} =$ 250 psf. The time-history records of some of the flight parameters of interest for this example are shown in the next few figures. Figure 45 shows the variation in altitude (-Z) and horizontal excursions (Y) from an extended vertical plane through the center of the runway. The deviation of the aircraft position from the desired flight path, discussed earlier in Section 16.3.1, is shown in Fig. 46. Figure 47 shows the variation in dynamic pressure, and Fig. 48 shows the variation in roll angle and angles of attack and sideslip over the flight history. In addition to these flight parameters, there is a plot of $C\mu$ vs. t (Fig. 49), mass flow rate $\dot{m}$ vs. t (Fig. 50), and integrated $\dot{m}$ or cumulative mass requirements with time (Fig. 51). This demonstrates the usage of the blowing system to meet the control demands of the flight control system in this particular landing task.

For a flight vehicle of the size used in this simulation study, a practical jet diameter would probably be in the range of 1.0 to 2.0 inches. With the $C\mu$ and q_∞

requirements as noted, i.e., $C\mu = 0.002$ and $q_\infty = 250$ psf, the range of pressure levels required at the nozzle would be (referring to Fig. 44) approximately 500 psi to 150 psi corresponding to the nozzle diameters of 1.0 to 2.0 inches. If the available pressure were in the range of 1000 psi, for example, the jets could be reduced to 0.7 inches.

Once a jet diameter and related supply pressure, P_0, are chosen (see Fig. 44), it can be determined what the resulting range of required mass flow rates must be, assuming a temperature a reservoir T_0.

From the mass flow rate equation shown earlier:

$$\dot{m} = 0.012982\ P_o\ d_j^2/T_o^{1/2}$$

where

$$d_j = 1.312\ \left(\frac{q_\infty}{P_o}\ A_{ref}\right)^{1/2}\ C\mu^{1/2}$$

Substituting this equation for d_j into the $\dot{m}$ equation:

$$\dot{m} = .022346\ q_\infty\ A_{ref}\ C\mu//T_o^{1/2}$$

For this example case:

where $C\mu = 0.002$, $q_\infty = 250$ psf, and $A_{ref} = 523.4$,

$$\dot{m} = (.022346)\ (250)\ (523.4)\ (.002)/T_o^{1/2}$$

$$\dot{m} = 5.8479/T_o^{1/2} \text{ slugs/sec or } 188.302/T_o^{1/2} \text{ lbm/sec}$$

The plot of $\dot{m}$ vs. T_0 for this example is shown in Fig. 52.

For the illustrated example, if we choose a nozzle diameter of 1 inch, referring to Fig. 44, the required maximum pressure P_0 will be 500 psi and with a total temperature of 530° R (70°F), the corresponding mass flow would be (see Fig. 52) approximately 8.1 lbm/sec. From the simulation example, the mass flow requirements during the landing task varied from 0 to approximately 8 lbm/sec, resulting in the total mass of blowing air required over the 265 second time span of the landing task of m_{total} = 274.8 lbm for the left nozzle and 261.7 lbm for the right nozzle for a total of 536.5 lbm.

17.4 Utility Of Jet Blowing For Forebody Vortex Control

The designer has an option to either obtain this quantity of air from stored gas or to provide a continuously replenished pressurized air system either by direct engine bleed from the compressor by-pass air or possibly by repressurizing high-pressure

bottles or containers on board at a rate consistent with the $\dot{m}$ demands. This regeneration could possibly be derived from a power take-off compressor driven by the engine in some fashion.

If this represents the blowing requirements for a typical landing task, i.e. , a maximum required $\dot{m}$ = 8.1 lbm/sec and with a duty cycle as shown in this example, what are the practical alternatives for supplying the required mass flow?

Without knowing the specific engine characteristics of a proposed engine, it is difficult to decide whether using bleed air from the engine compressor is possible or not. From information on typical fighter configurations, an assessment has been made to determine whether bleed air from a fighter aircraft propulsion system can be considered. It is known that the level of total engine bleed air of today's typical twin engine fighter aircraft is in the range up to 8 lbm/sec, depending on altitude and throttle setting etc. That is not to say that all of the engine bleed would be available from these presently configured engines for a forebody control system, but it is not out of the question to consider engine bleed as a source, particularly if the duty cycle over the normal range of maneuvers is not high. If the design of a vehicle was expected to include sufficient bleed air for a pneumatic forebody blowing system, it is possible that the design of the engine and other related systems could take this into account early in the design.

An accurate assessment of the duty cycle for any particular vehicle would depend on the requirement for enhanced control and the frequency with which it would be employed in a typical flight mission. Trade-off studies comparing the advantages and disadvantages of a blowing system to an enhanced conventional control system would have to be made using extensive simulation evaluation to determine the complexity of a blowing system, including the hardware requirements in terms of weight, cost, volume, etc., as well as the control system requirements and enhancement of conventional control surfaces.

For example, to solve a directional stability problem at medium to high angles of attack, the vertical tail (and rudder) could be enlarged in order to be more effective, or one could consider using an active control system on the forebody, which is more effective in producing yawing moments, and integrate the control actuation into the flight control system. The advantage could be reduced tail height, which means less weight and less drag at all conditions including, particularly, cruise conditions where the enlarged tail is not necessary. However, the penalties for providing vortex control would also have to be evaluated, such as weight, requirements for more engine capacity, complexity of the active control system, fail-safe operation, engine out limitations, etc.

There could also be a system which relies on storable high pressure air for short duty cycles that would not depend on real-time generation of the high-pressure gas source. This would have an impact on safety considerations and efficient scheduling of the use of blowing nozzles so that the demand for replenishment of the high pressure gas source could be met efficiently at a time when the blowing system is not required.

Serious consideration of forebody vortex control with pneumatic jets and the related hardware and flight control system software will require careful analysis and evaluation of tradeoffs. For some vehicles it may not be practical. For others it may be the answer to providing a high-gain, highly-effective control input source that cannot be obtained in any other practical way. The result of this study shows that it is at least possible to consider a forebody pneumatic control system as a candidate for high-attitude aerodynamic control.

18.0 CONCLUSIONS

Data from the static wind tunnel test described in Volume II were smoothed, interpolated and incorporated into a six-degree-of-freedom simulation data base. The database included the static aerodynamic effects of pneumatic forebody vortex control. The free-to-roll wind tunnel test revealed a wing rock limit cycle oscillation at high angles of attack, as expected.

The non-linear aerodynamics causing the wing rock limit cycle were closely modeled by a second-order expression. The formula had three terms that were included as functions of angle of attack. The role in the limit cycle motion played by each of the terms was determined, allowing the observed motion from the wind tunnel to be quickly and easily reproduced. A non-linear, one-degree-of-freedom simulation was used in this part of the study.

For the manned simulation, a representative hypersonic aircraft was sized and mass properties were estimated based on other similar configurations and aircraft preliminary design methods. The aircraft had an overall length of 75 ft and a maximum gross weight of 100,000 lbs. The resultant high wing loading forced the angle of attack to be very large in low-speed flight conditions. The wind tunnel model and test conditions were a near-perfect dynamically scaled test of this hypothetical aircraft.

Different forms of pneumatic forebody vortex control were investigated and two systems, in addition to a conventionally control system, were selected for further study in the manned simulation. A landing and approach task and high angle of attack loaded rolls were used to evaluate the control systems. The simulation clearly demonstrated the utility of blowing control in a properly designed flight control system.

Mass flow rates and total mass requirements from the flight maneuvers were used as basis for a discussion of the design of a jet blowing system. Potential sources for the high pressure gas supply were identified and design guidelines were discussed.

19.0 ACKNOWLEDGMENTS

Support for this work is provided by NASA-Ames Research Center under contract NAS2-12989. The technical monitor is Mr. Larry Meyn of the Fixed-Wing Aerodynamics Branch. We would also like to acknowledge the support of Eidetics personnel who were instrumental in the simulation exercise: Don Farmer, Bill Clark and Jim Cobasko.

20.0 REFERENCES

1. Murri, D. G. and Rao, D. M., "Exploratory Studies of Actuated Forebody Strakes for Yaw Control at High Angles of Attack," AIAA-87-2557-CP, August 1987.

2. Malcolm, G. N., Ng, T. T., Lewis, L. C., and Murri, D. G., "Development of Non-Conventional Control Methods for High Angle of Attack Flight Using Vortex Manipulation," AIAA-89-2192, July 31, August 1-2, 1989.

3. Zilliac, G., Degani, D., and M. Tobak, "Asymmetric Vortices on a Slender Body of Revolution," AIAA-90-0388, January 1990.

4. Moskovitz, C., Hall, R., and DeJarnette, F., "Experimental Investigation of a New Device to Control the Asymmetric Flowfield on Forebodies at Large Angles of Attack," AIAA-90-0068, January 1990.

5. Ng, T. T. and Malcolm, G. N., "Aerodynamic Control Using Forebody Strakes," AIAA-91-0618, January 1991.

6. Suárez, C. J., Malcolm, G. N., and Ng, T. T., "Forebody Vortex Control with Miniature, Rotatable Nose-Boom Strakes", AIAA-92-0022, January 1992.

7. Guyton, R. W., and Maerki, G., "X-29 Forebody Jet Blowing", AIAA-92-0017, January 1992.

8. LeMay, S. P., Sewall, W. G., and Henderson, J. F., "Forebody Vortex Flow Control on the F-16C Using Tangential Slot and Jet Nozzle Blowing", AIAA-92-0019, January 1992.

9. Tavella, D. A., Schiff, L. B., and Cummings, R. M., "Pneumatic Vortical Flow Control at High Angles of Attack," AIAA-90-0098, January 1990.

10. Rosen, B. and Davis, W., "Numerical Study of Asymmetric Air Injection to Control High Angle-of-Attack Forebody Vortices on the X-29 Aircraft," AIAA-90-3004, August 1990.

11. Ng, T. T. and Malcolm, G. N., "Aerodynamic Control Using Forebody Blowing and Suction," AIAA-91-0619, January 1991.

12. Ng, T. T., Suárez, C. J., and Malcolm, G. N., "Forebody Vortex Control Using Slot Blowing," AIAA-91-3254, September 1991.

13. Ng, T. T., "Aerodynamic Control of NASP-type Vehicles through Vortex Manipulation", Eidetics International TR89-009, 1989.

14. Hoak, D. E., and Carlson, J. W., "USAF Stability and Control DATCOM," Air Force Flight Dynamics Laboratory, Wright-Patterson AFB, OH.

15. Baber, H. T. Jr., "Characteristics of the Advanced Supersonic Technology AST-105-1 Configured for Transpacific Range with Pratt and Whitney Aircraft Variable Stream Engines", NASA-TM-78818, March 1979.

16. Malcolm, G. N., and Ng, T. T., "Forebody Vortex Manipulation for Aerodynamic Control of Aircraft Methods at High Angles of Attack," SAE TP-892220, September 1989.

17. Grantham, W. D., Smith, P. M., and Deal, P. L., "A Simulator Study for the Development and Evaluation of Operating Procedures on a Supersonic Cruise Research Transport to Minimize Airport-Community Noise", NASA-TP-1742, November 1980.

18. Fox, C. H. Jr., Luckring, J. M., Morgan, H. L. Jr., and Huffman, J. K., "Subsonic Longitudinal and Lateral-Directional Static Aerodynamic Characteristics of a Slender Wing-Body Configuration", NASA TM-1011, February 1988.

19. Hahne, D. E., Luckring, J. M., Covell, P. F., Phillips, W. P., Gatlin, G. M., Shaughnessy, J. D., and Nguyen, L. T., "Stability Characteristics of a Conical Aerospace Plane Concept", SAE TP-892313, September 1989.

20. Hahne, D. E., Riebe, G. D., Riley, D. R., and Pegg, R. J., "Exploratory Wind-Tunnel Investigation of the Low-Speed Aerodynamic Characteristics of a Conical Aerospace Plane Concept", NASA TP-2860, January 1989.

21. Levin, D., and Katz, J., "Self-Induced Roll Oscillations of Low-Aspect Ratio Rectangular Wings", AIAA-90-2811, August 1990.

22 Levin, D., and Katz, J., "Dynamic Load Measurements with Delta Wings Undergoing Self-Induced Roll-Oscillations", AIAA-82-1320, 1982.

23. Nguyen, L. T., Yip, L., and Chambers, J. R., " Self-Induced Wing Rock of Slender Delta Wings", AIAA-81-1883, August 1981.

24. Raymer, D. P., *Aircraft Design: A Conceptual Approach*, AIAA Education Series, Washington, DC, 1989.

25. Wolowicz, C. H., Bowman, J. S. Jr., and Gilbert, W. P., "Similitude Requirements and Scaling Relationships as Applied to Model Testing", NASA TP-1435, August 1979.

26. Mosher, S. M., and Skow, A. M., "ARENA II. Man In The Loop, Multi-Mission Air Combat Simulation", Eidetics International S91-010, Torrance, CA, 1991.

27. Etkin, B., *Dynamics of Atmospheric Flight*, John Wiley and Sons, New York, NY, 1972.

28. Authors unknown, *"Flying Qualities of Piloted Aircraft"*, MIL-STD-1797 (USAF), 1987.

FIGURES

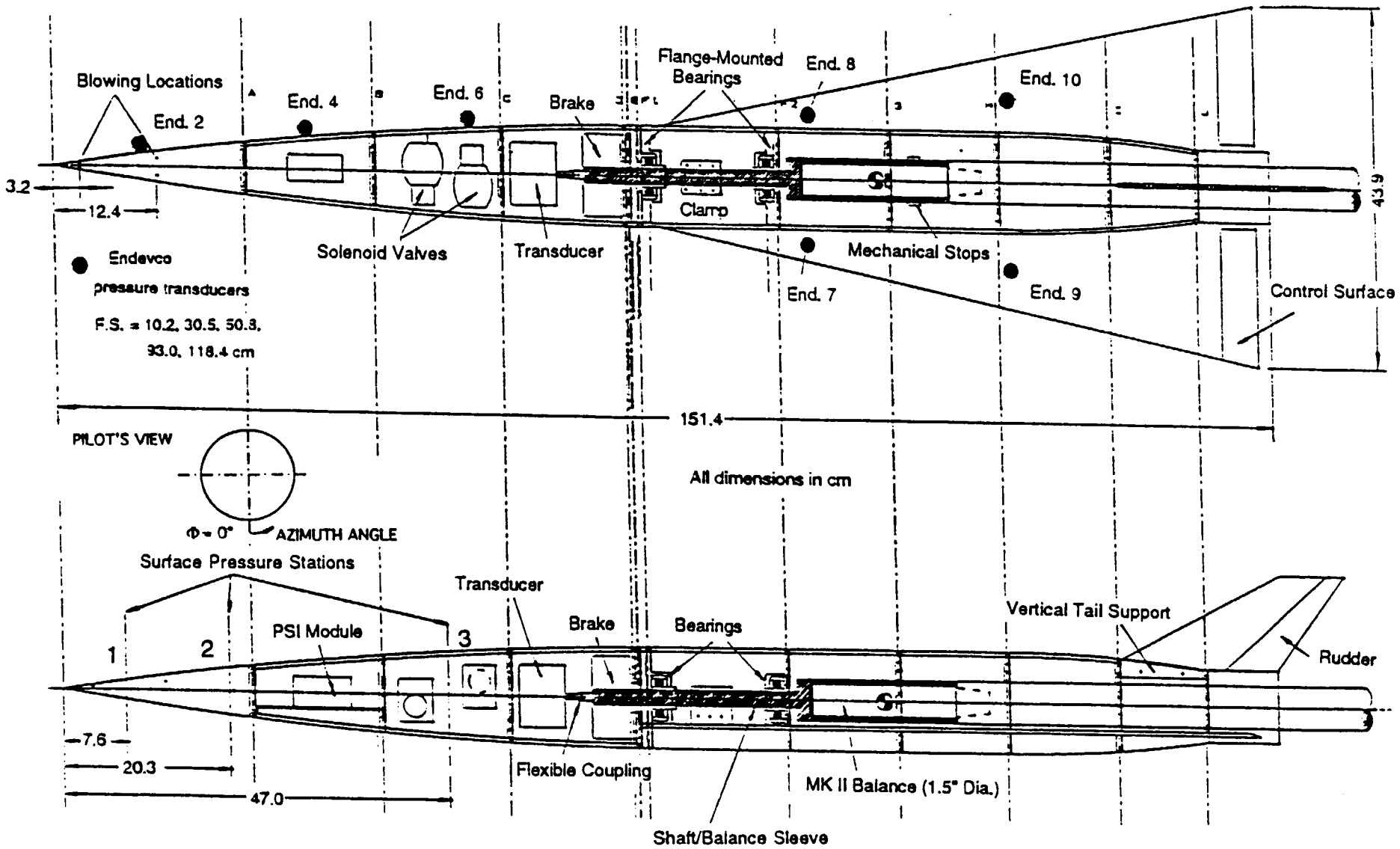

Figure 1 - Schematics of Wind Tunnel Model

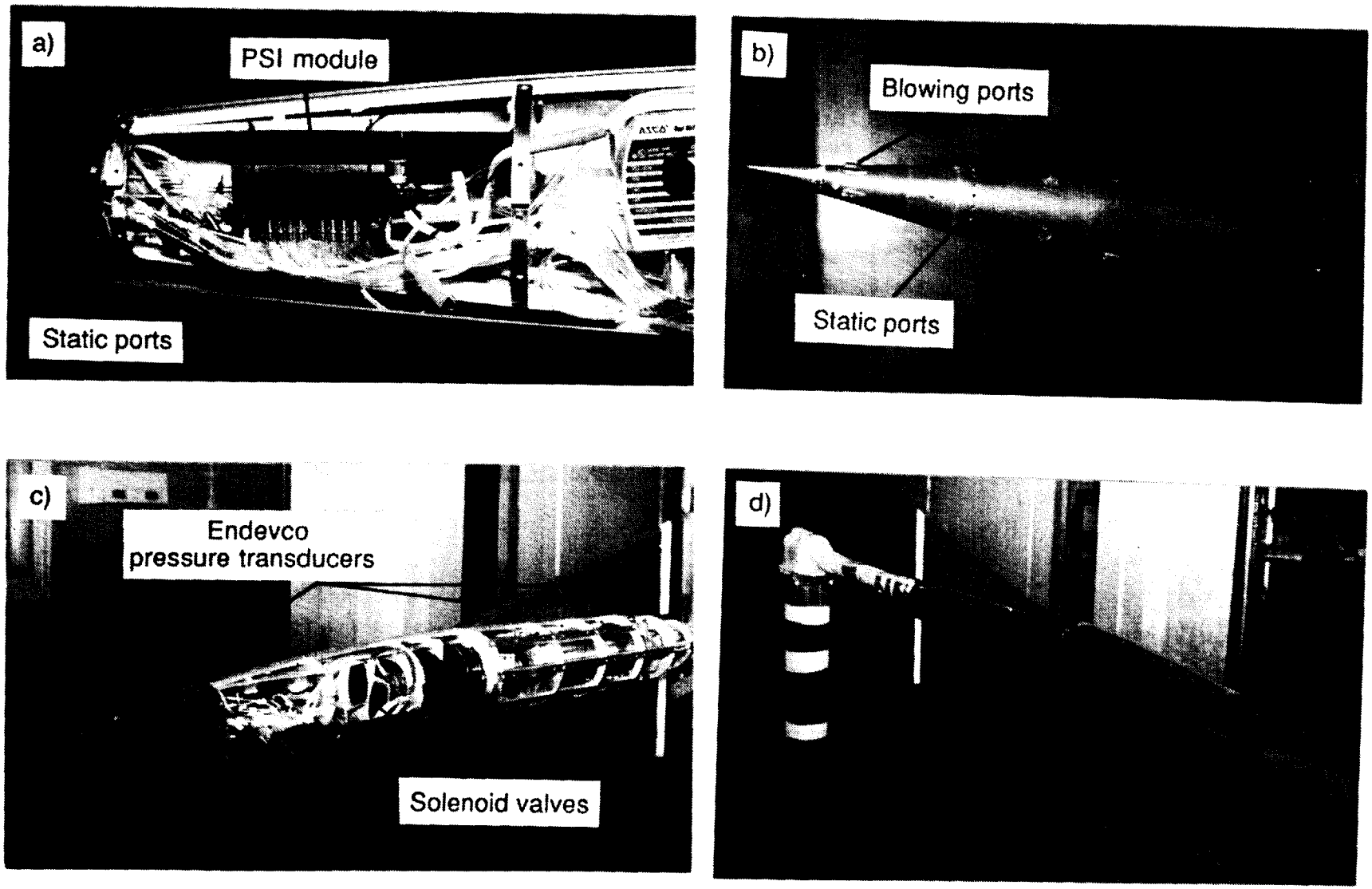

Figure 2 - Photos of Wind Tunnel Model

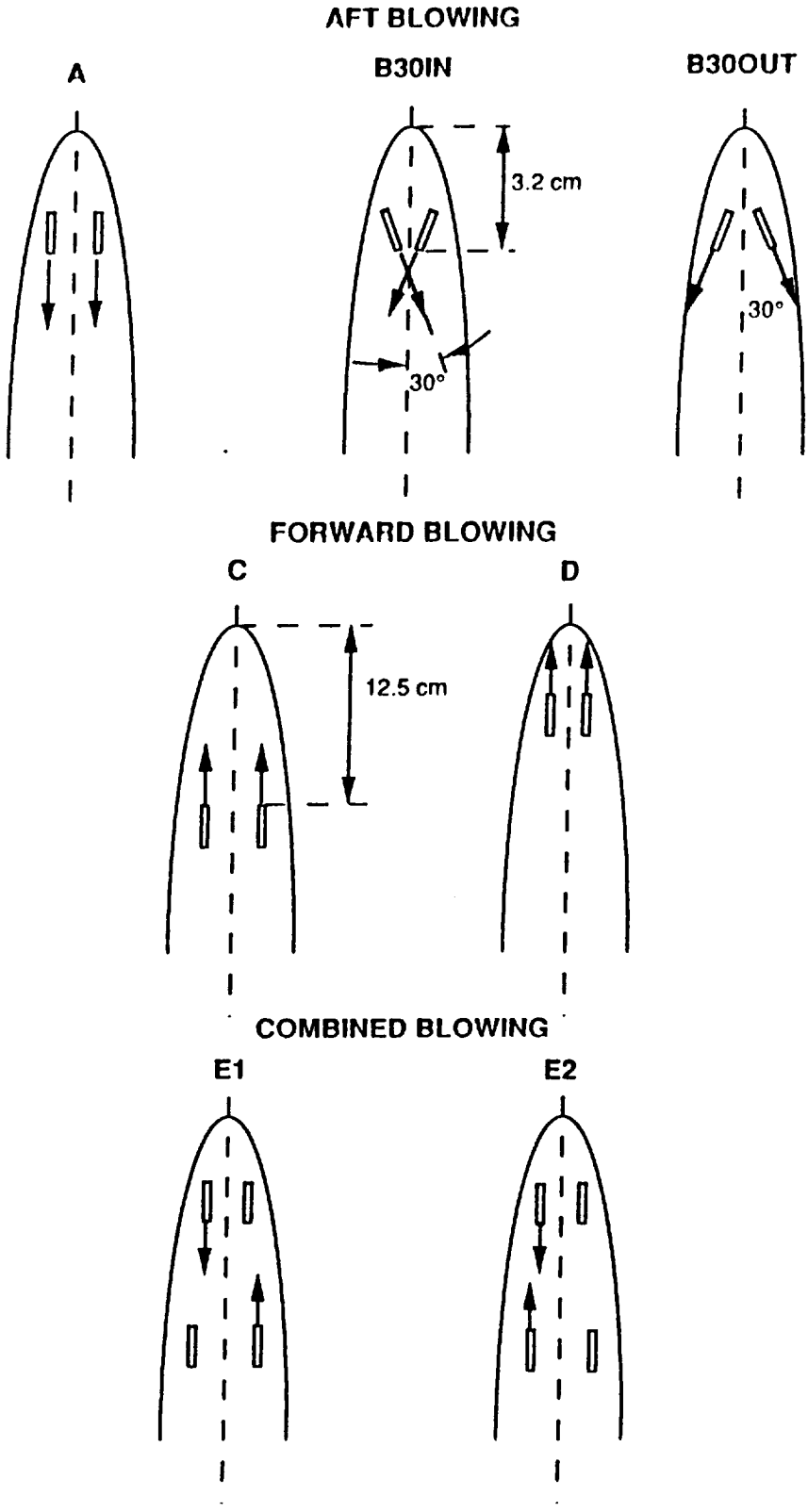

Figure 3 - Schematics of Different Blowing Schemes

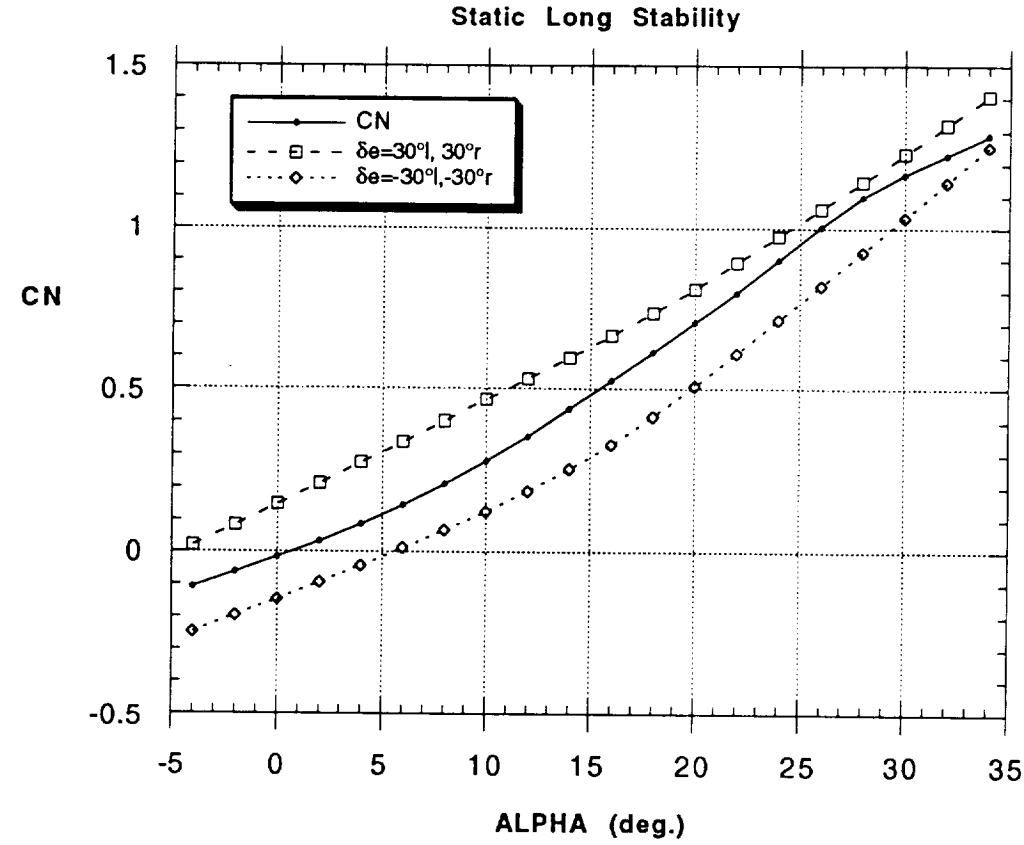

a)

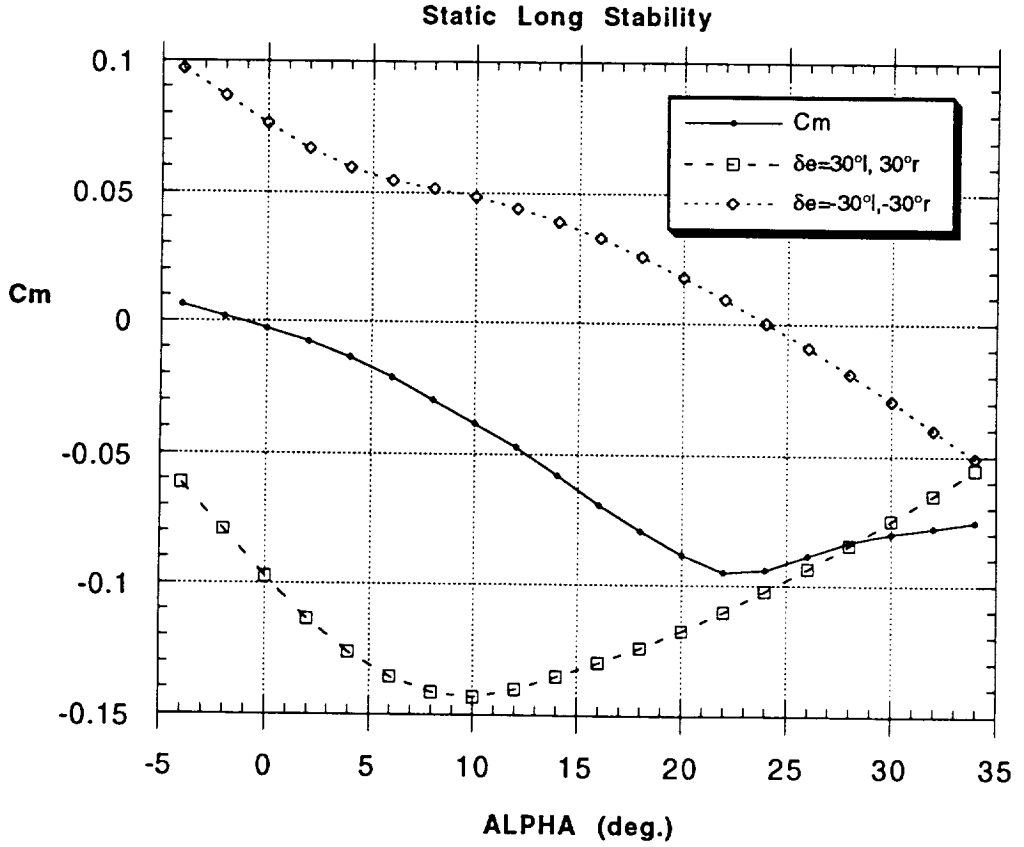

b)

Figure 4 - Static Aerodynamic Model (Longitudinal Characteristics)
a) CN, b) Cm

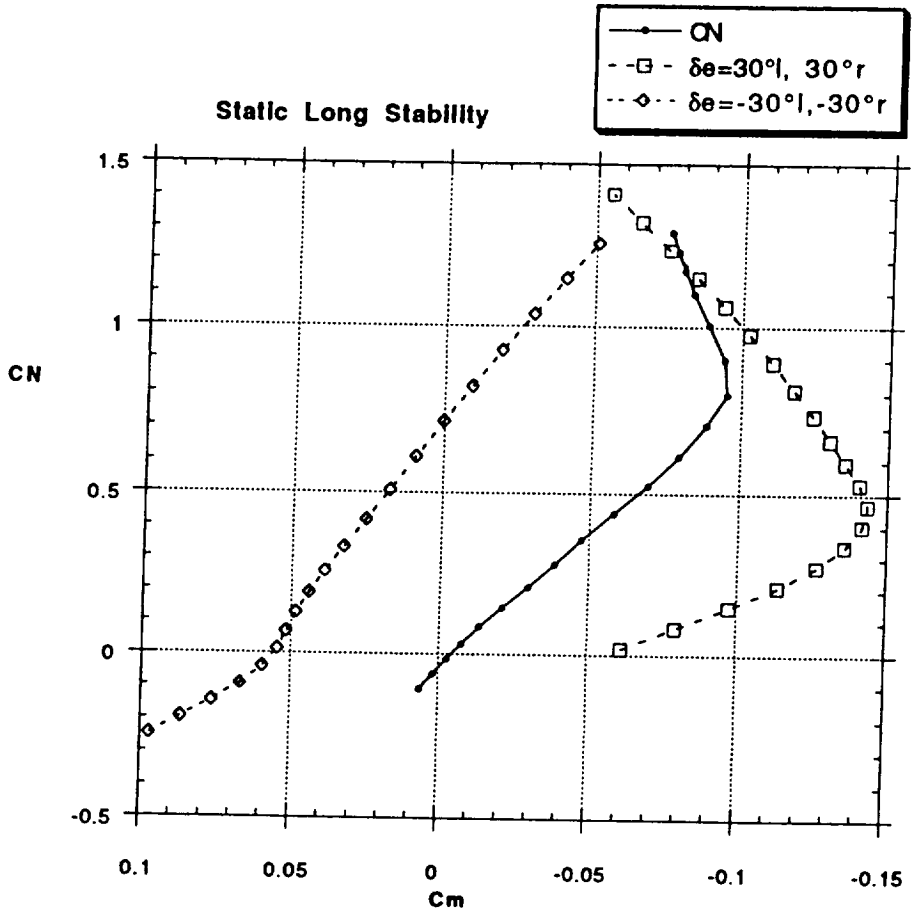

a)

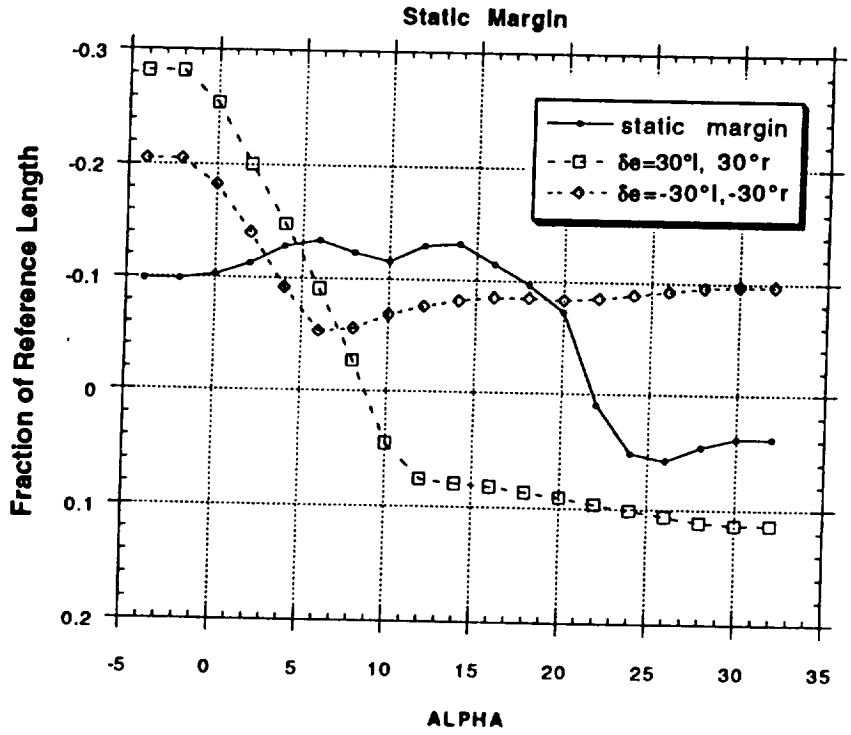

b)

Figure 5 - Static Aerodynamic Model (Longitudinal Characteristics)
a) Static Stability, b) Static Margin

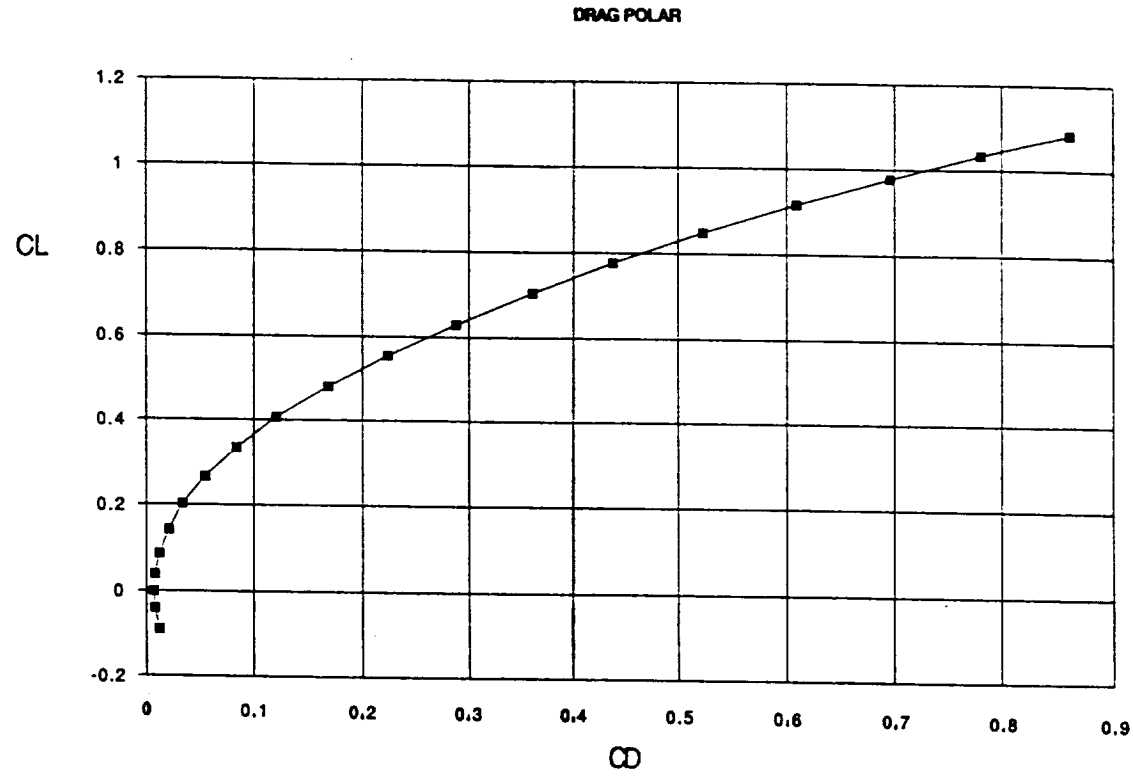

Figure 6 - Static Aerodynamic Model
Basic Drag Polar (from DATCOM)

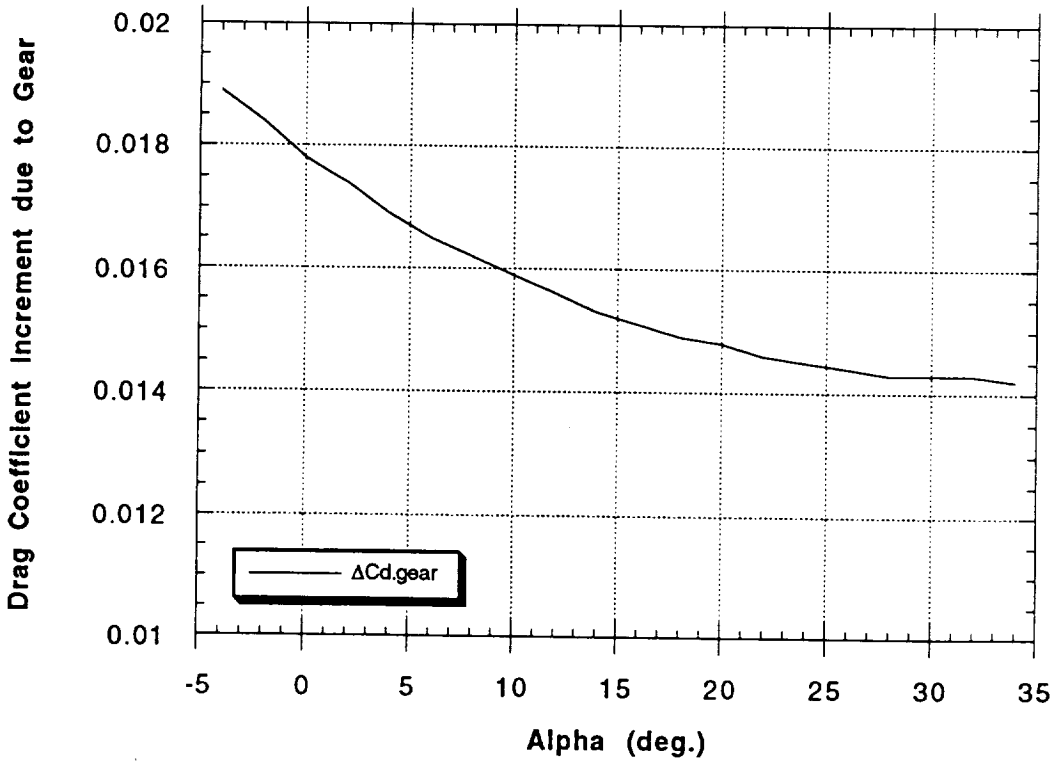

Figure 7 - Drag Coefficient Increment due to Landing Gear Extension

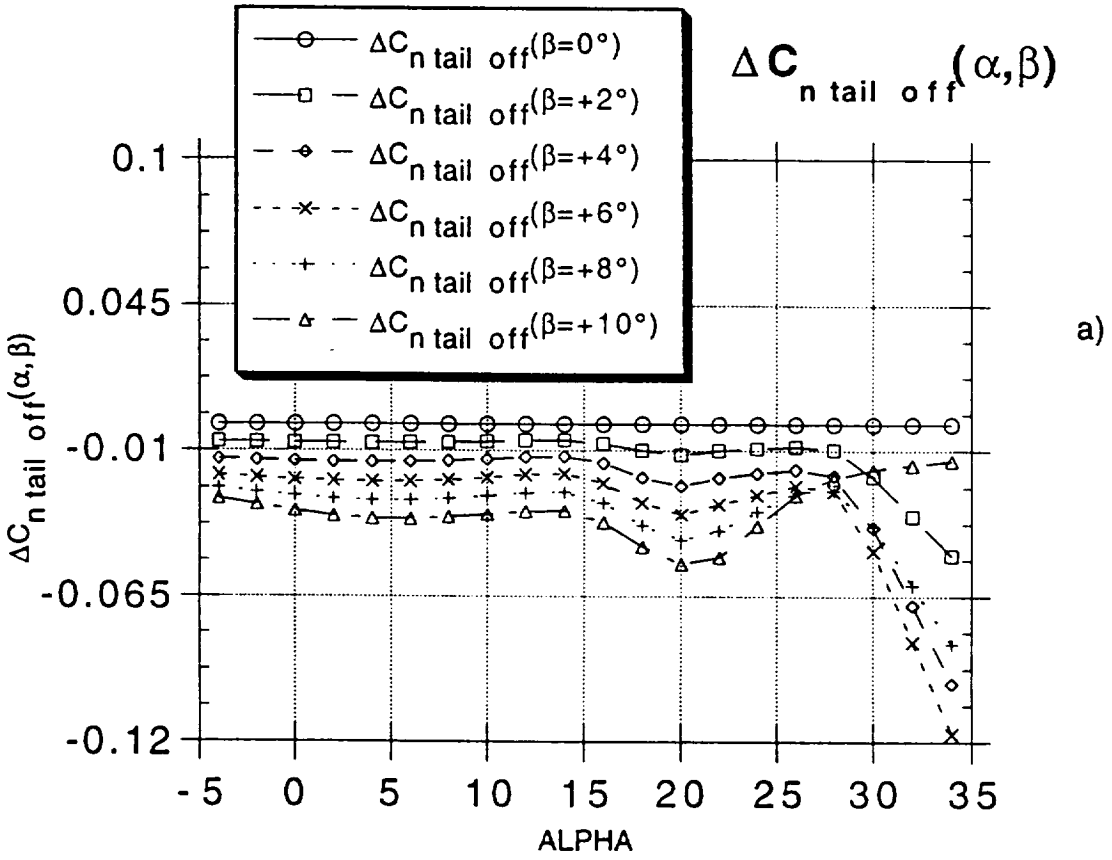

a)

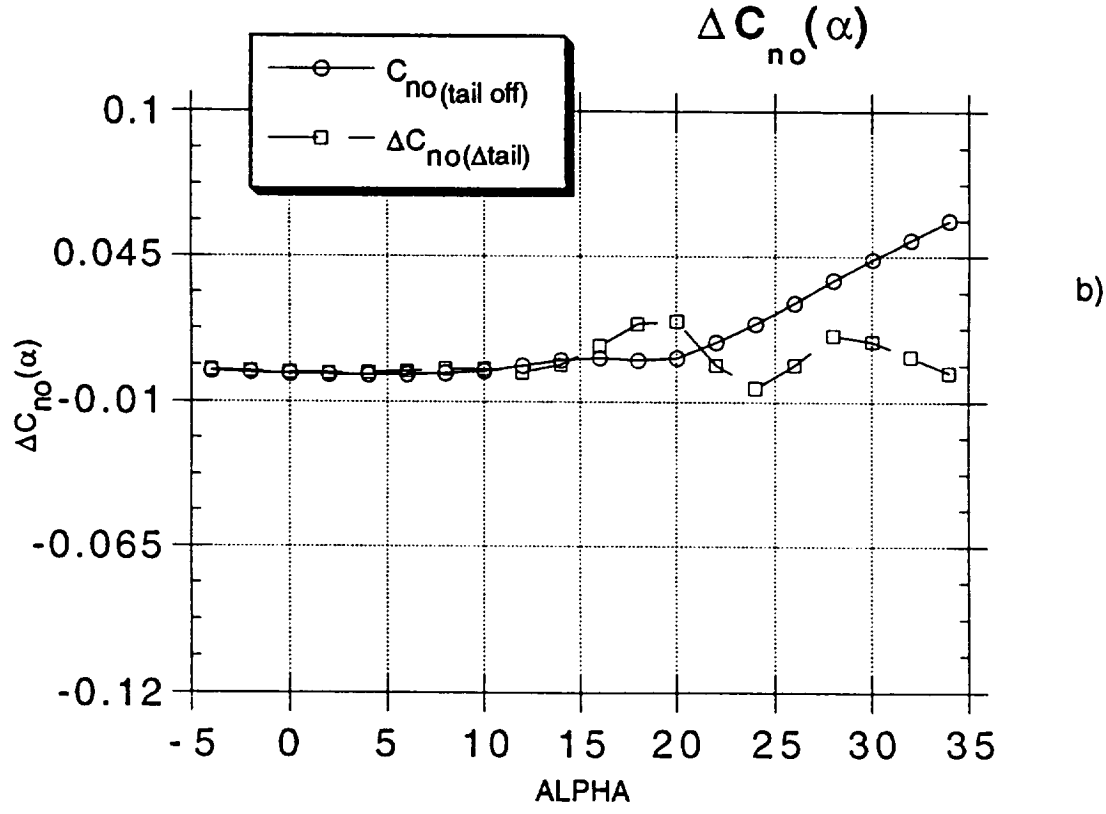

b)

Figure 8 - Static Aerodynamic Model (Directional Characteristics) Directional Aerodynamics and Conventional Control Effects on Yawing Moment

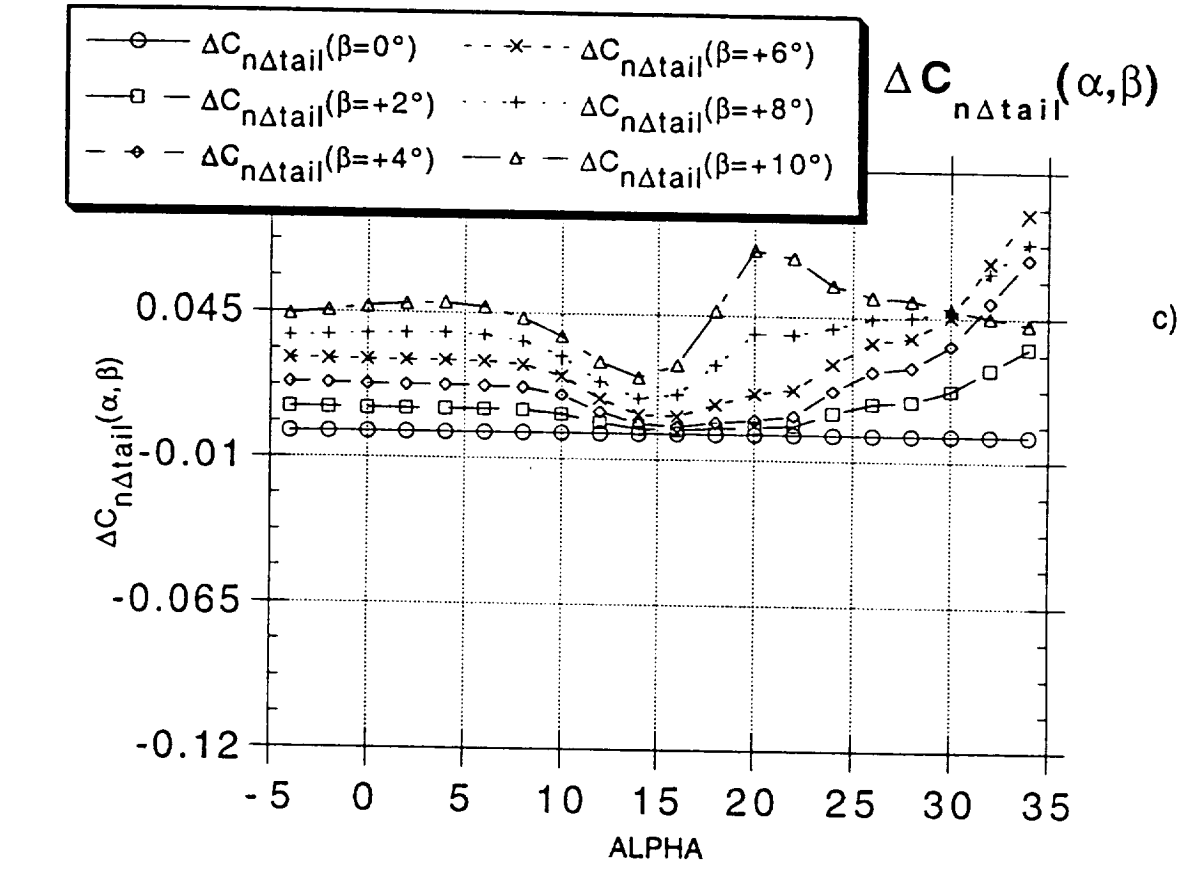

c)

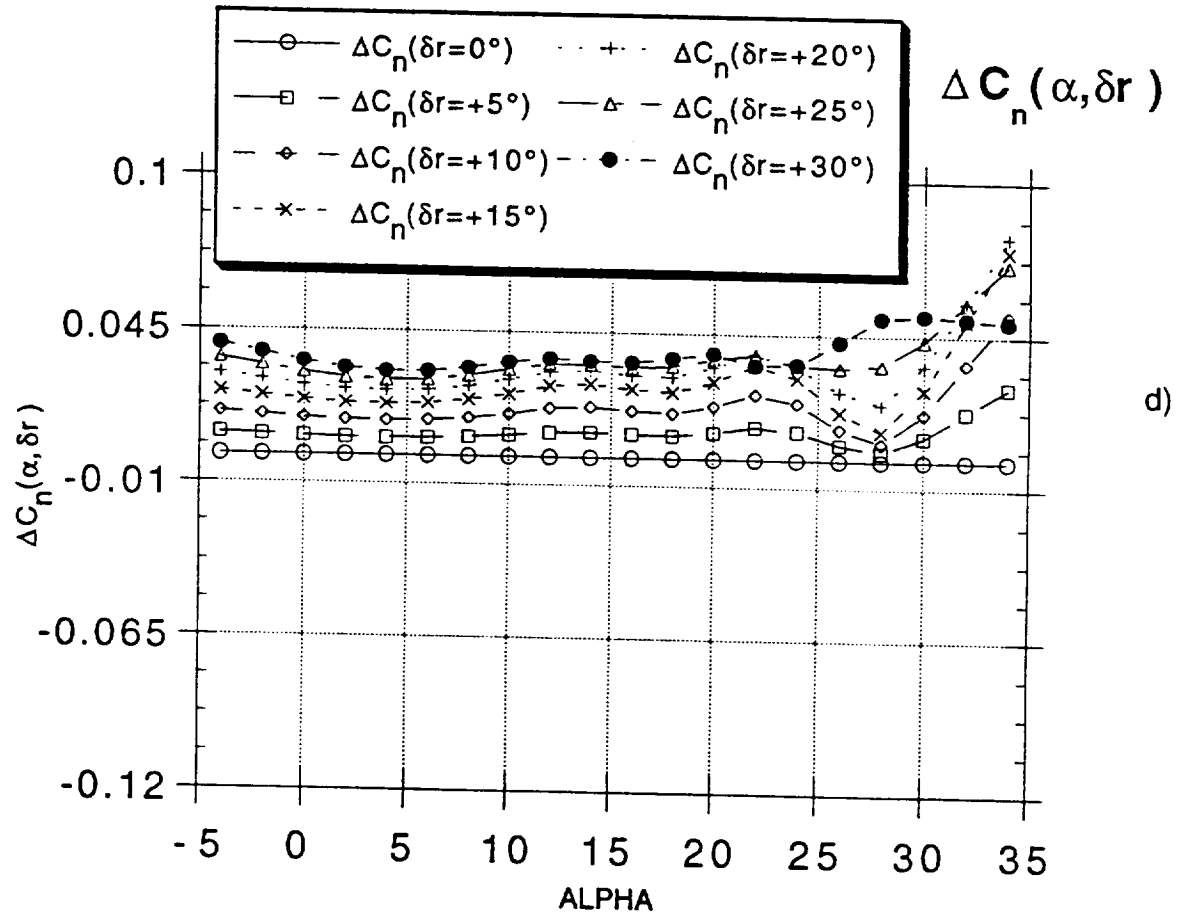

d)

Figure 8 - Continued

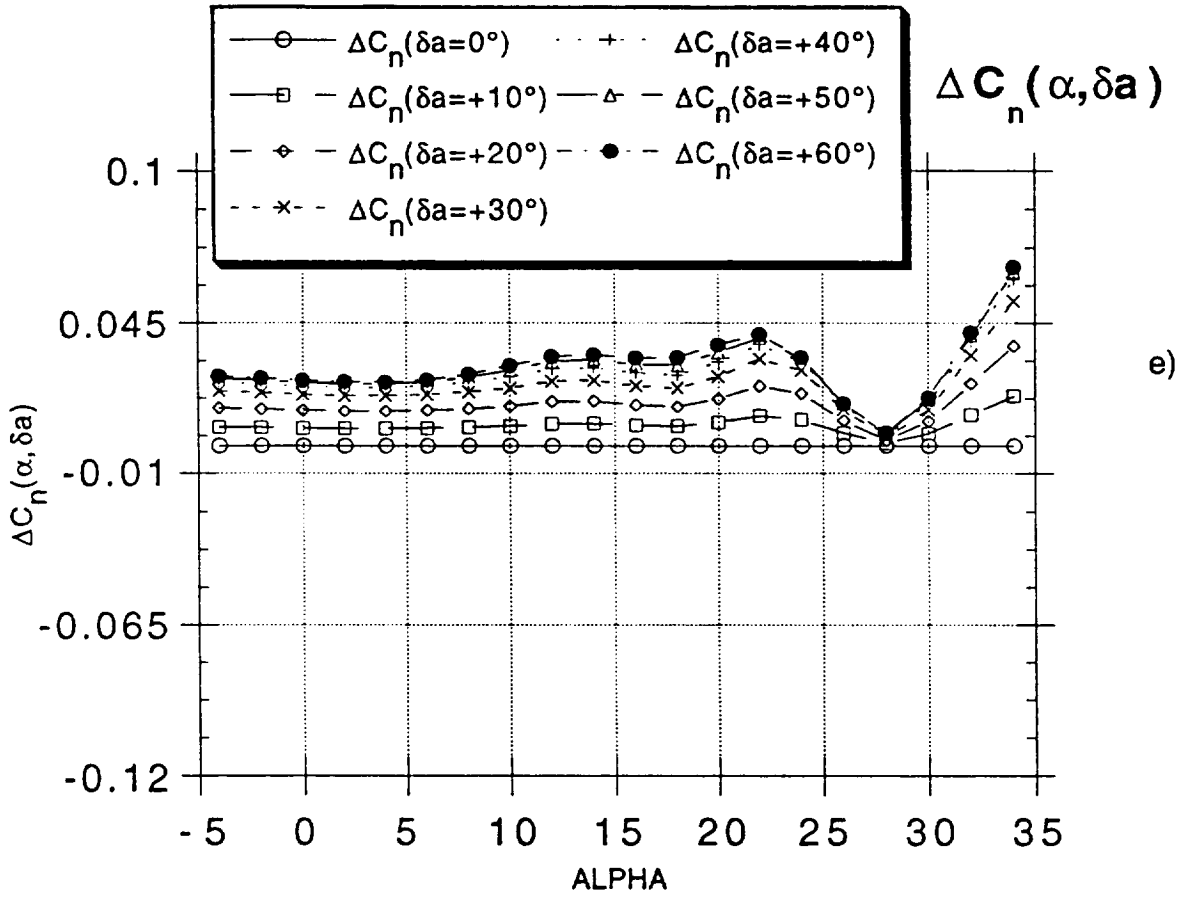

e)

Figure 8 - Concluded

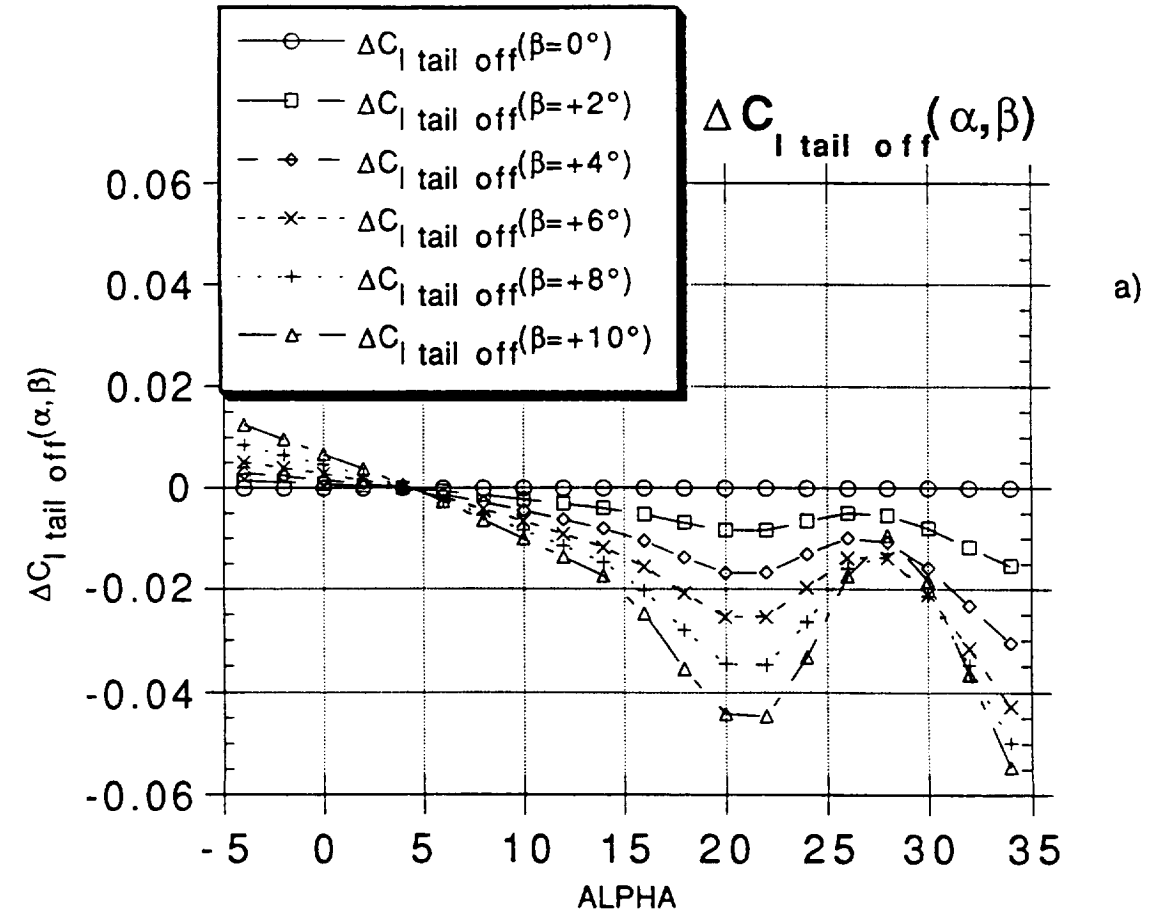

a)

Figure 9 - Static Aerodynamic Model (Lateral Characteristics) Lateral Aerodynamics and Conventional Control Effects on Rolling Moment

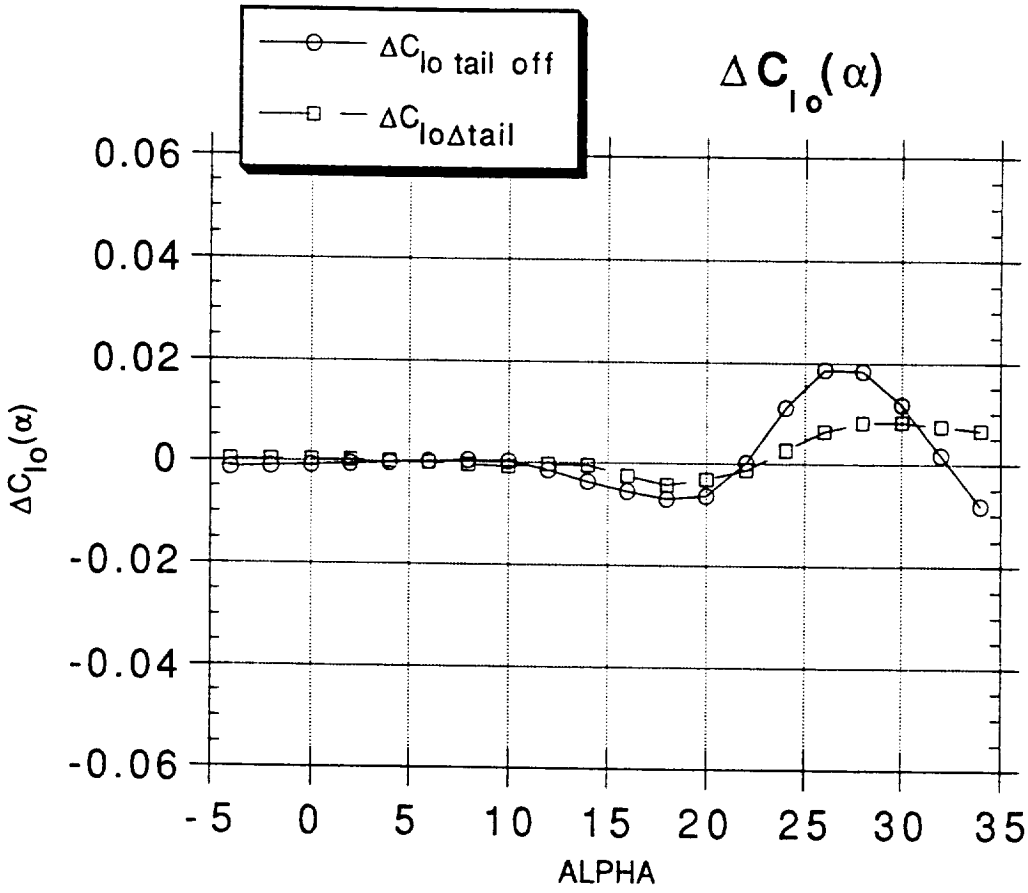

b)

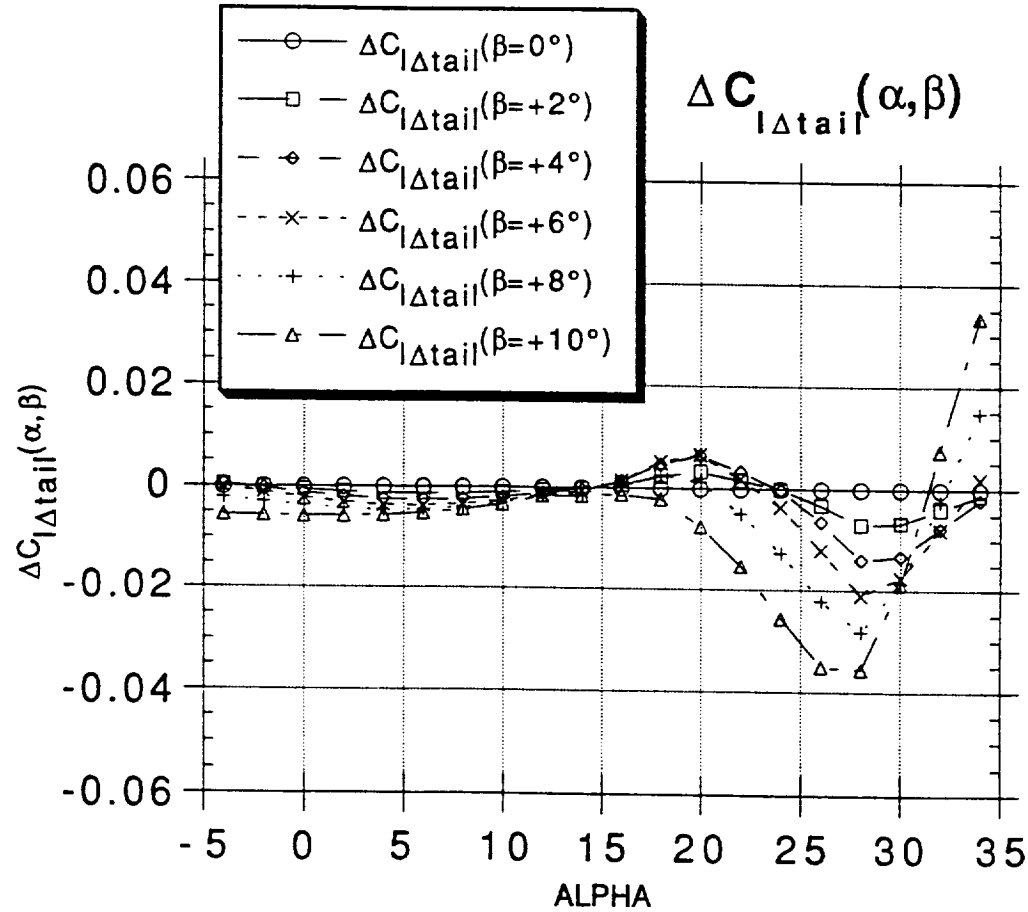

c)

Figure 9 - Continued

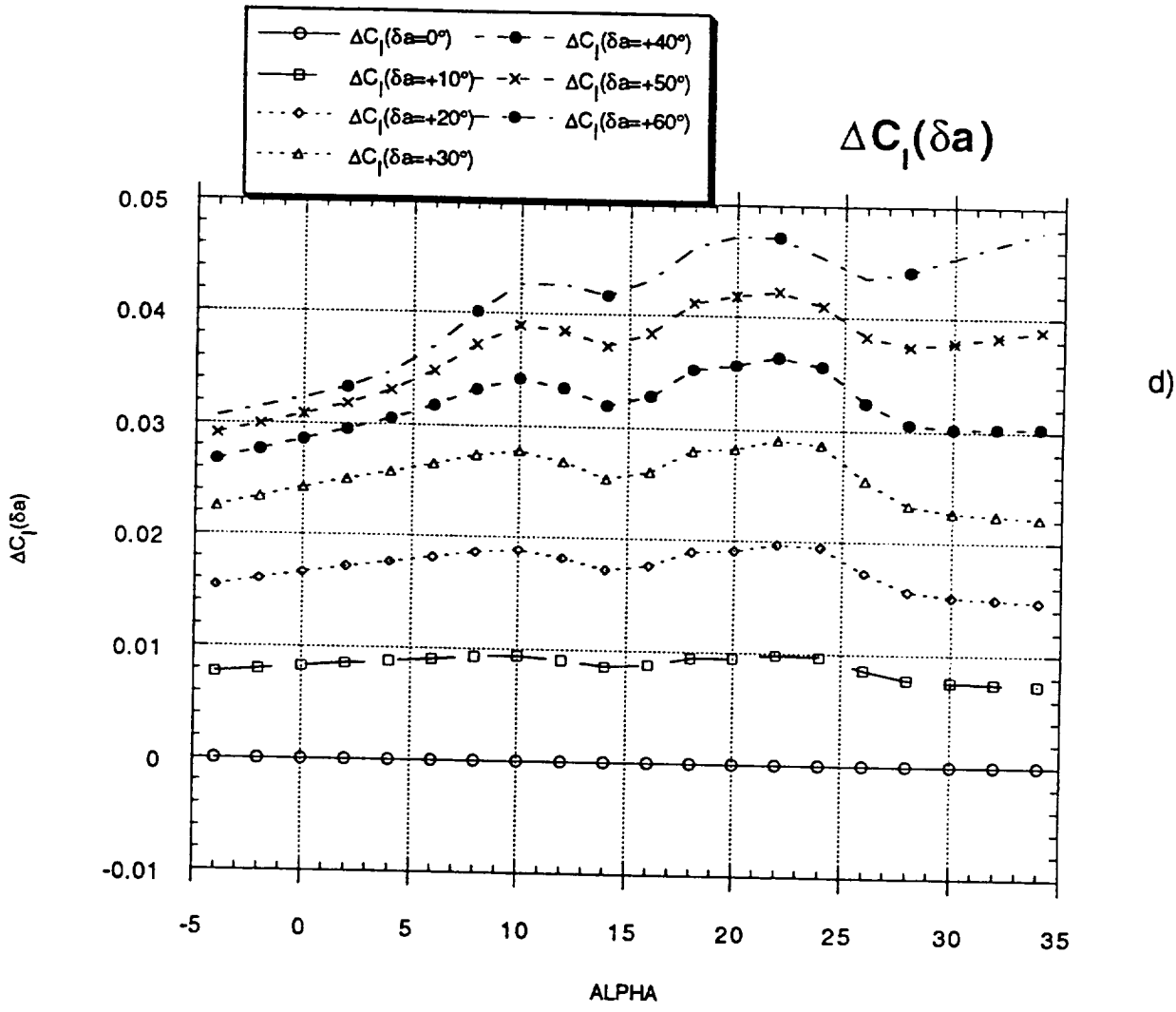

d)

Figure 9 - Concluded

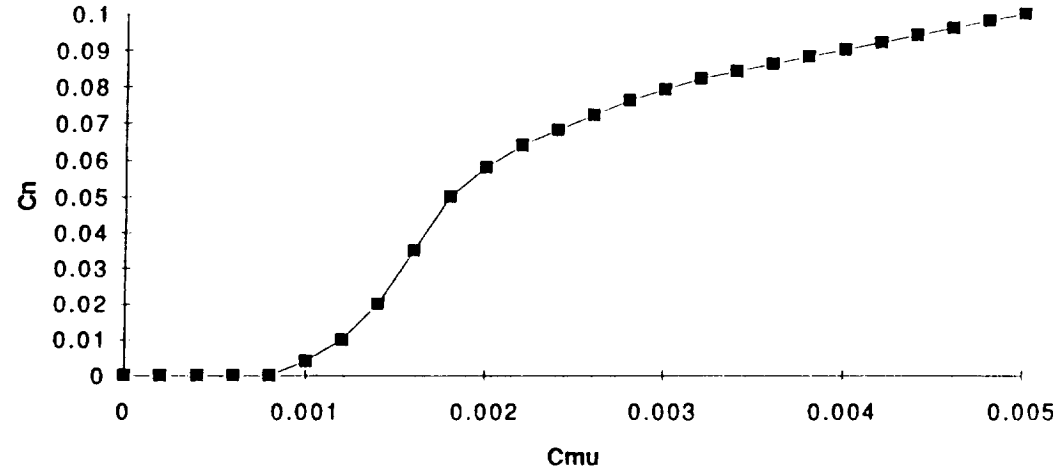

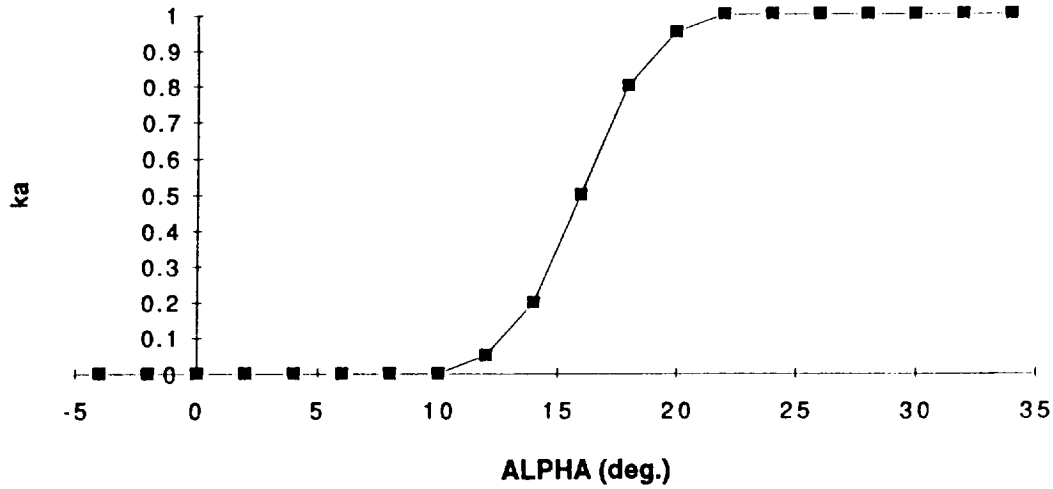

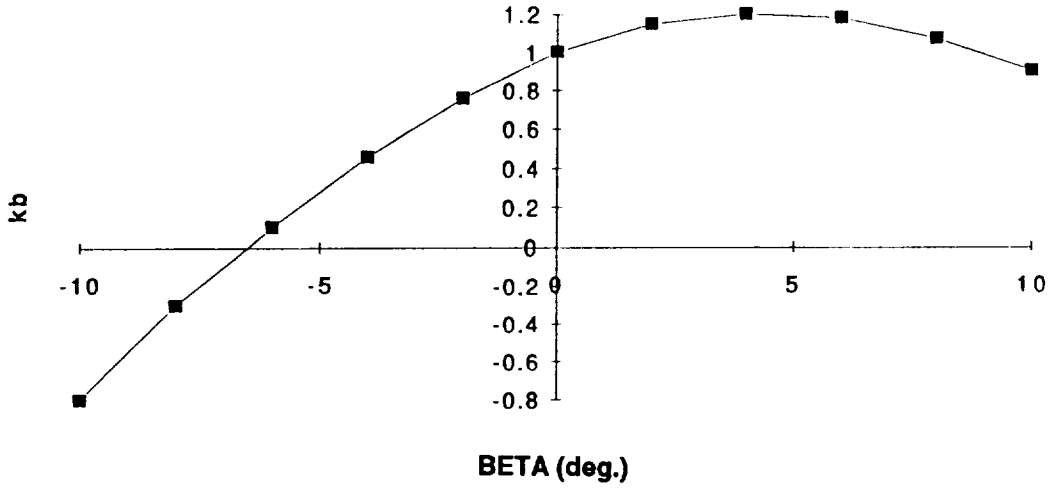

Figure 10 - Aerodynamic Model of Pneumatic Control Effect on Yawing Moment

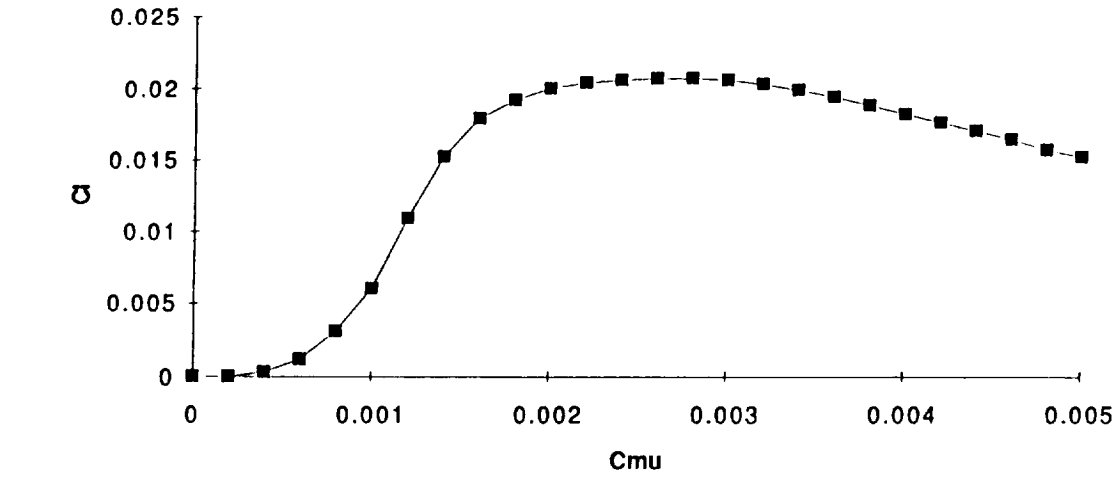

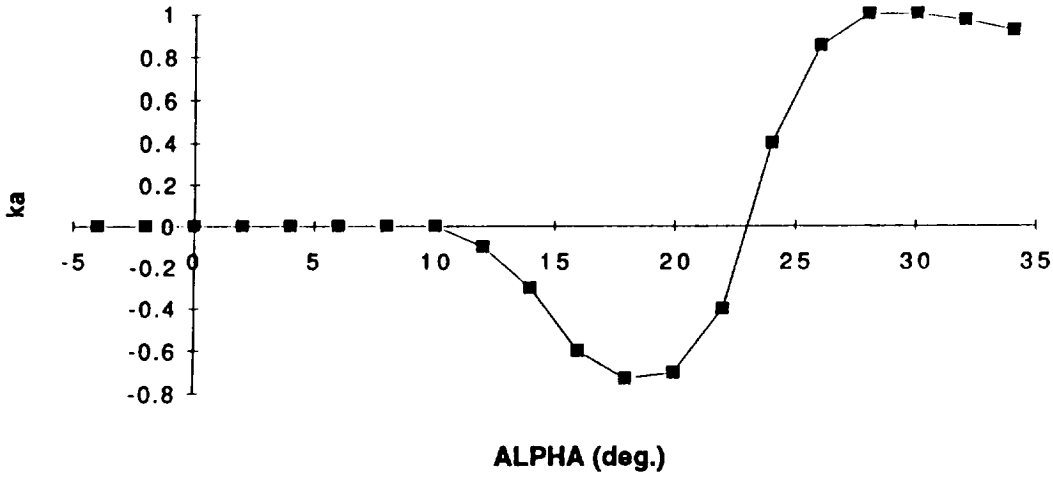

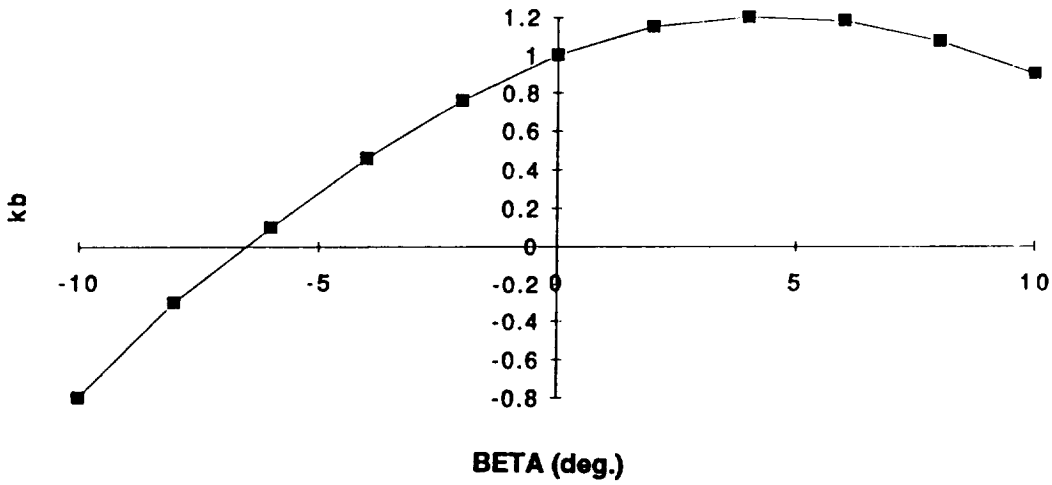

Figure 11 - Aerodynamic Model of Pneumatic Control Effect on Rolling Moment

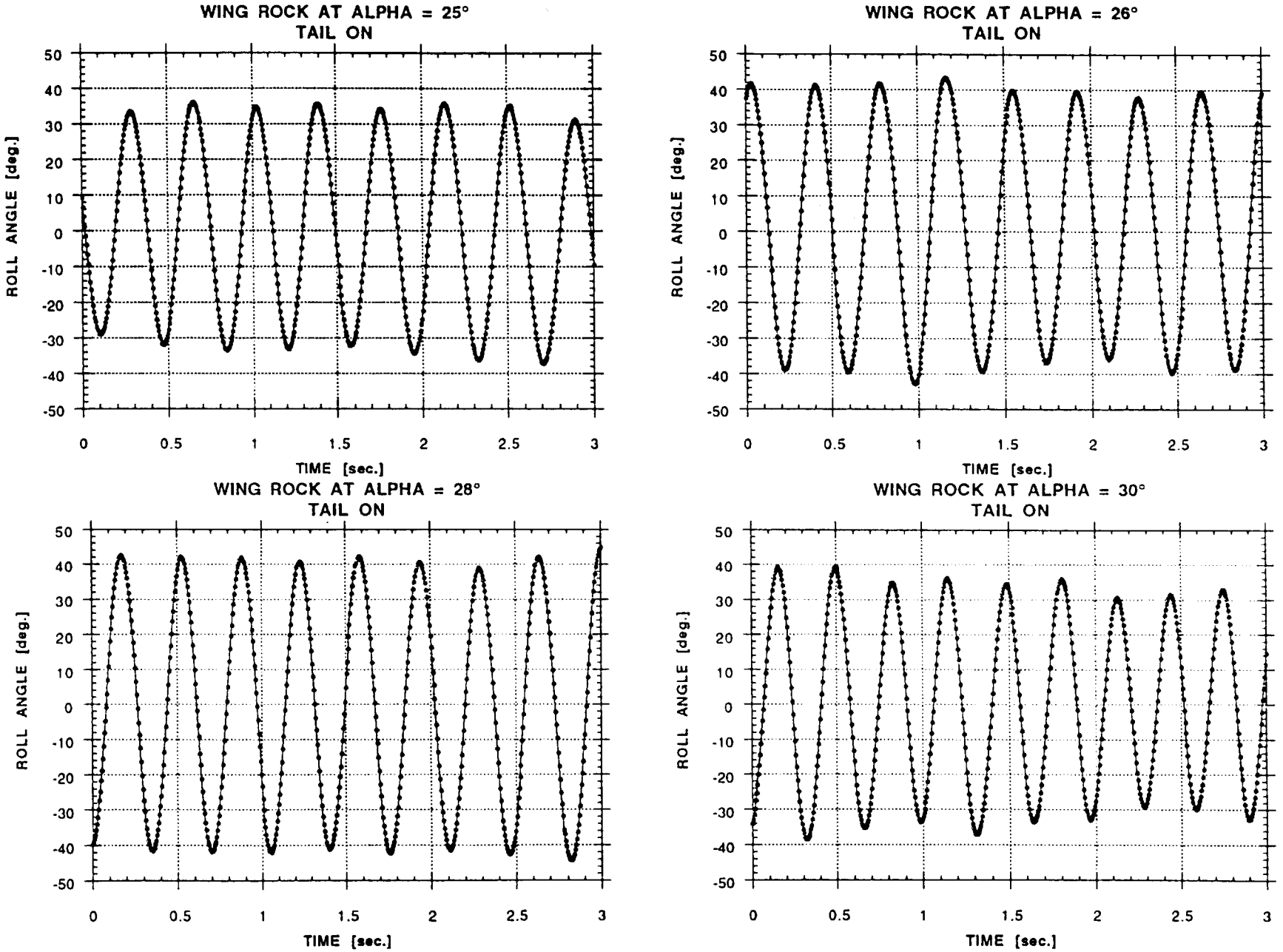

Figure 12 - Roll Angle History of Wing Rock at Various Angles of Attack (Wind Tunnel Test)

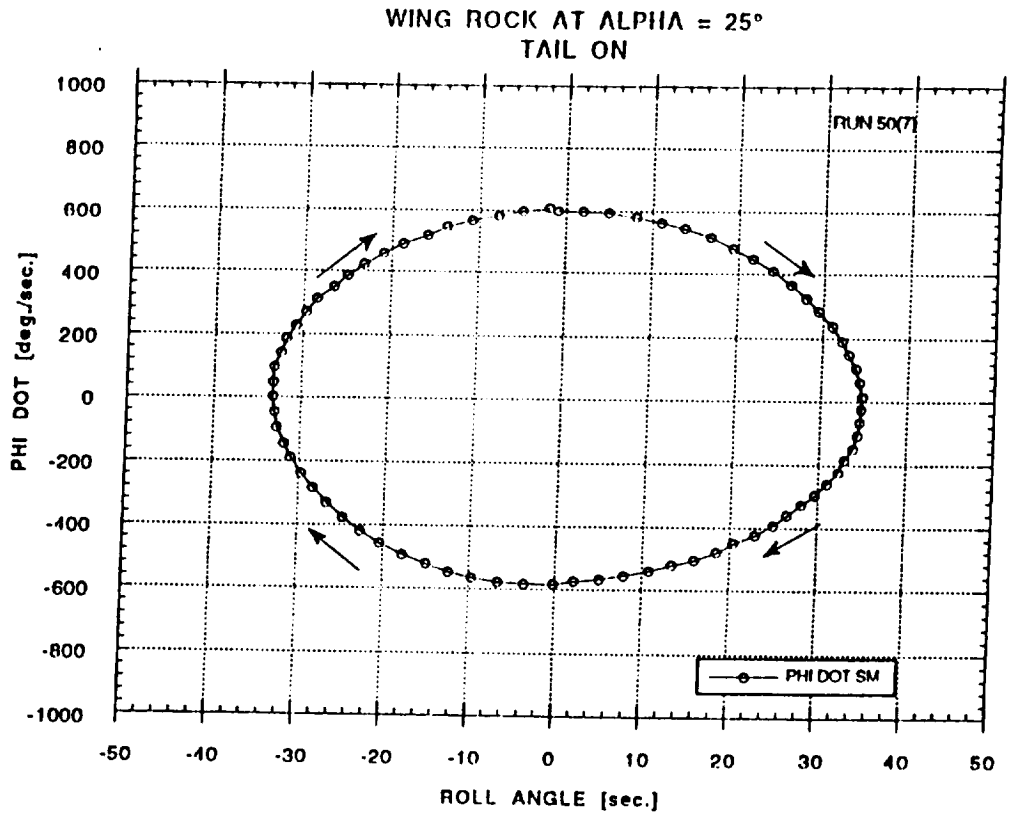

a)

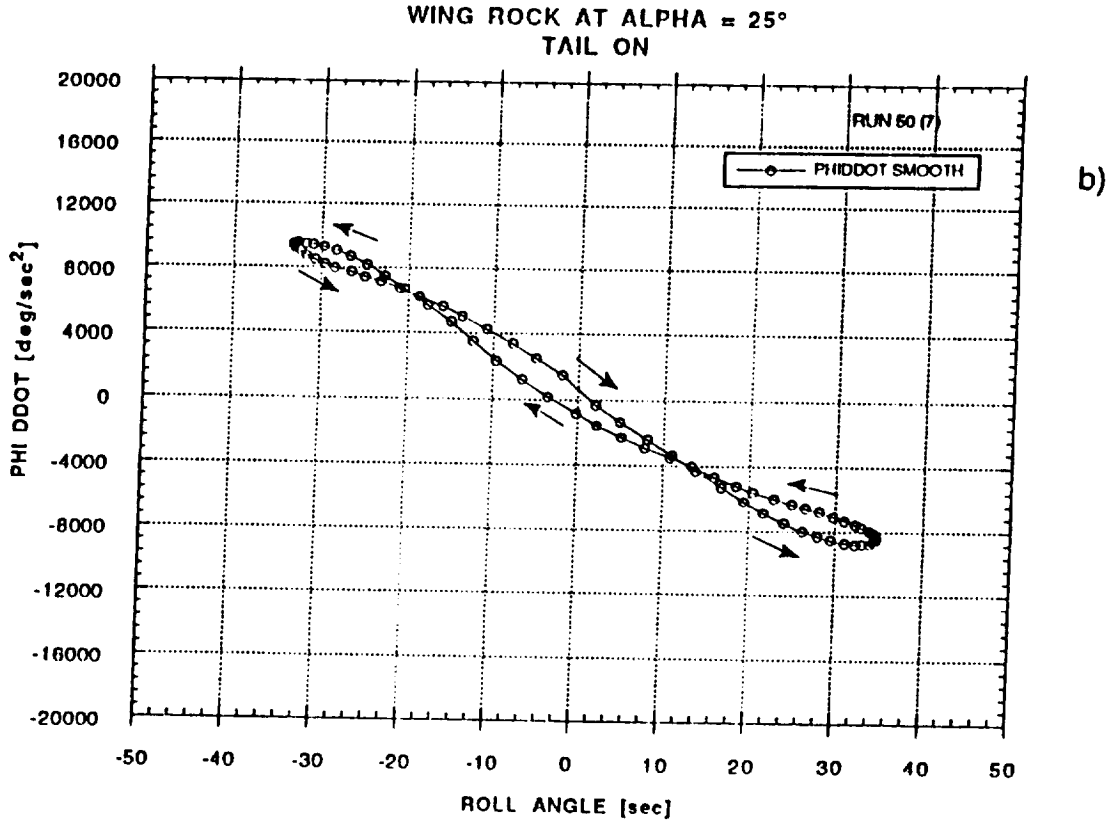

b)

Figure 13 - Phase Plots at $\alpha = 25°$ (q = 958 Pa, Tail-On) (Wind Tunnel Test)

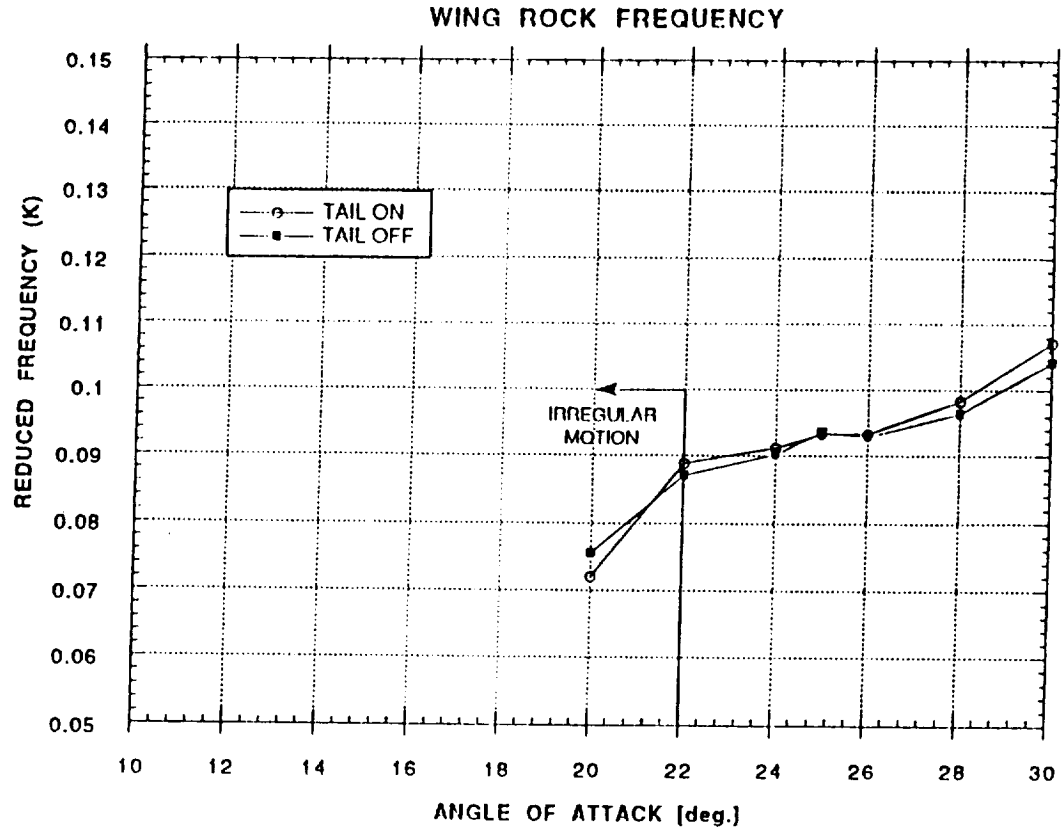

Figure 14 - Reduced Frequency of Wing Rock Motion (q = 958 Pa)

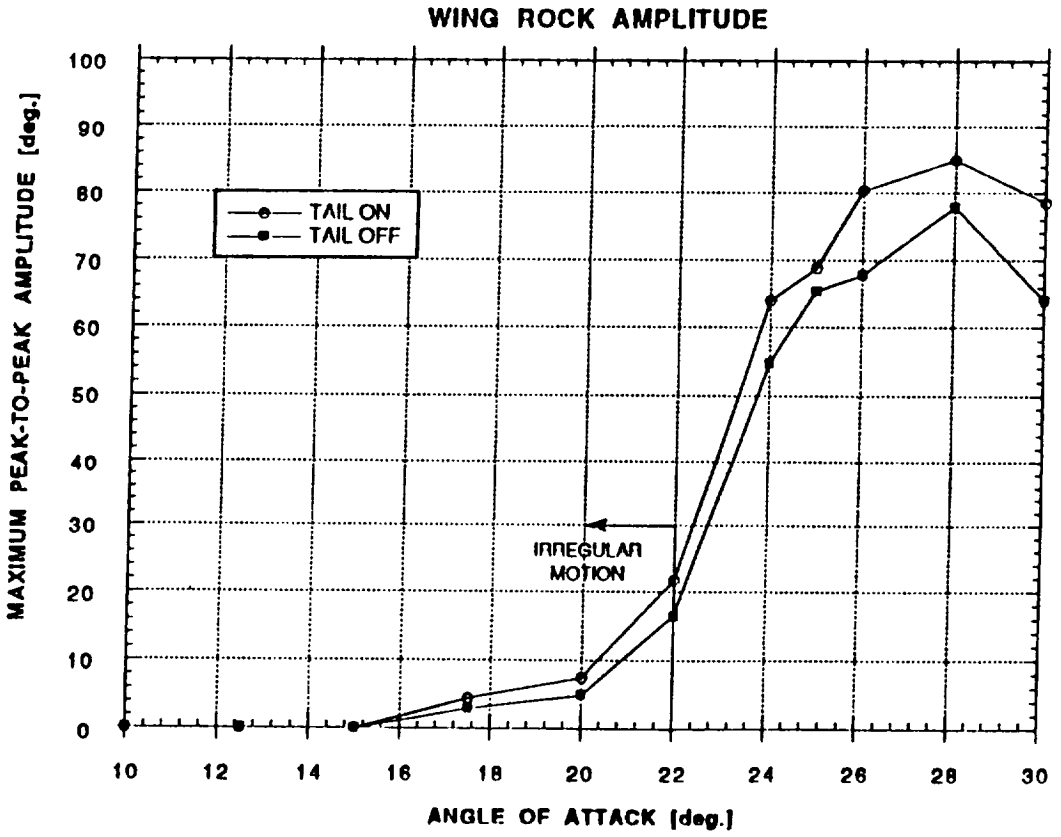

Figure 15 - Maximum Peak-to-Peak Amplitude of Wing Rock (q = 958 Pa)

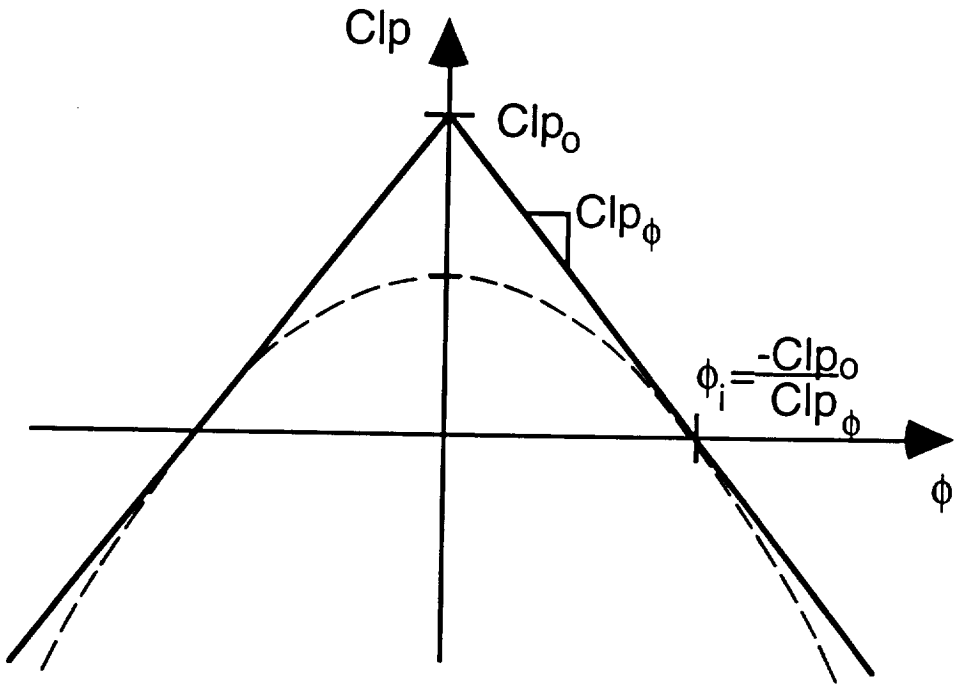

Figure 16 - Wing Rock Mathematical Model
Relationship between Damping Term and Roll Angle

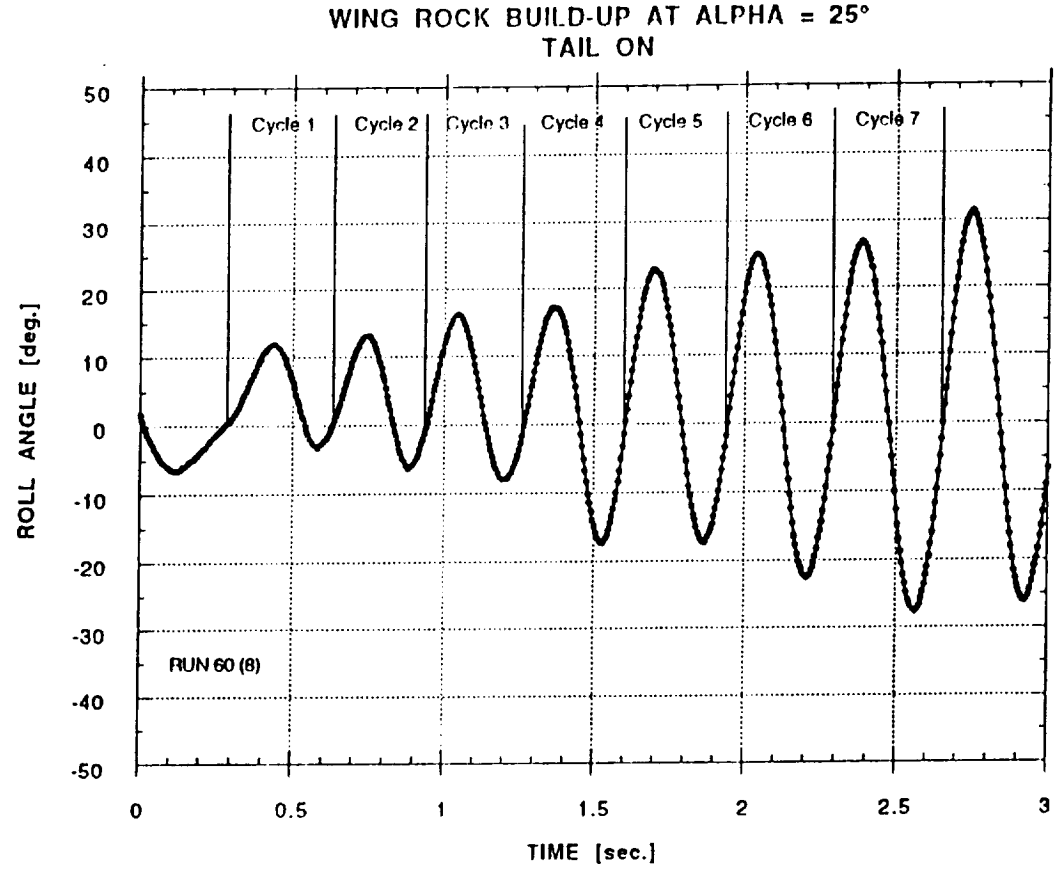

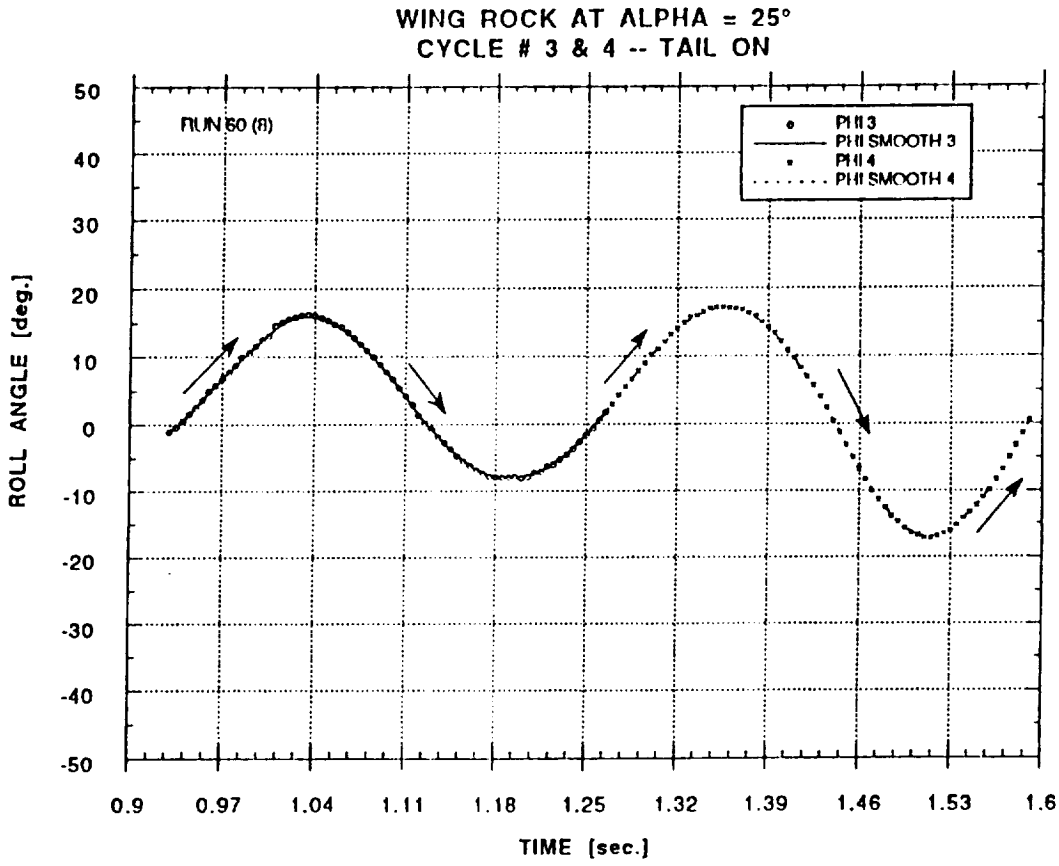

Figure 17 - Wing Rock Build-up at $\alpha = 25°$ (q = 958 Pa, Tail-On) (Wind Tunnel Test)

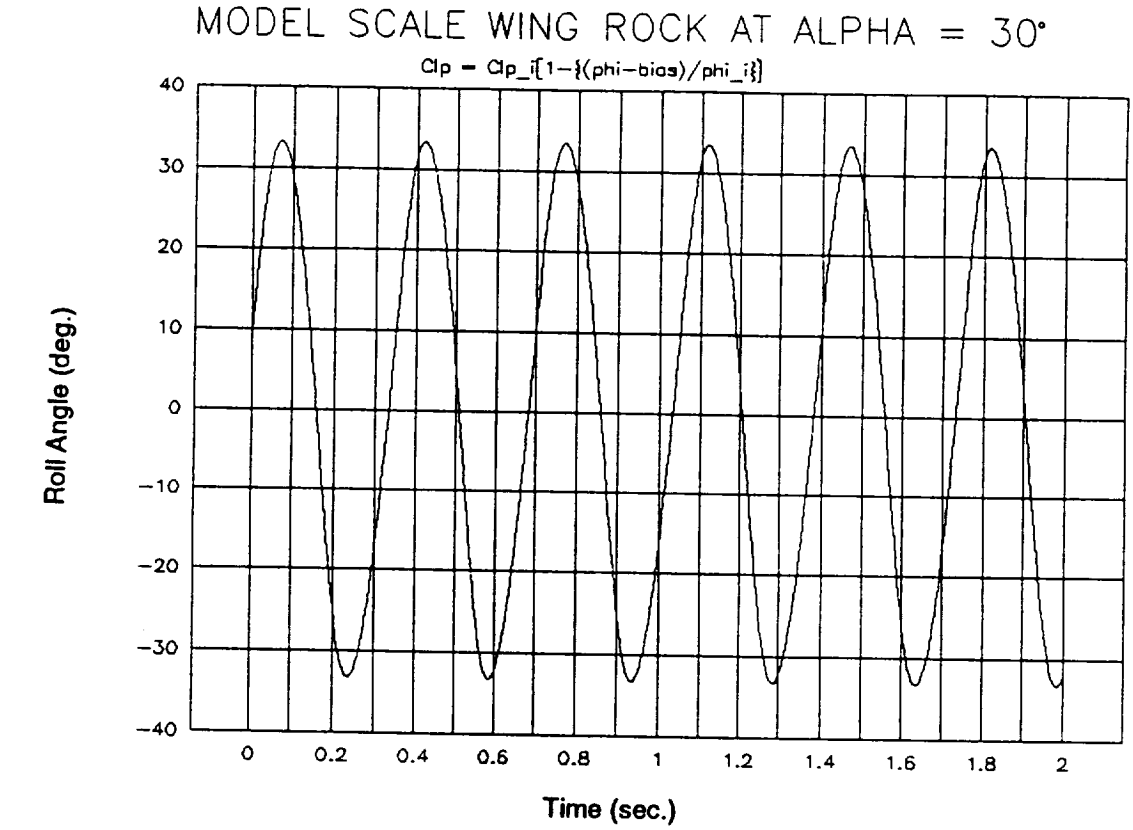

a)

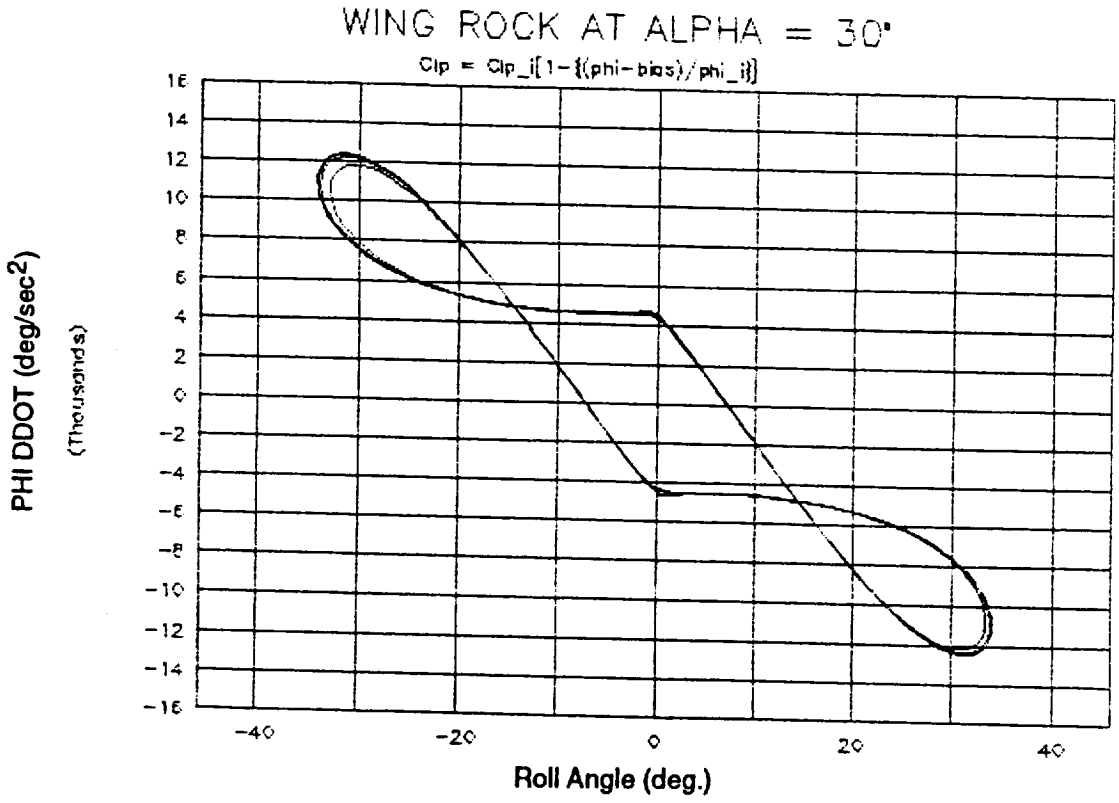

b)

Figure 18 - Results of First Order Wing Rock Model at $\alpha = 30°$
a) Roll Angle History, b) Phase Plot

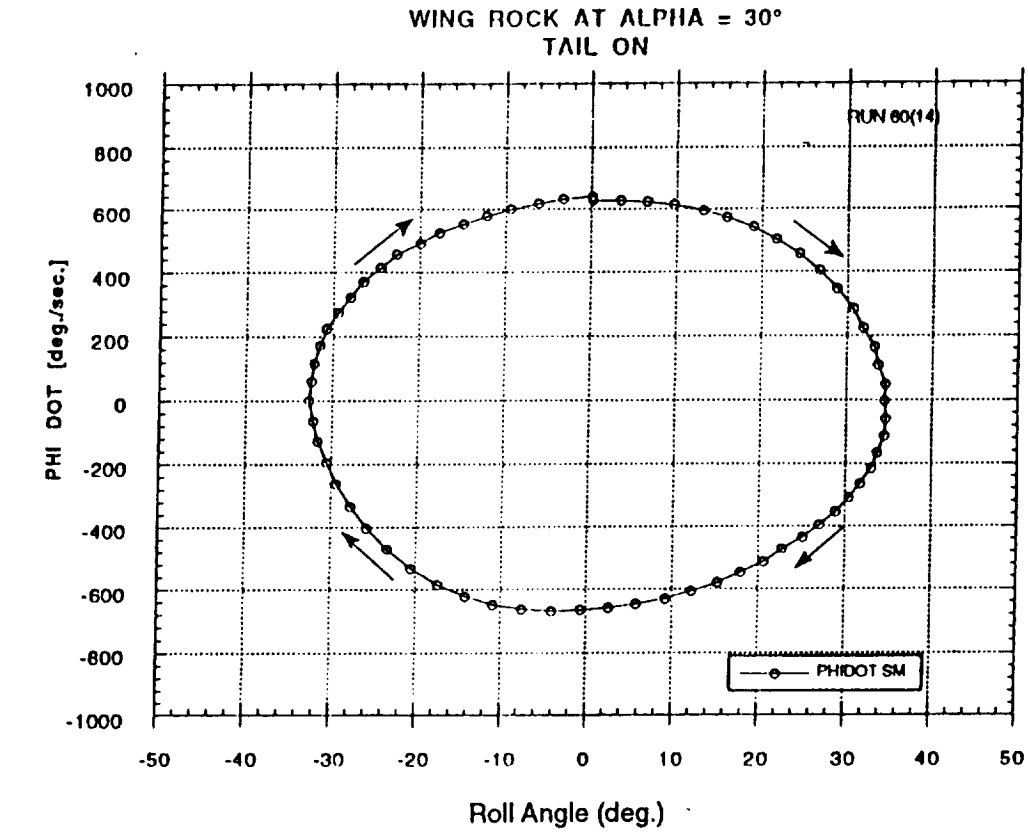

a)

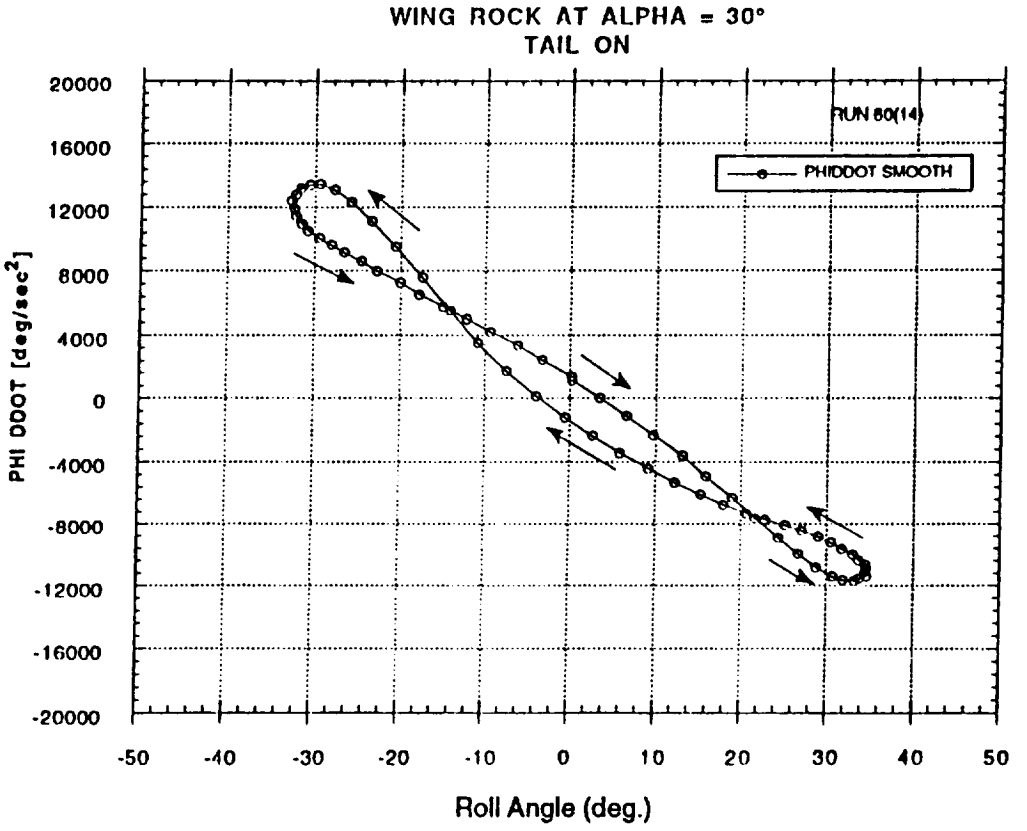

b)

Figure 19 - Phase Plots at $\alpha = 30°$ (q = 958 Pa, Tail-On) (Wind Tunnel Test)

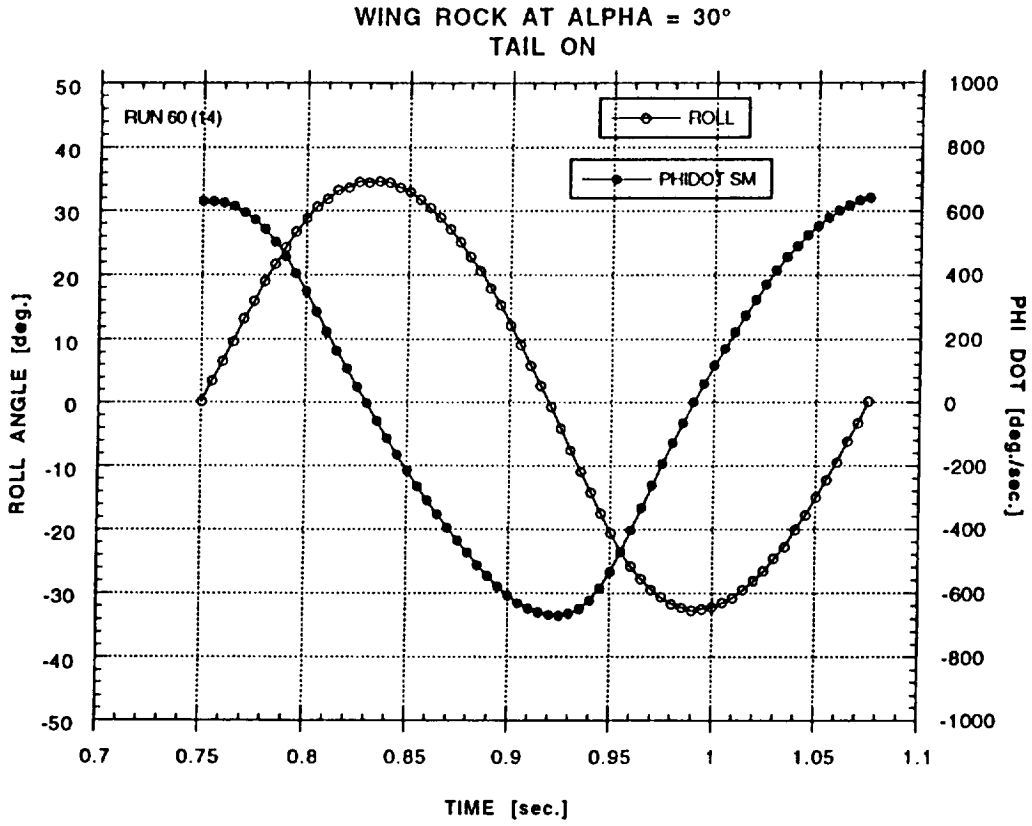

a)

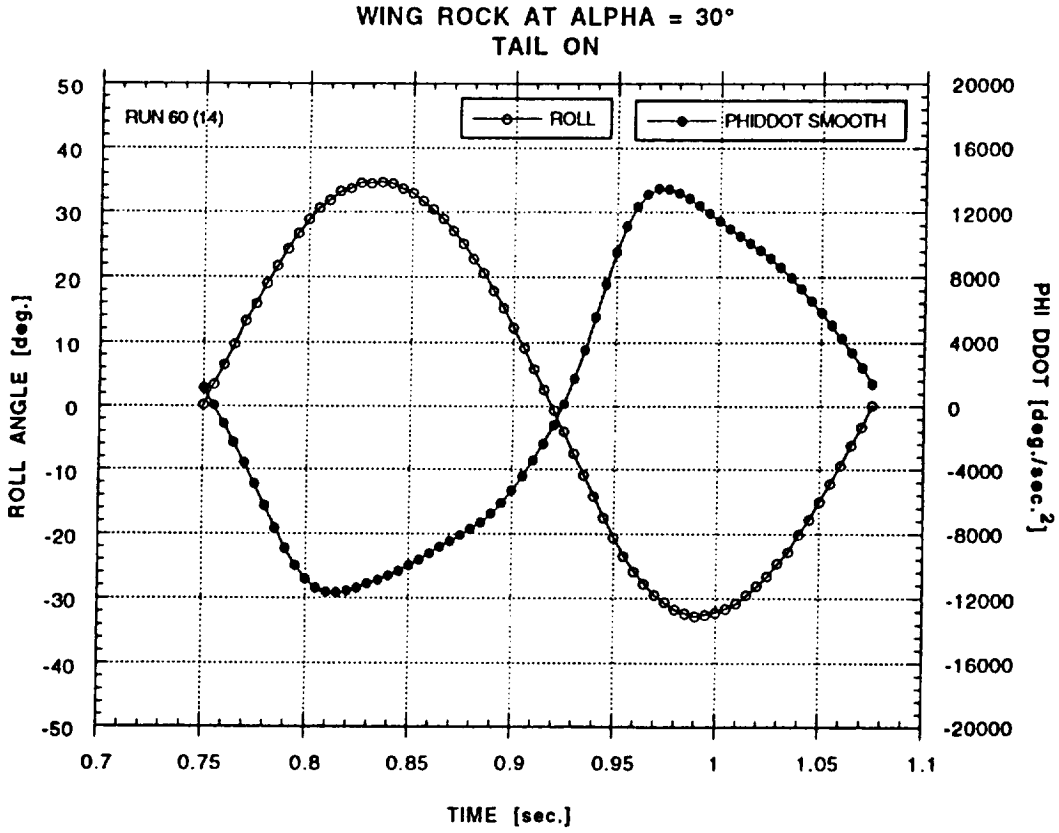

b)

Figure 20 - Angular Velocity and Acceleration at $\alpha = 30°$ (Wind Tunnel Test)

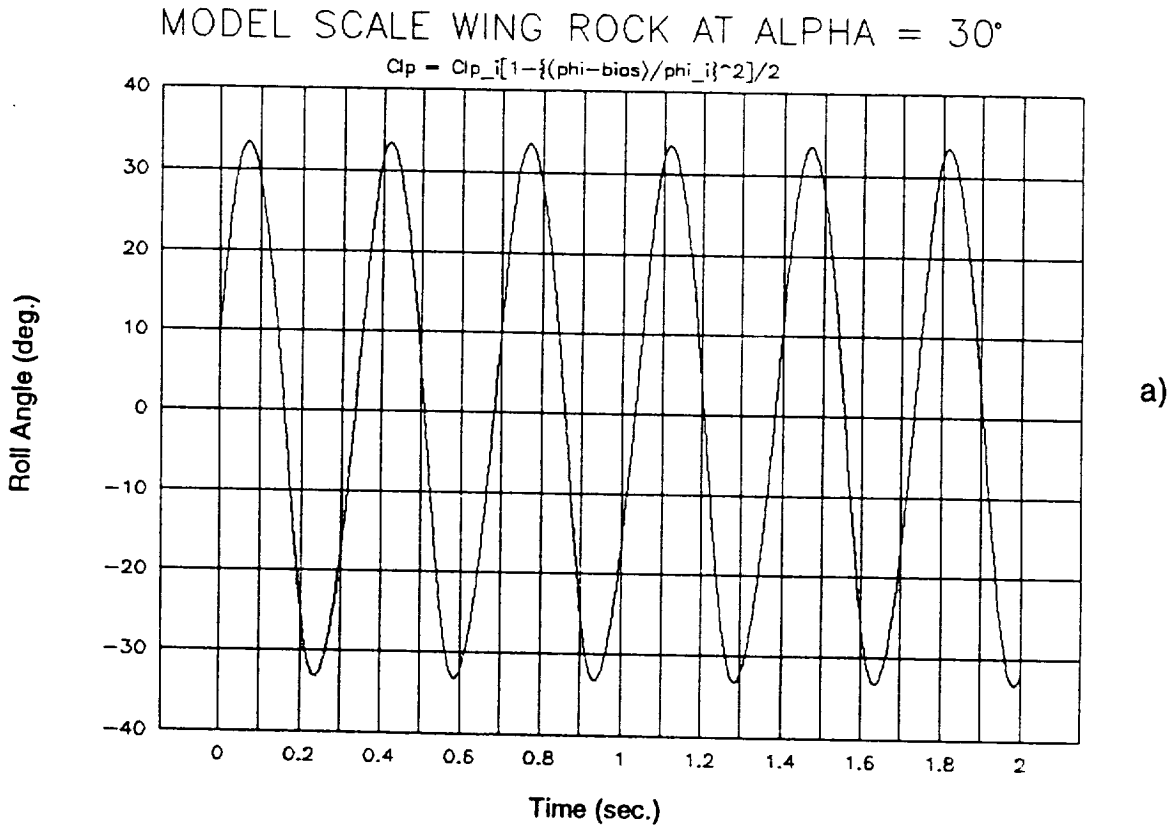

a)

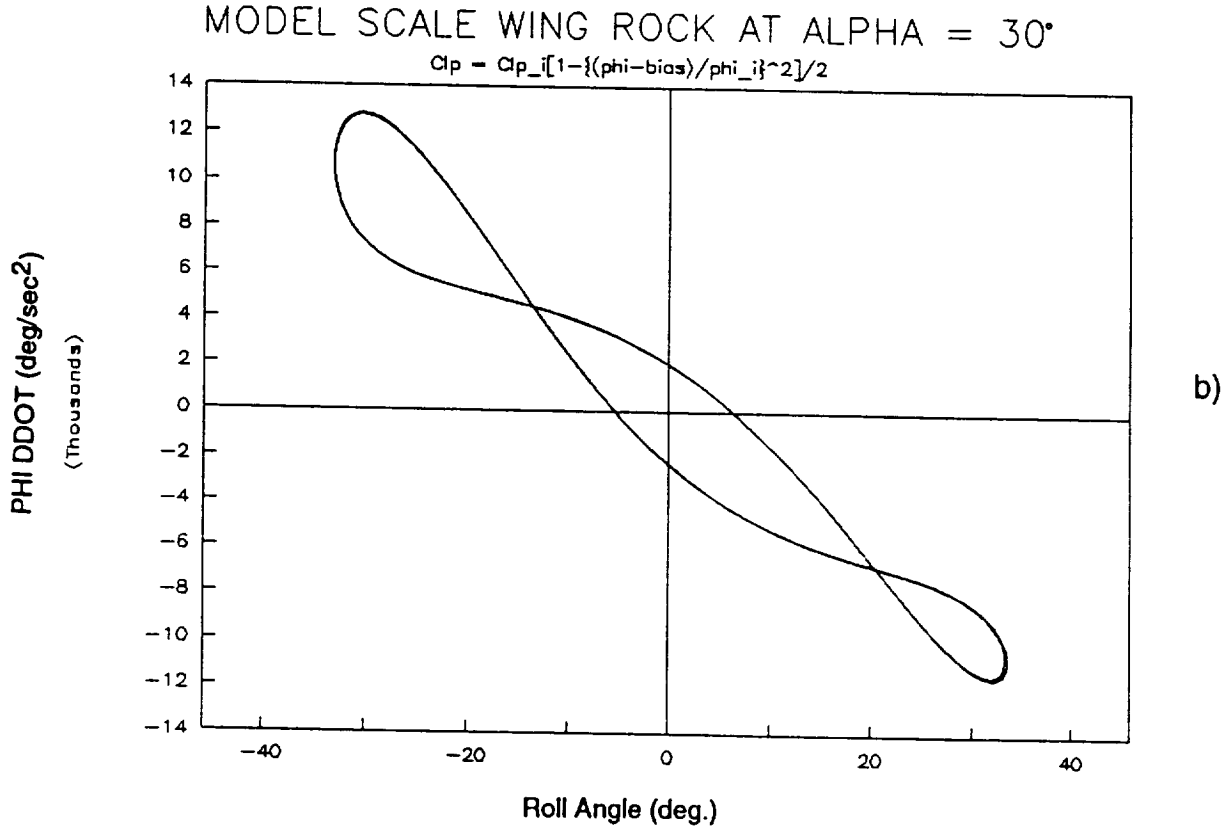

b)

Figure 21 - Results of Second Order Wing Rock Model at $\alpha = 30°$
a) Roll Angle History, b) Phase Plot

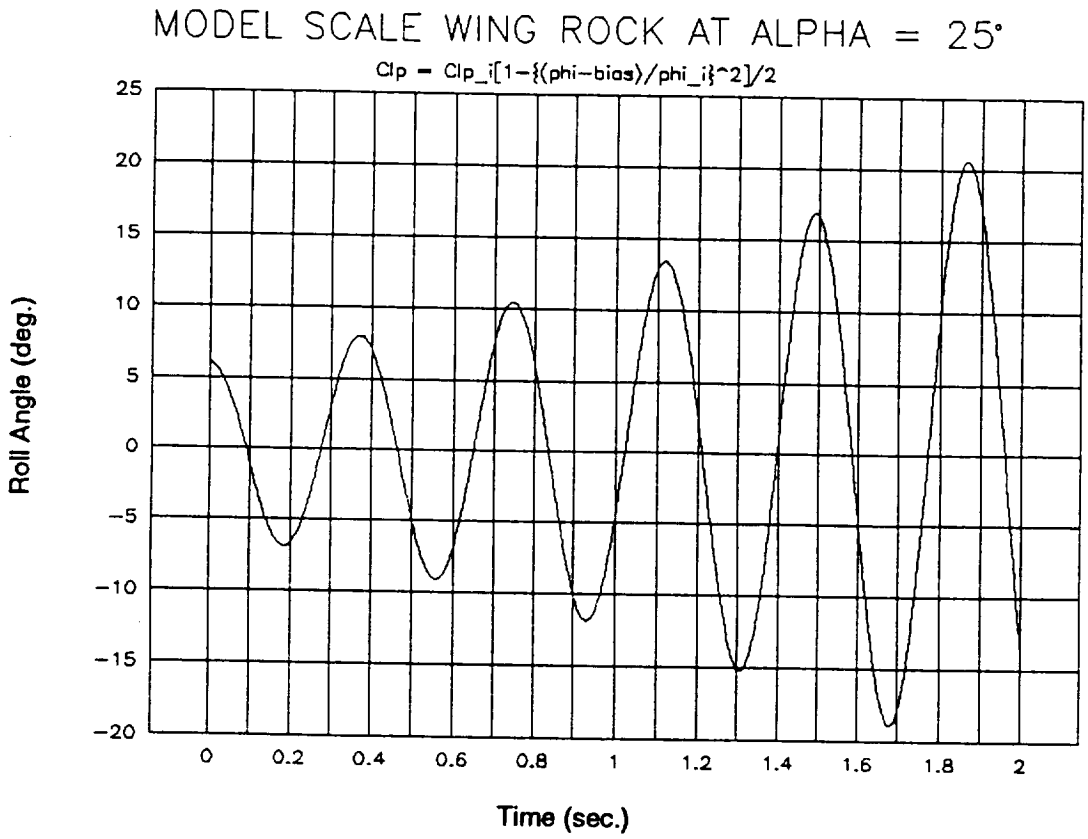

a)

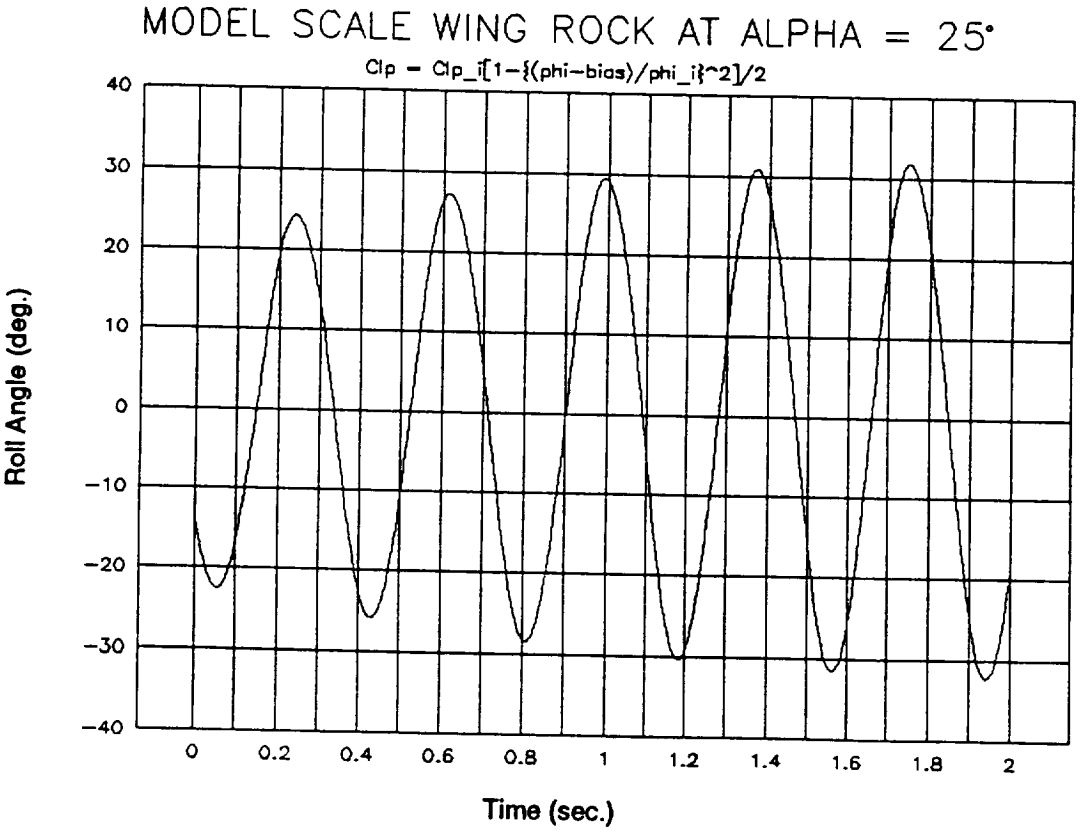

b)

Figure 22 - Results of Second Order Wing Rock Model at $\alpha = 25°$
Wing Rock Build-up for a) t = 0 to 2 sec., b) t = 2 to 4 sec.

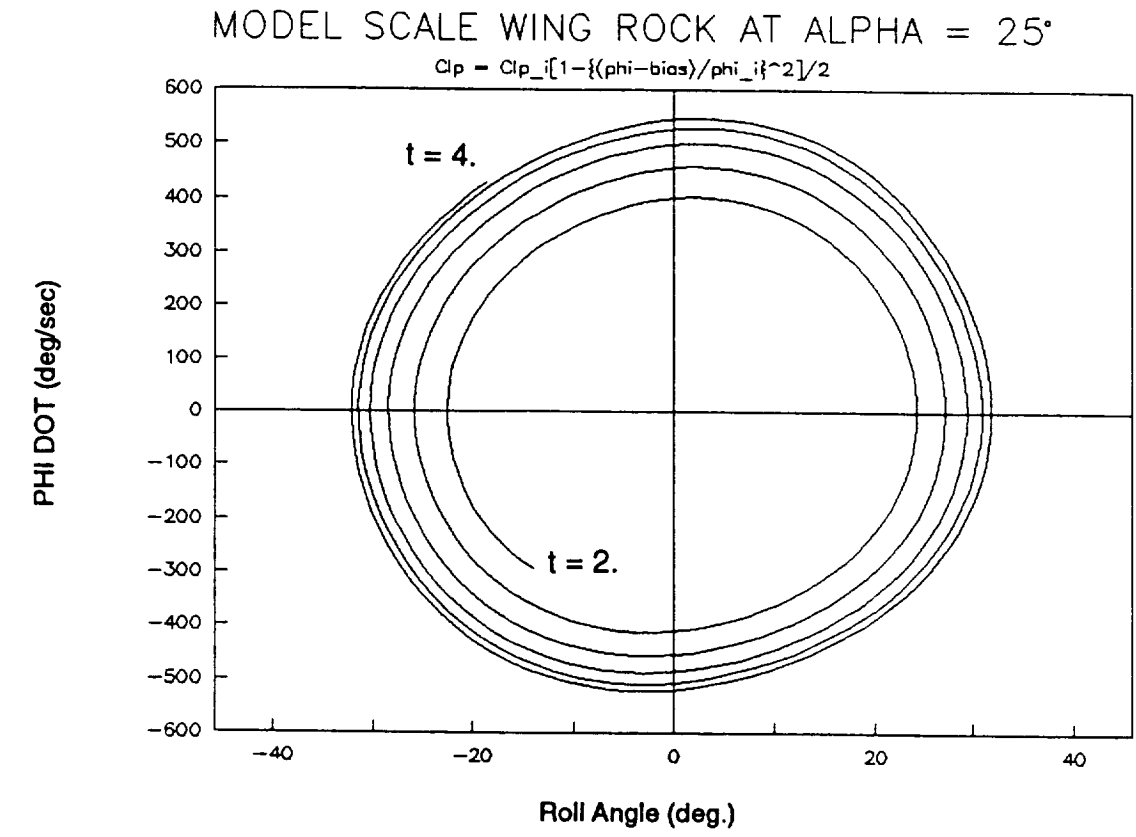

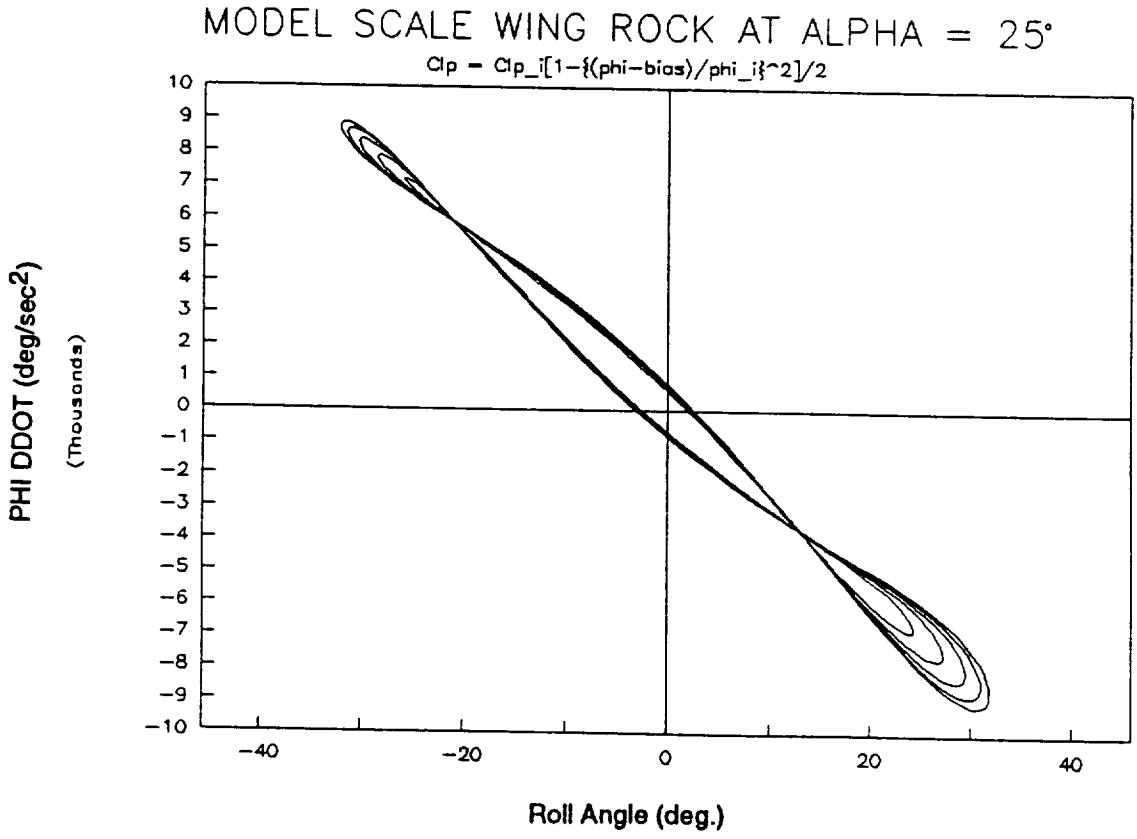

Figure 23 - Phase Plots at $\alpha = 25°$ for the Motion Shown in Figure 22 (Part b)

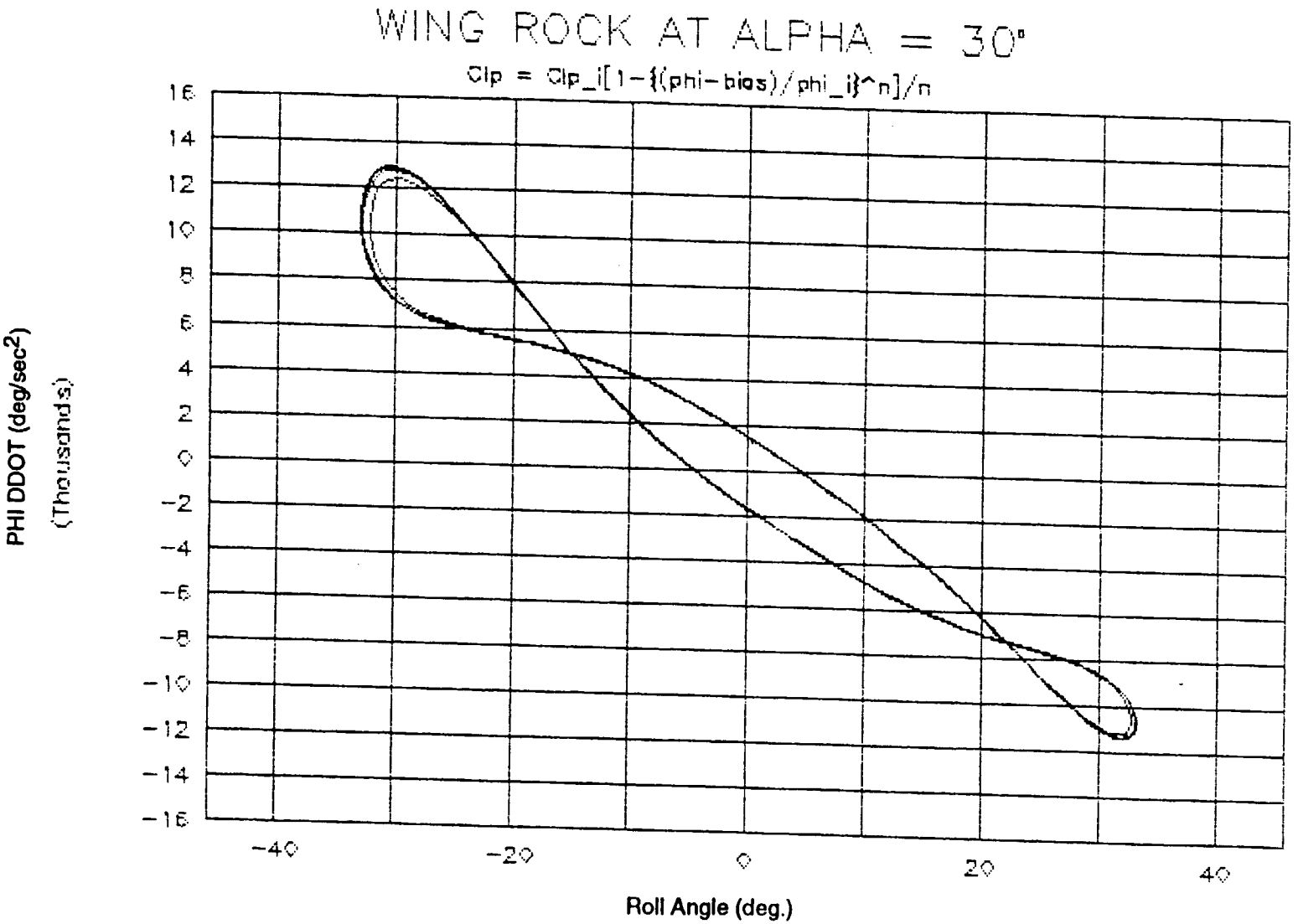

Figure 24 - Results of n^{th} Order Wing Rock Model at $\alpha = 30°$ Phase Plot

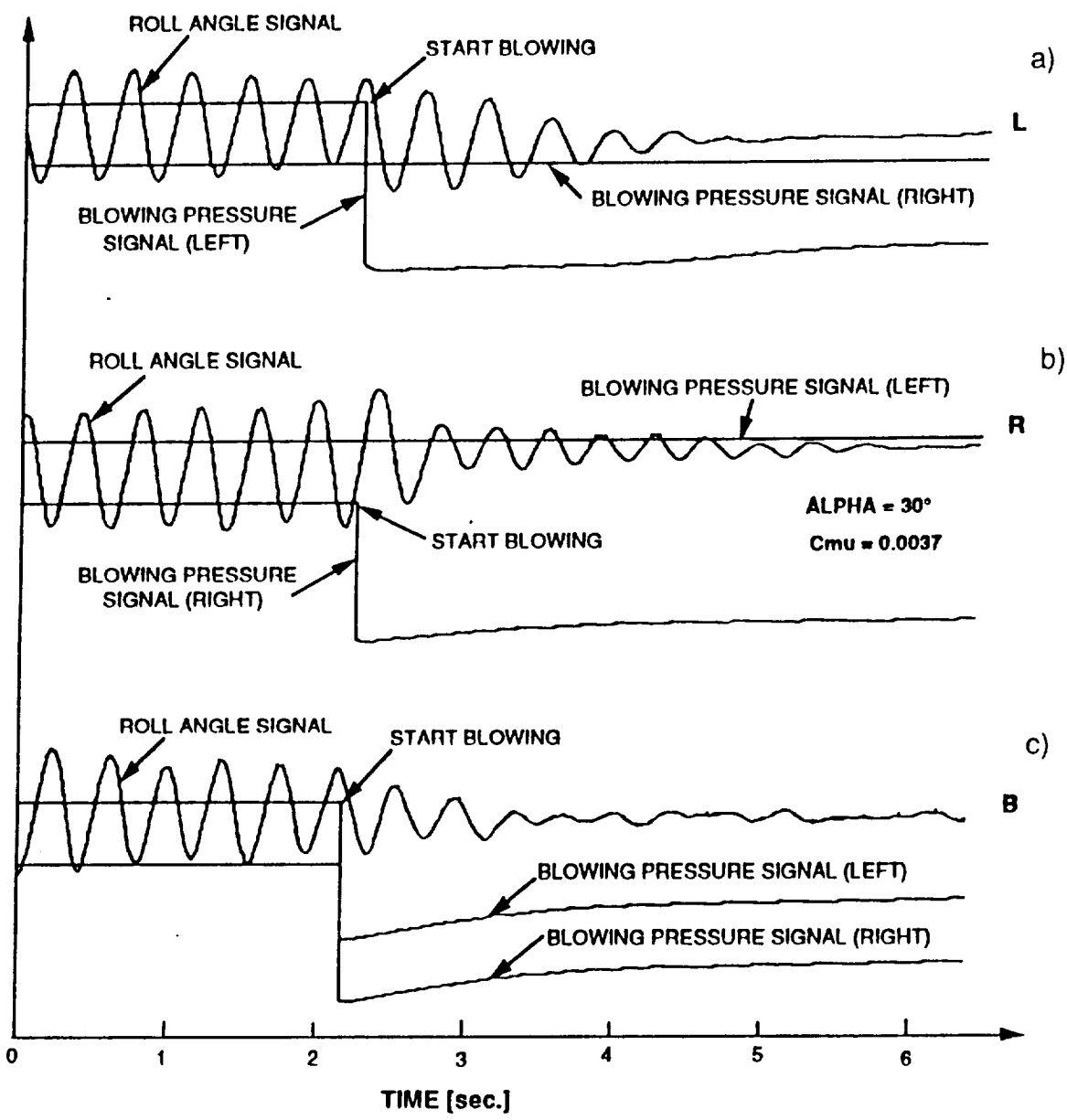

Figure 25 - Effect of Aft Blowing on Wing Rock at $\alpha = 30°$
(Wind Tunnel Test, Tail-On, $C\mu = 0.0037$)
a) Left Nozzle, b) Right Nozzle, c) Simultaneous Blowing

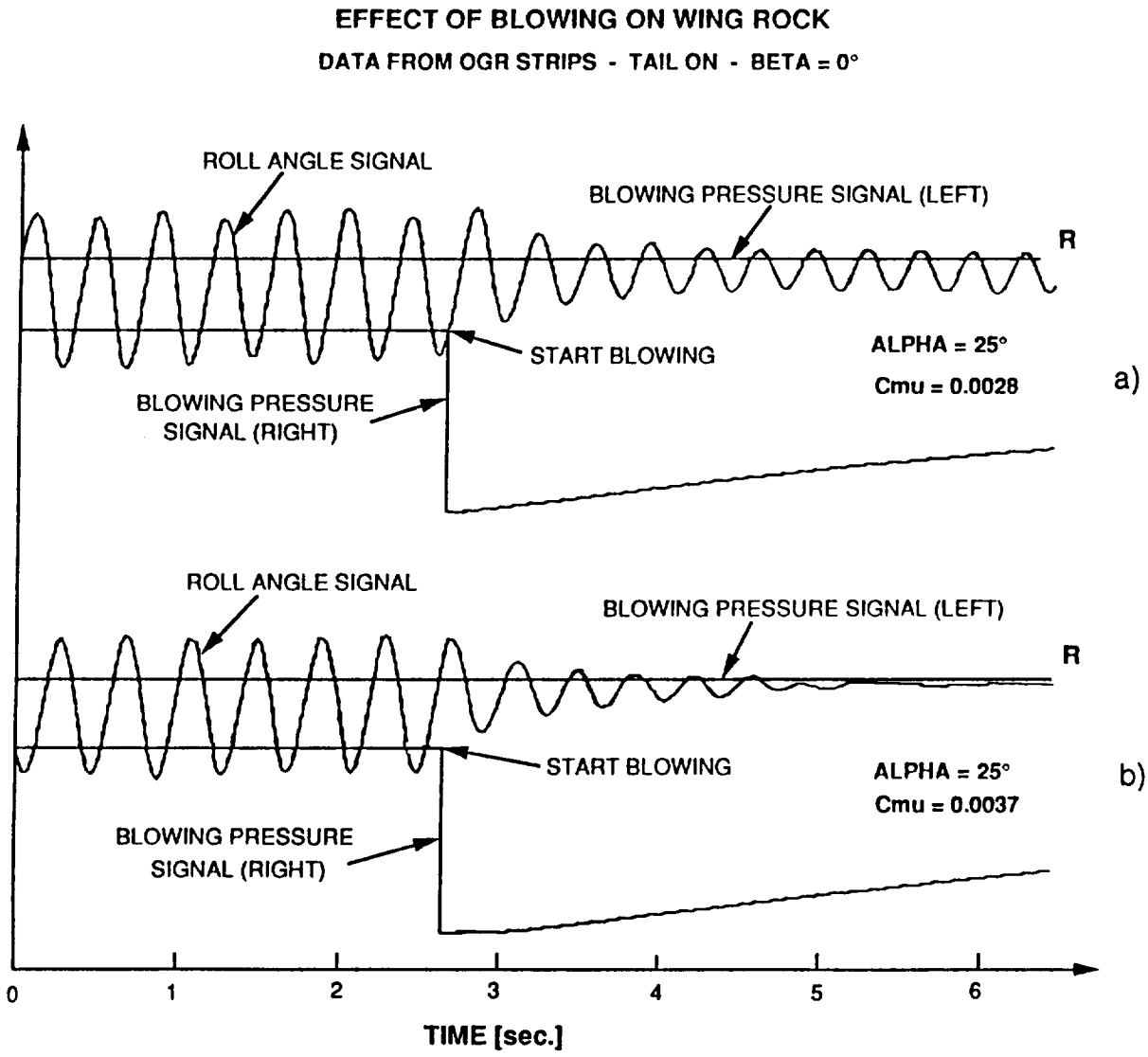

Figure 26 - Effect of Aft Blowing on Wing Rock at $\alpha = 25°$
(Wind Tunnel Test, Tail-On)
a) Right Nozzle, $C\mu = 0.0028$; b) Right Nozzle, $C\mu = 0.0037$

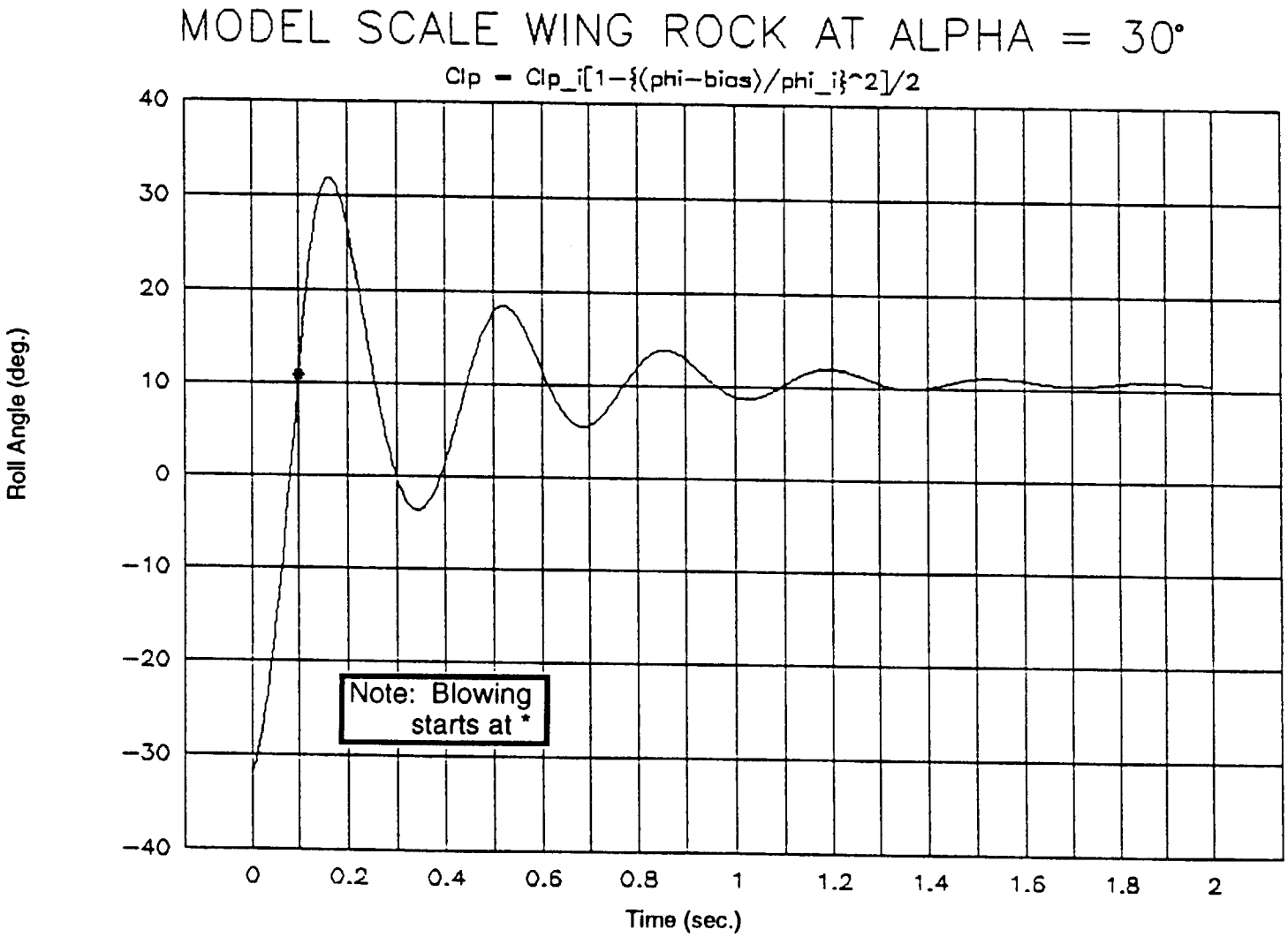

Figure 27 - Results of Second Order Wing Rock Model at $\alpha = 30°$
Wing Rock Suppression, $C\mu = 0.0037$

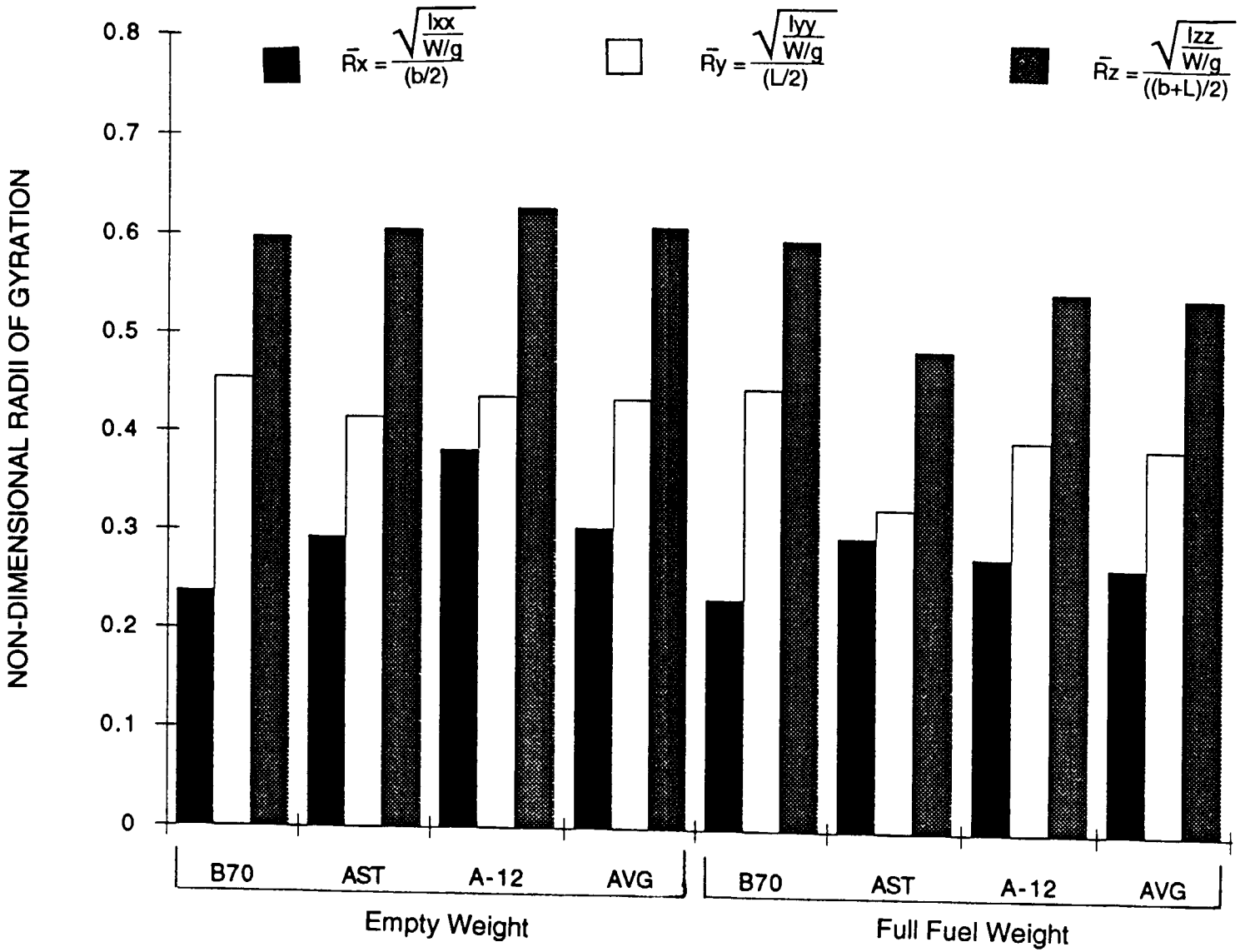

Figure 28 - Non-Dimensional Inertias for Three Example Aircraft

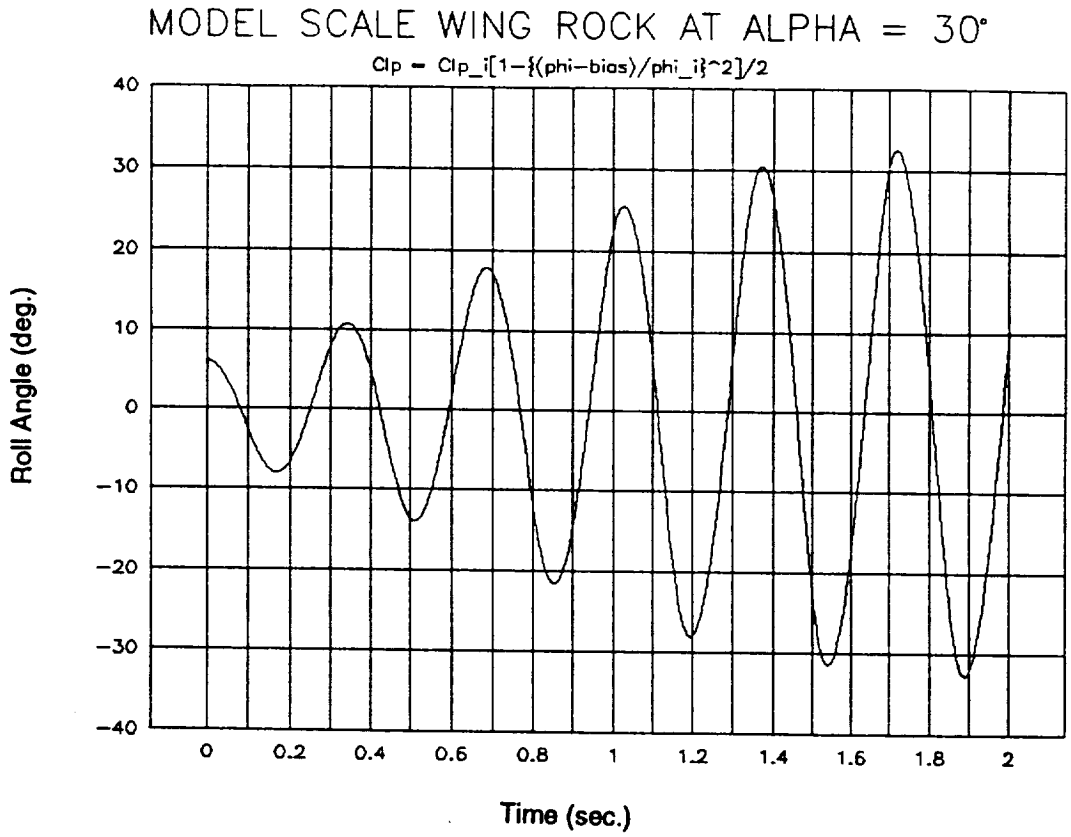

a)

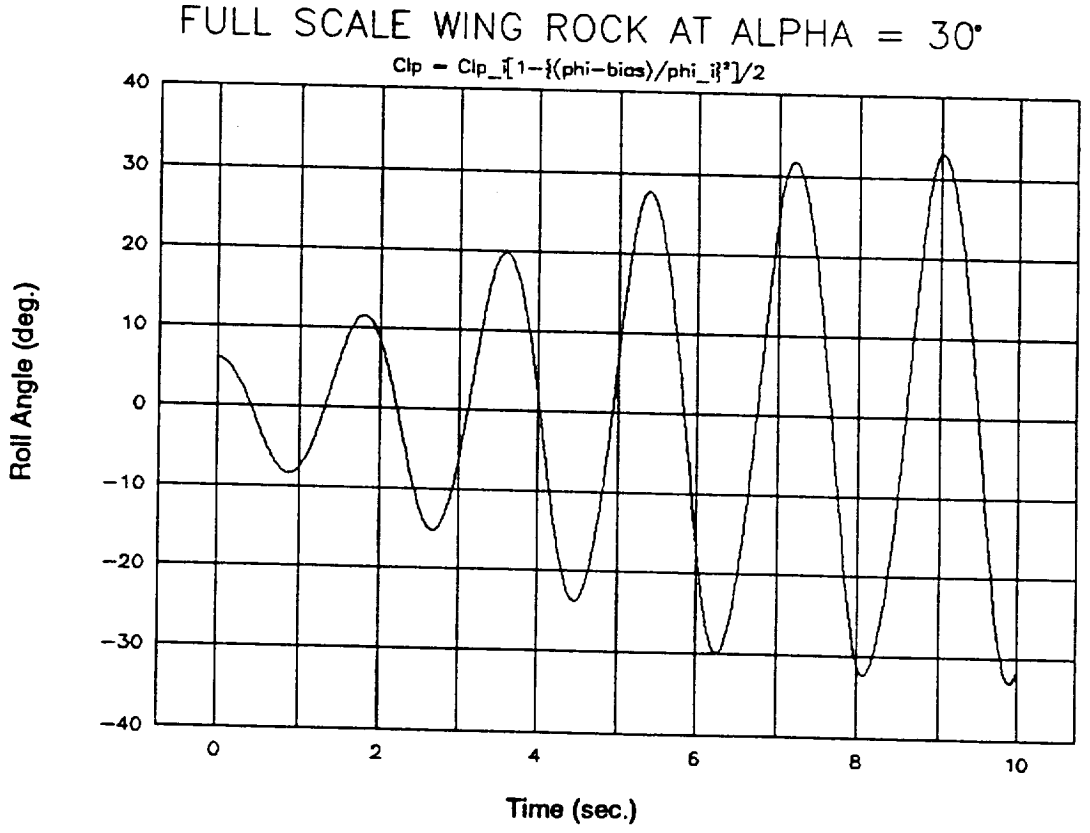

b)

Figure 29 - Comparison of Wind Tunnel Model and Full Scale Configuration (Wing Rock Build-up)
a)-b) Roll Angle, c)-d) Phase Plots

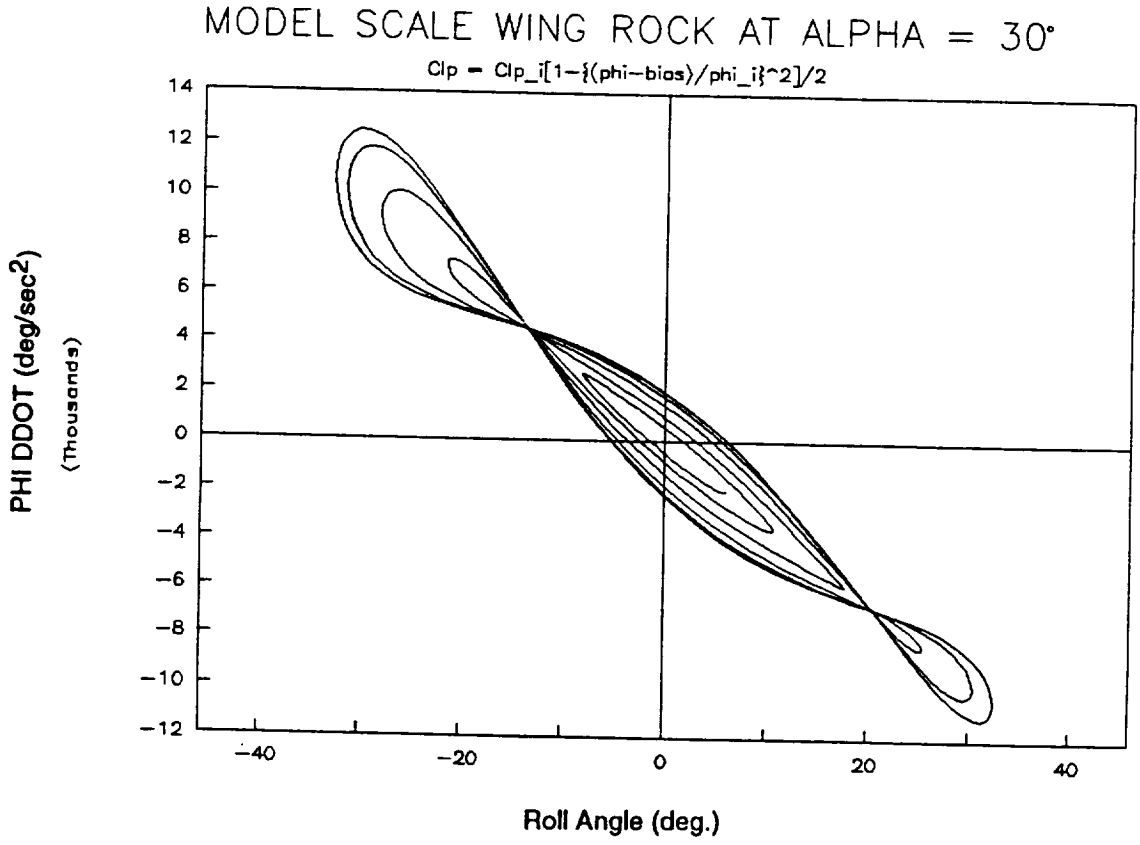

c)

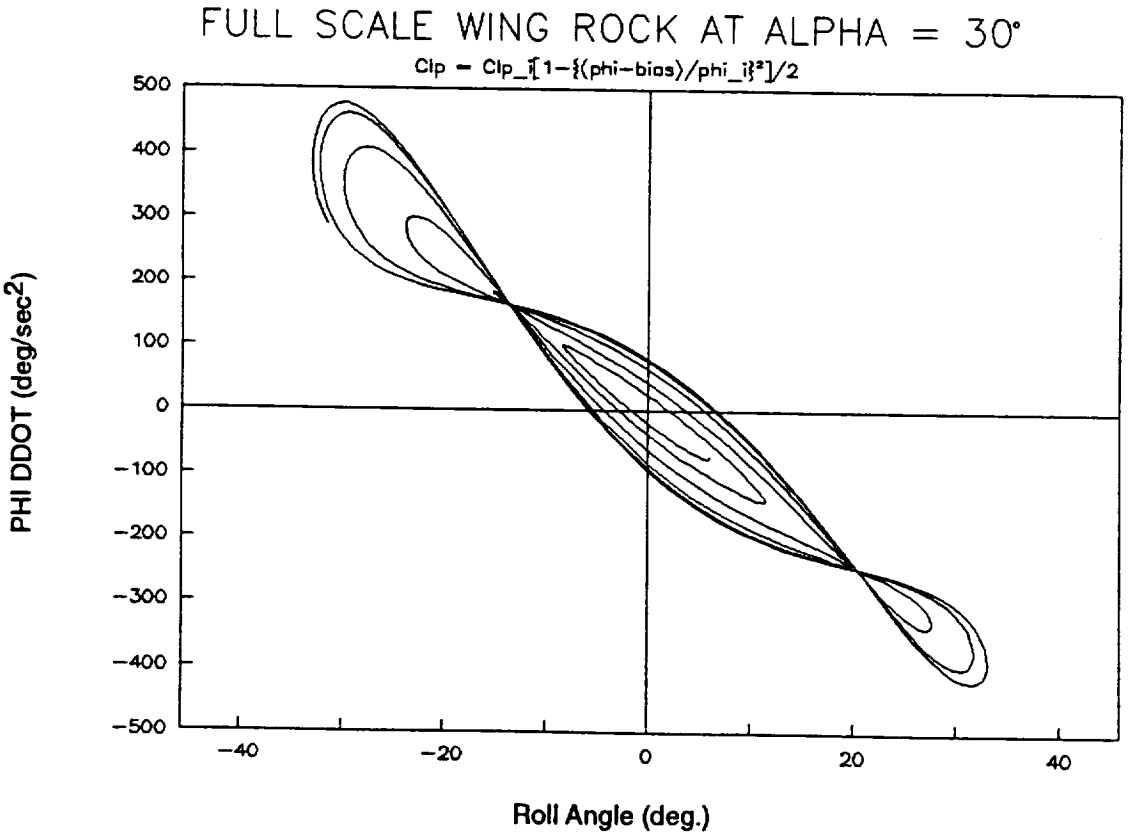

d)

Figure 29 - Concluded

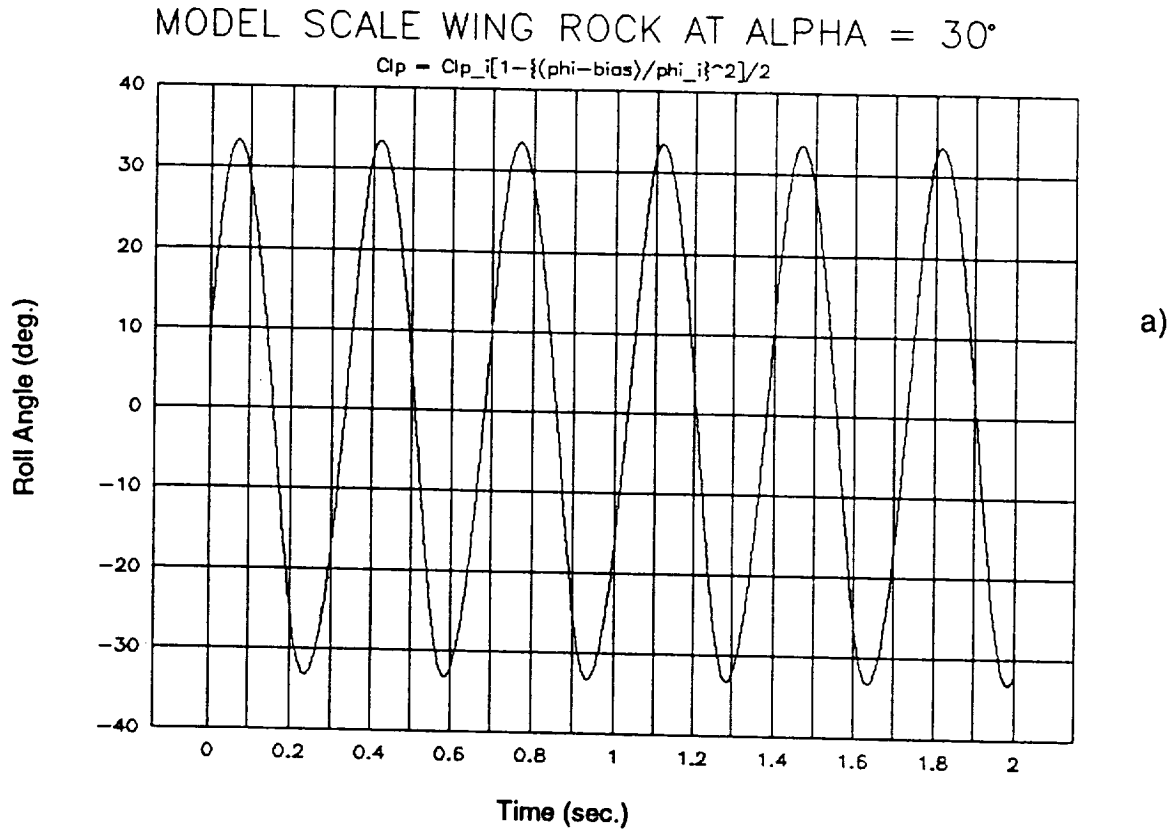

a)

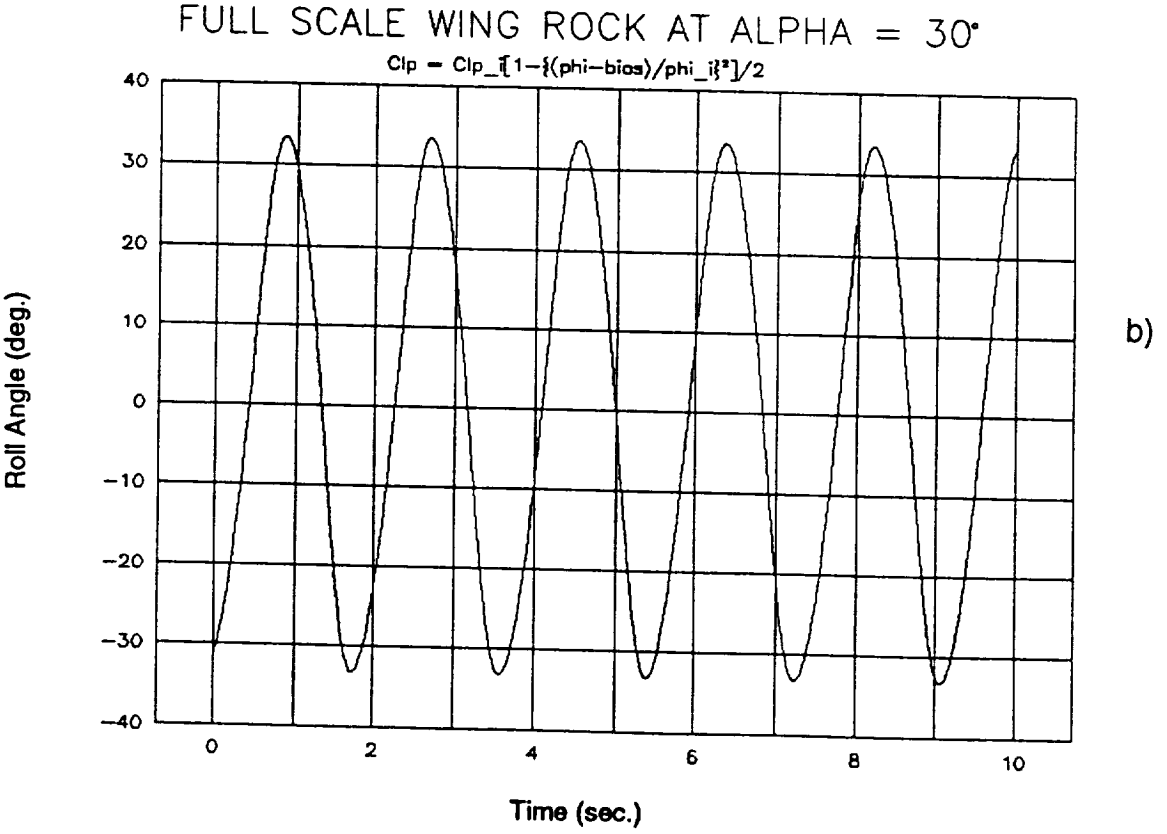

b)

Figure 30 - Comparison of Wind Tunnel Model and Full Scale Configuration (Steady Wing Rock)
a)-b) Roll Angle, c)-d) Phase Plots

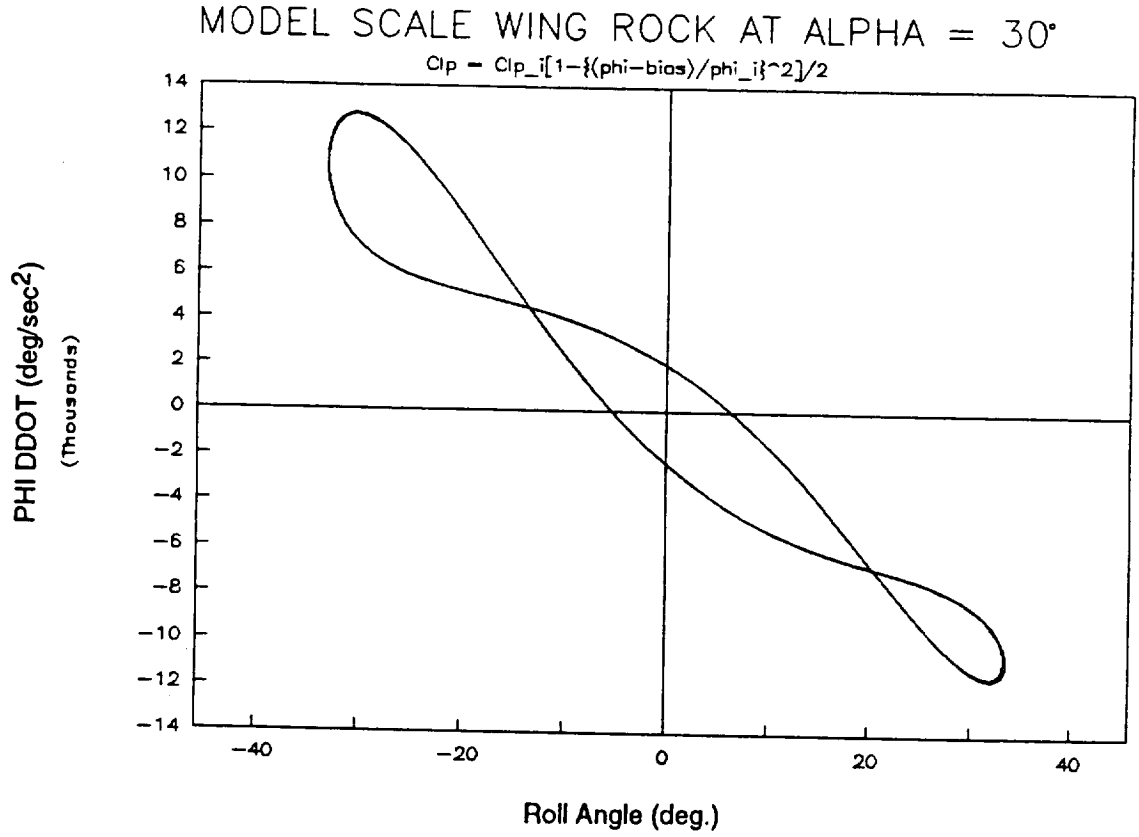

c)

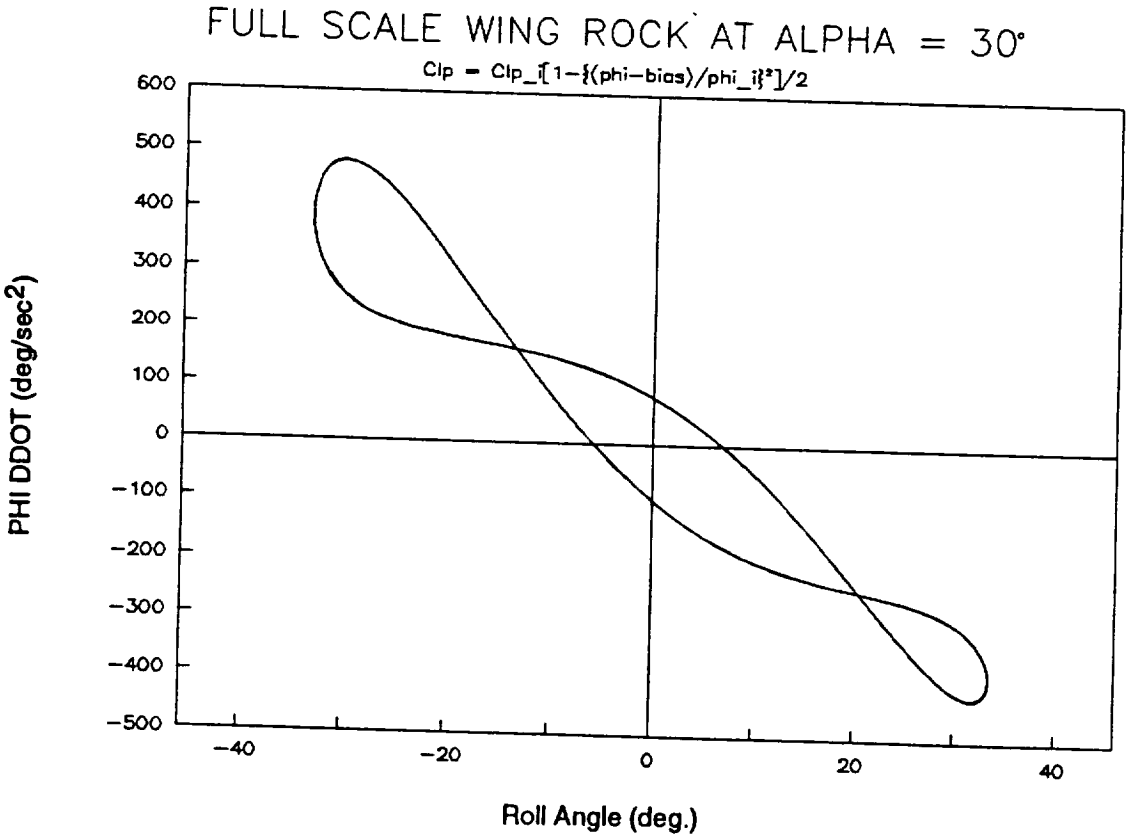

d)

Figure 30 - Concluded

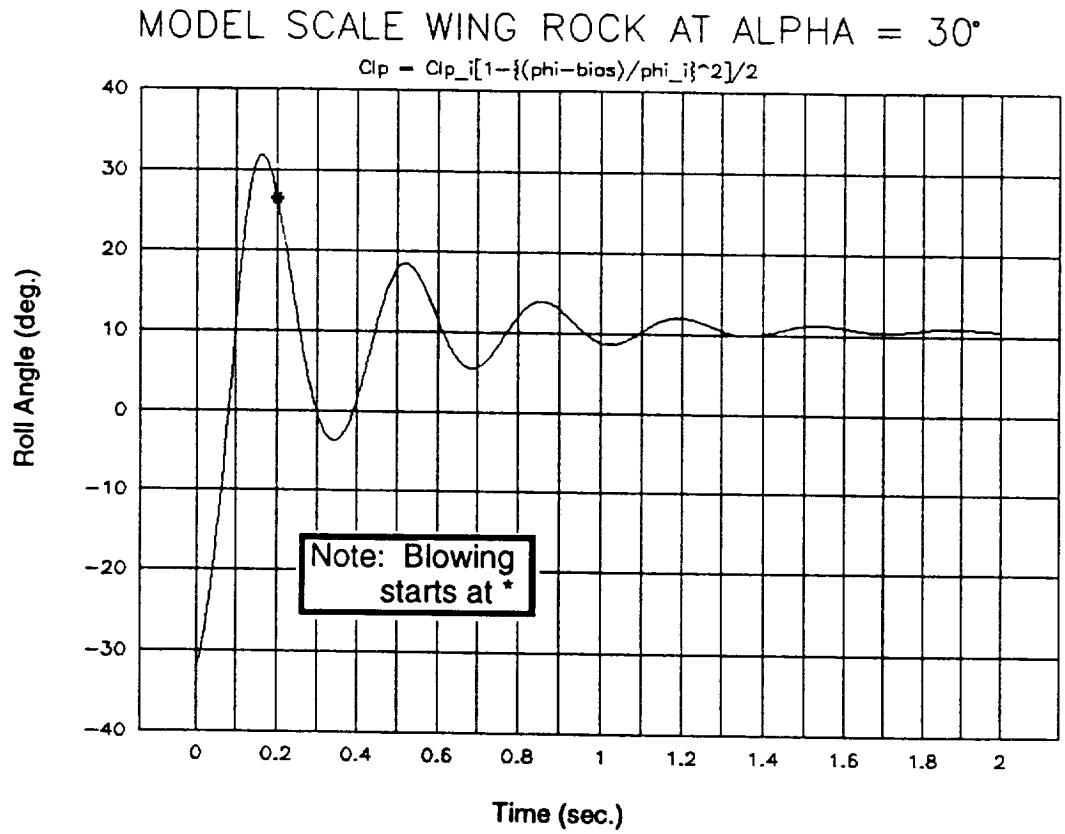

a)

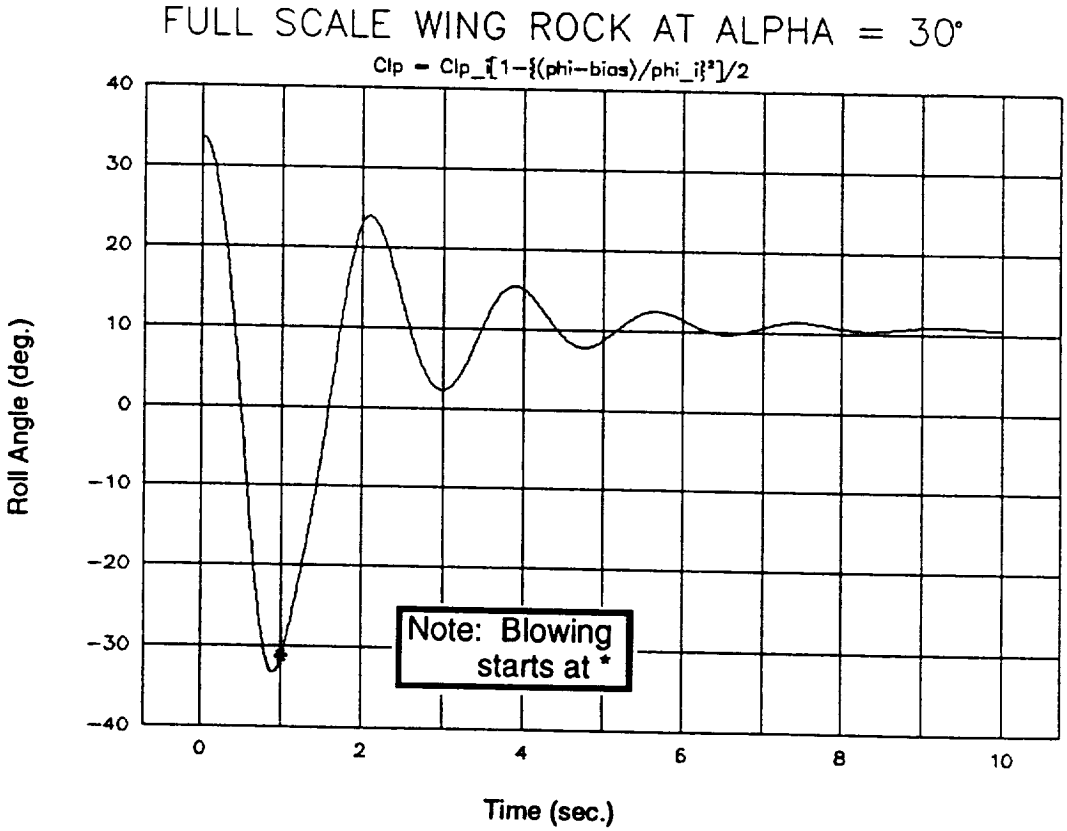

b)

Figure 31 - Comparison of Wind Tunnel Model and Full Scale Configuration (Wing Rock Suppression, $C\mu = 0.0037$)
a)-b) Roll Angle, c)-d) Phase Plots

C-2

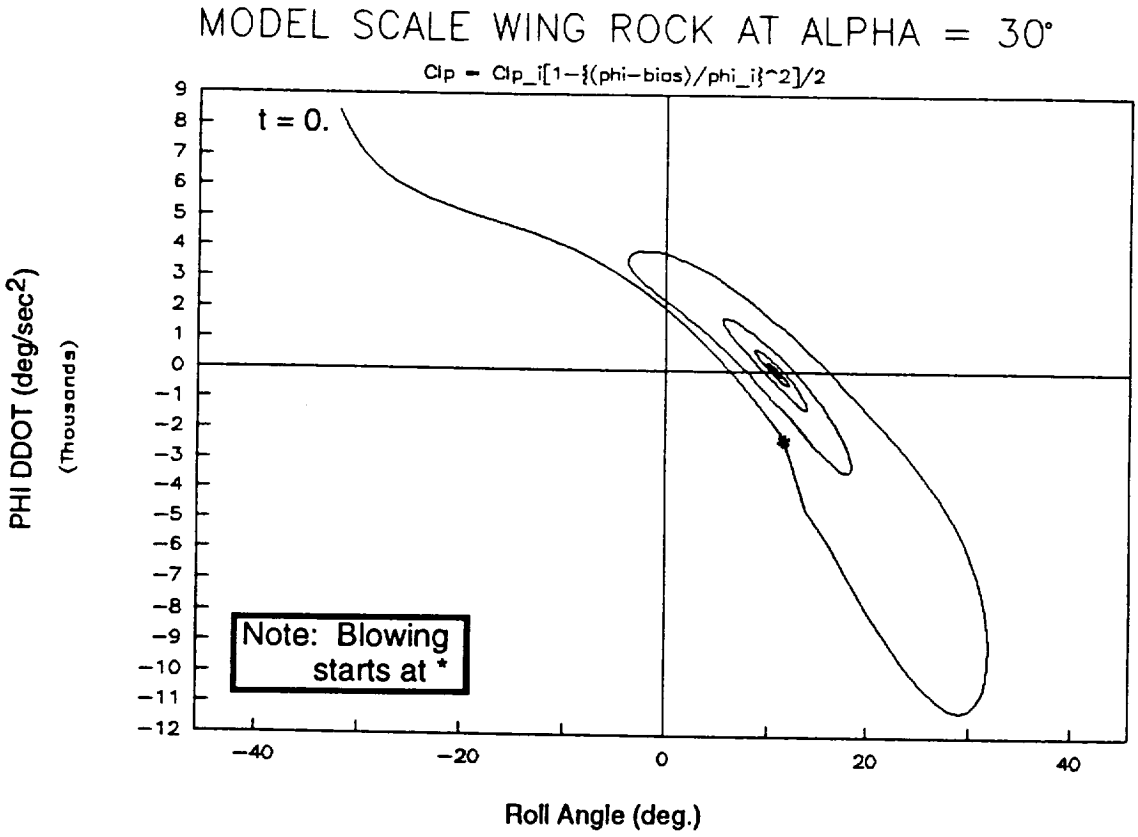

c)

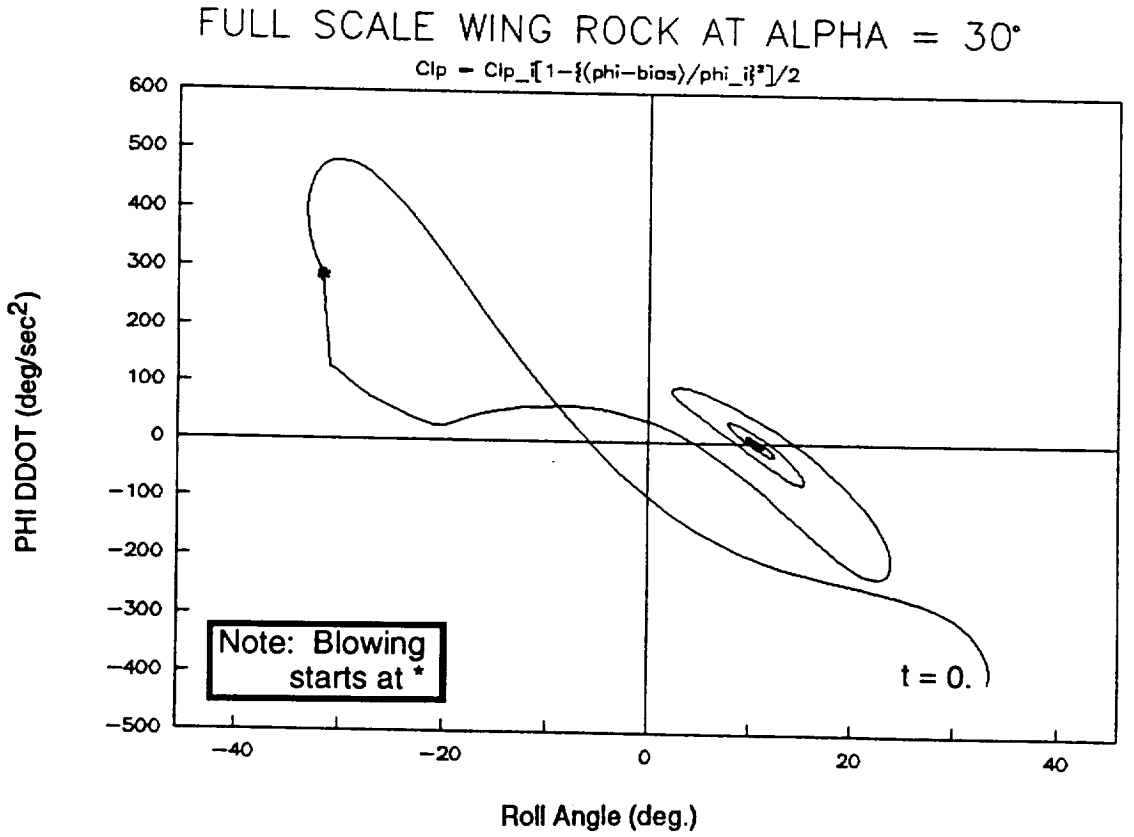

d)

Figure 31 - Concluded

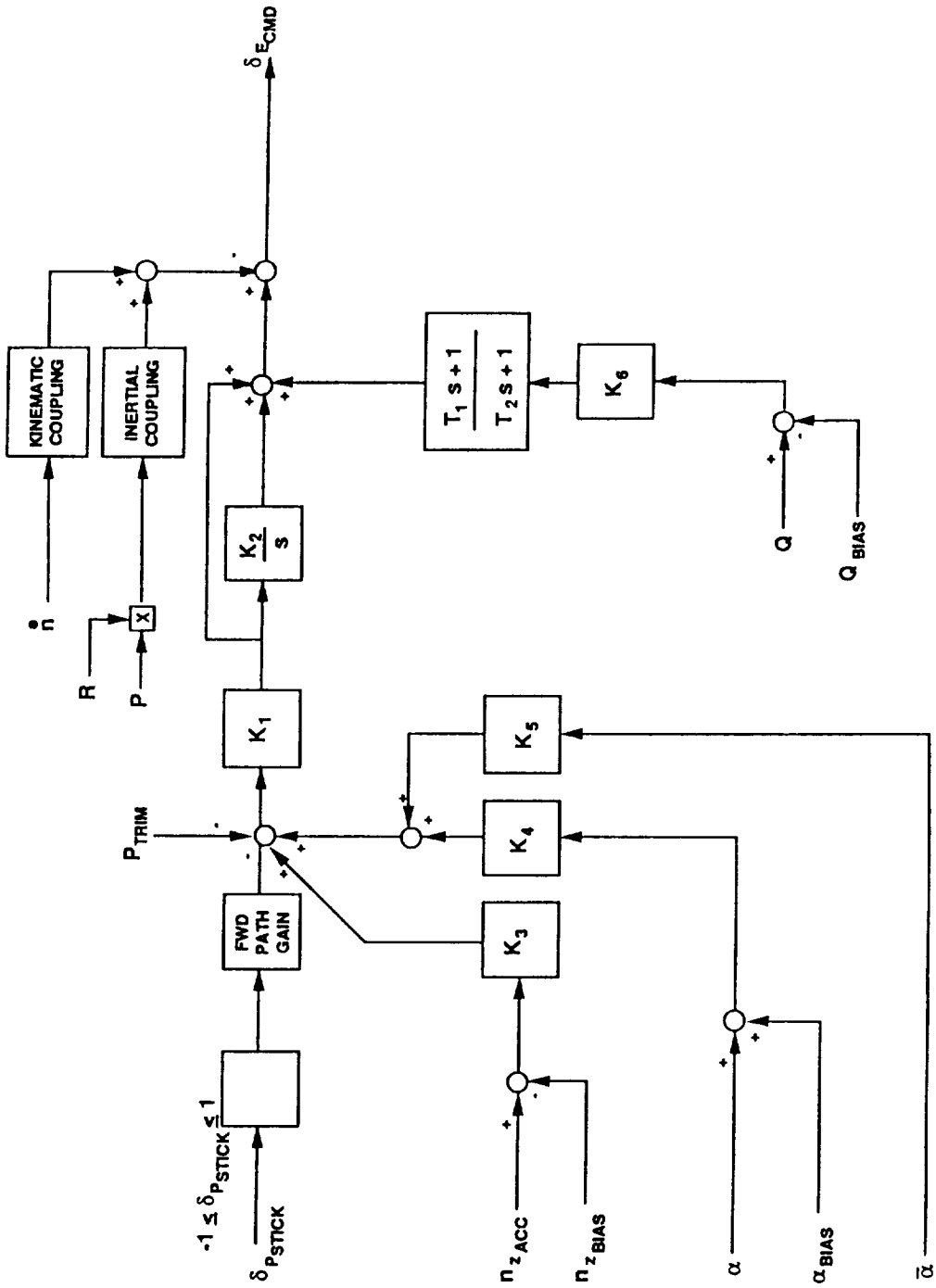

Figure 32 - Longitudinal Flight Control System

a)

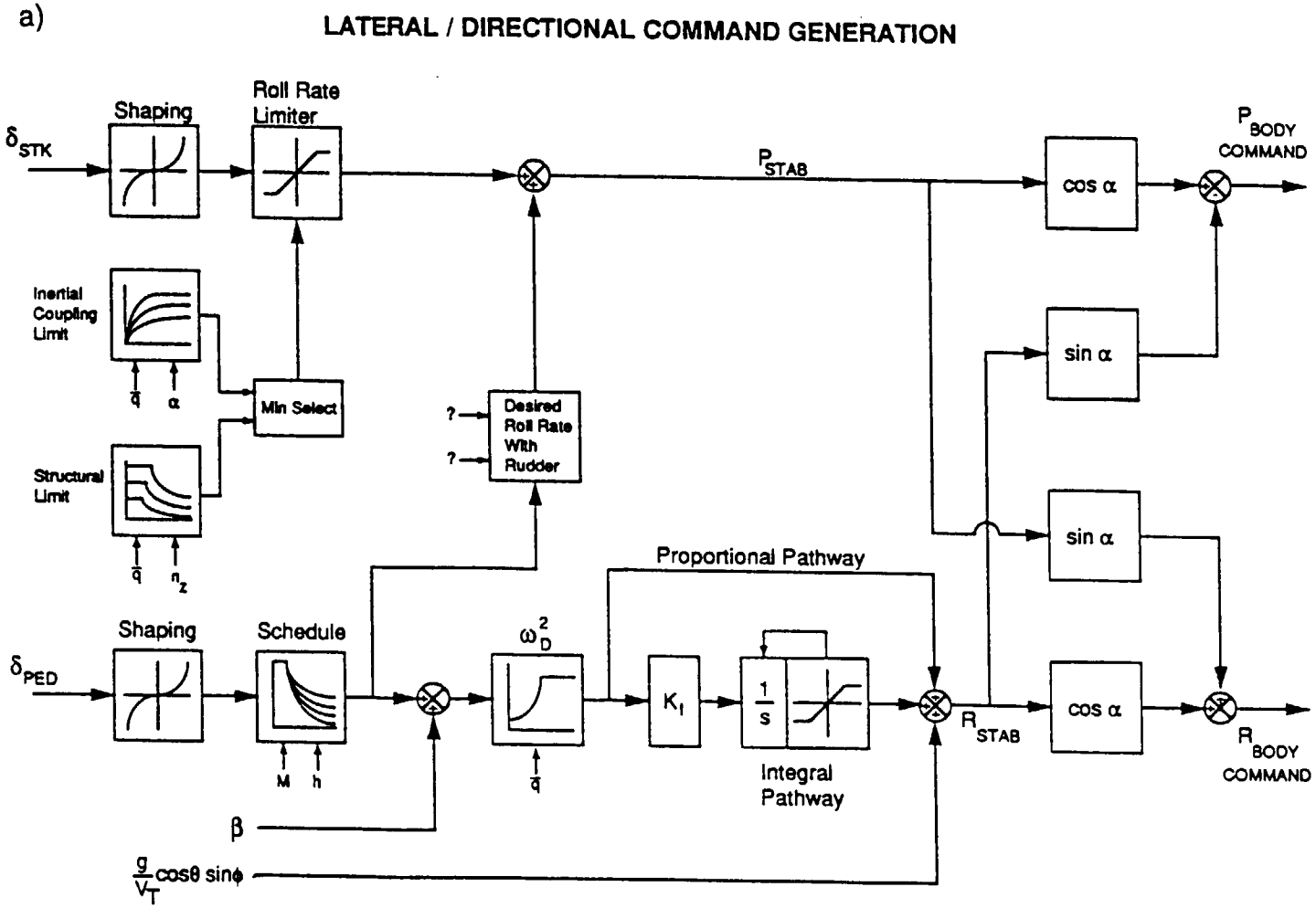

Figure 33 - Lateral-Directional Flight Control System

b)

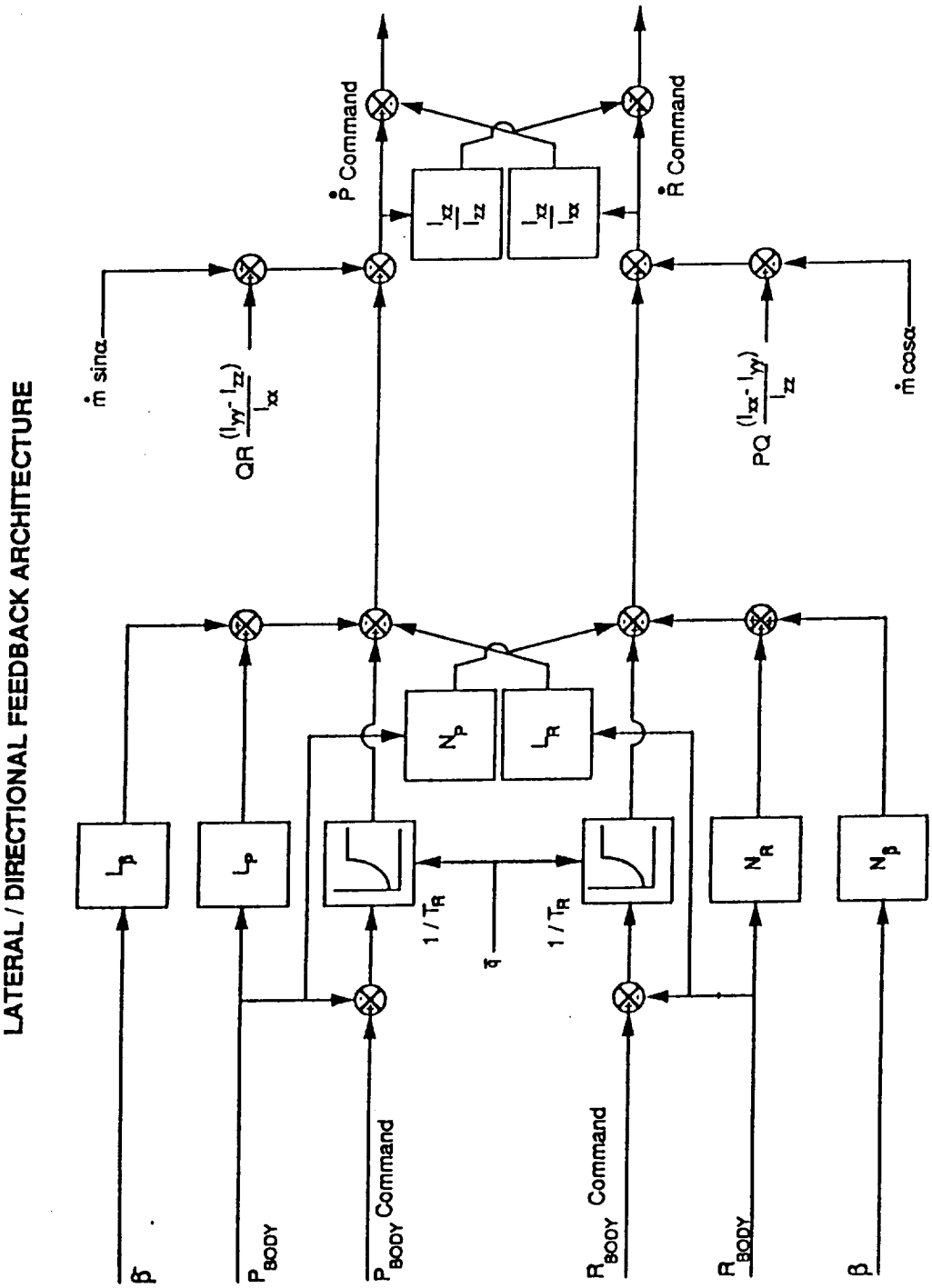

Figure 33 - Continued

c)

LATERAL/DIRECITIONAL CONTROL MIXER

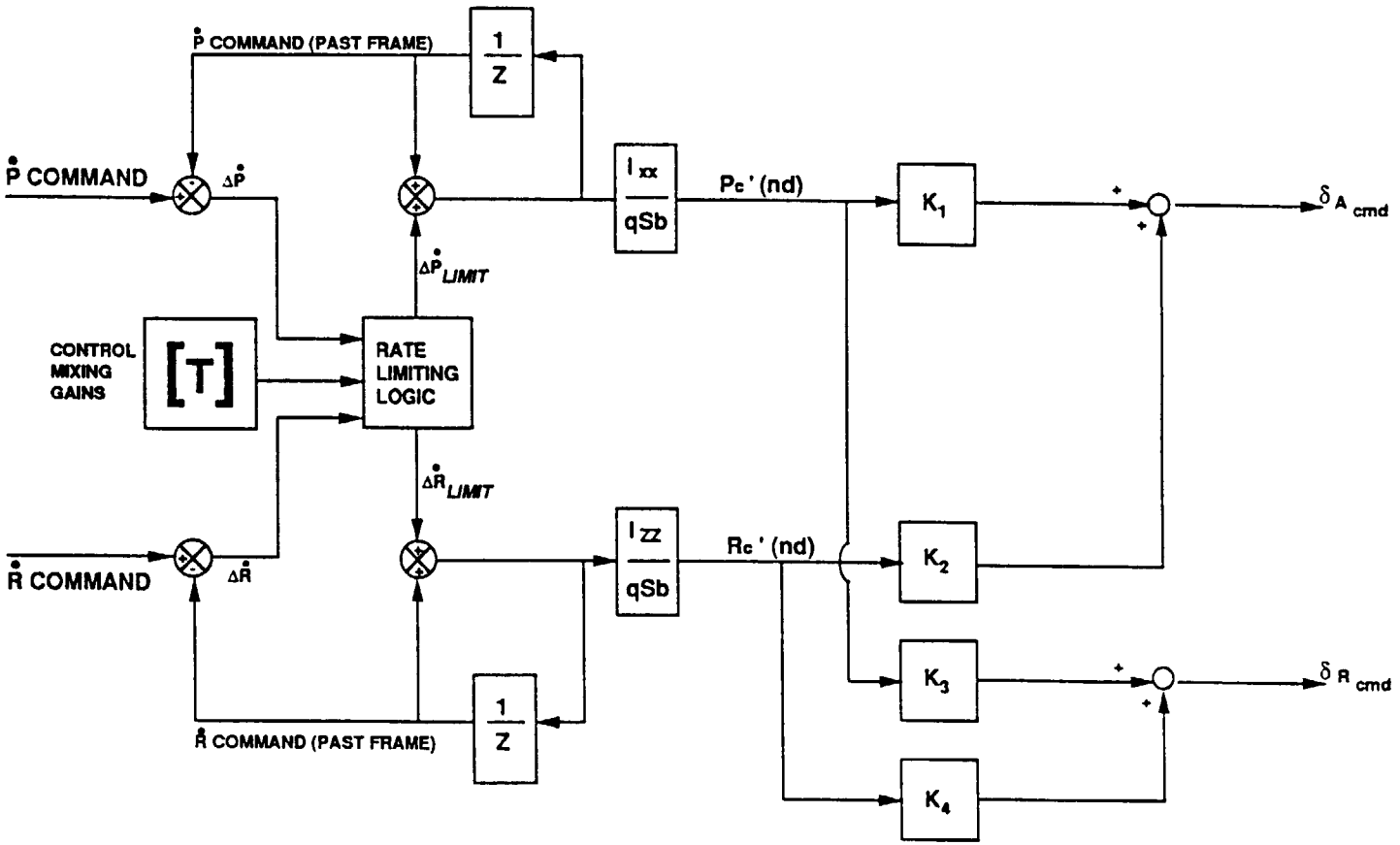

Figure 33 - Concluded

ARENA HARDWARE CONFIGURATION

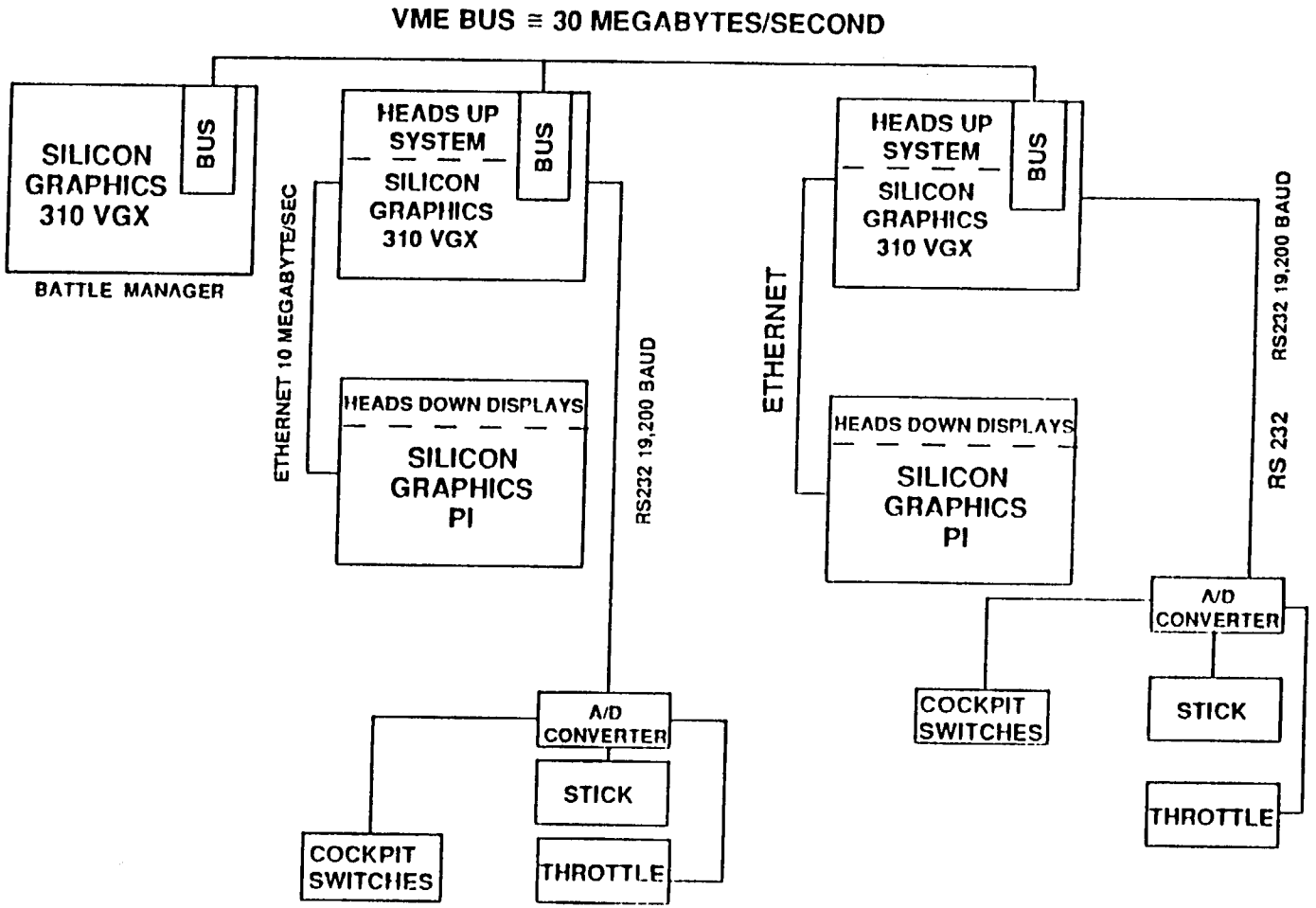

Figure 34 - Arena Hardware Configuration

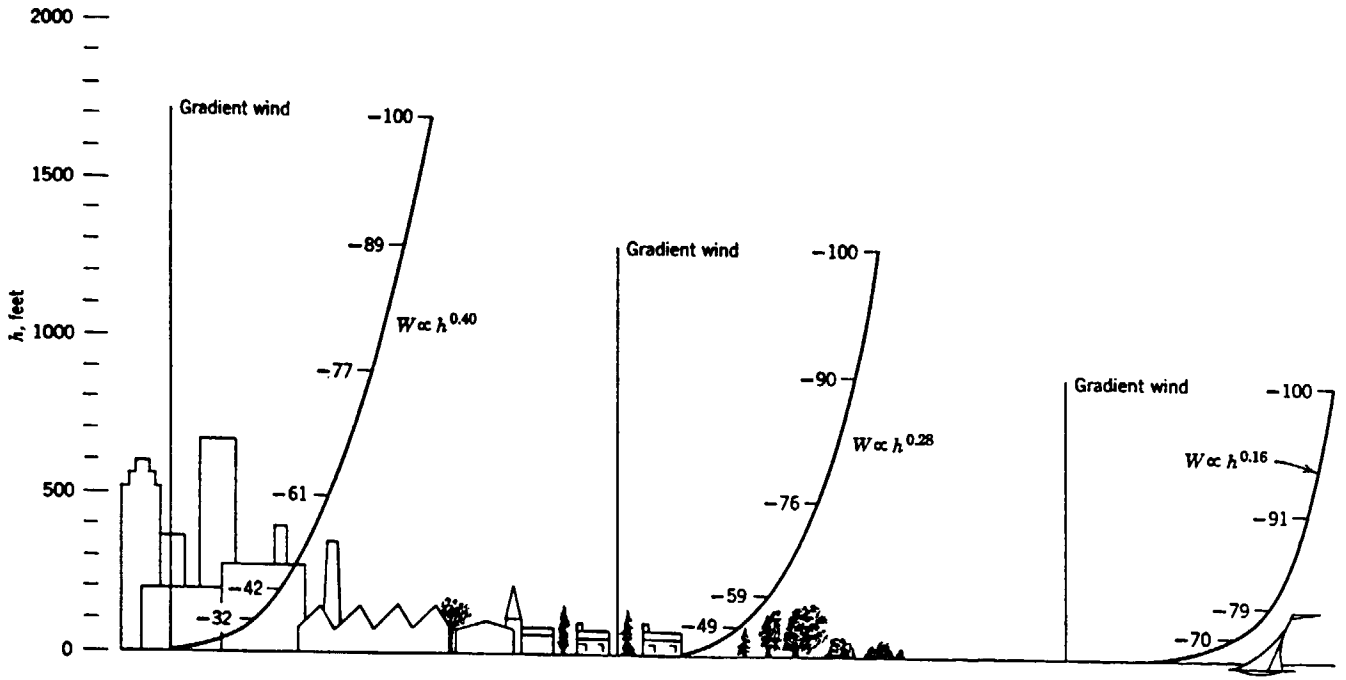

Figure 35 - Profiles of Mean Wind Velocity over Level Terrains of Different Roughness (from Ref. 27)

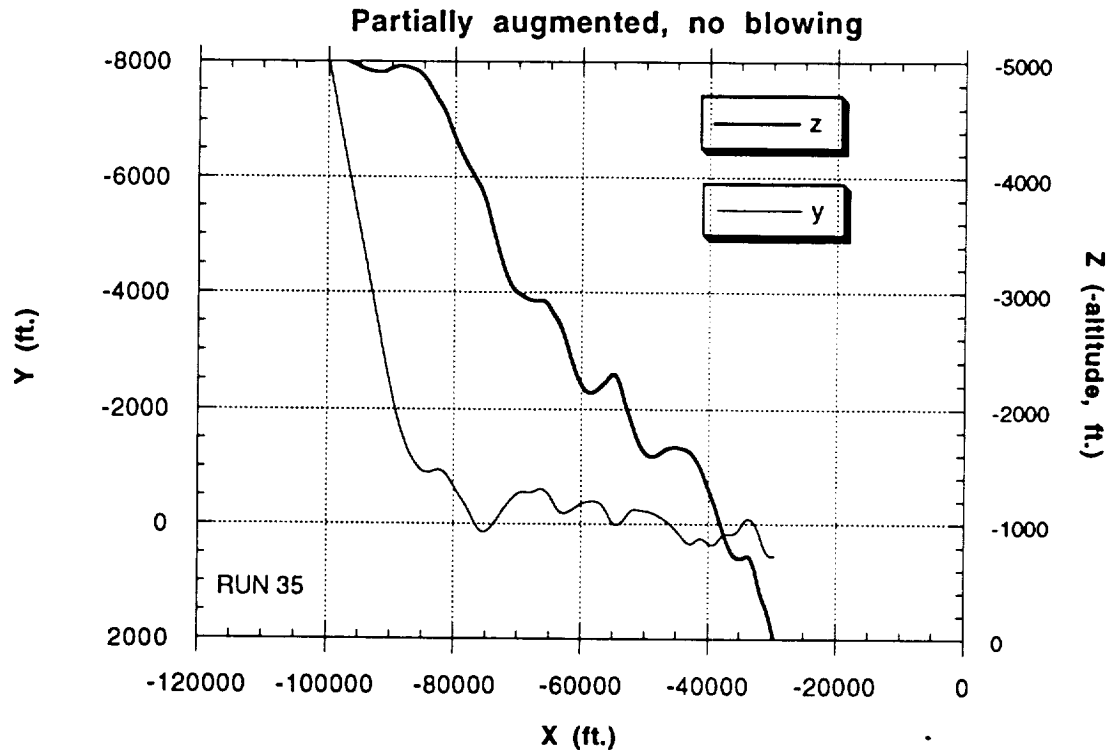

a) Variation in Altitude (-Z) and Horizontal Excursions (Y)

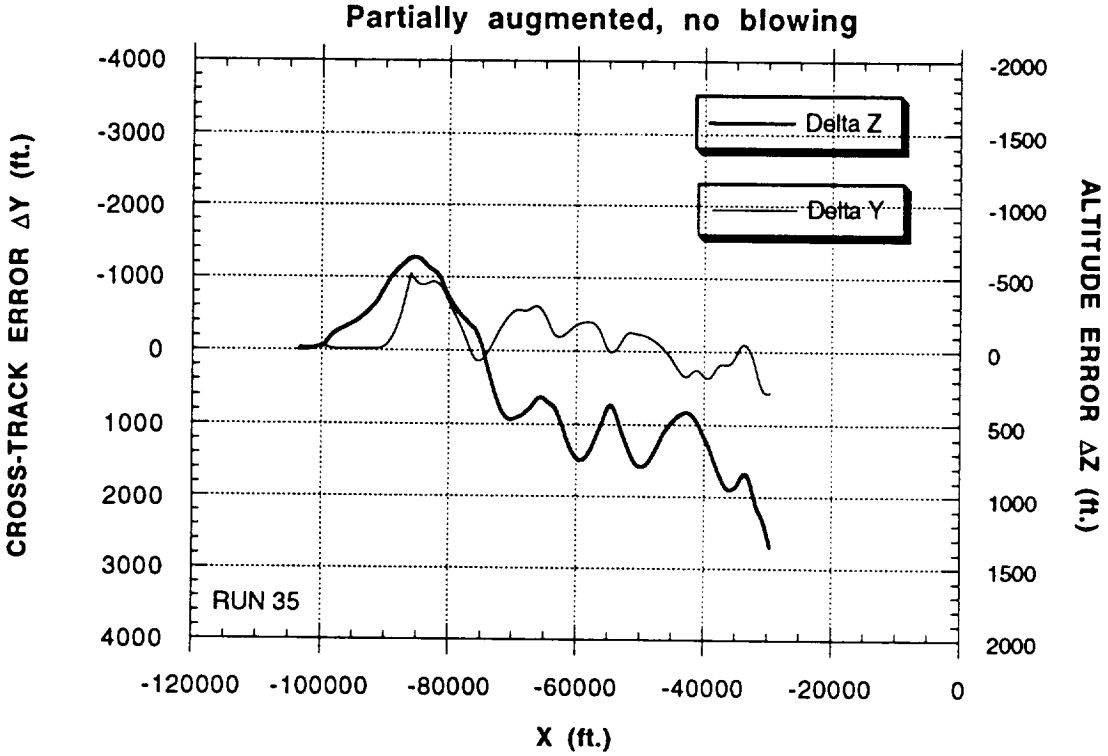

b) Cross-Track and Altitude Errors

Figure 36 - Approach and Landing Simulation for the NASP-type Configuration with Partially Augmented Flight Control System (No Forebody Blowing)

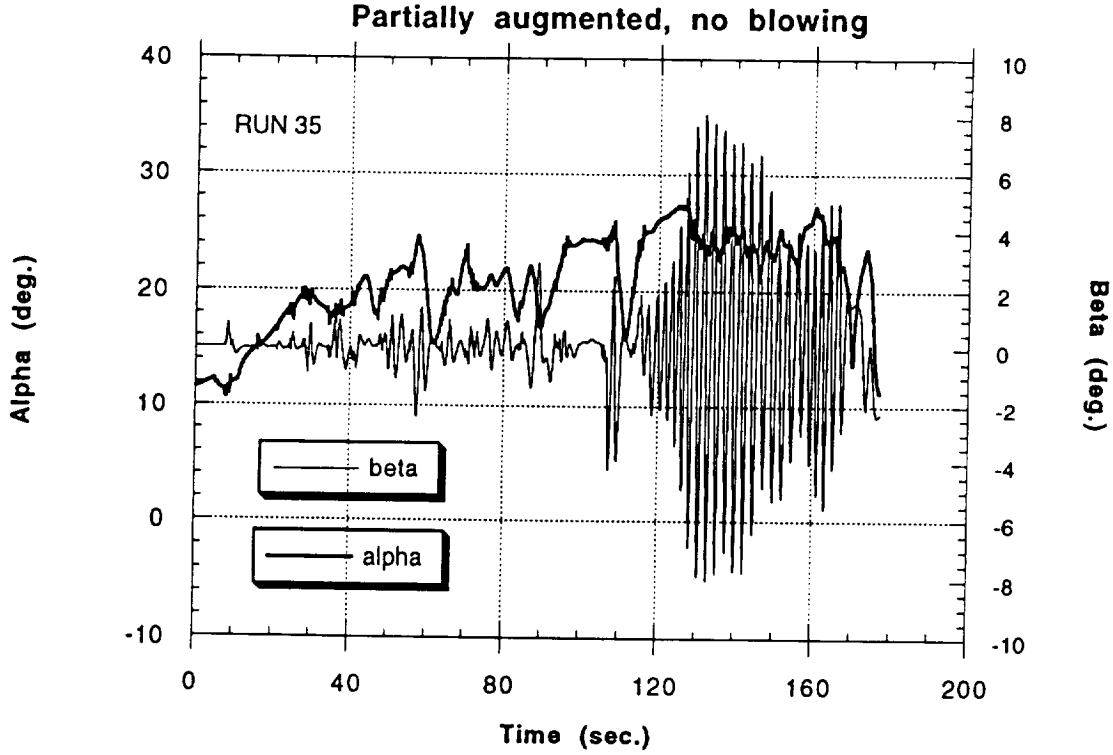

c) Angles of Attack and Sideslip

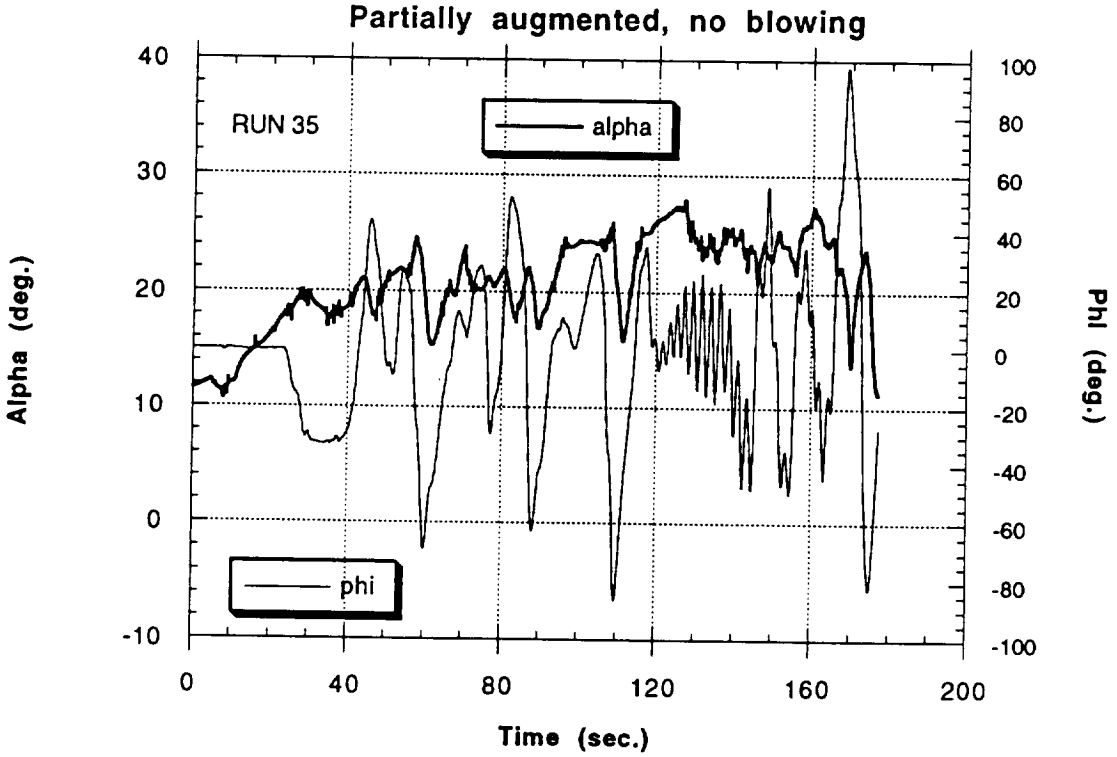

d) Angles of Attack and Roll

Figure 36 - Continued

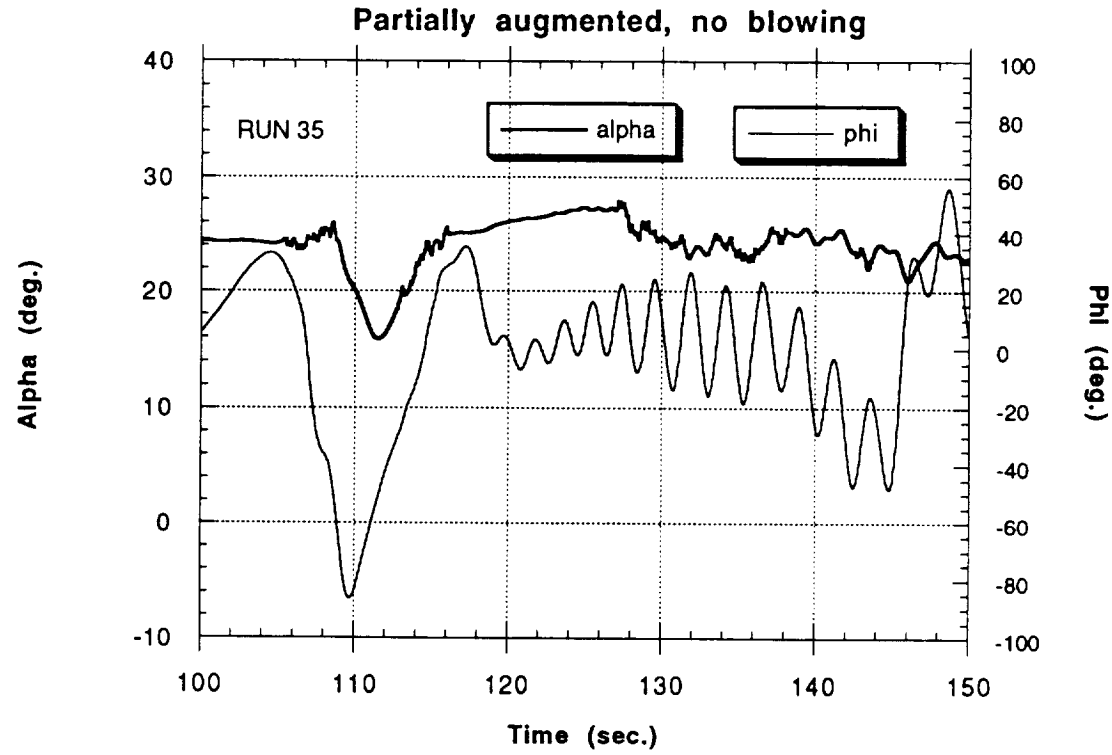

e) Angles of Attack and Roll

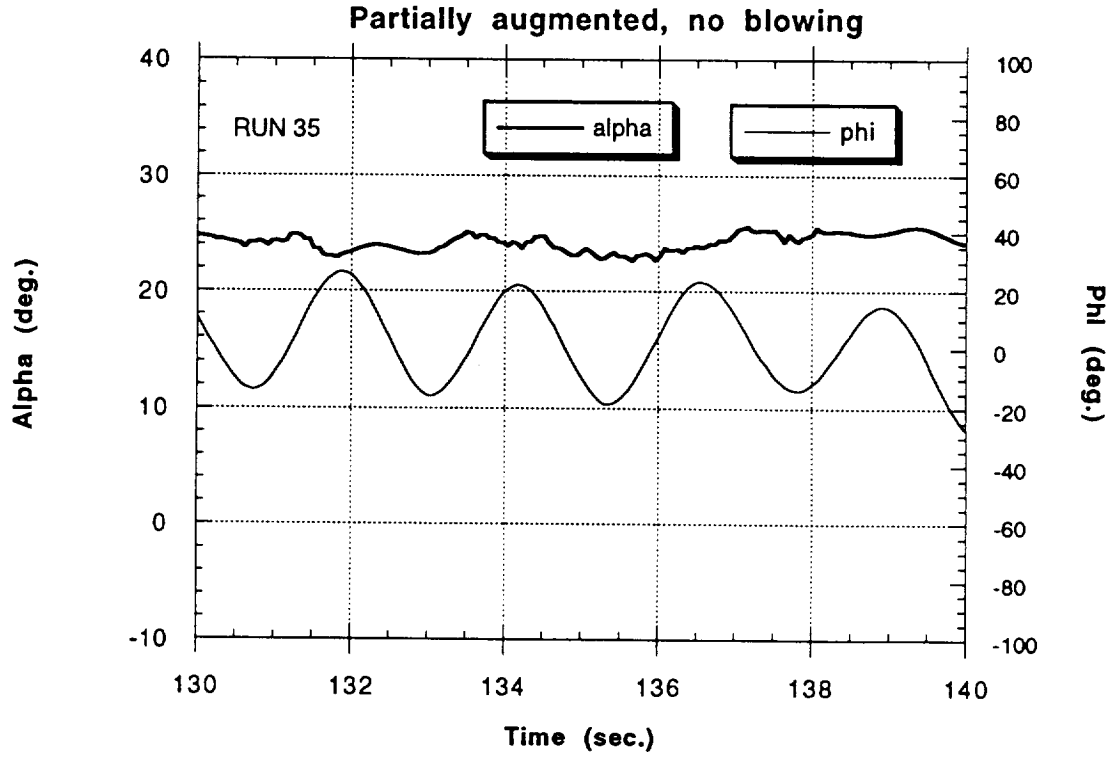

f) Angles of Attack and Roll

Figure 36 - Continued

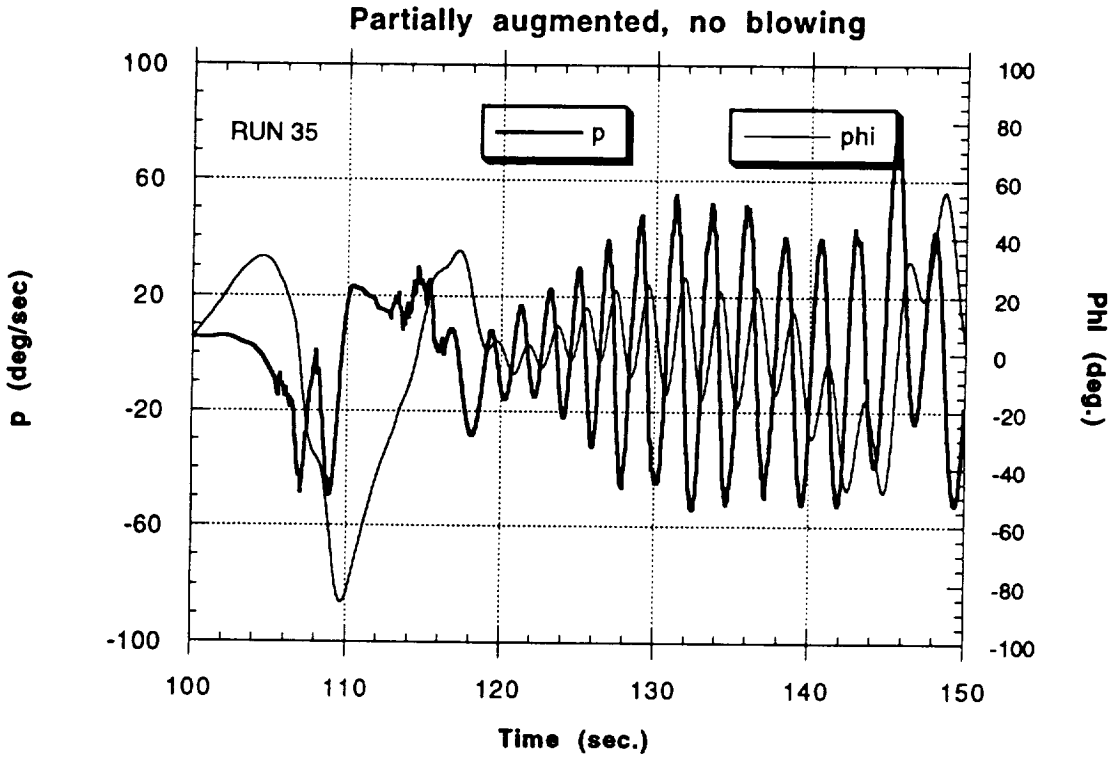

g) Roll Angle and Roll Rate

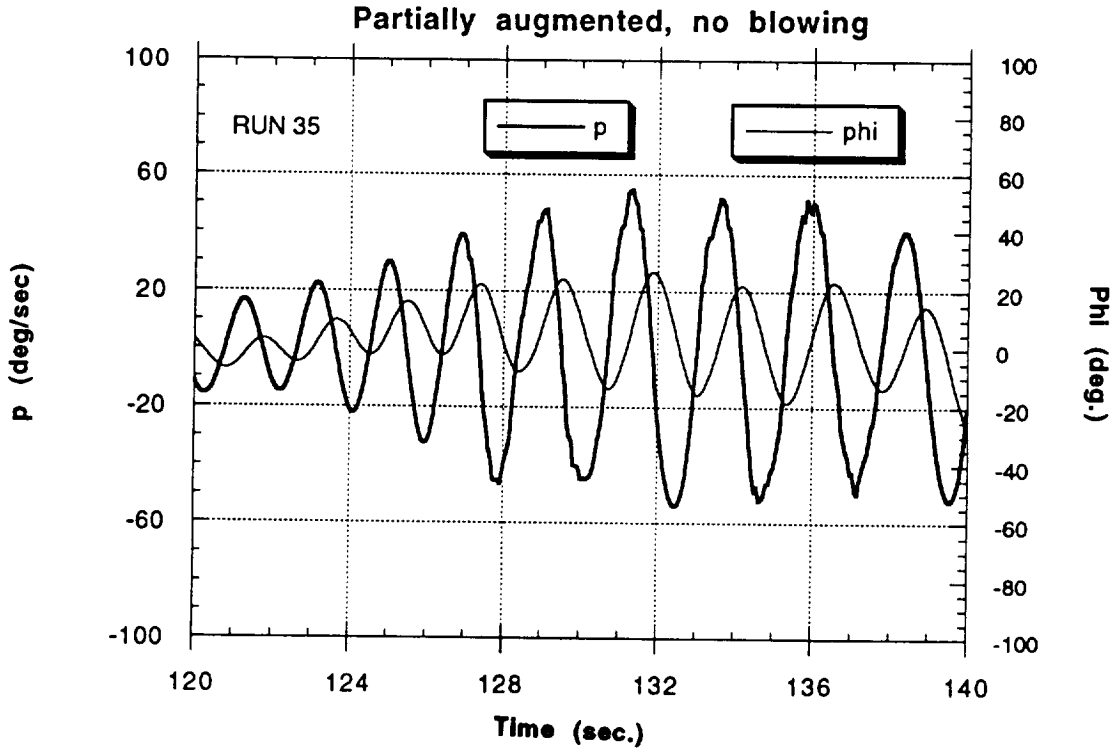

h) Roll Angle and Roll Rate (Different Time Scale)

Figure 36 - Continued

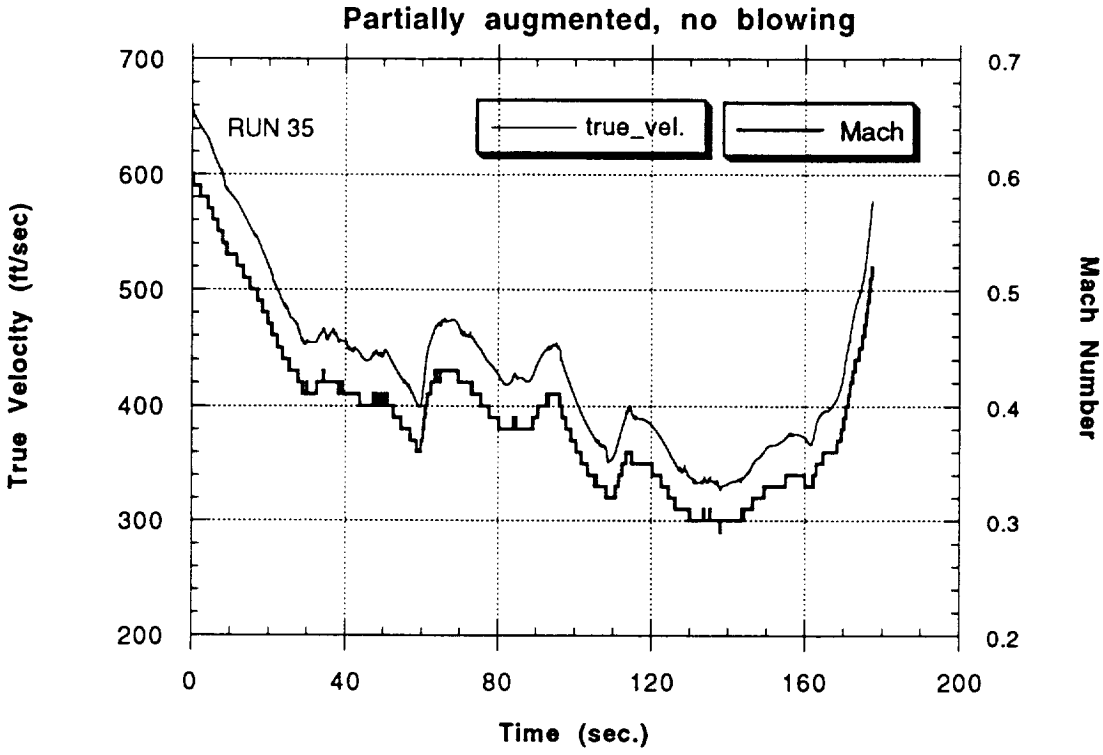

i) Flight Velocity and Mach Number

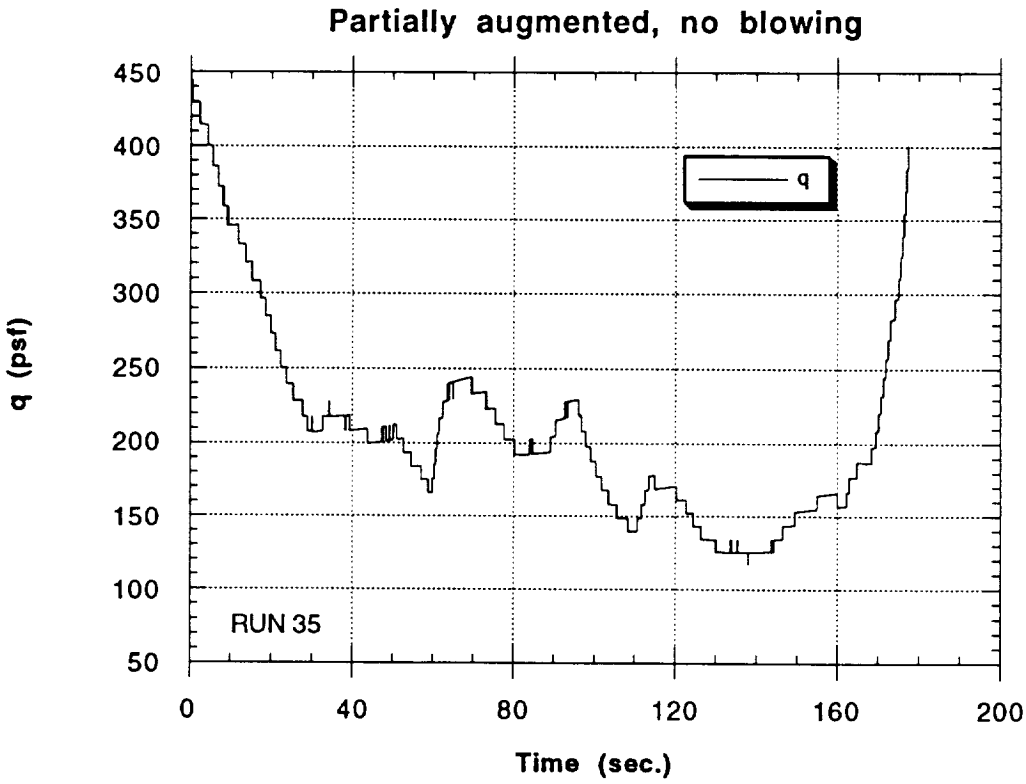

j) Dynamic Pressure

Figure 36 - Continued

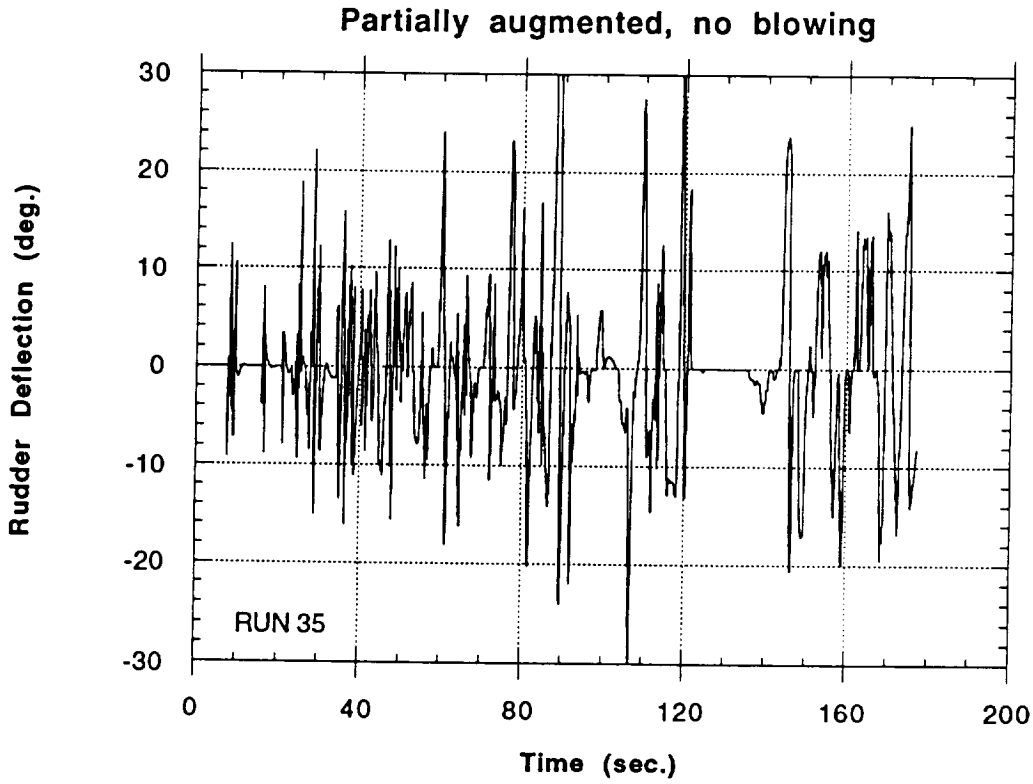

k) Rudder Deflection Angle

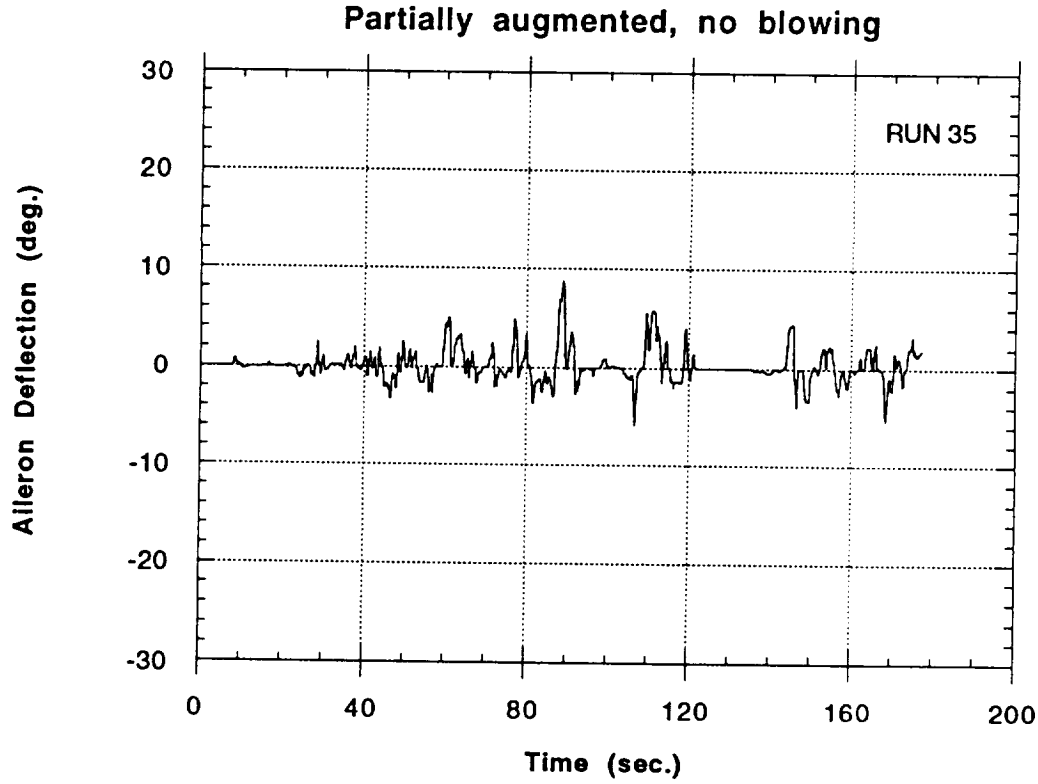

l) Aileron Deflection Angle

Figure 36 - Concluded

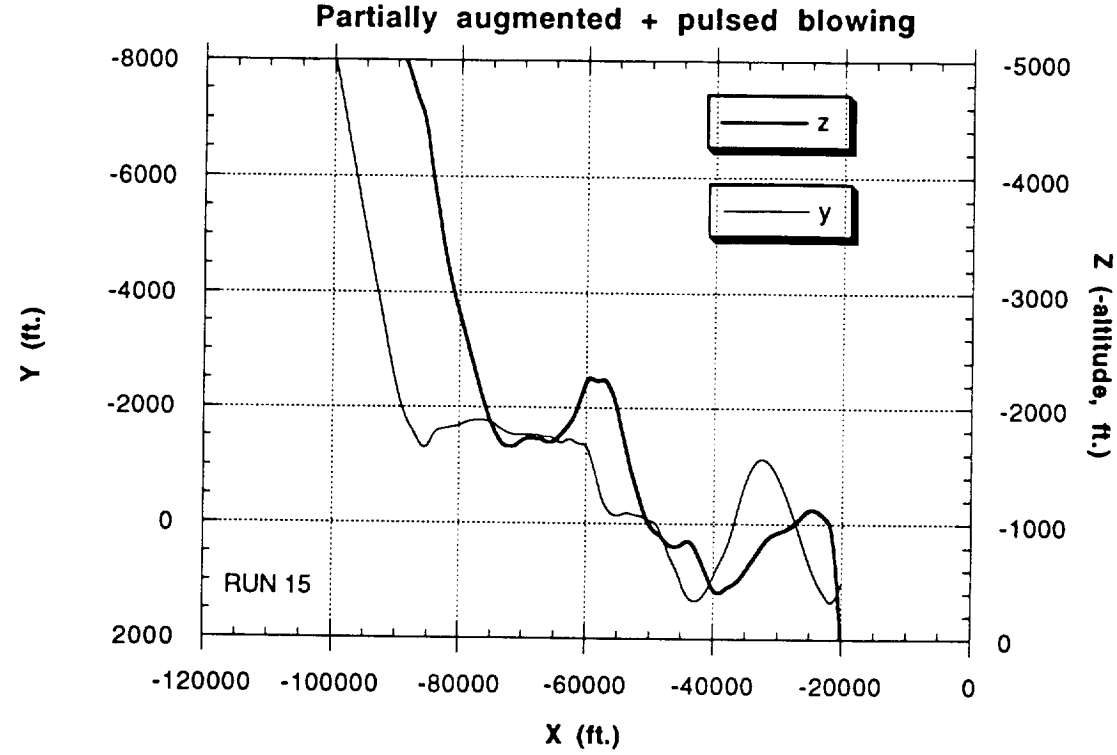

a) Variation in Altitude (-Z) and Horizontal Excursions (Y)

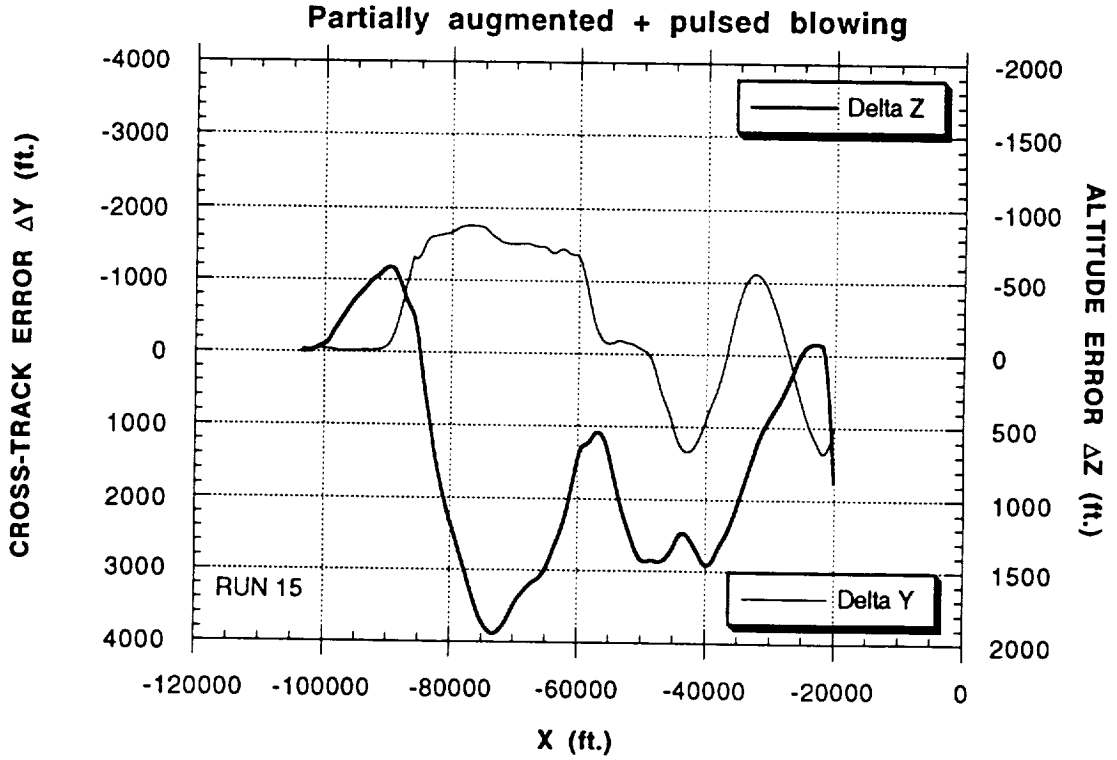

b) Cross-Track and Altitude Errors

Figure 37 - Approach and Landing Simulation for the NASP-type Configuration with Partially Augmented Flight Control System and Pulsed Forebody Blowing

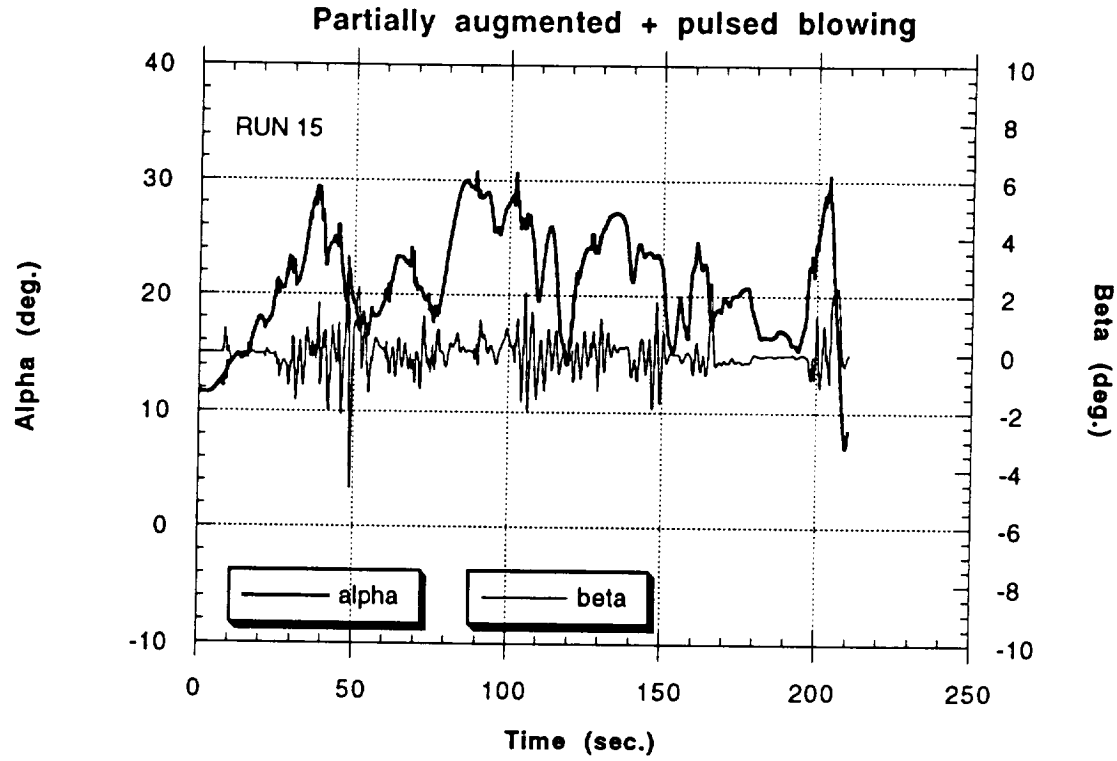

c) Angles of Attack and Sideslip

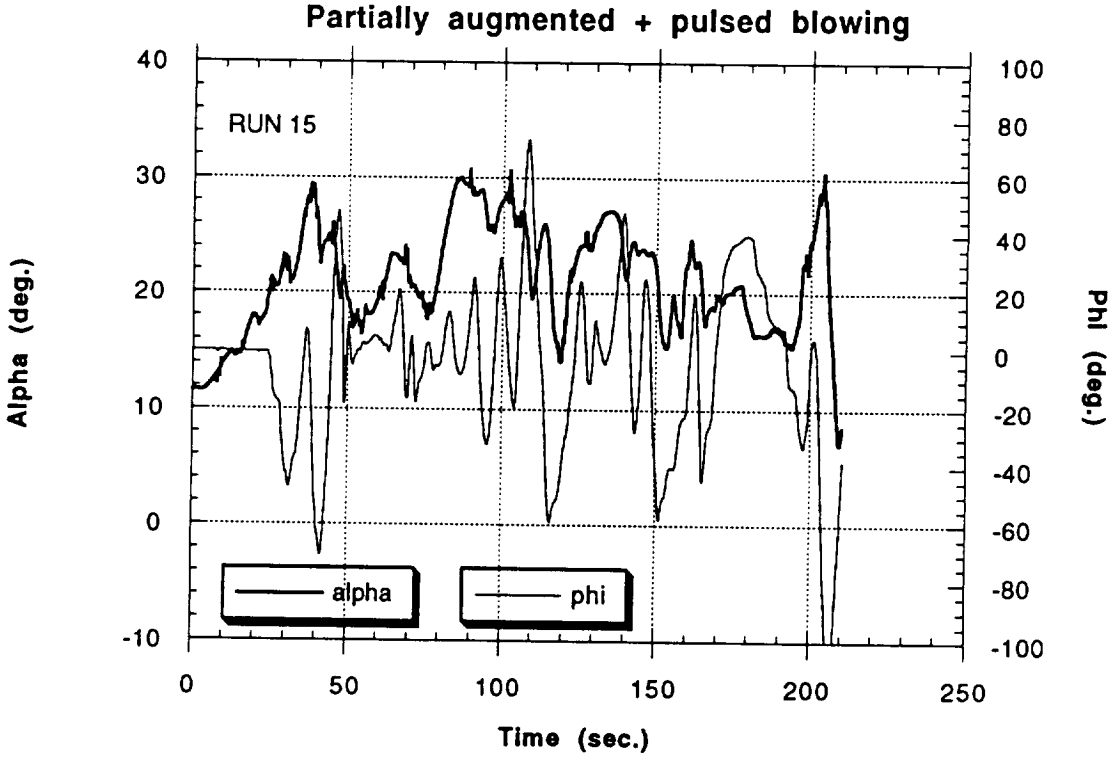

d) Angles of Attack and Roll

Figure 37 - Continued

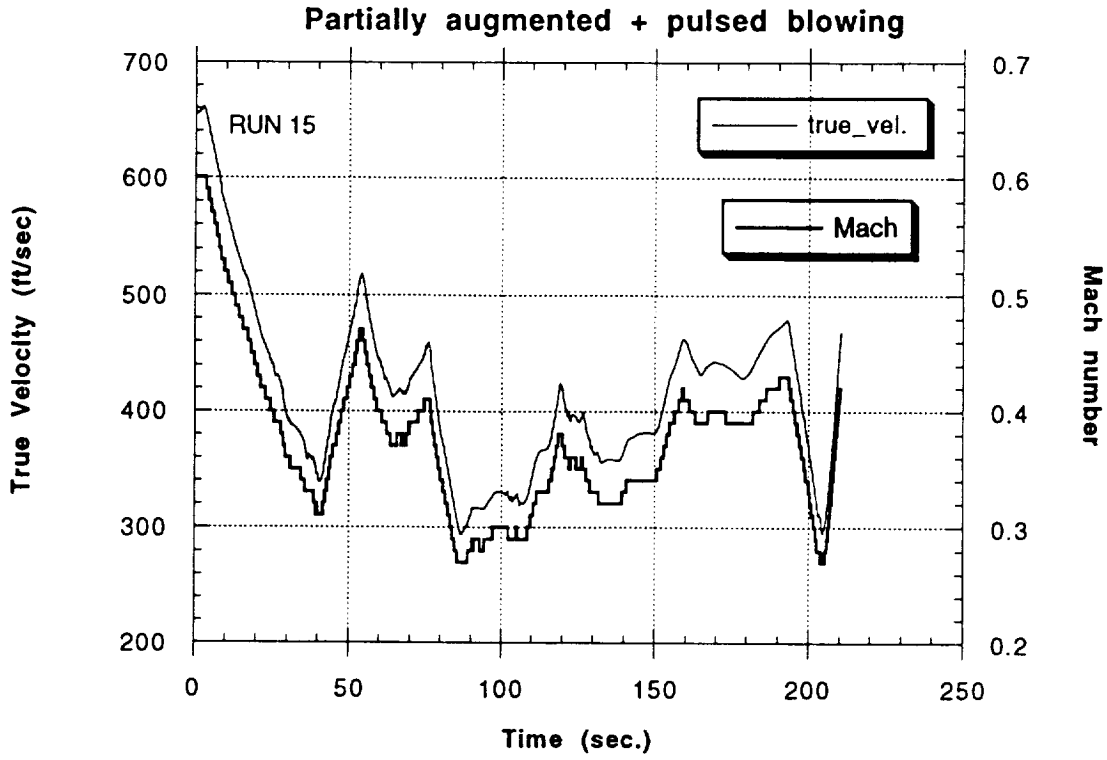

e) Flight Velocity and Mach Number

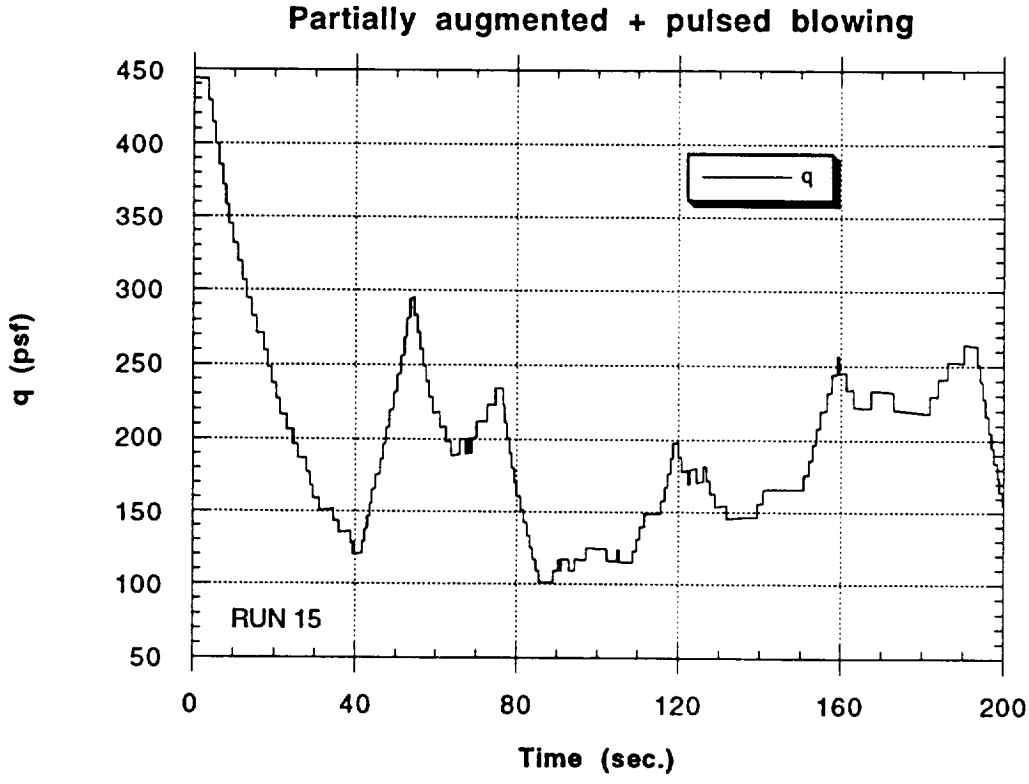

f) Dynamic Pressure

Figure 37 - Continued

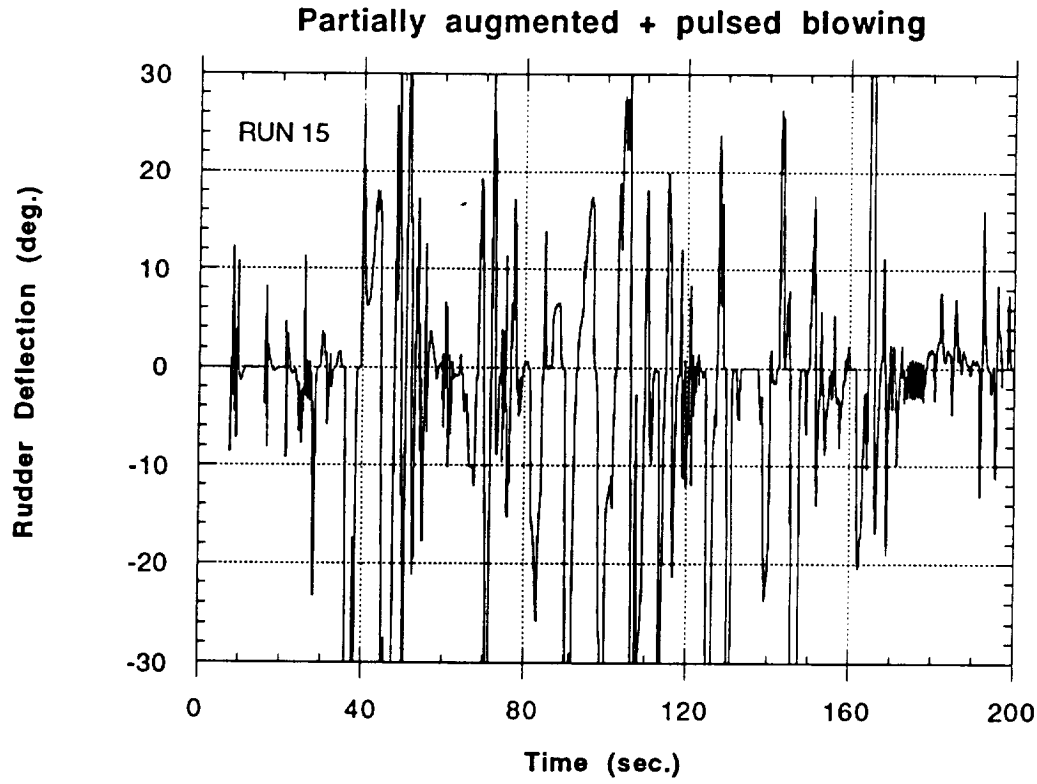

g) Rudder Deflection Angle

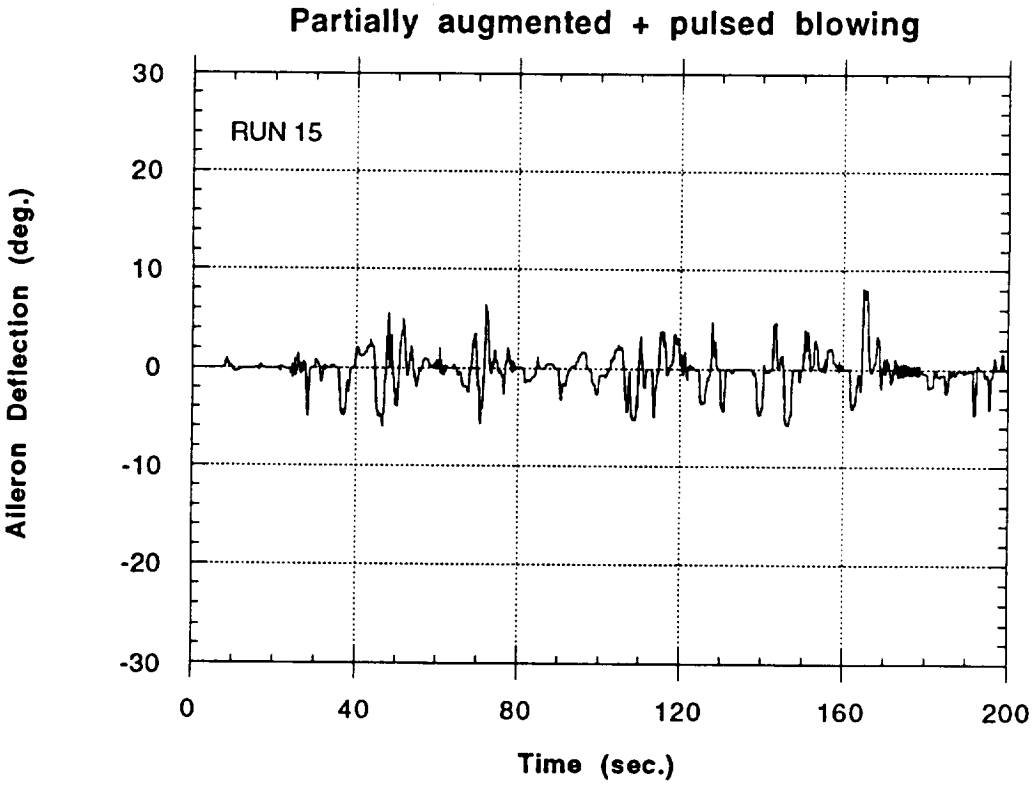

h) Aileron Deflection Angle

Figure 37 - Continued

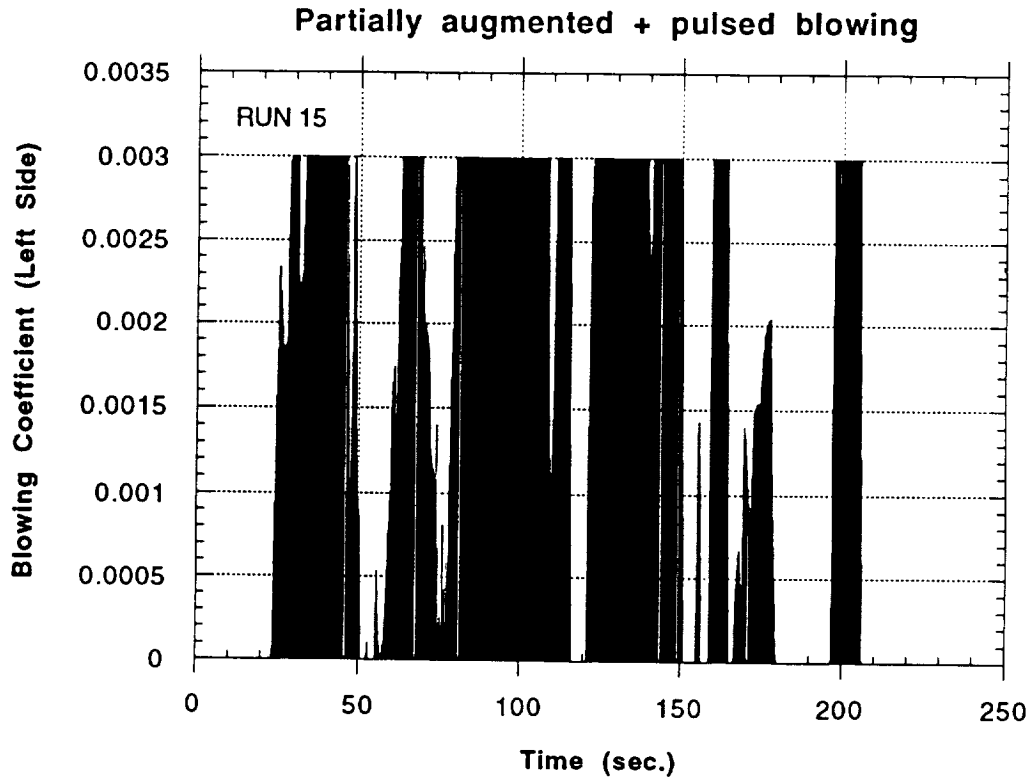

i) Blowing Coefficient (Left Nozzle)

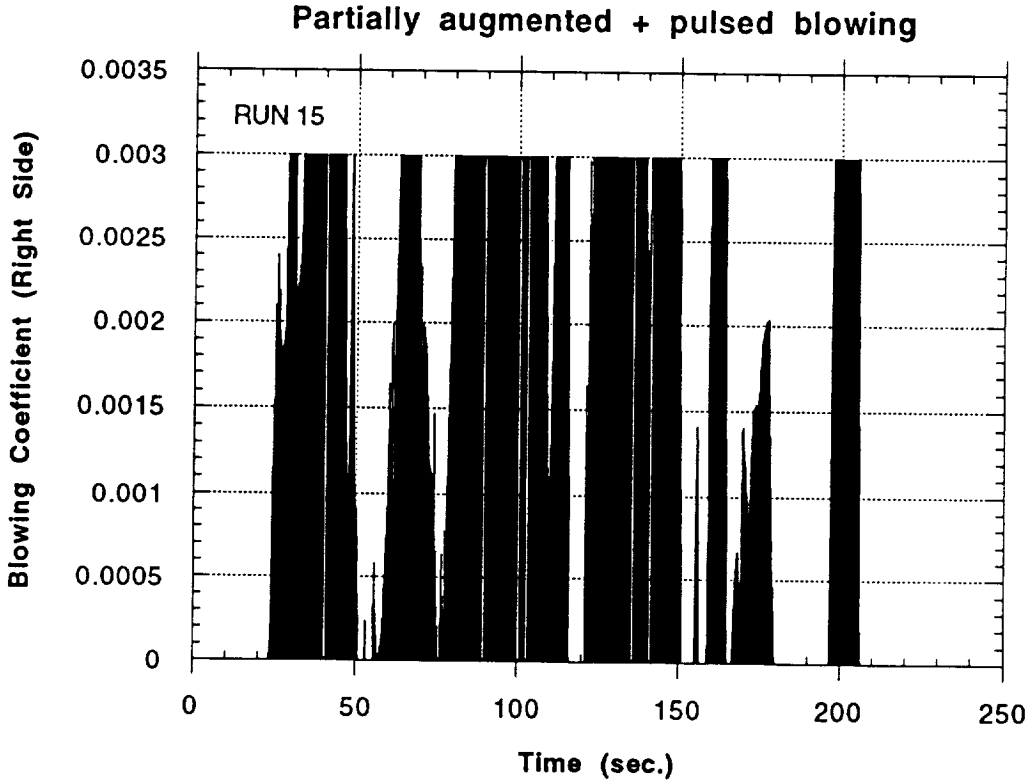

j) Blowing Coefficient (Right Nozzle)

Figure 37 - Continued

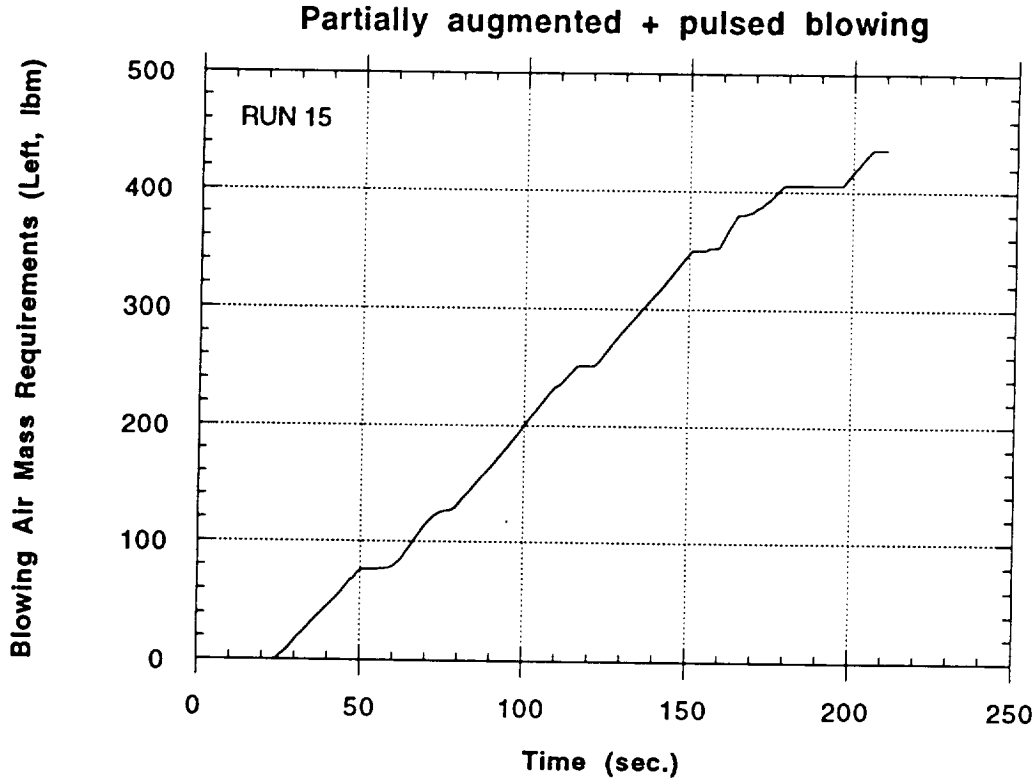

k) Accumulative Total Mass Flow Requirements (Left)

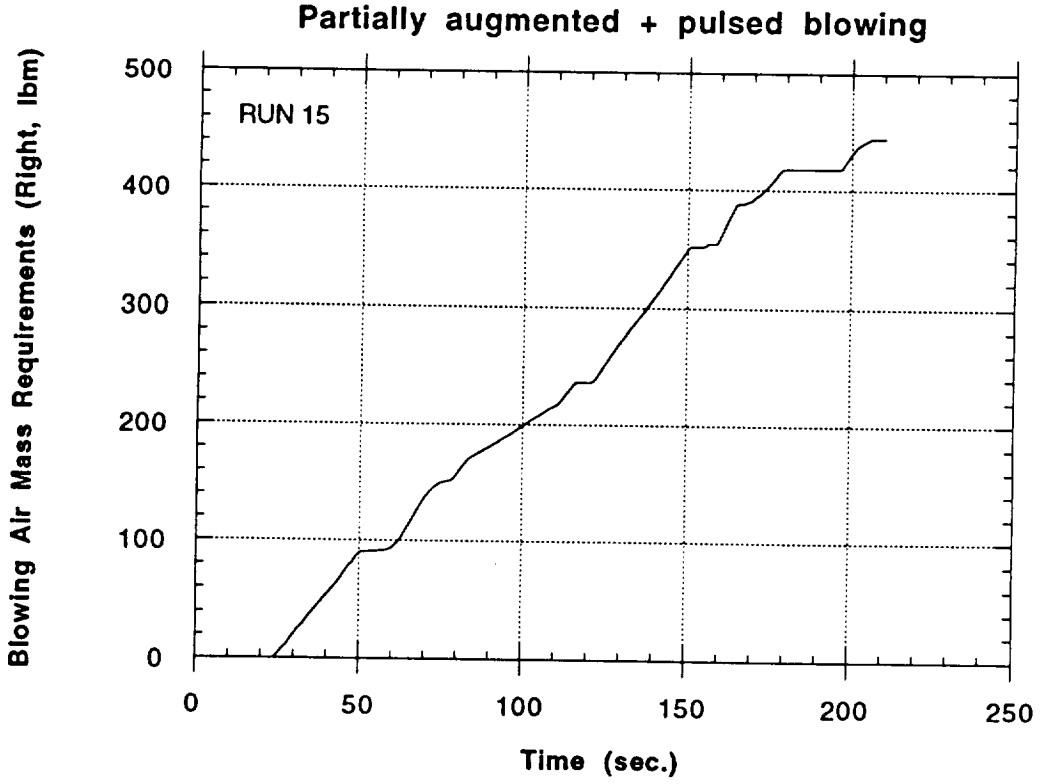

l) Accumulative Total Mass Flow Requirements (Right)

Figure 37 - Concluded

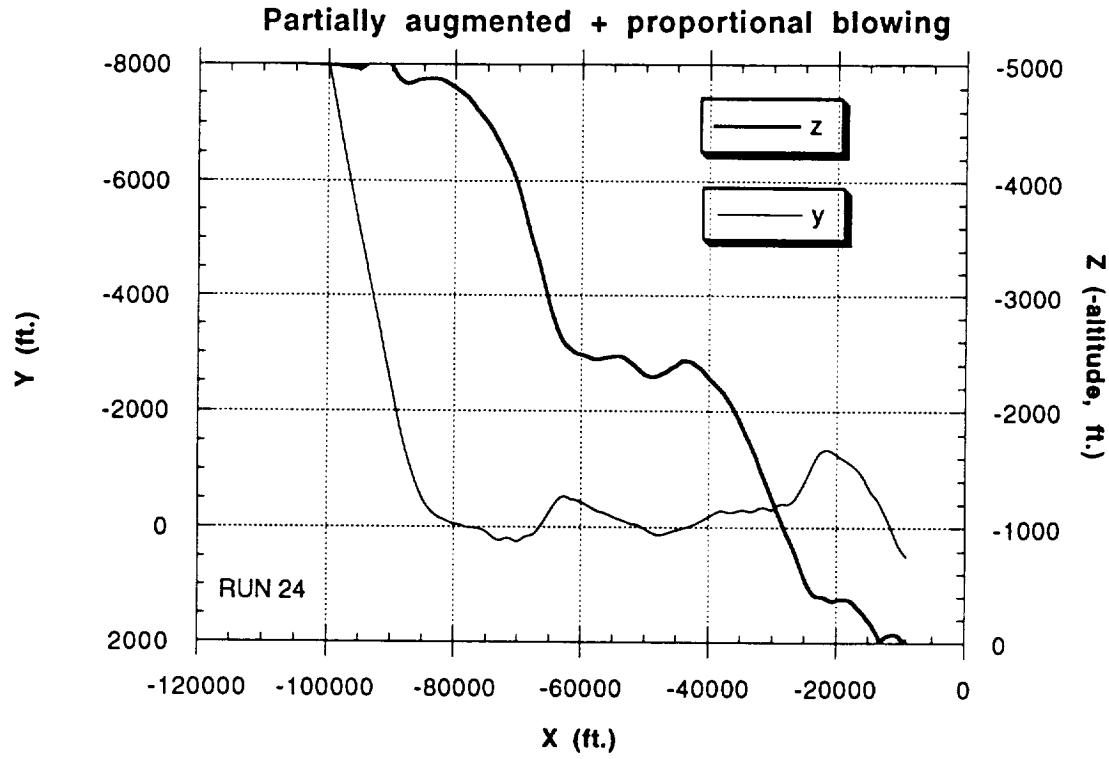

a) Variation in Altitude (-Z) and Horizontal Excursions (Y)

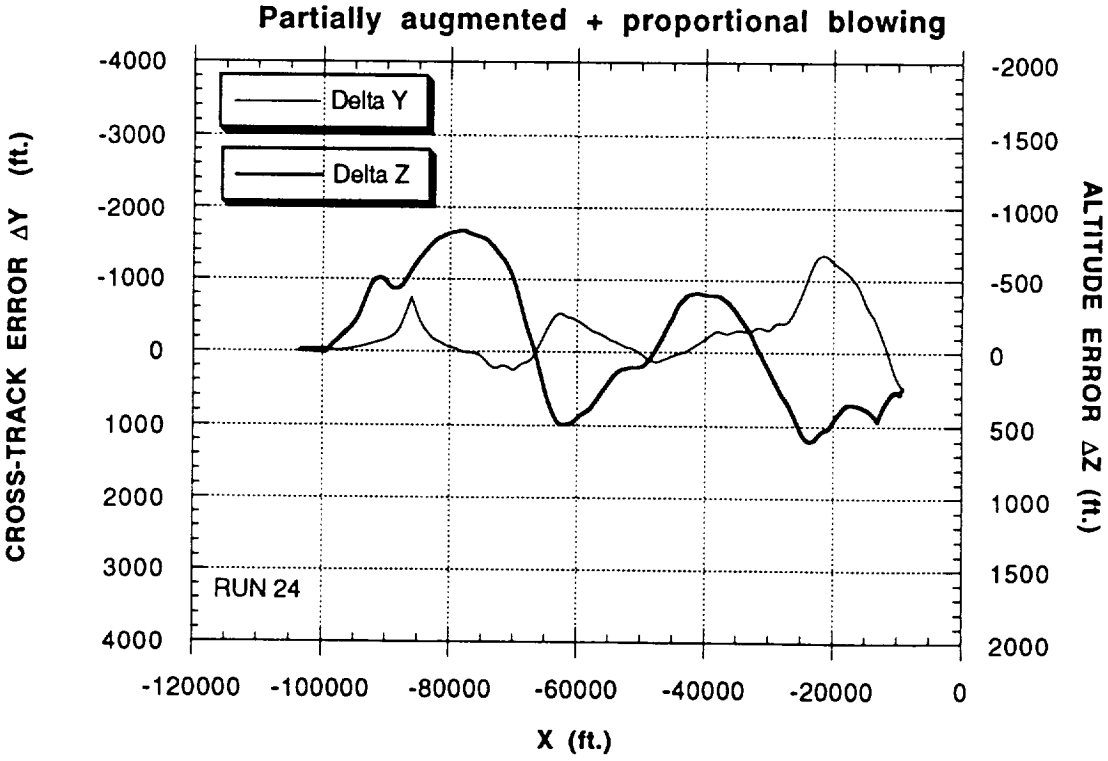

b) Cross-Track and Altitude Errors

Figure 38 - Approach and Landing Simulation for the NASP-type Configuration with Partially Augmented Flight Control System and Proportional Forebody Blowing

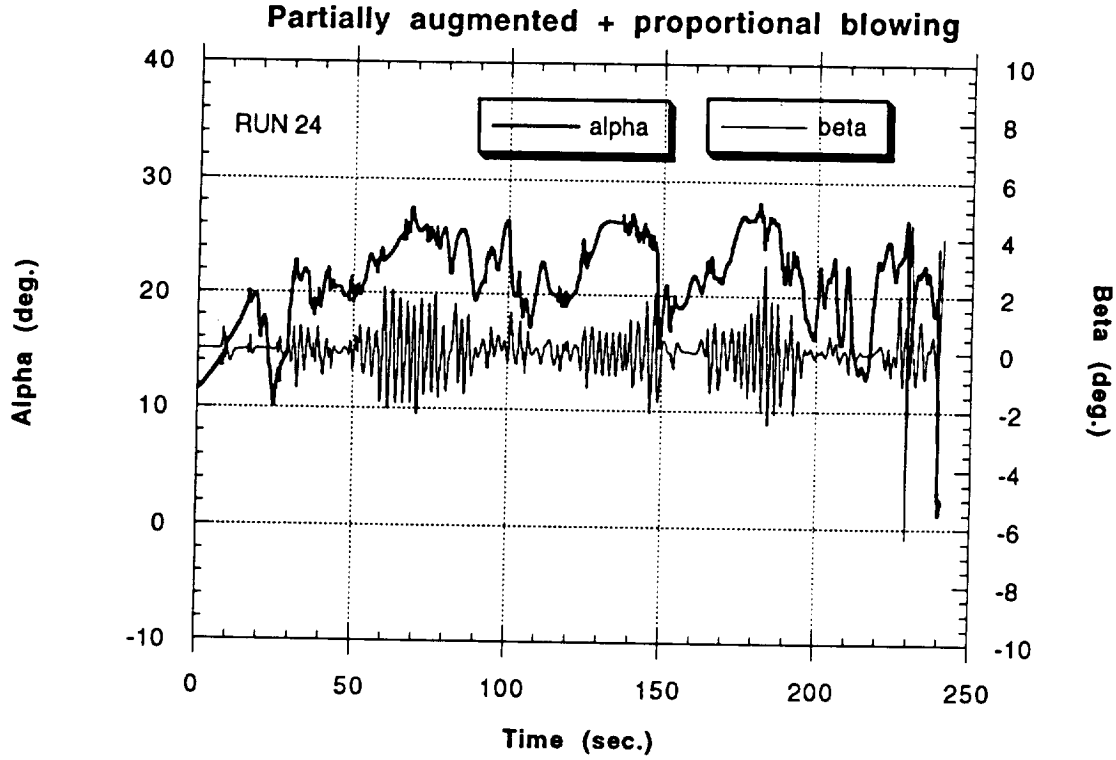

c) Angles of Attack and Sideslip

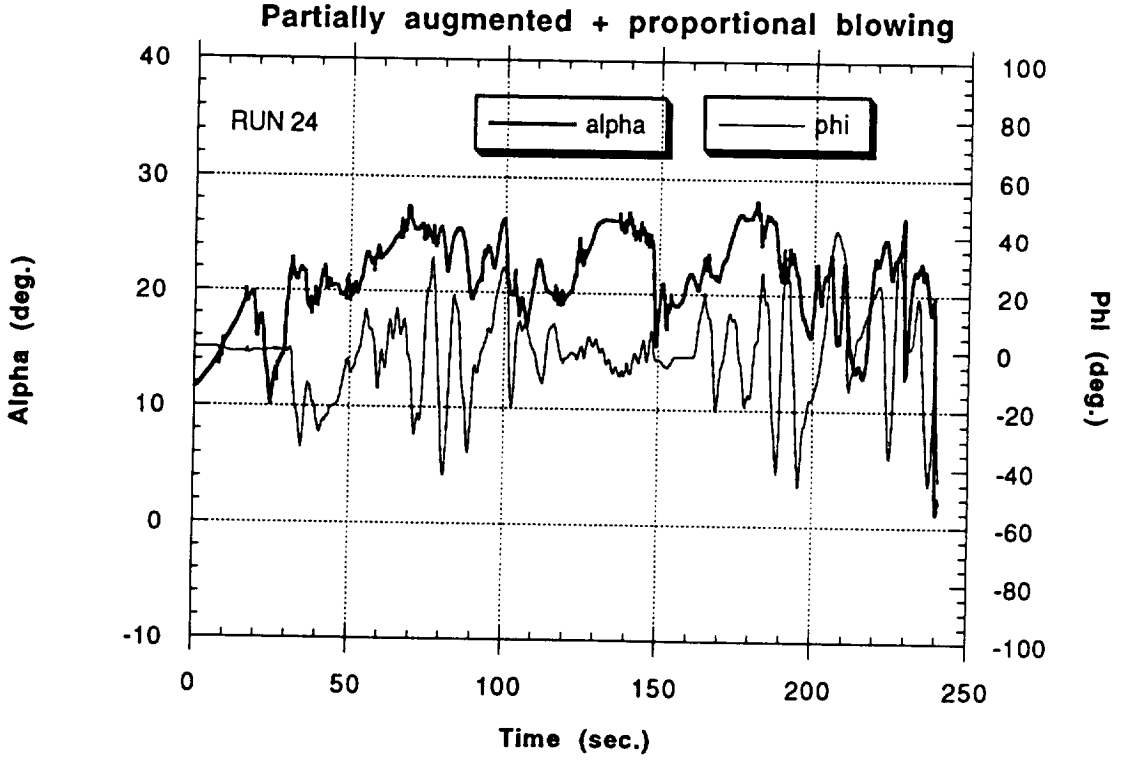

d) Angles of Attack and Roll

Figure 38 - Continued

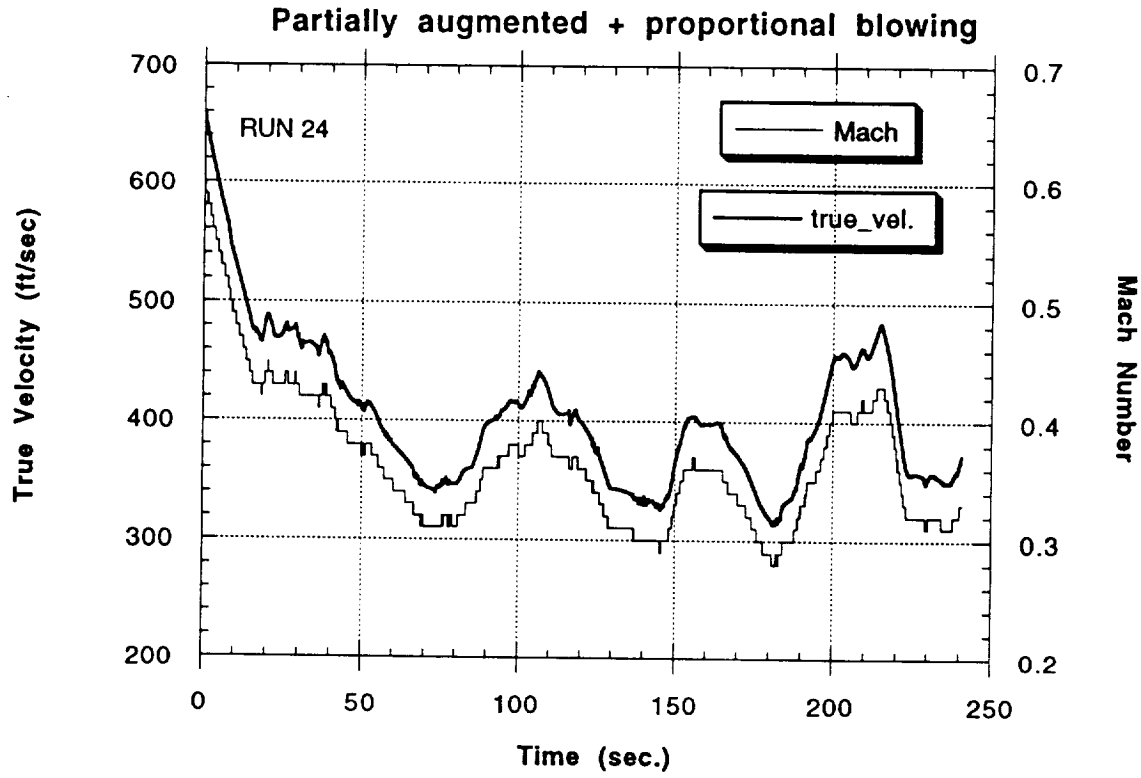

e) Flight Velocity and Mach Number

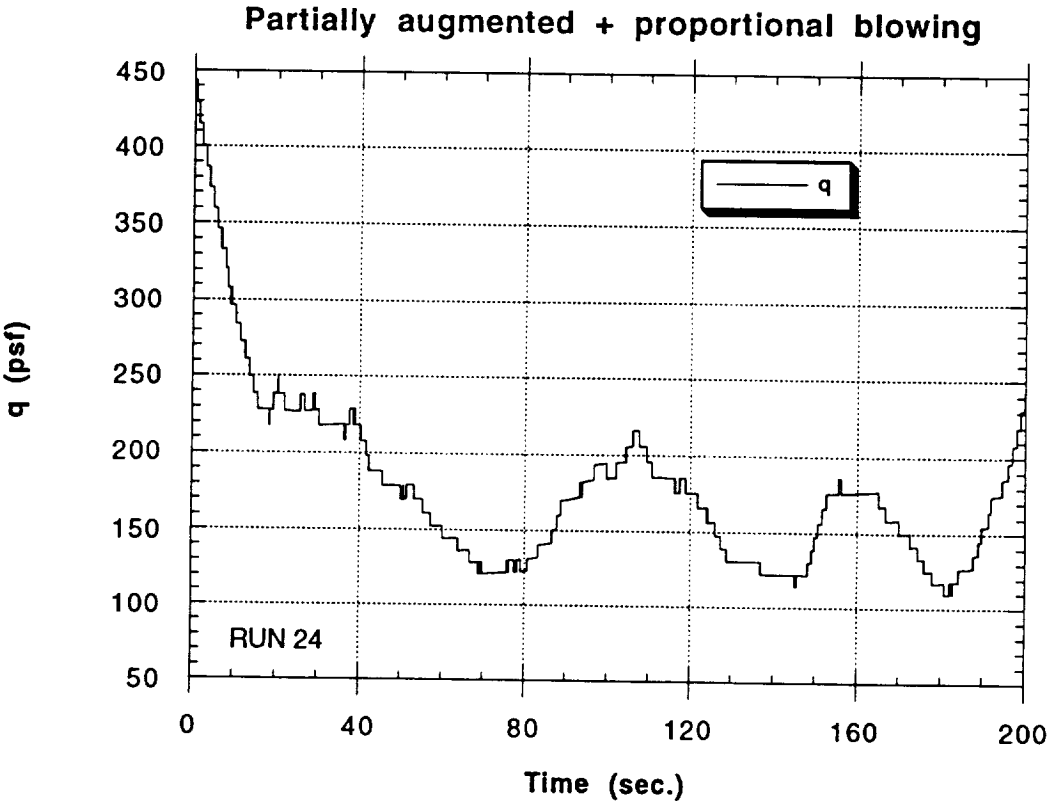

f) Dynamic Pressure

Figure 38 - Continued

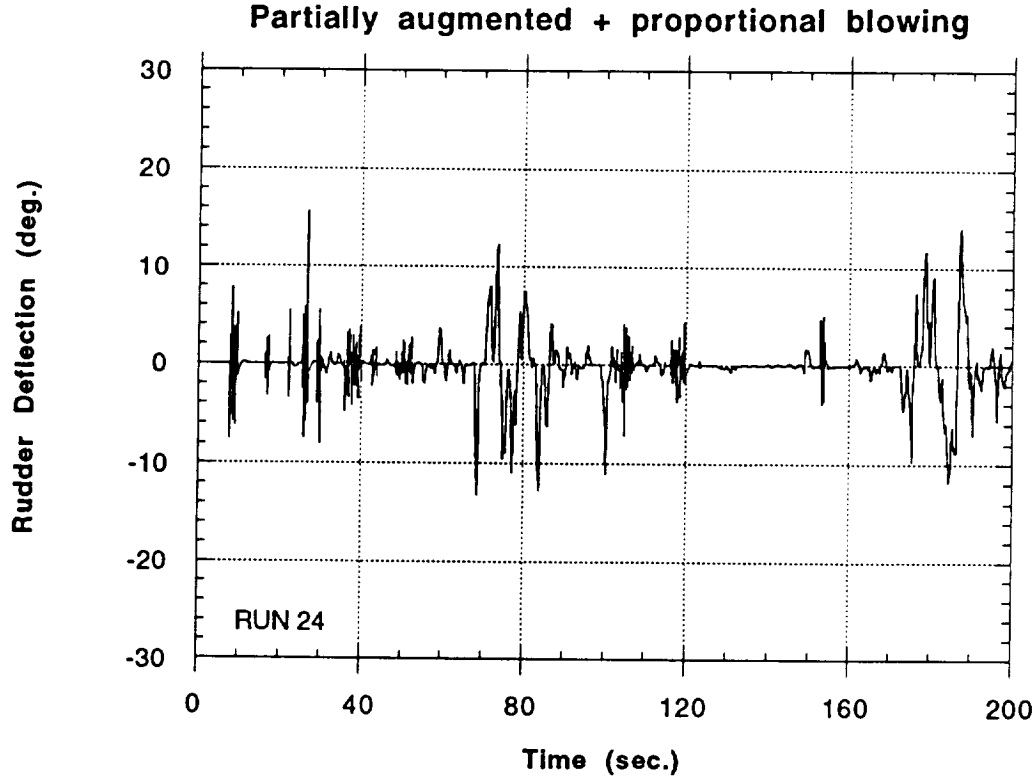

g) Rudder Deflection Angle

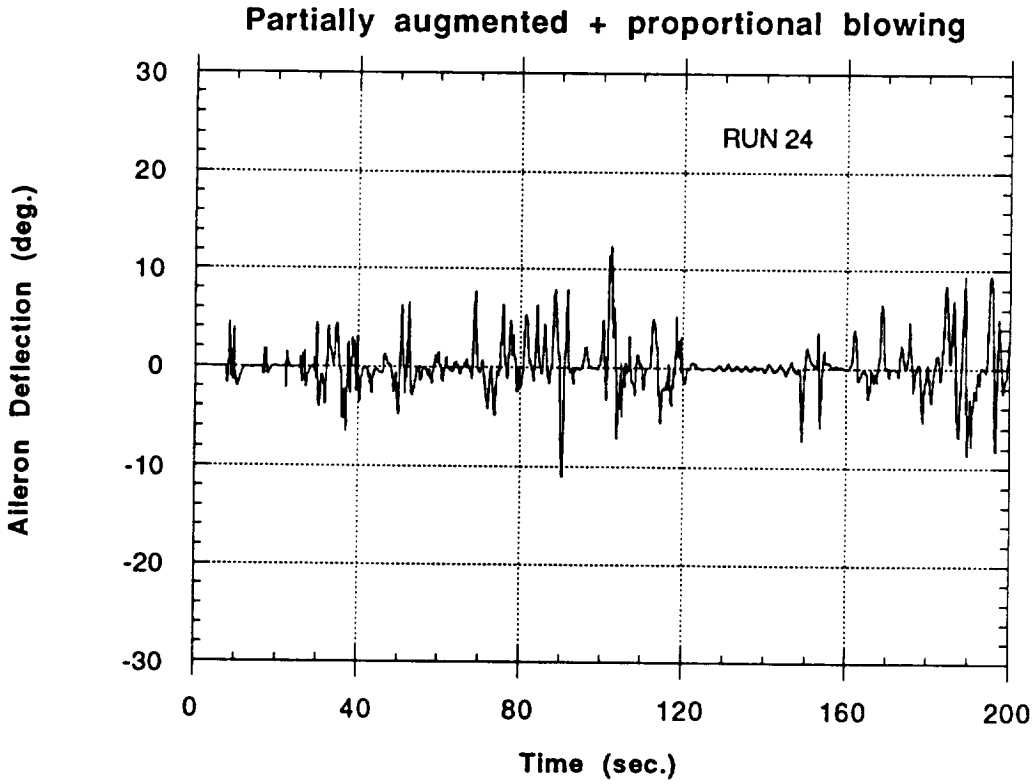

h) Aileron Deflection Angle

Figure 38 - Continued

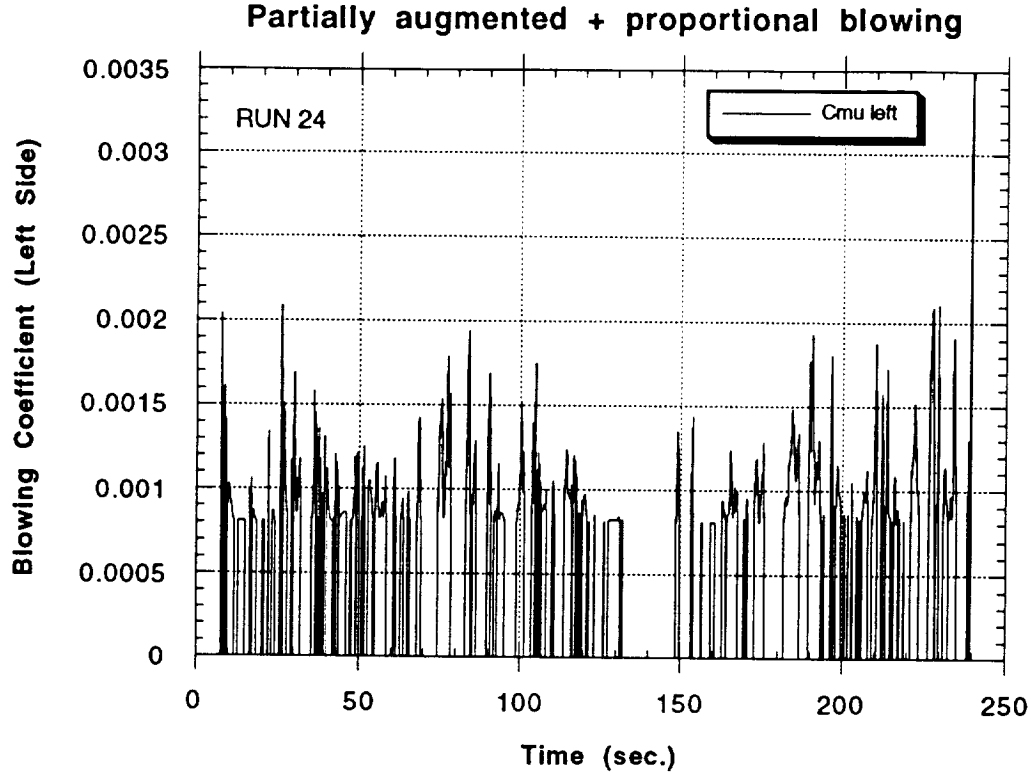

i) Blowing Coefficient (Left Nozzle)

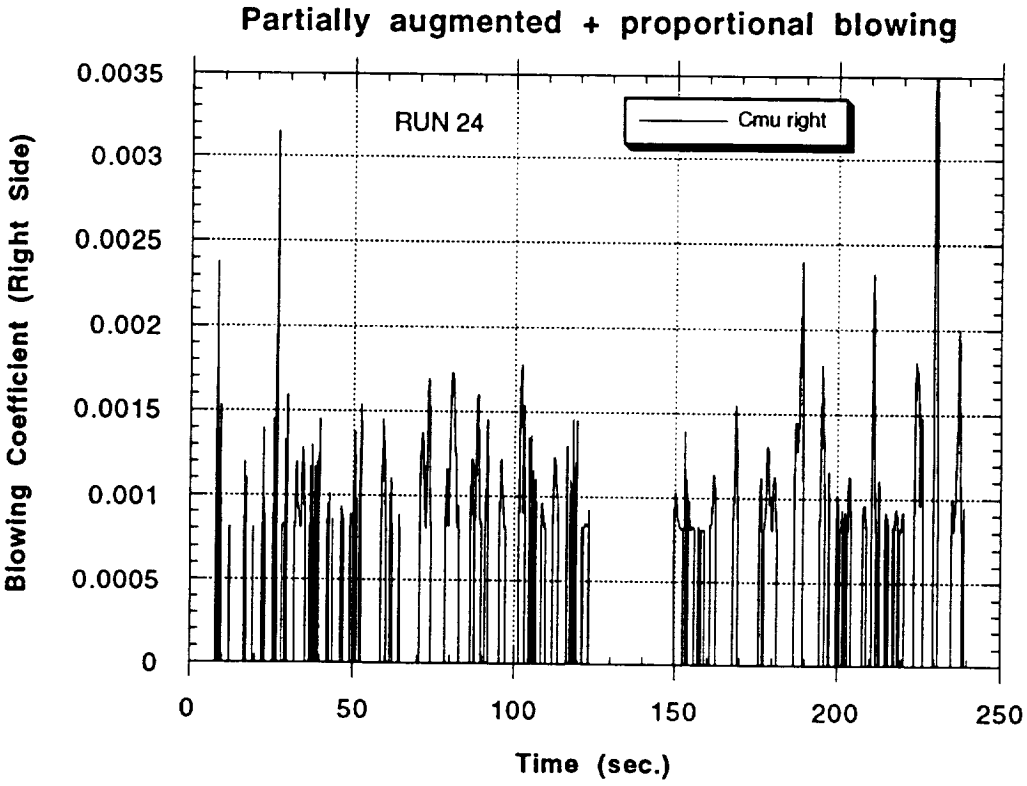

j) Blowing Coefficient (Right Nozzle)

Figure 38 - Continued

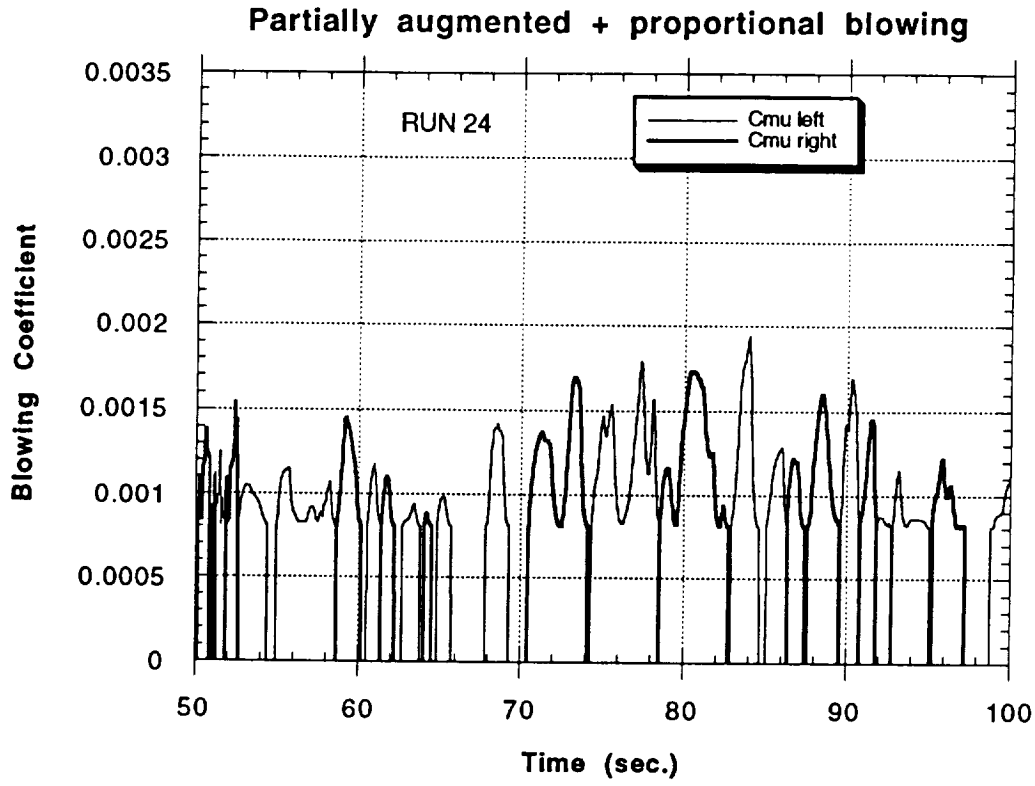

k) Blowing Coefficient (Expanded Time Scale)

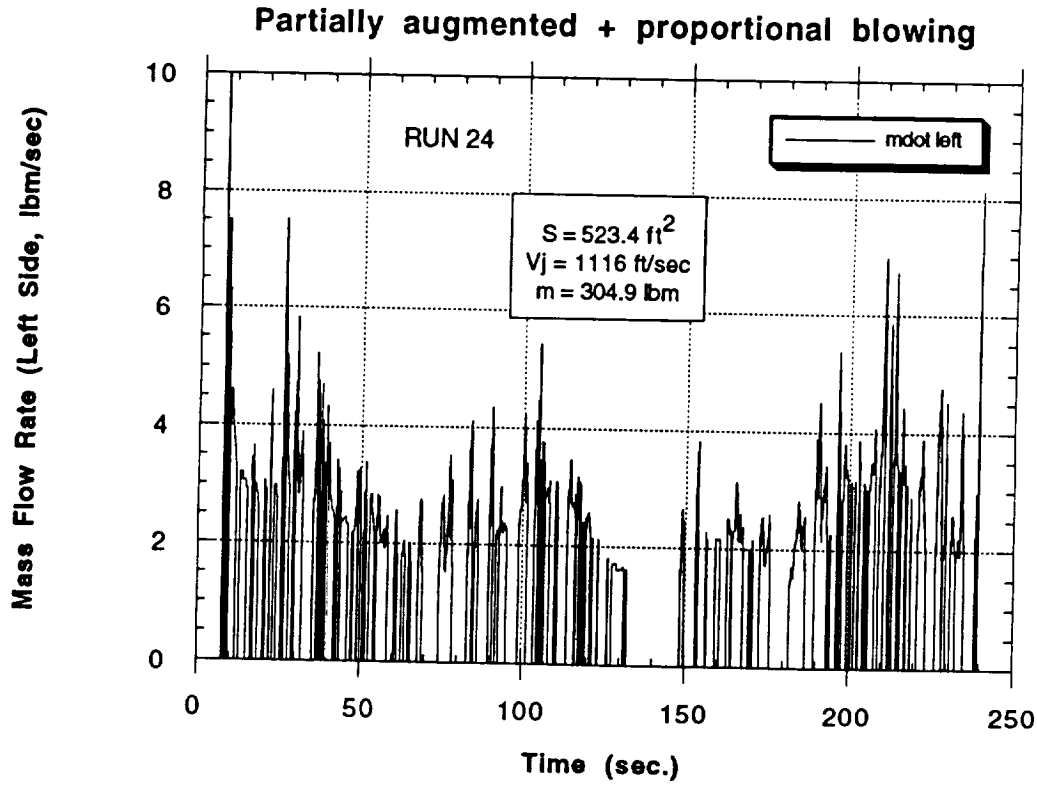

l) Mass Flow Rate (Left Nozzle)

Figure 38 - Continued

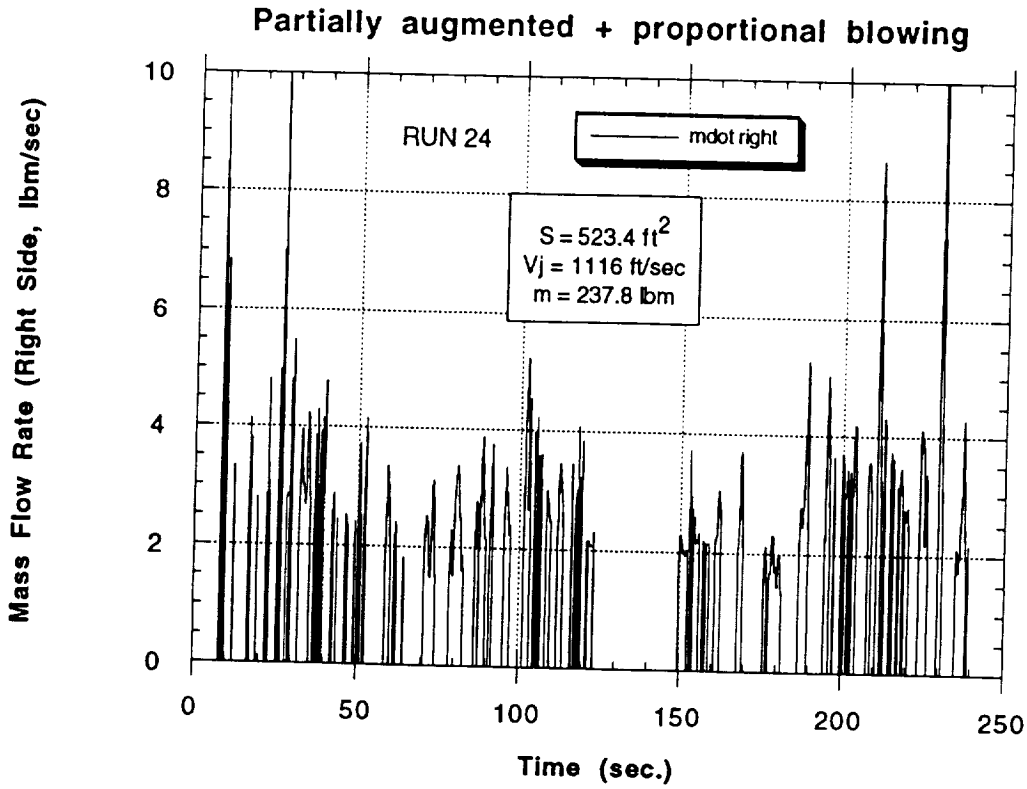

m) Mass Flow Rate (Right Nozzle)

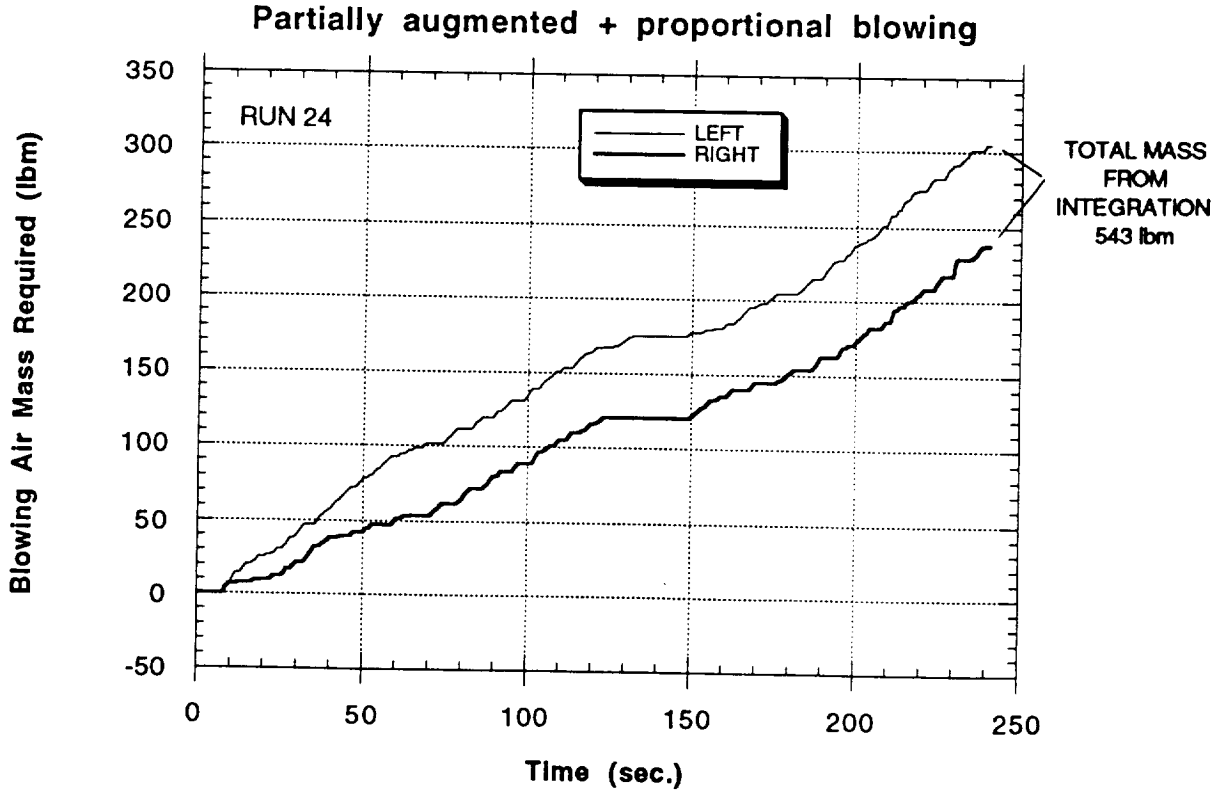

n) Accumulative Total Mass Flow Requirements (Left and Right)

Figure 38 - Concluded

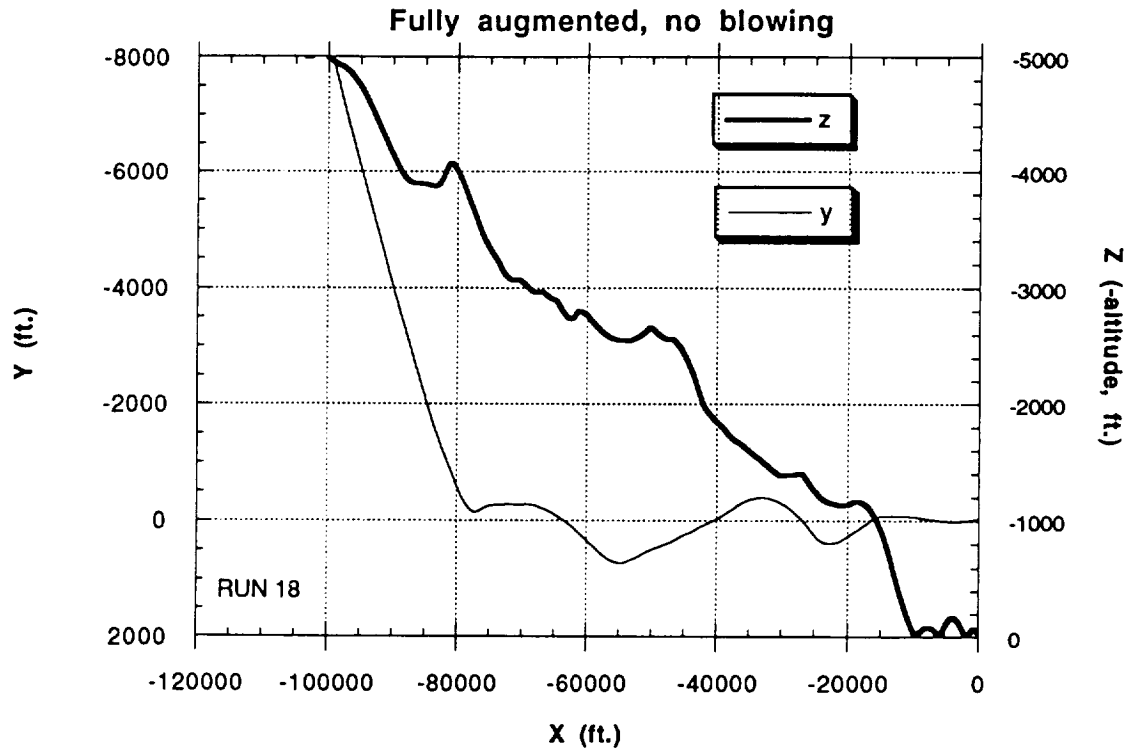

a) Variation in Altitude (-Z) and Horizontal Excursions (Y)

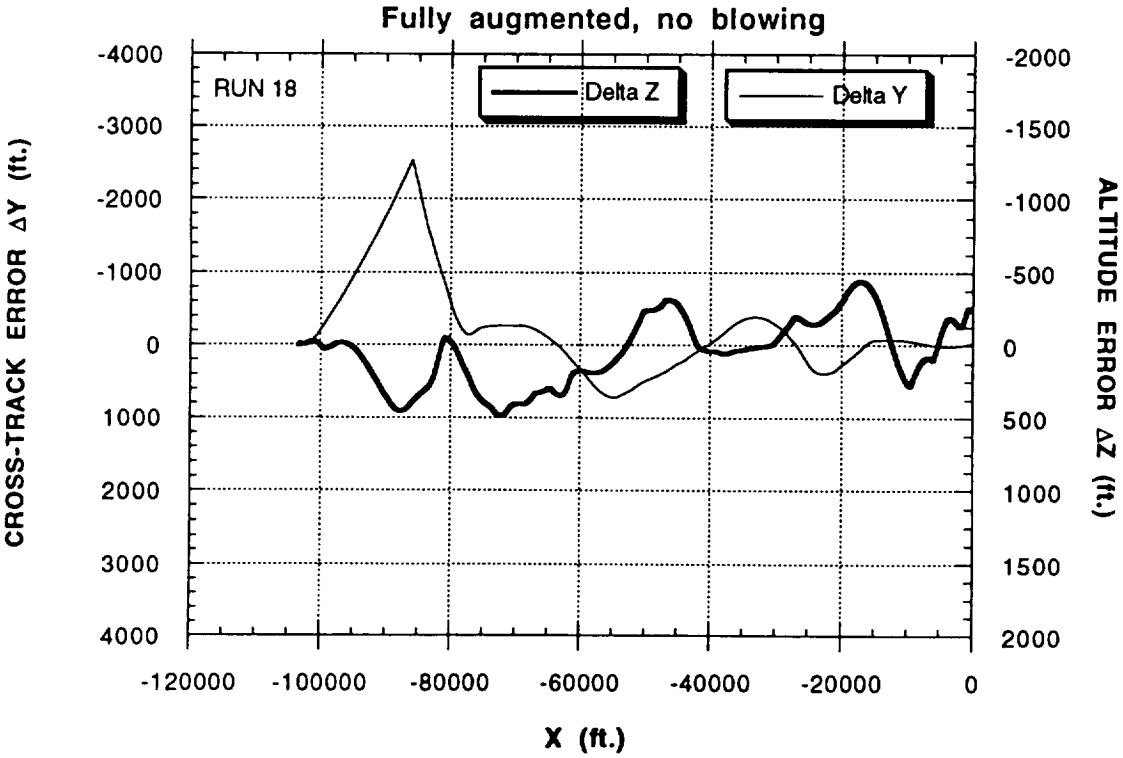

b) Cross-Track and Altitude Errors

Figure 39 - Approach and Landing Simulation for the NASP-type Configuration with Fully Augmented Flight Control System (No Forebody Blowing)

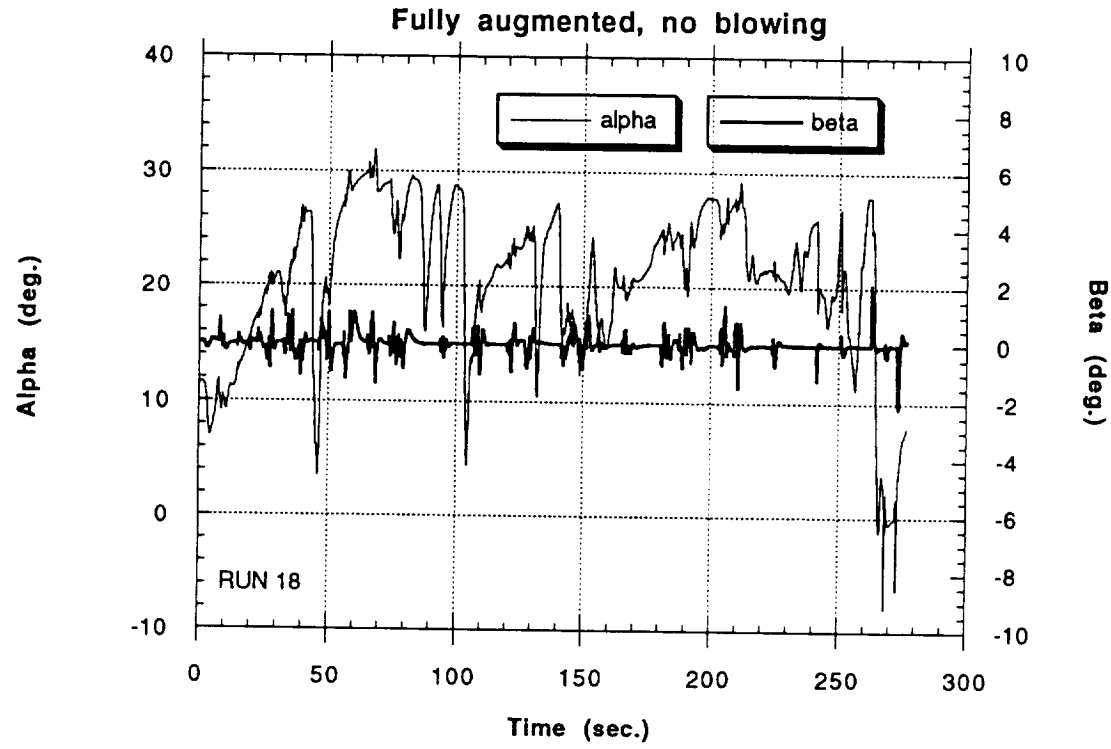

c) Angles of Attack and Sideslip

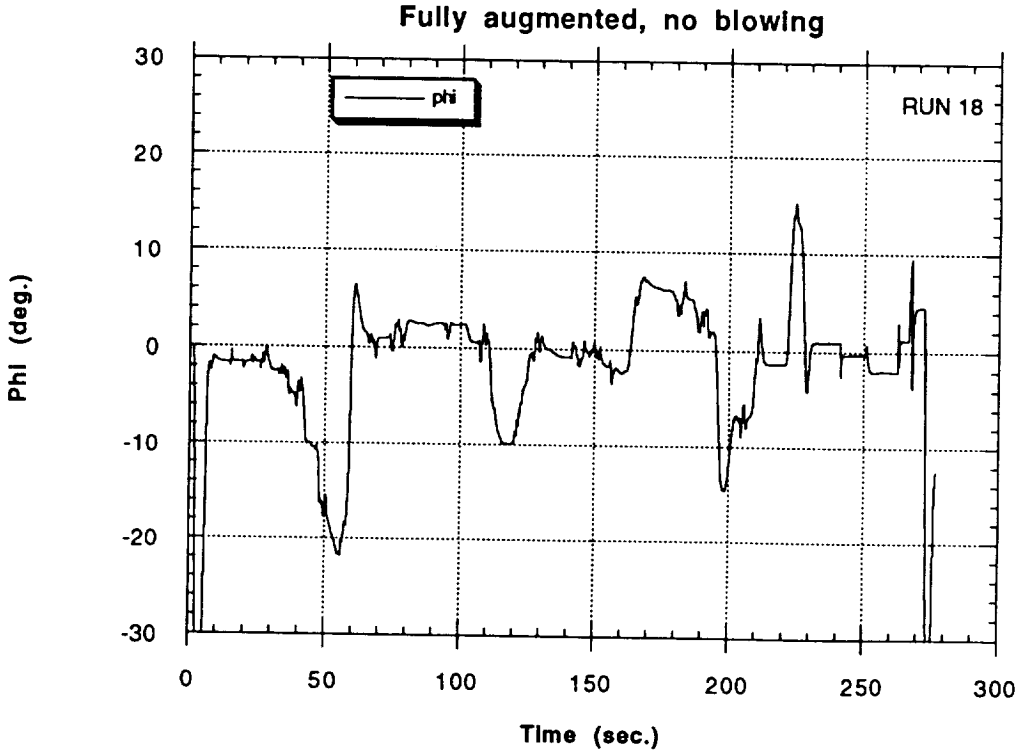

d) Roll Angle

Figure 39 - Continued

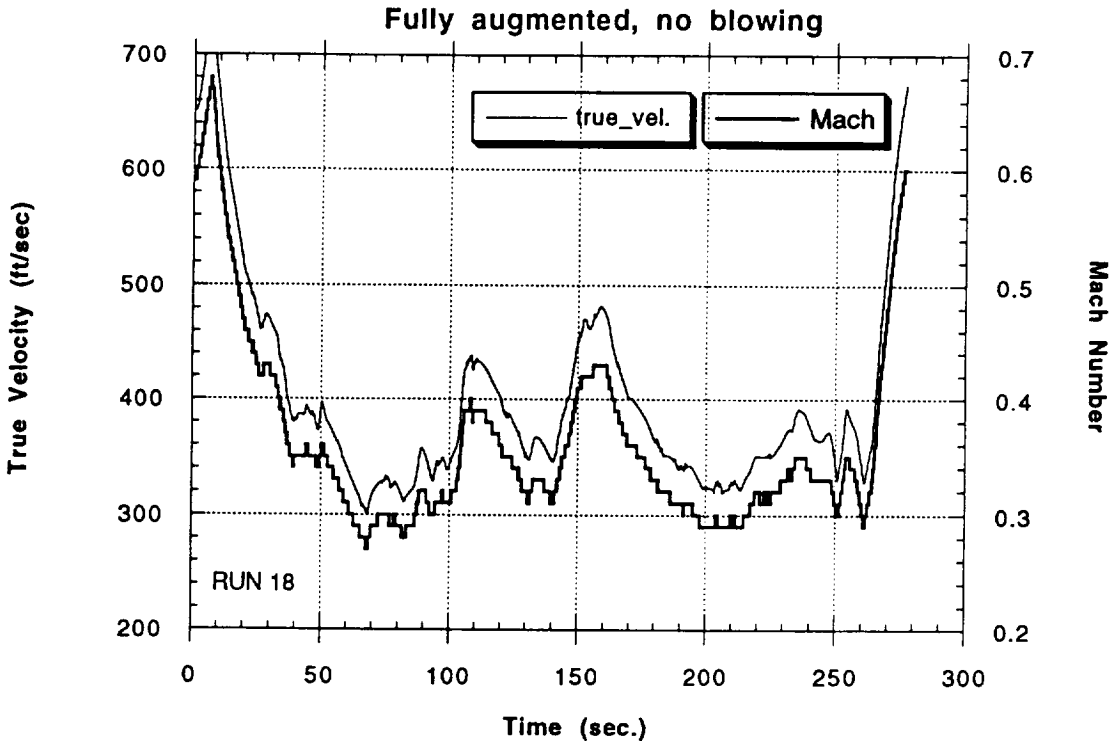

e) Flight Velocity and Mach Number

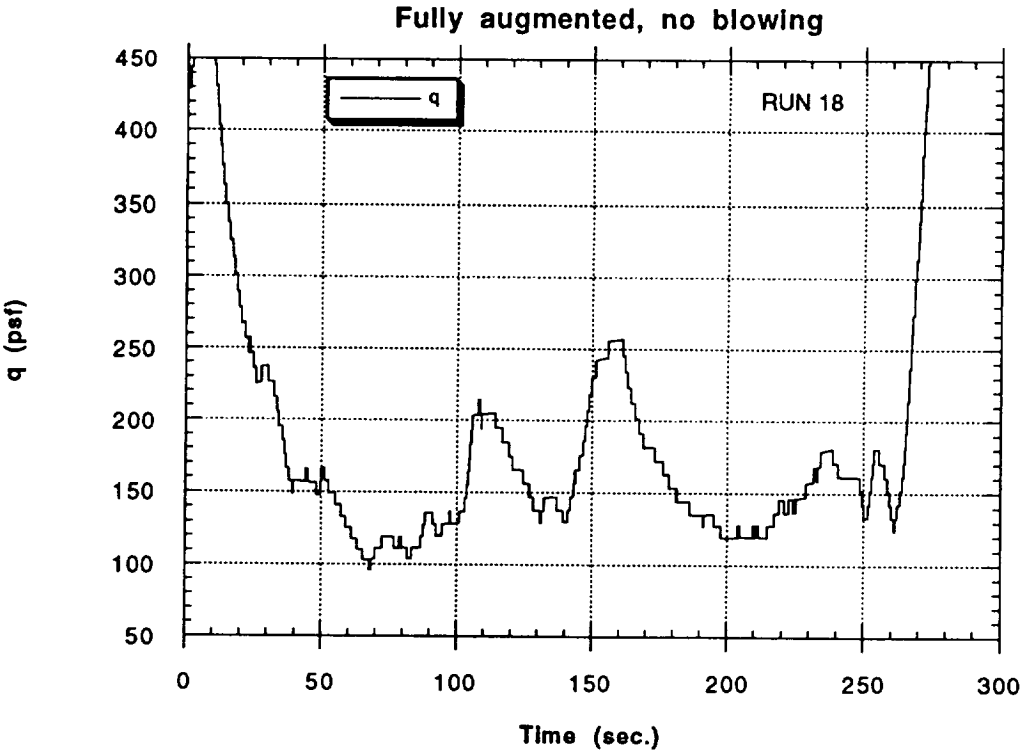

f) Dynamic Pressure

Figure 39 - Continued

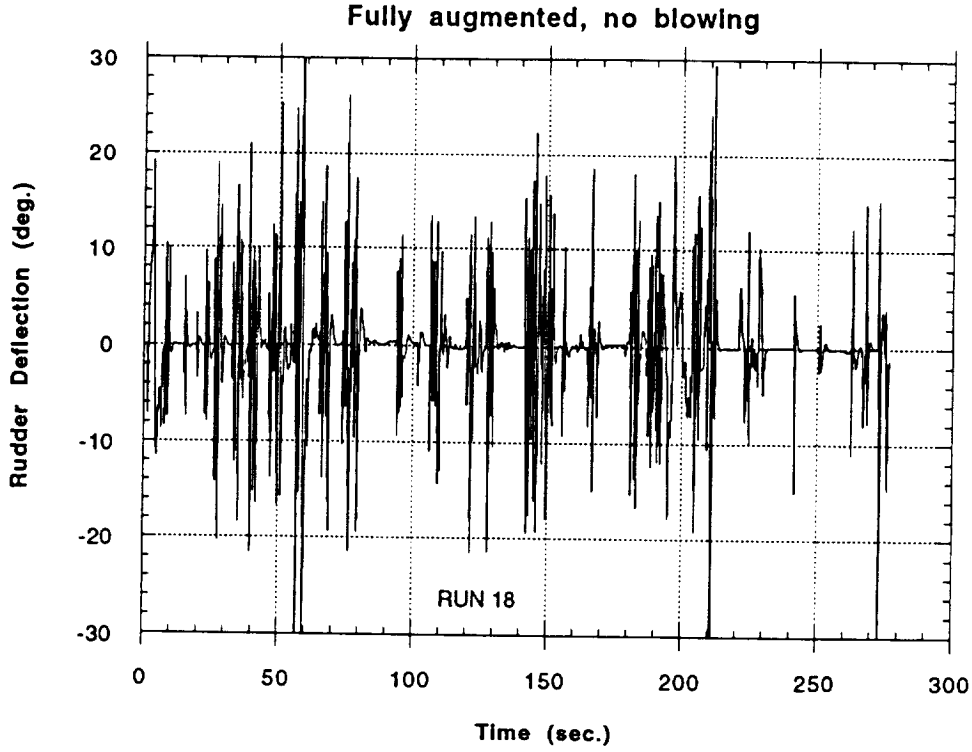

g) Rudder Deflection Angle

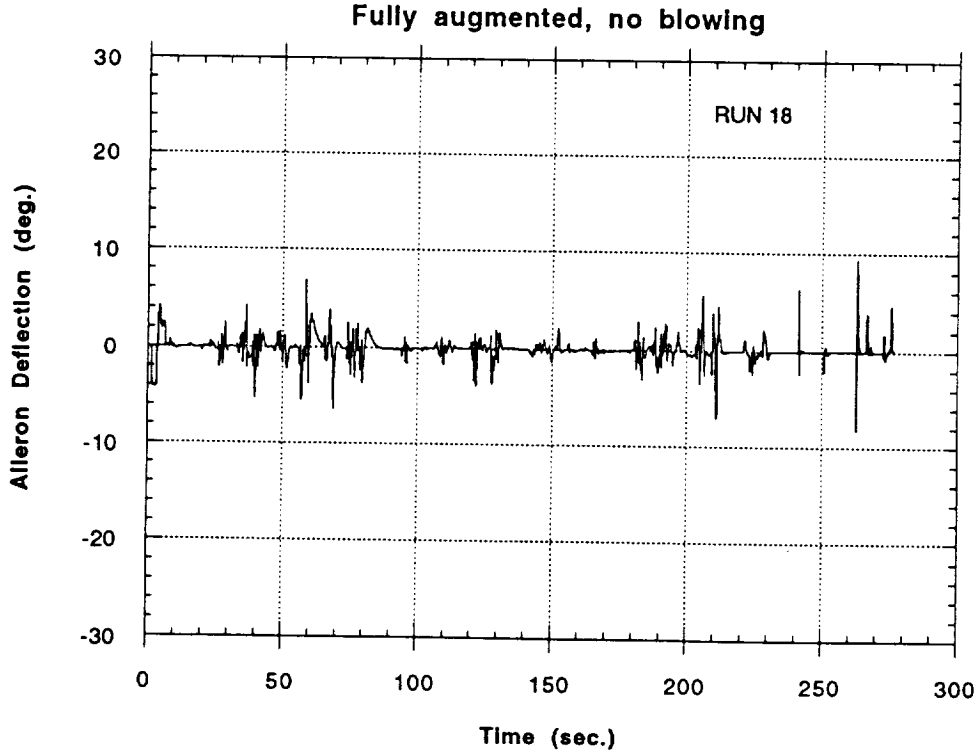

h) Aileron Deflection Angle

Figure 39 - Concluded

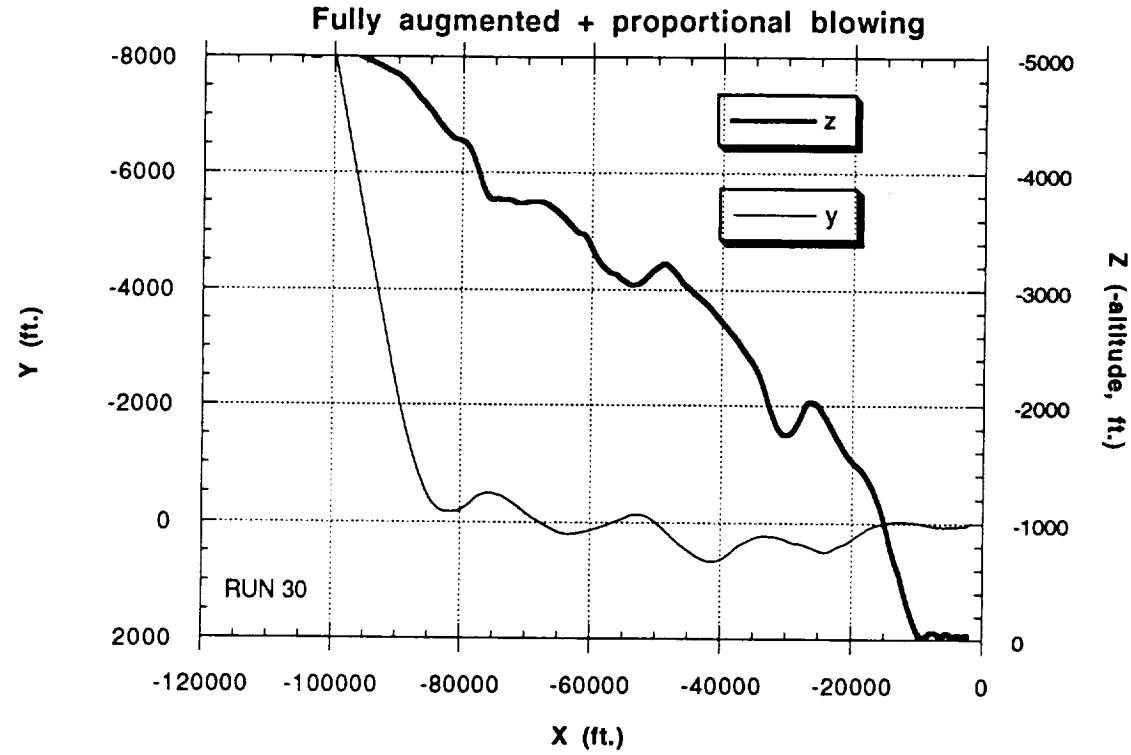

a) Variation in Altitude (-Z) and Horizontal Excursions (Y)

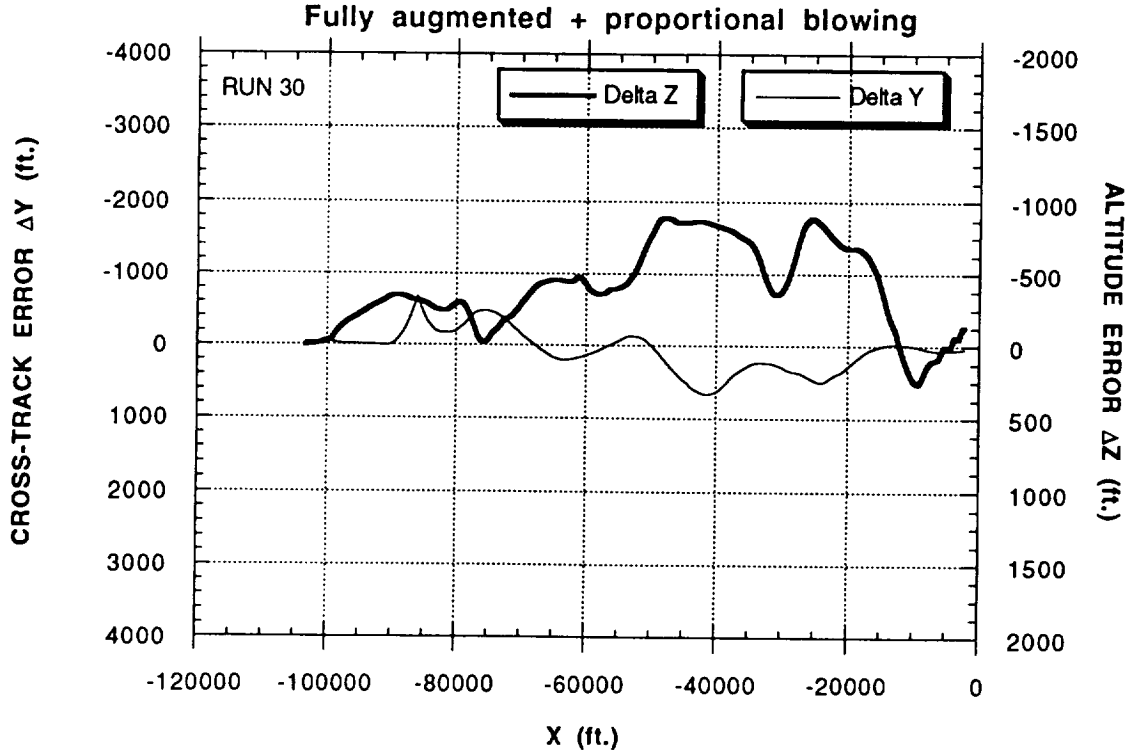

b) Cross-Track and Altitude Errors

Figure 40 - Approach and Landing Simulation for the NASP-type Configuration with Fully Augmented Flight Control System and Proportional Forebody Blowing

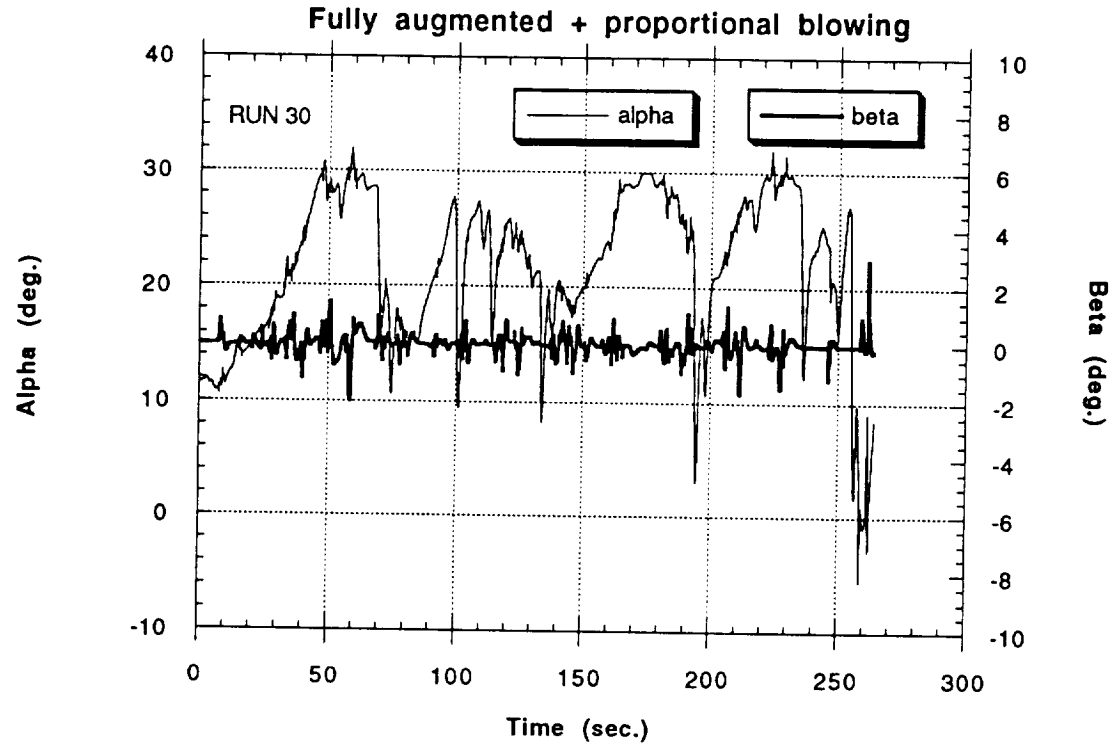

c) Angles of Attack and Sideslip

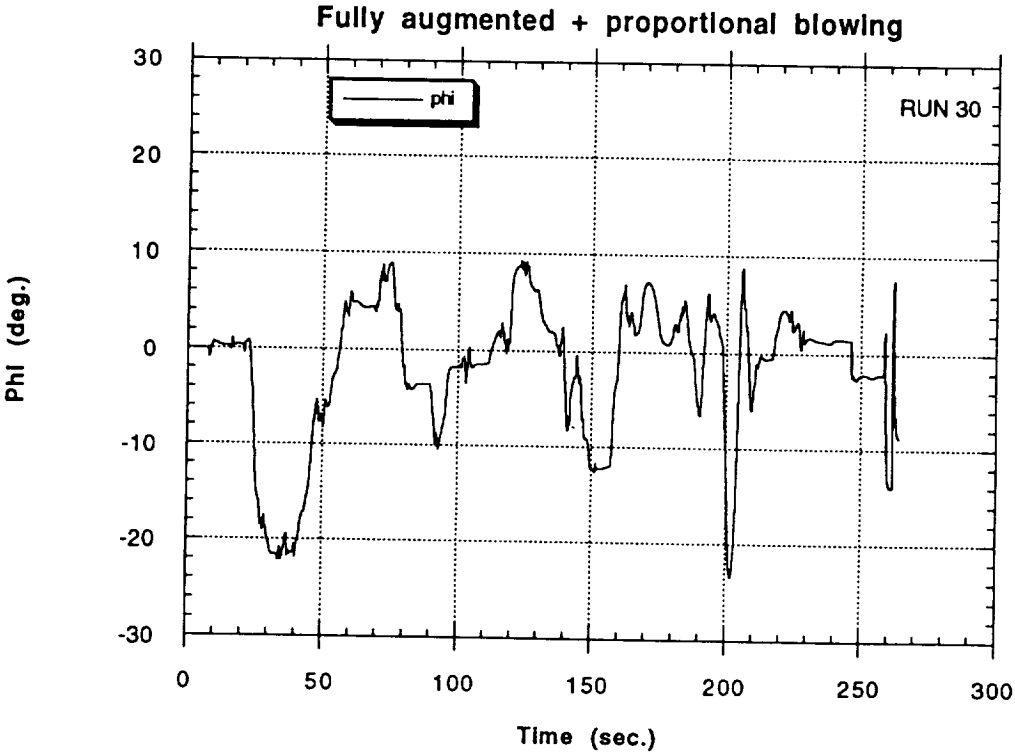

d) Roll Angle

Figure 40 - Continued

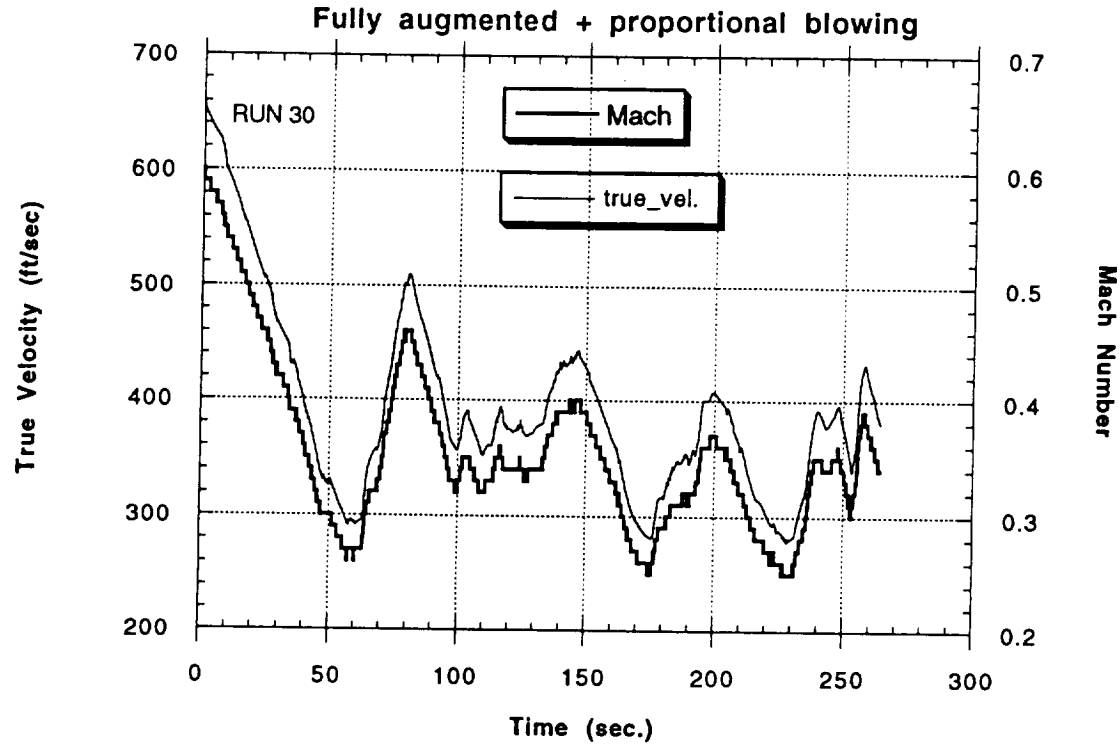

e) Flight Velocity and Mach Number

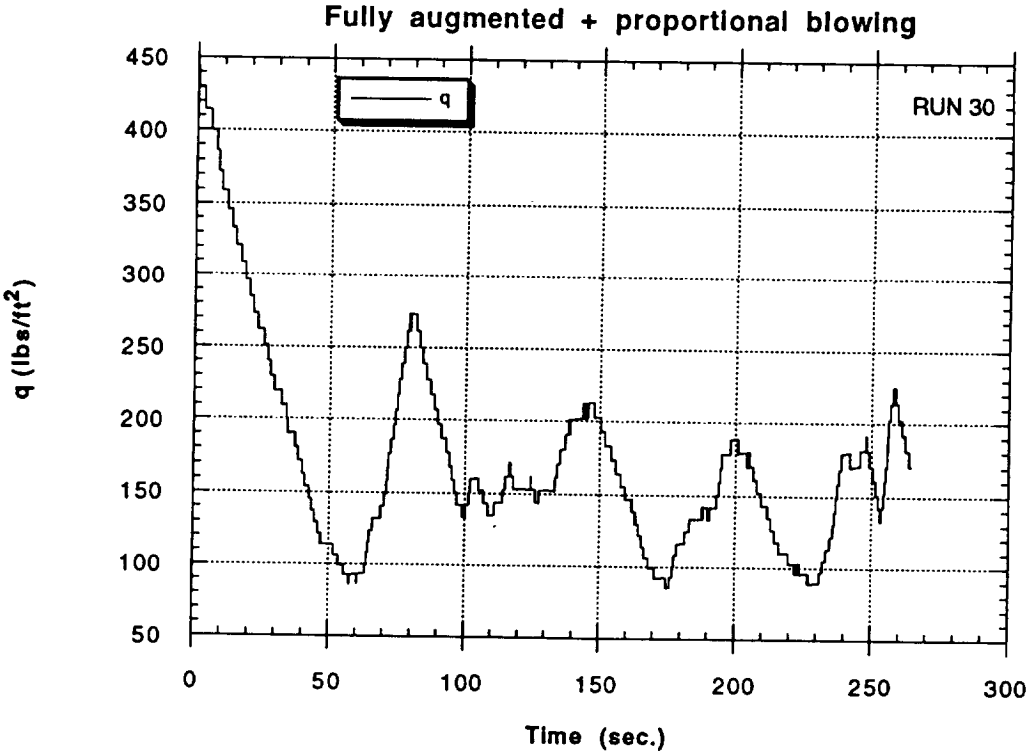

f) Dynamic Pressure

Figure 40 - Continued

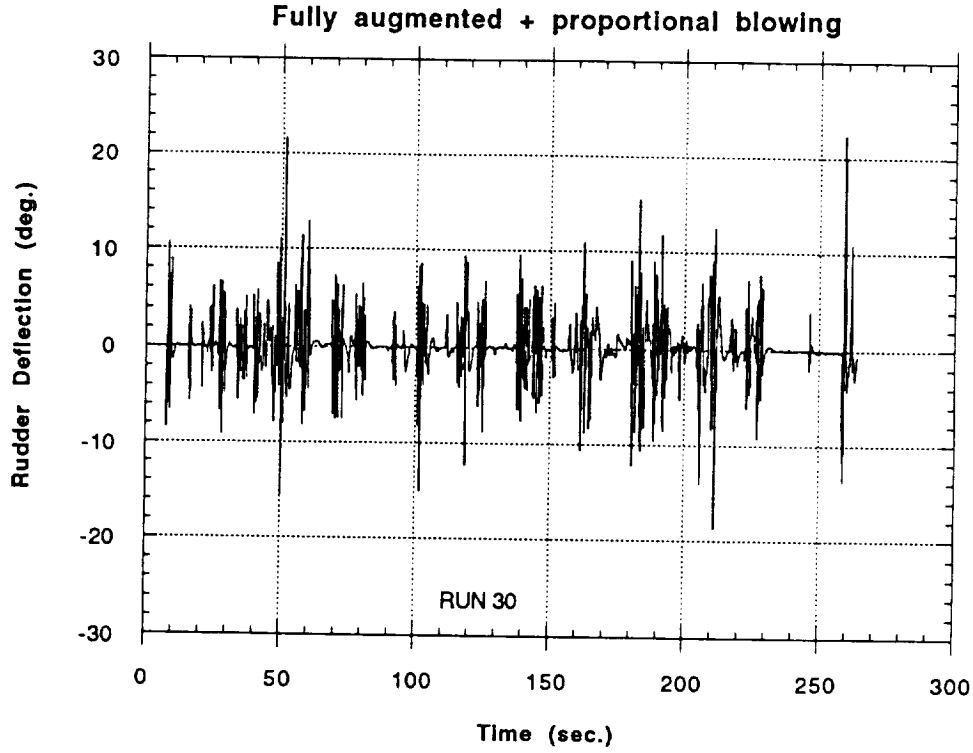

g) Rudder Deflection Angle

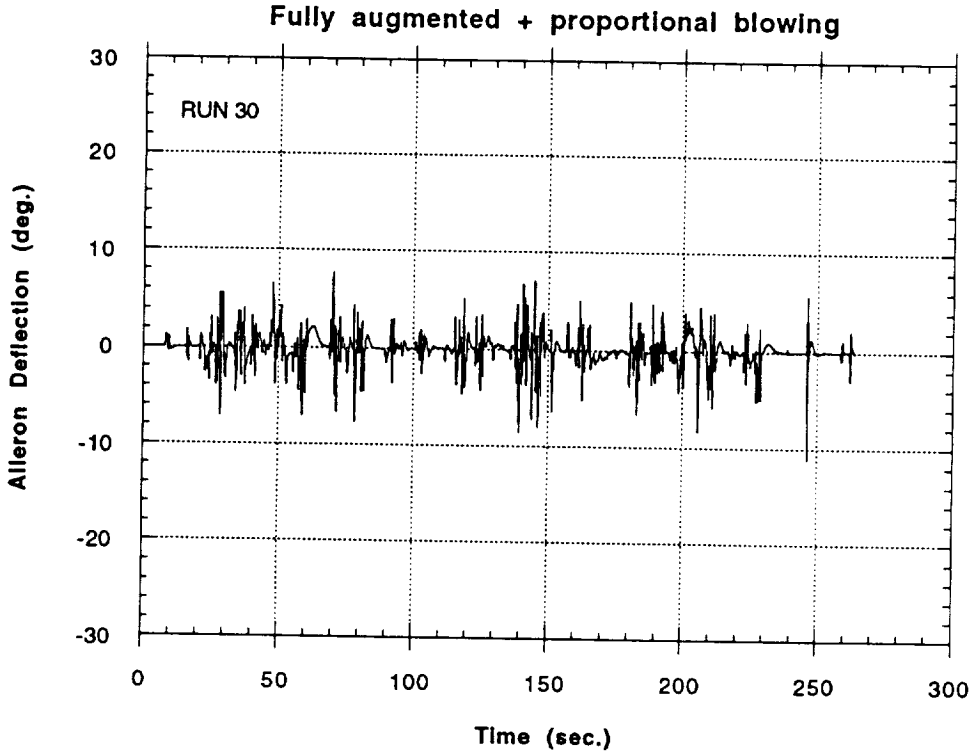

h) Aileron Deflection Angle

Figure 40 - Continued

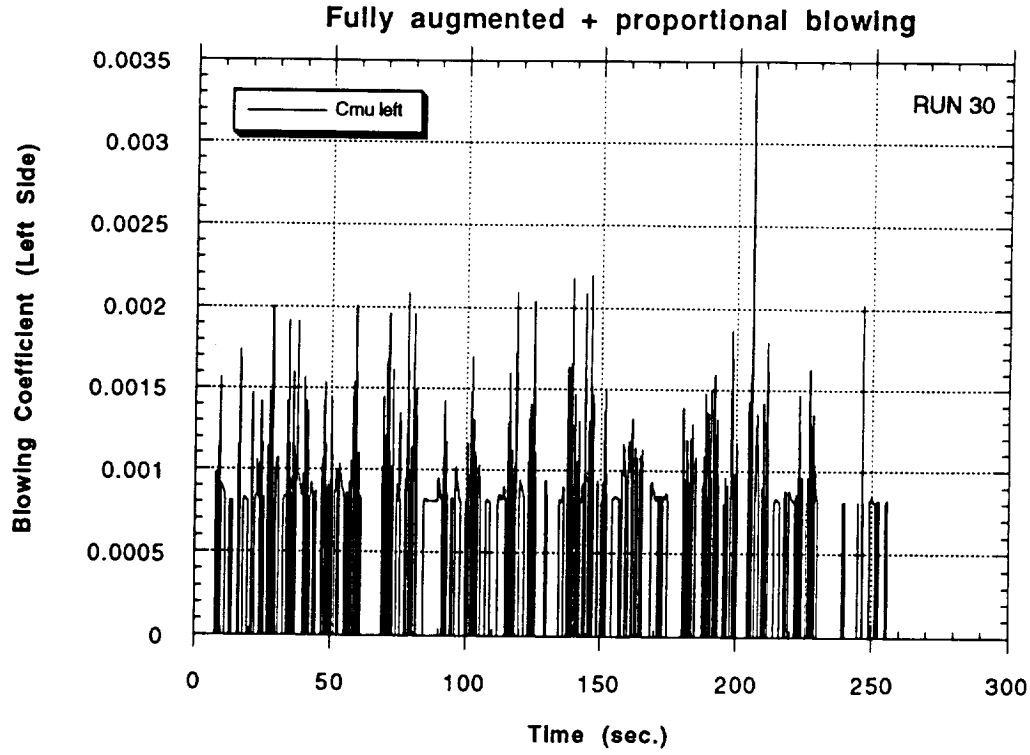

i) Blowing Coefficient (Left Nozzle)

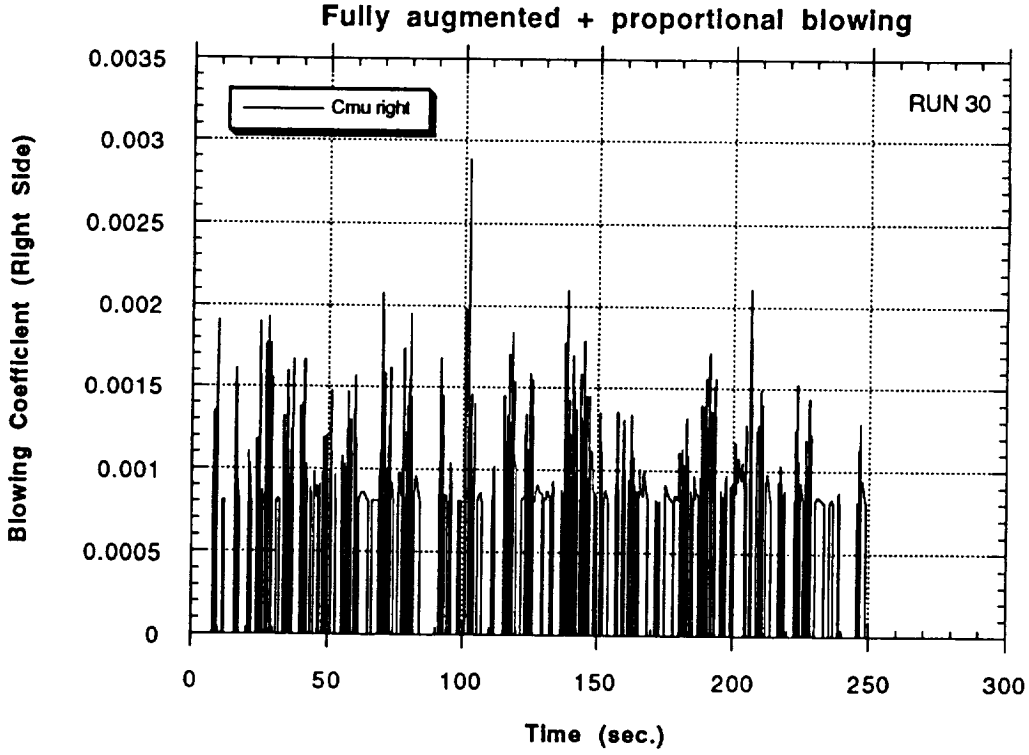

j) Blowing Coefficient (Right Nozzle)

Figure 40 - Continued

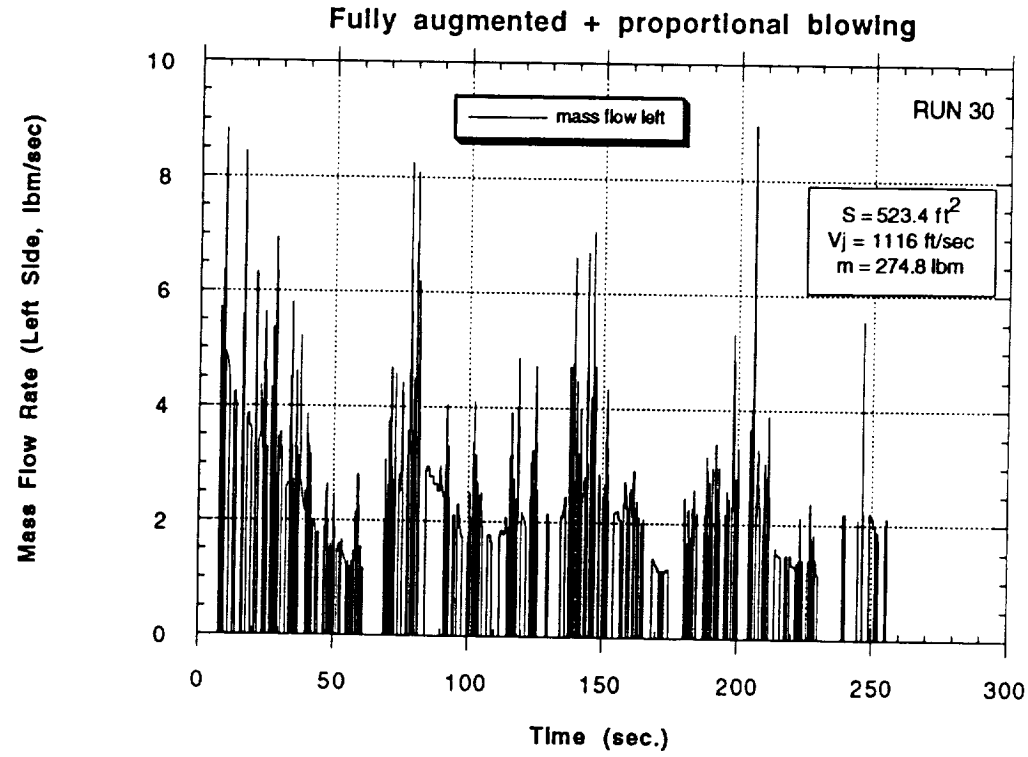

k) Mass Flow Rate (Left Nozzle)

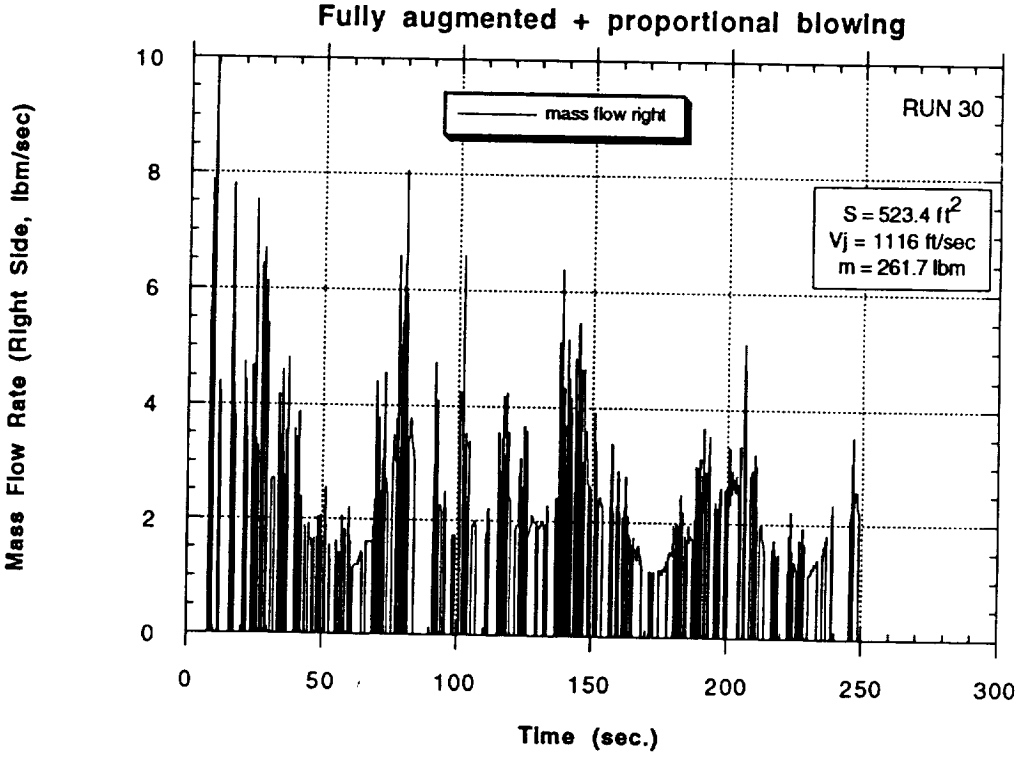

l) Mass Flow Rate (Right Nozzle)

Figure 40 - Continued

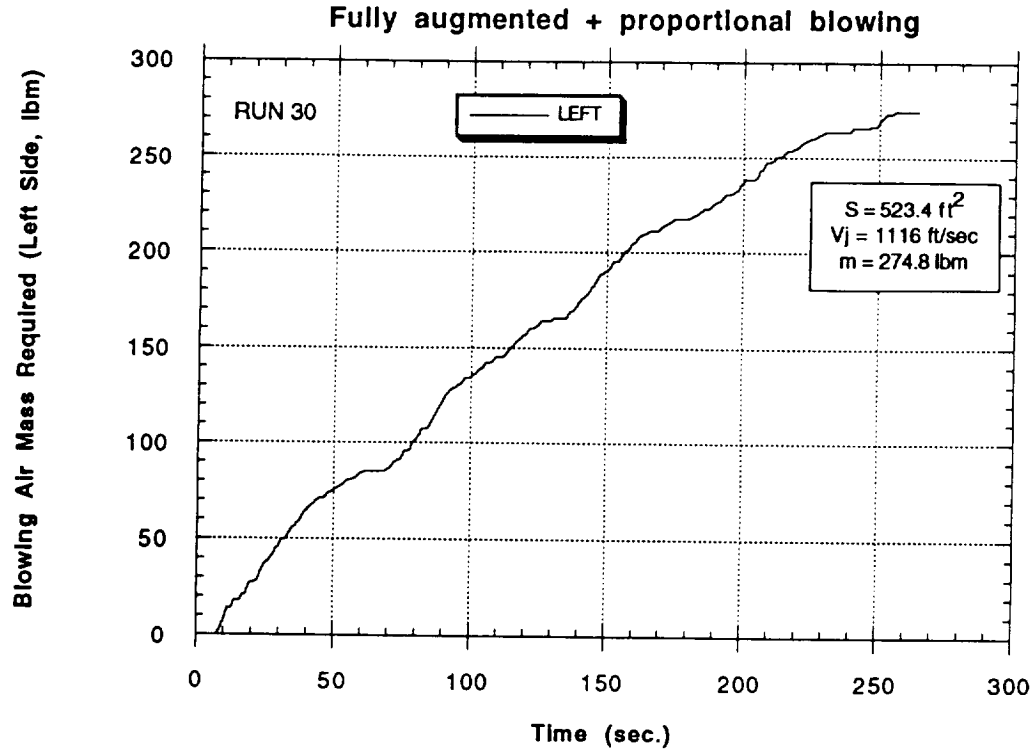

m) Accumulative Total Mass Flow Requirements (Left)

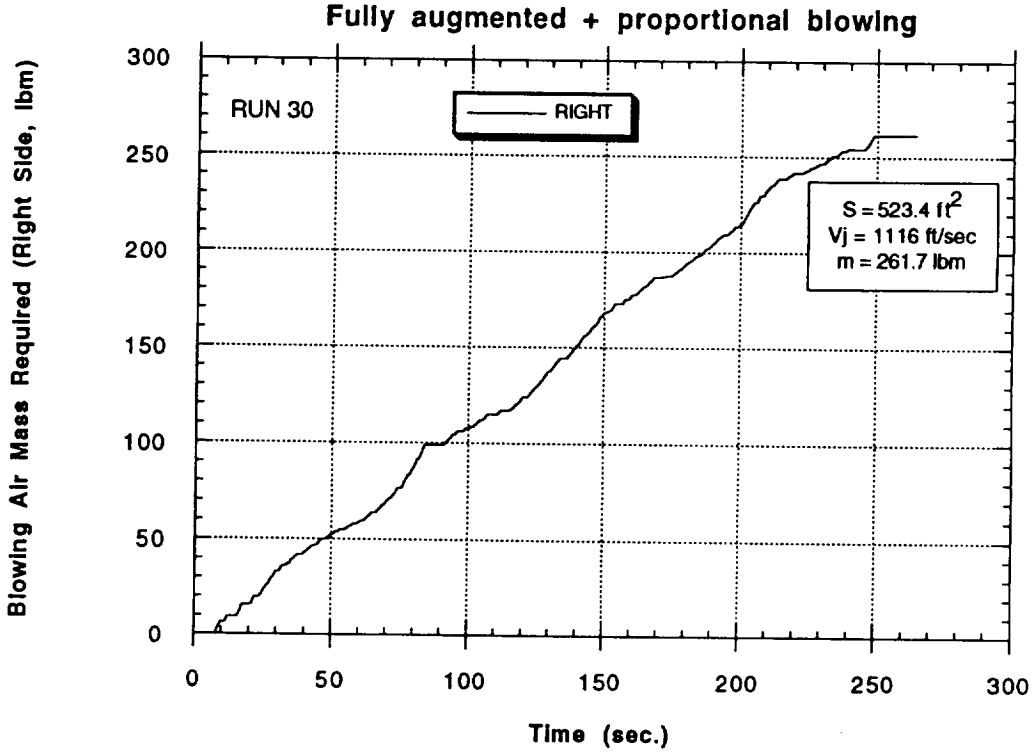

n) Accumulative Total Mass Flow Requirements (Right)

Figure 40 - Concluded

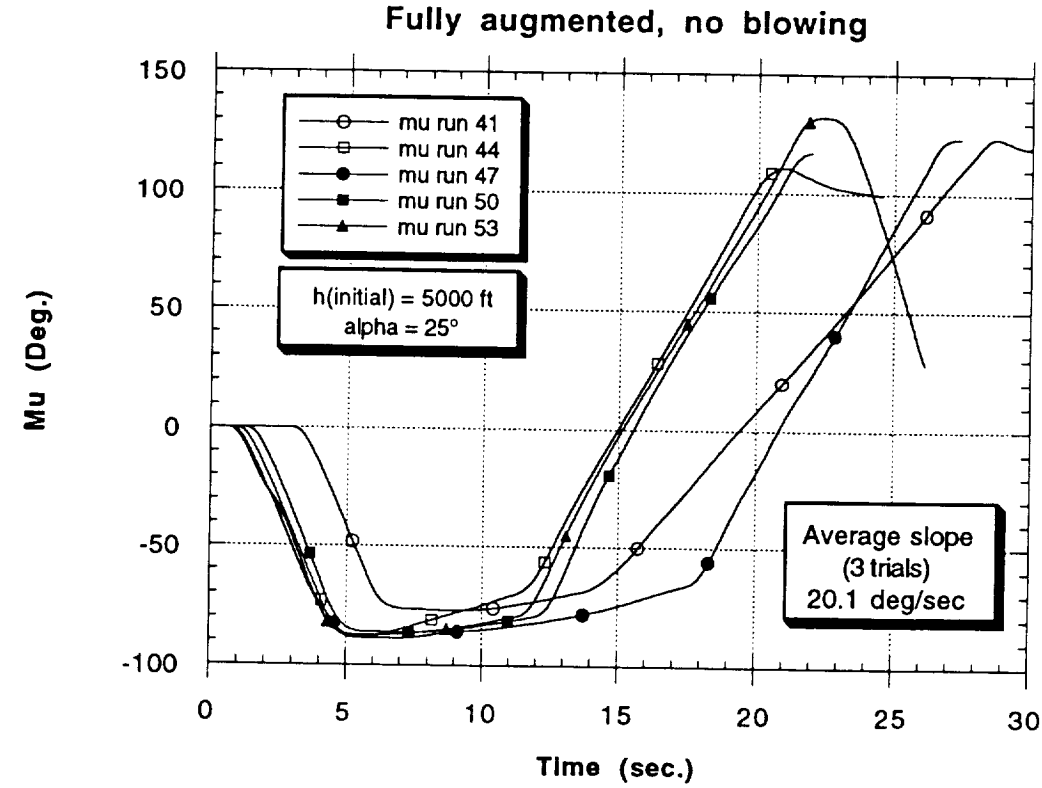

a) Velocity Vector Roll Angle

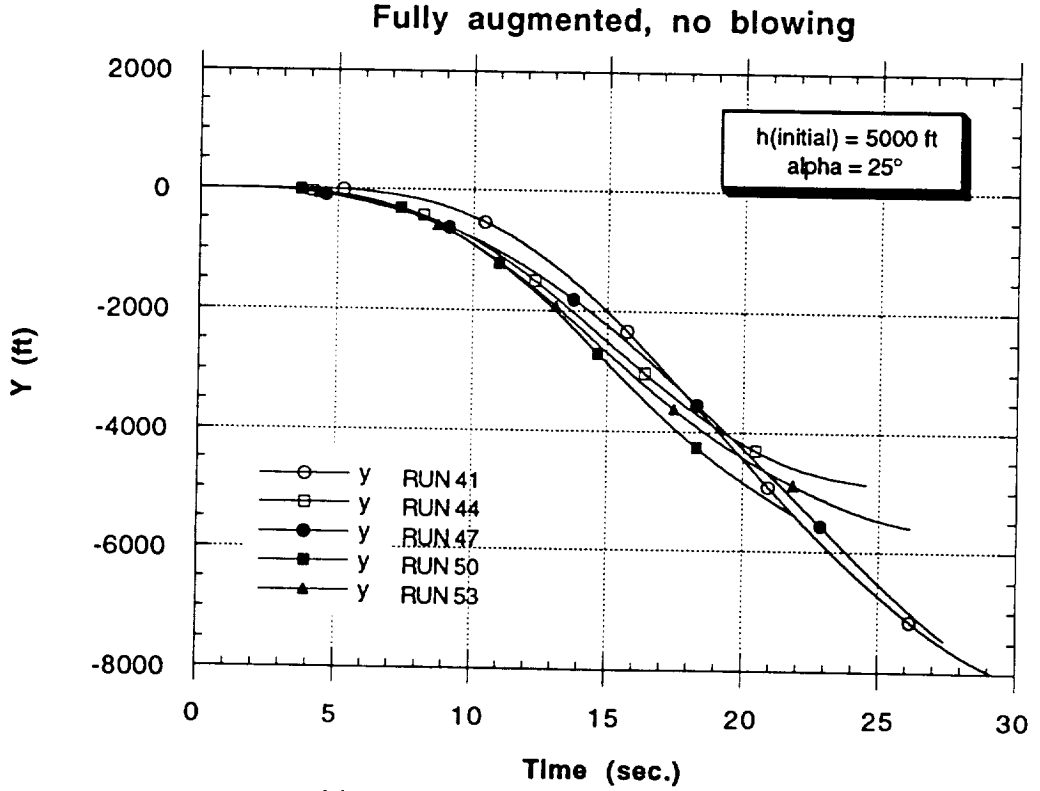

b) Cross-Track (Y-Coordinate)

Figure 41 - Loaded Roll Simulation for the NASP-type Configuration with Fully Augmented Flight Control System (Multiple Trials). No Forebody Blowing

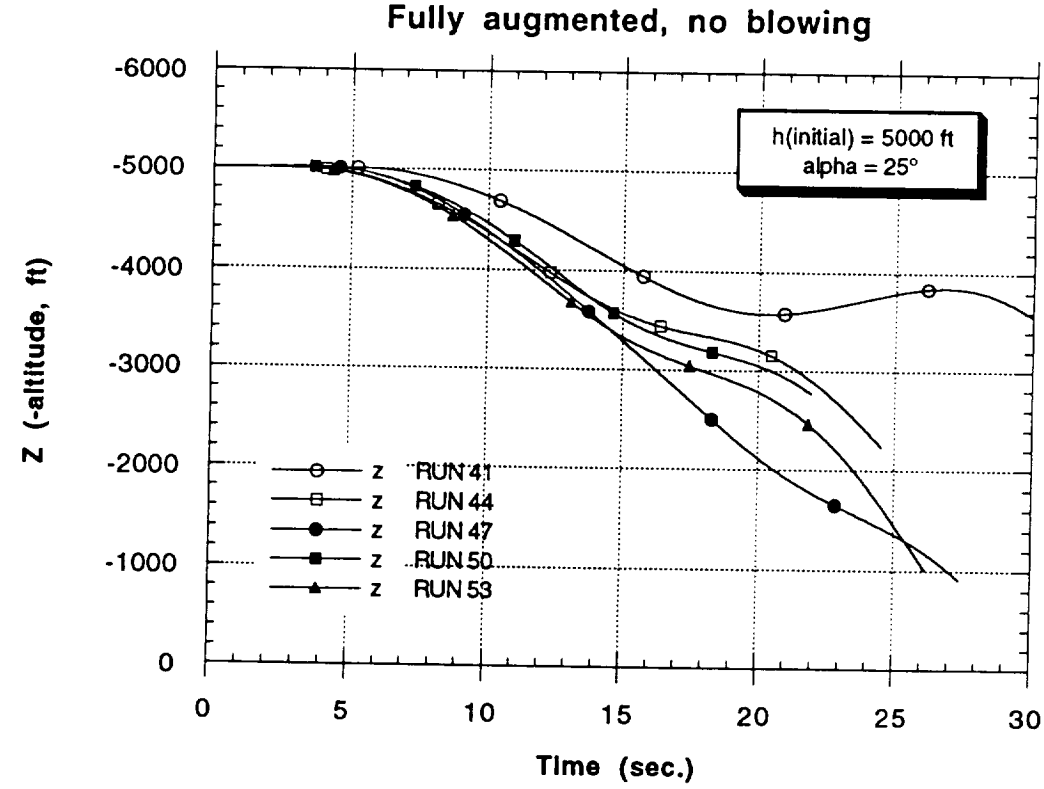

c) Altitude (-Z)

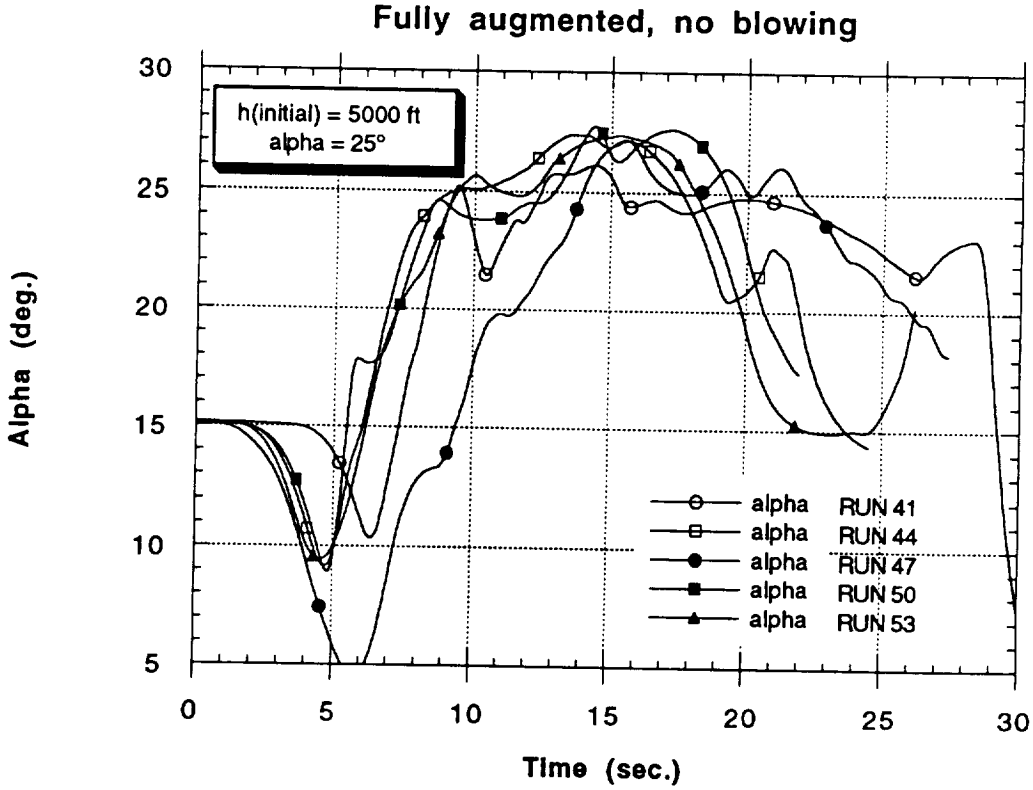

d) Angle of Attack

Figure 41 - Continued

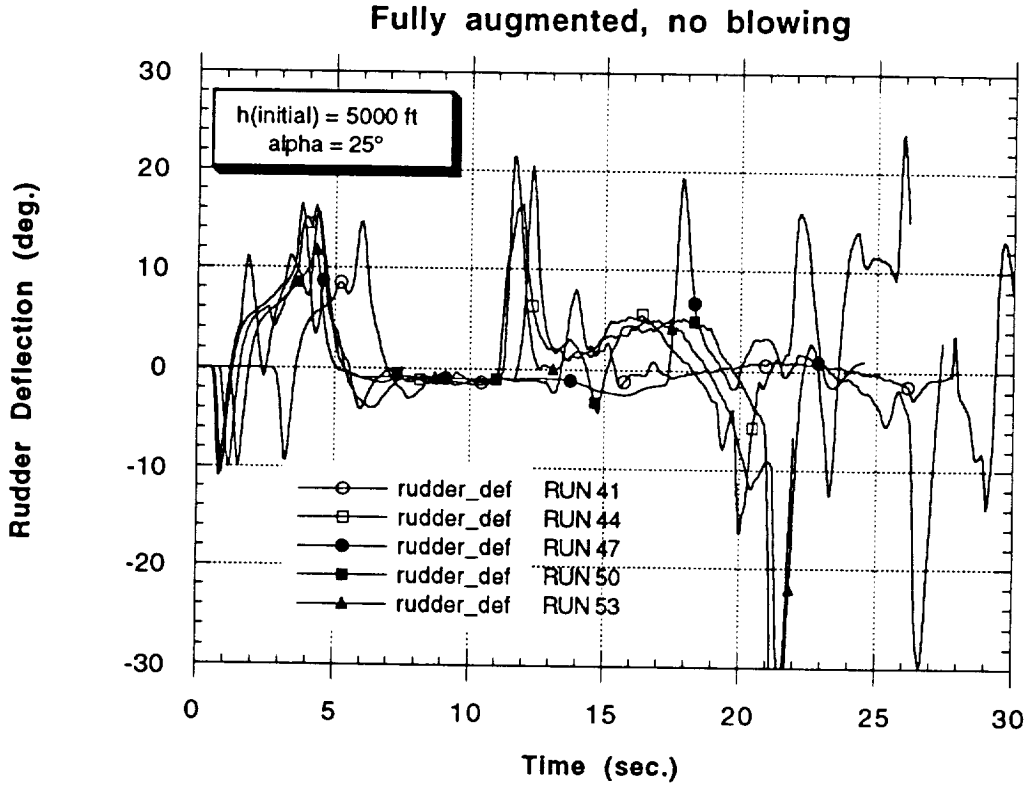

e) Rudder Deflection Angle

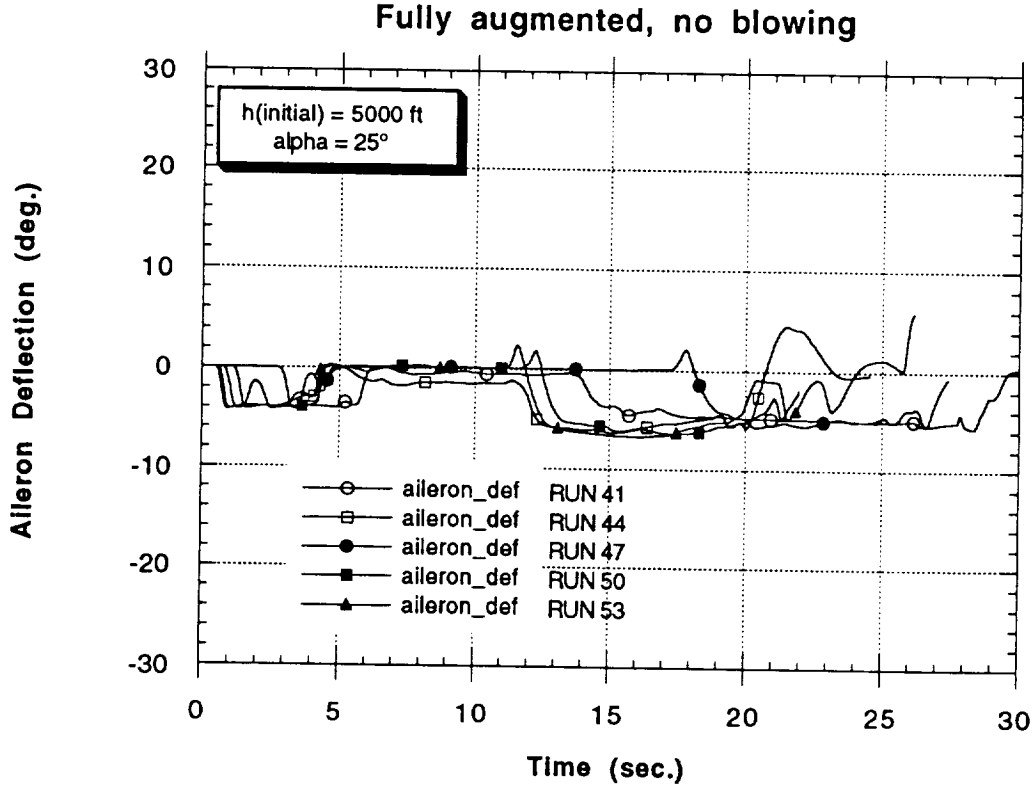

f) Aileron Deflection Angle

Figure 41 - Continued

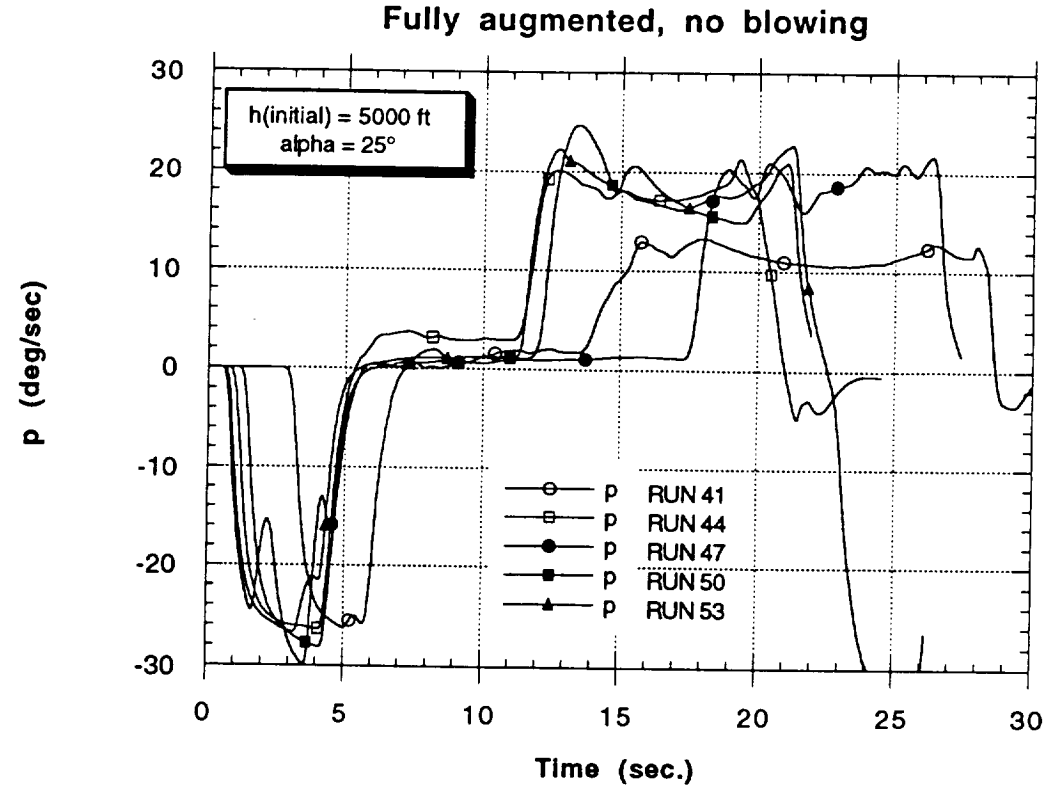

g) Body-Axis Roll Rate

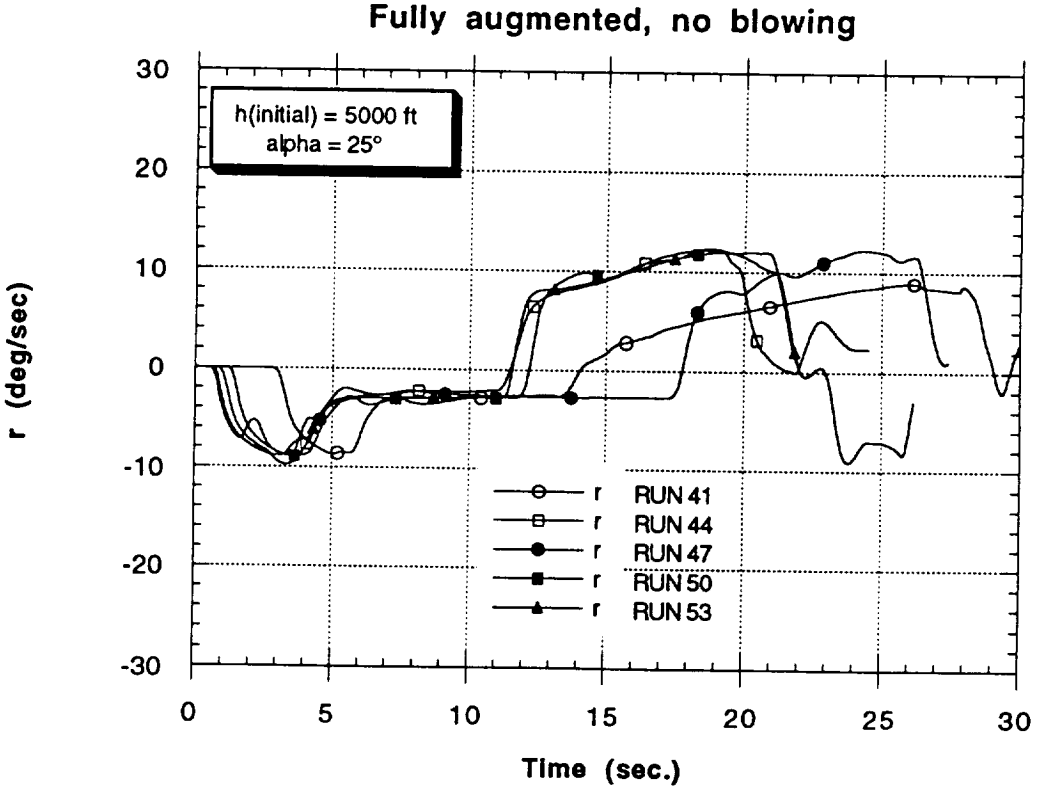

h) Body-Axis Yaw Rate

Figure 41 - Concluded

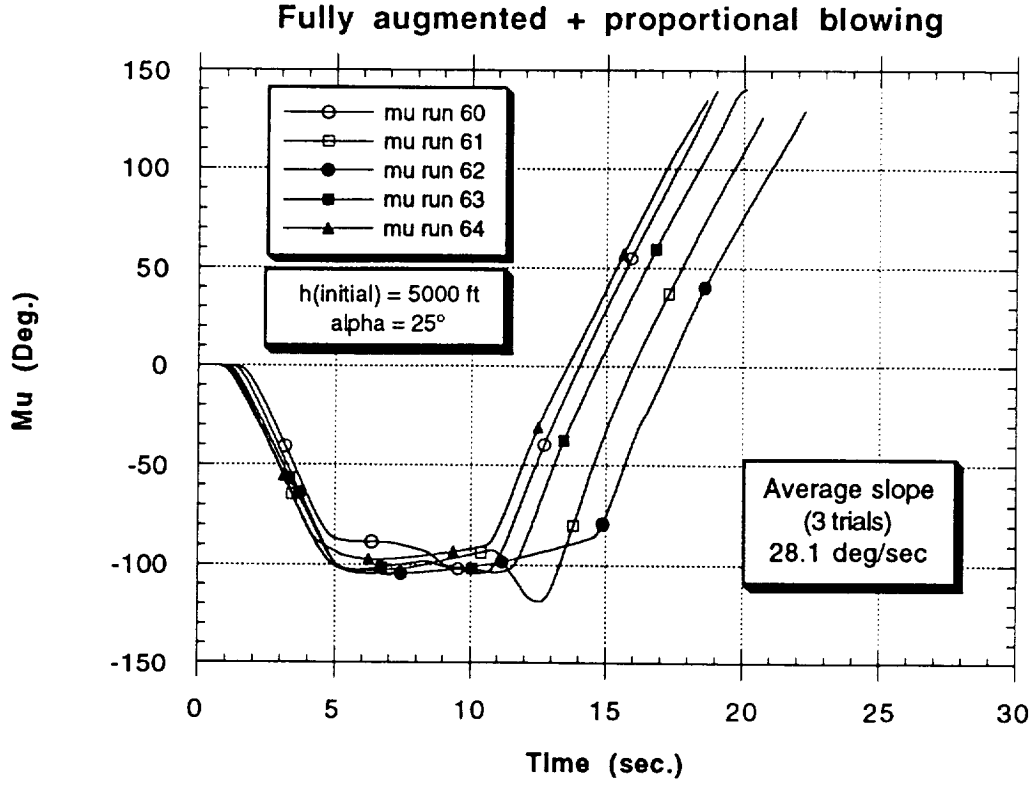

a) Velocity Vector Roll Angle

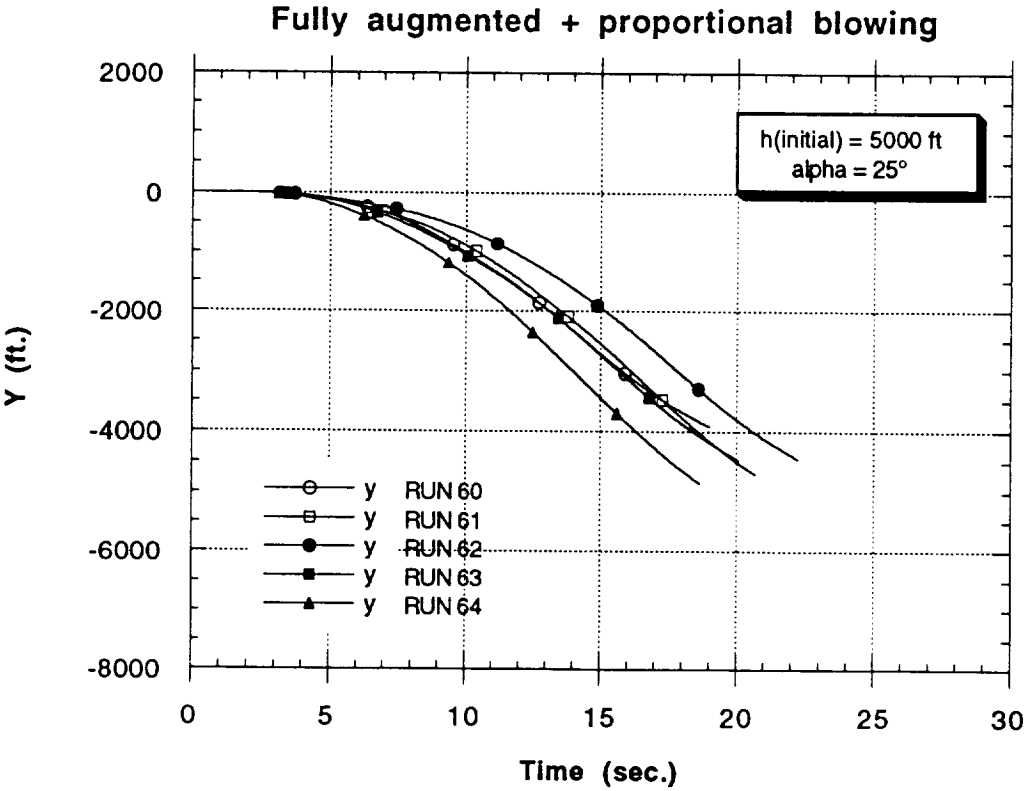

b) Cross-Track (Y-Coordinate)

Figure 42 - Loaded Roll Simulation for the NASP-type Configuration with Fully Augmented Flight Control System and Proportional Forebody Blowing (Multiple Trials)

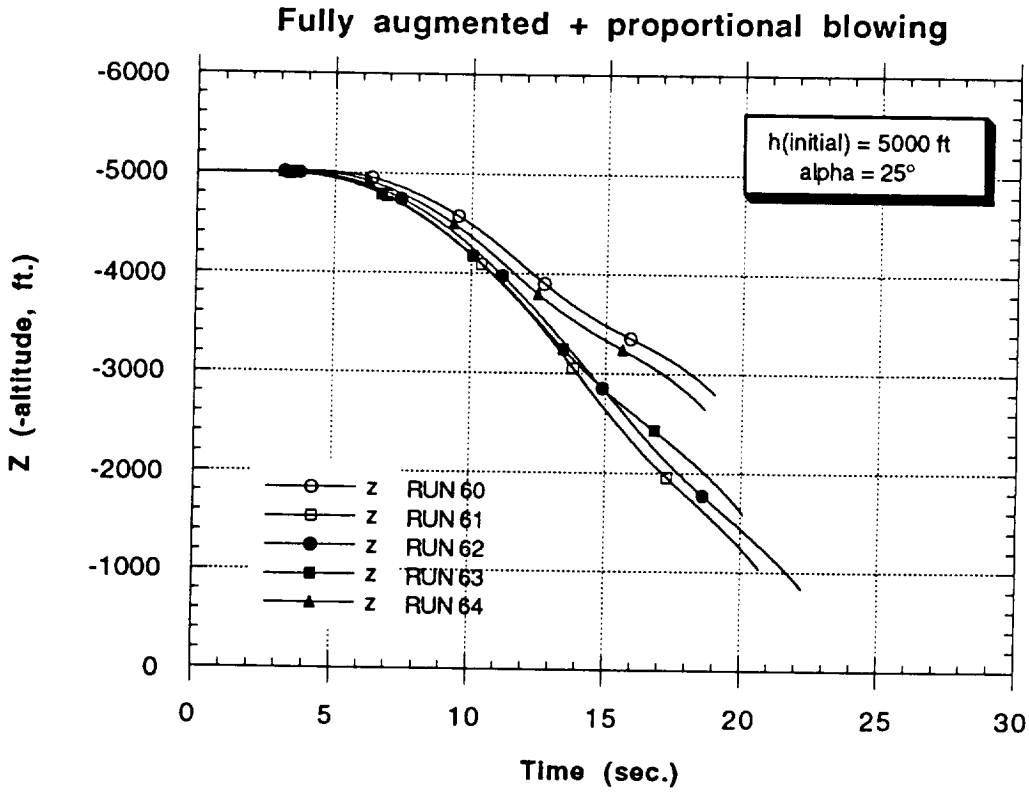

c) Altitude (-Z)

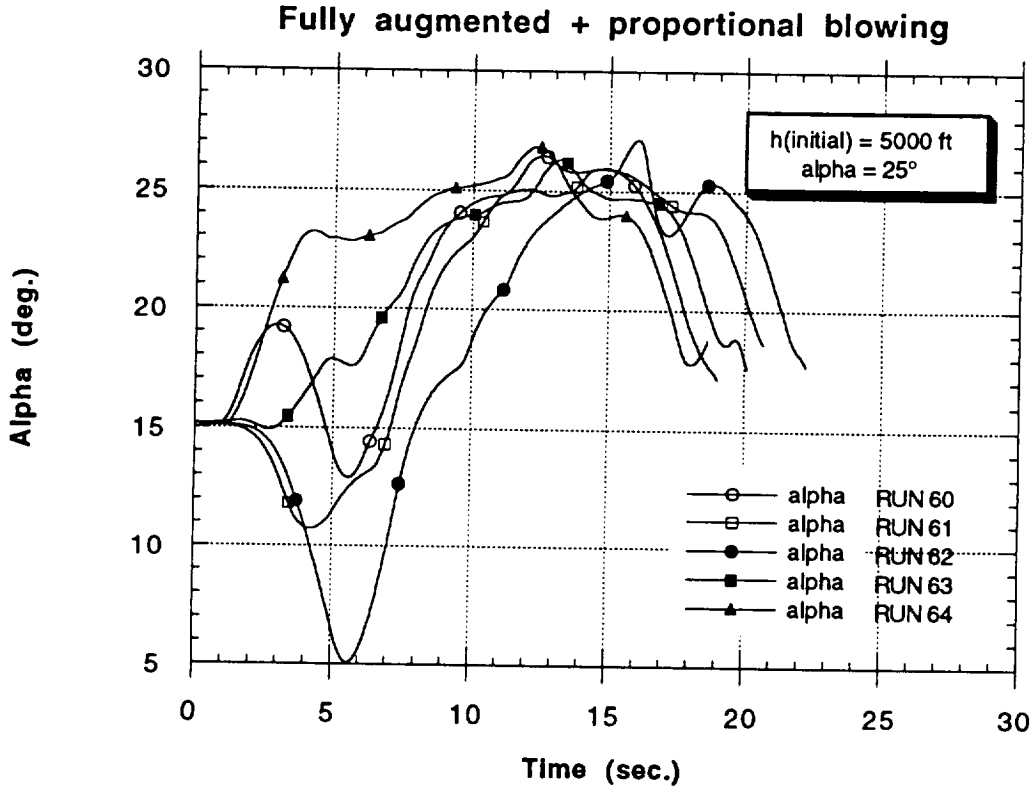

d) Angle of Attack

Figure 42 - Continued

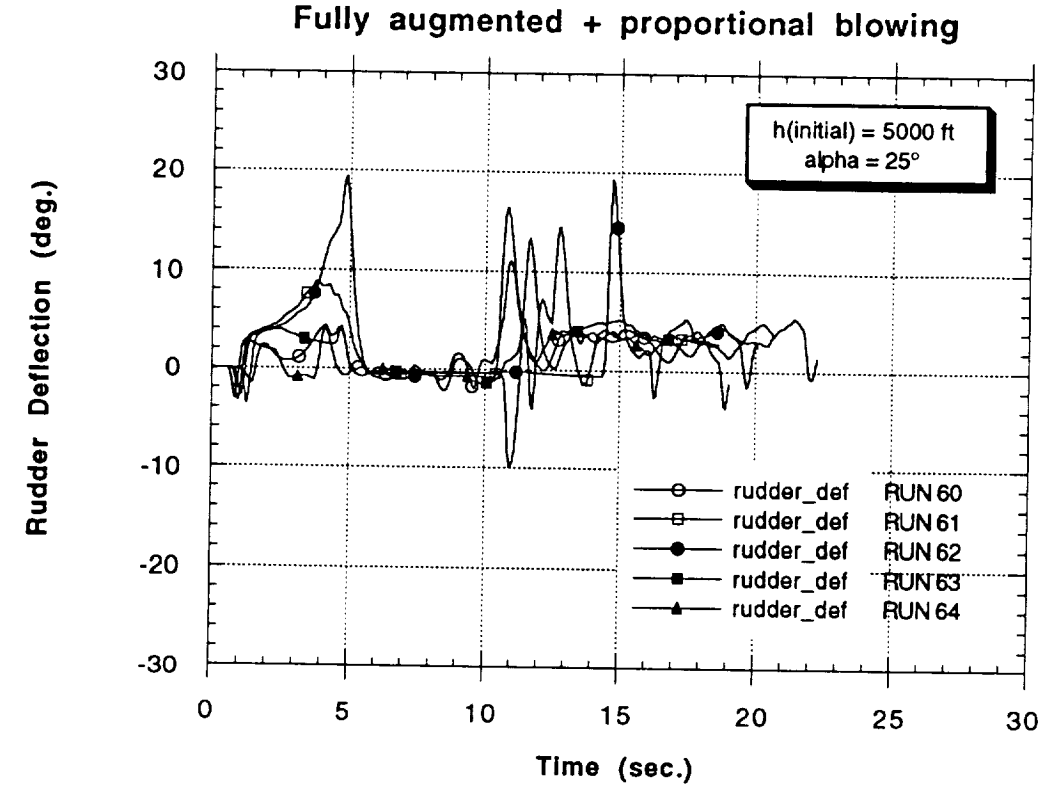

e) Rudder Deflection Angle

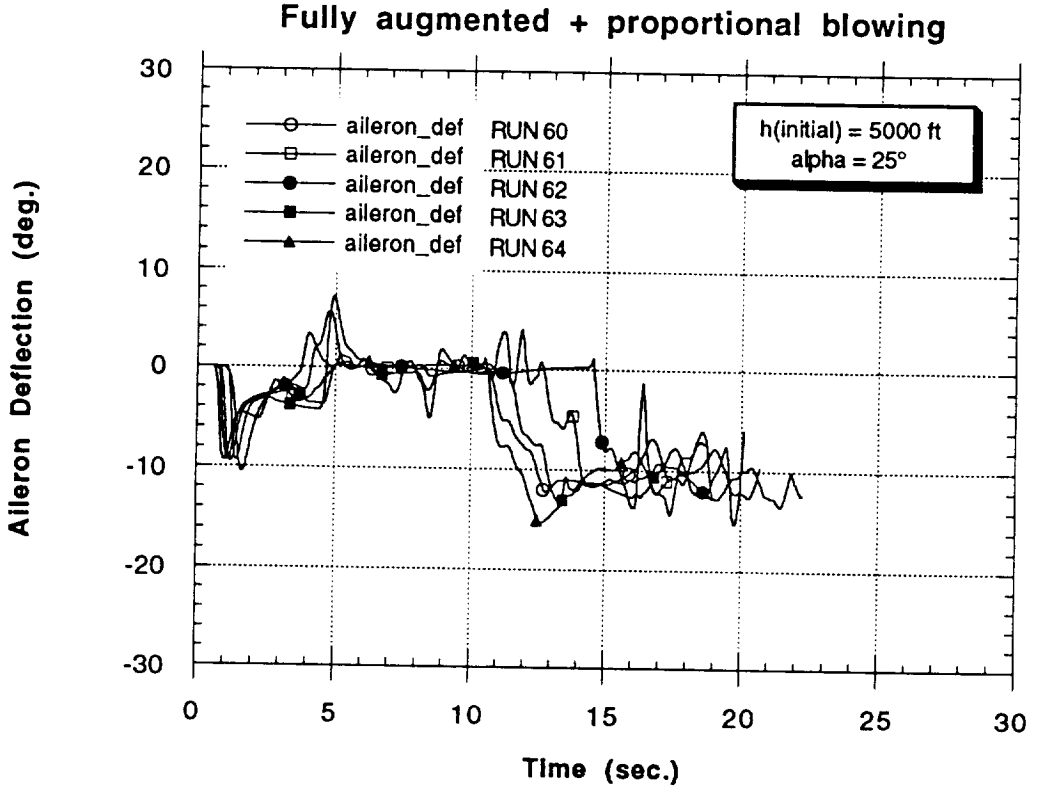

f) Aileron Deflection Angle

Figure 42 - Continued

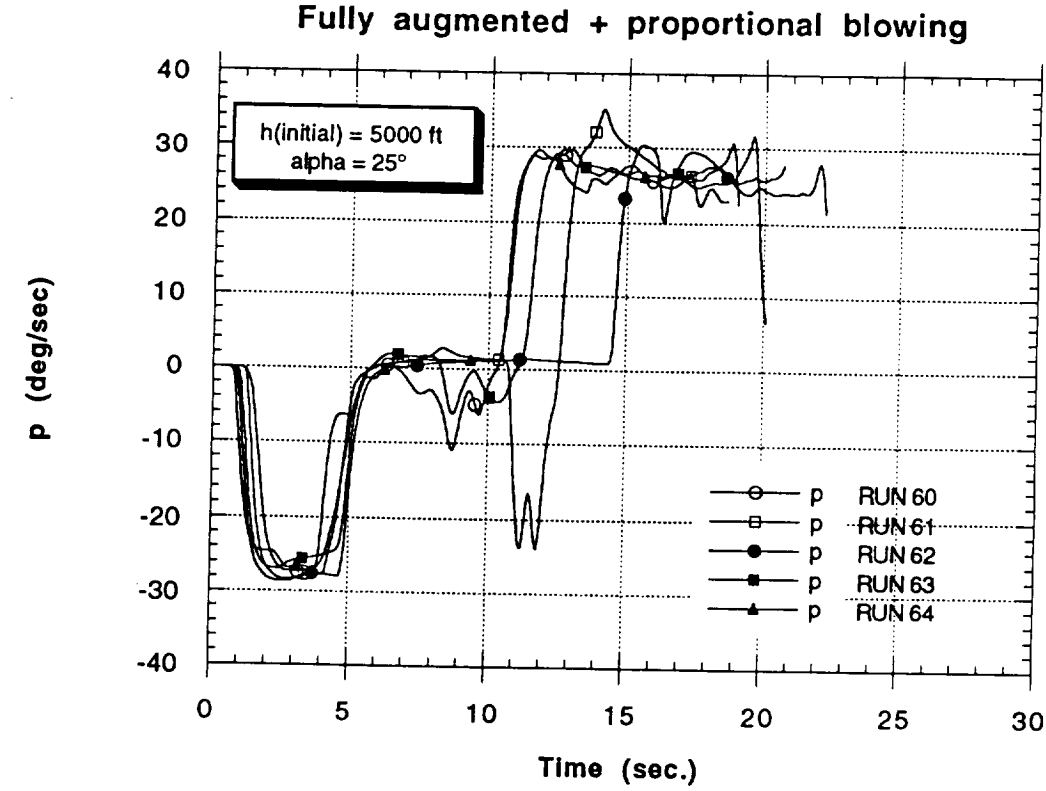

g) Body-Axis Roll Rate

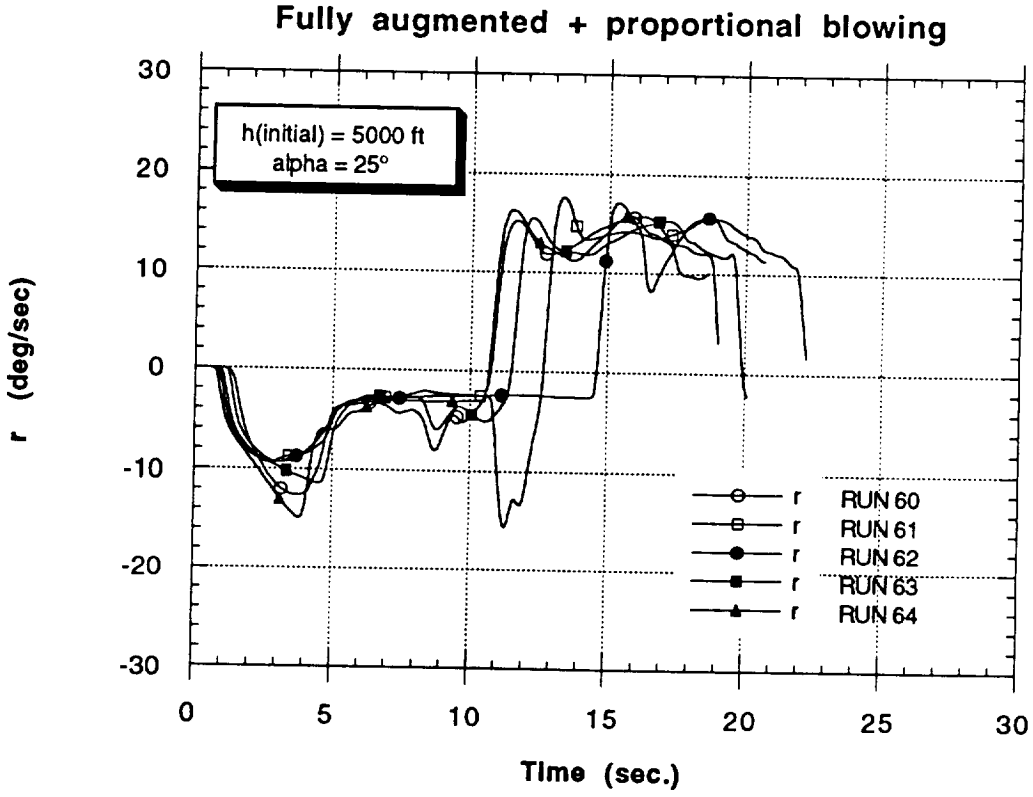

h) Body-Axis Yaw Rate

Figure 42 - Continued

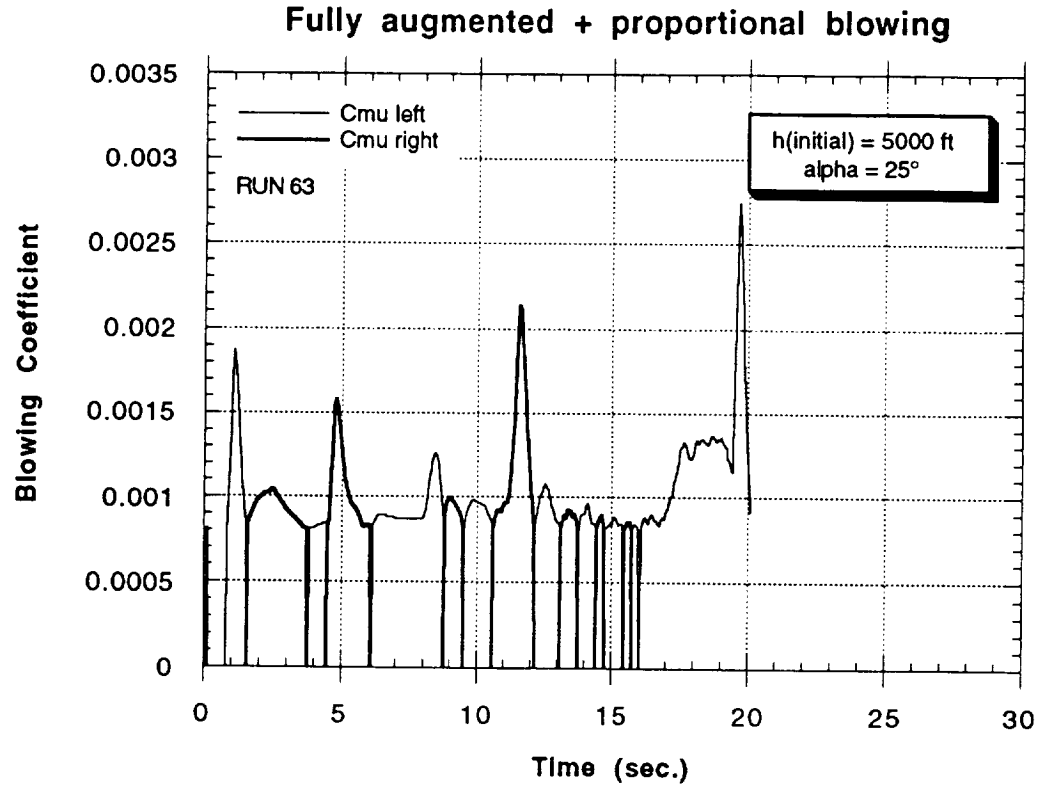

i) Blowing Coefficient

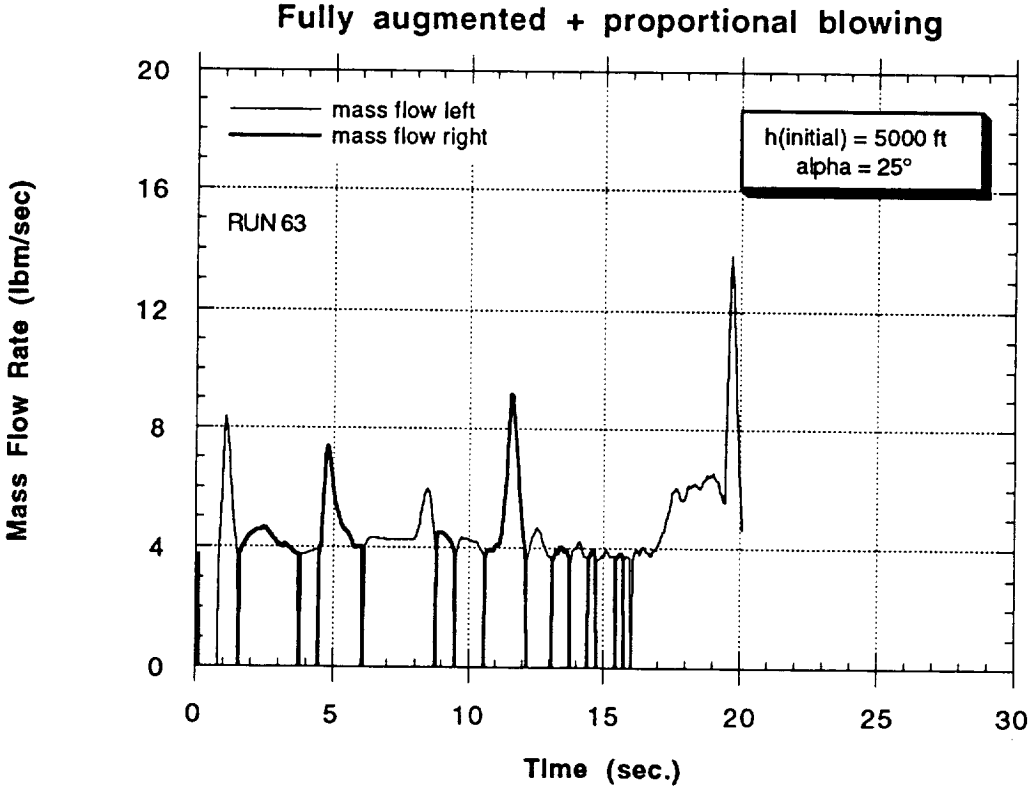

h) Mass Flow Rate

Figure 42 - Continued

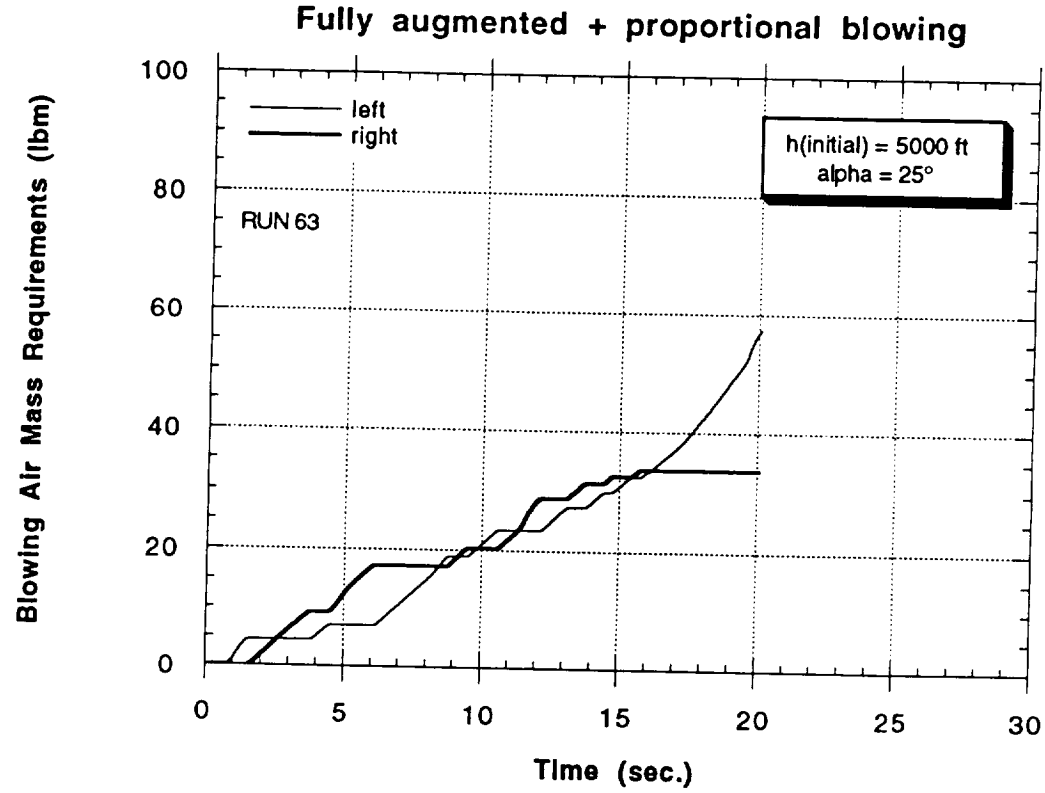

j) Accumulative Total Mass Requirements

Figure 42 - Concluded

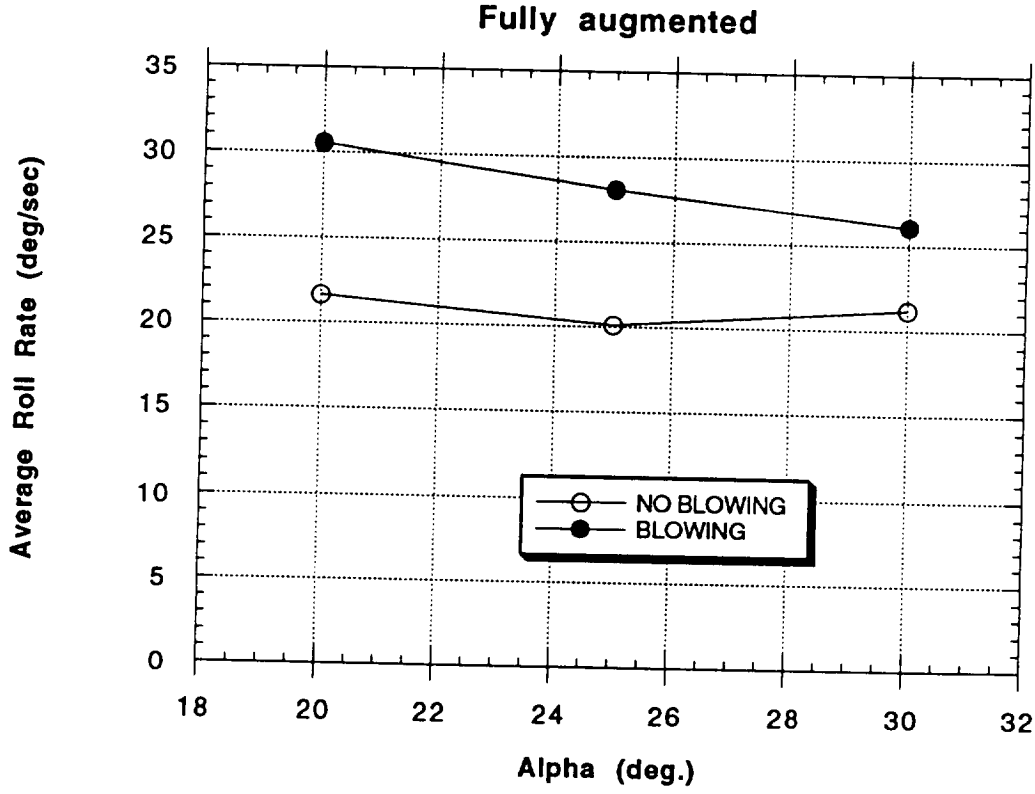

Figure 43 - Comparison Between Velocity Vector Roll Rate for the Non-Blowing and Blowing Cases

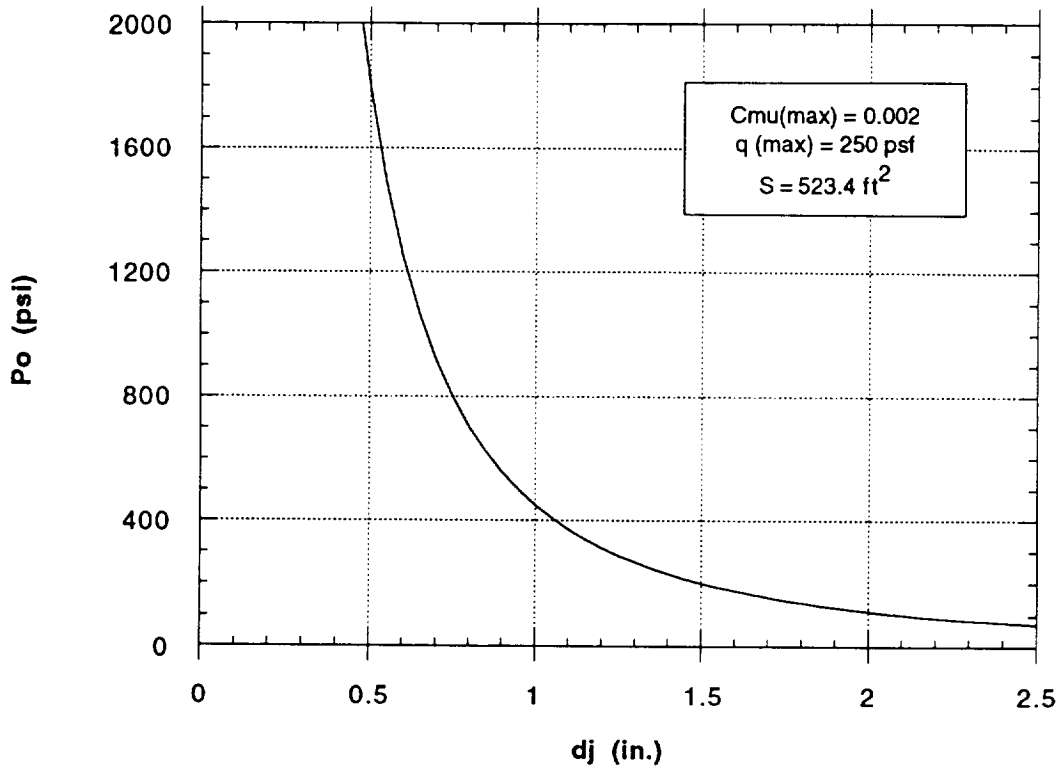

Figure 44 - Nozzle Total Pressure Requirements vs. Nozzle Diameter for Stated Reference Conditions

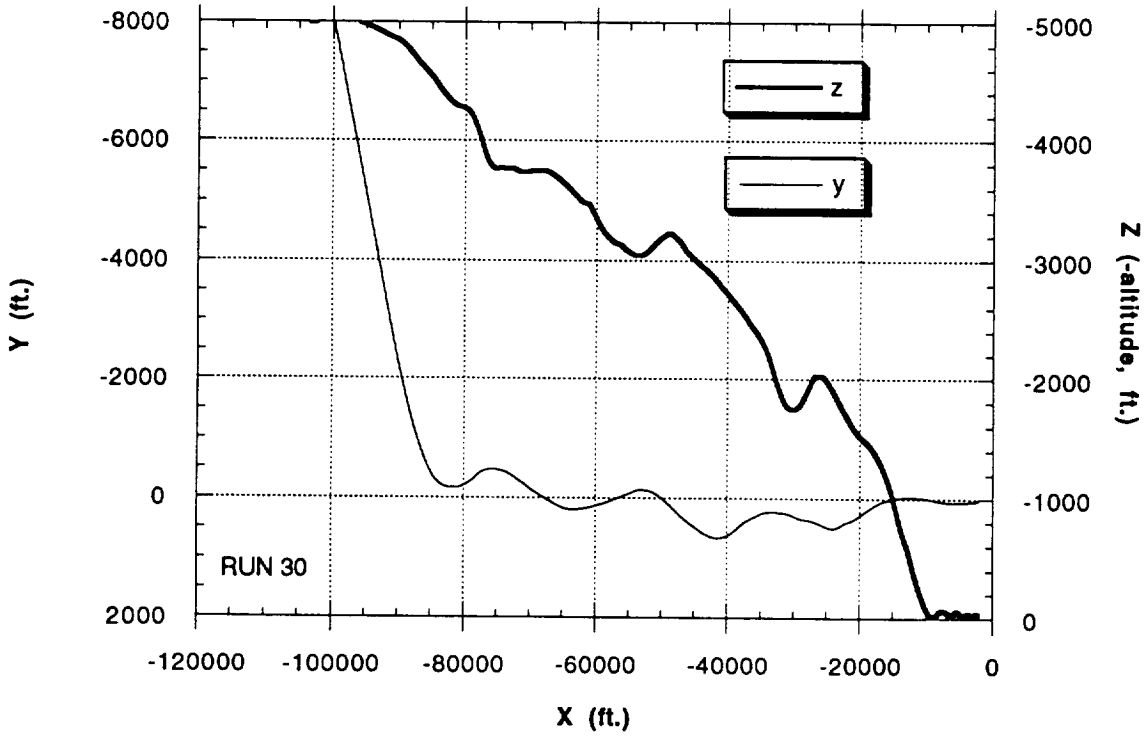

Figure 45 - Variation in Altitude and Lateral Excursions from Extended Vertical Plane Centered on the Runway for Simulated Approach and Landing Task With Fully Augmented Control System Including Proportional Forebody Blowing

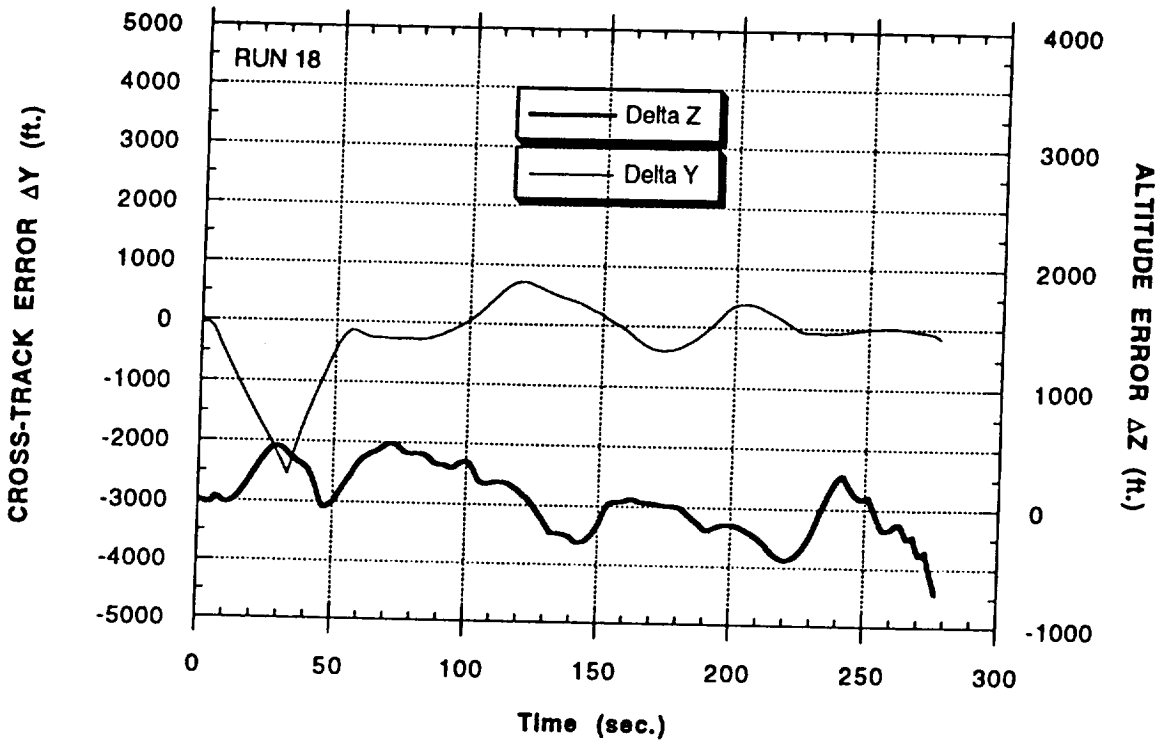

Figure 46 - Deviation from the Flight Path for Example Approach and Landing Task Described in Fig. 45

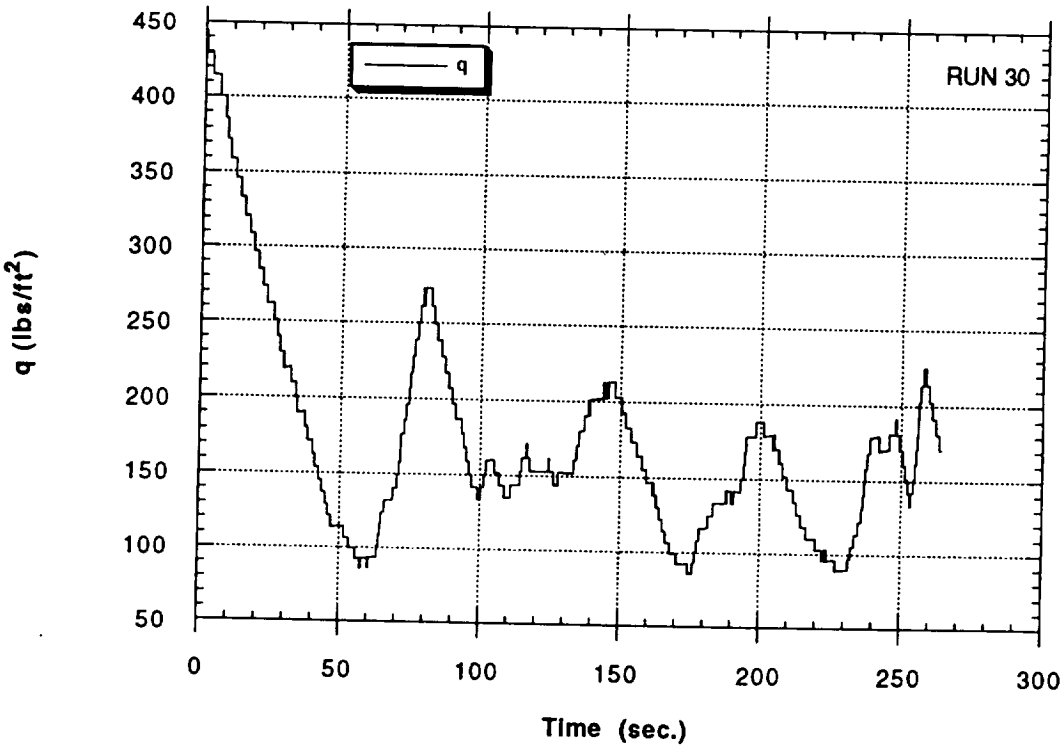

Figure 47 - Variation in Dynamic Pressure for Example Approach and Landing Task Shown in Fig. 45

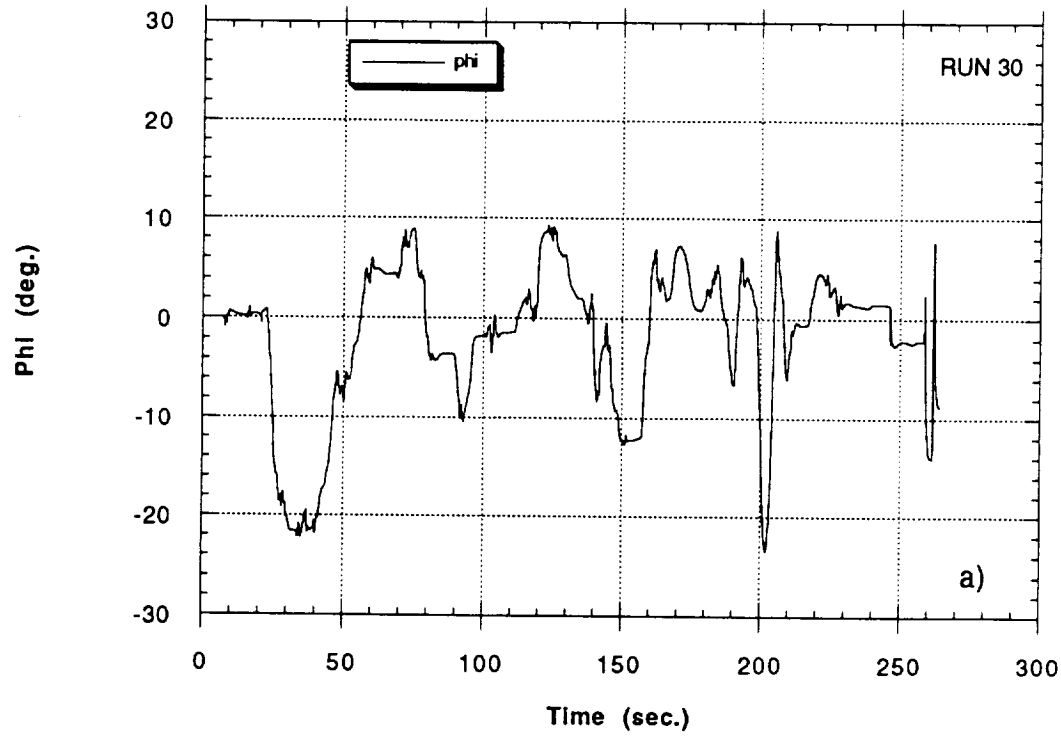

a) Roll Angle

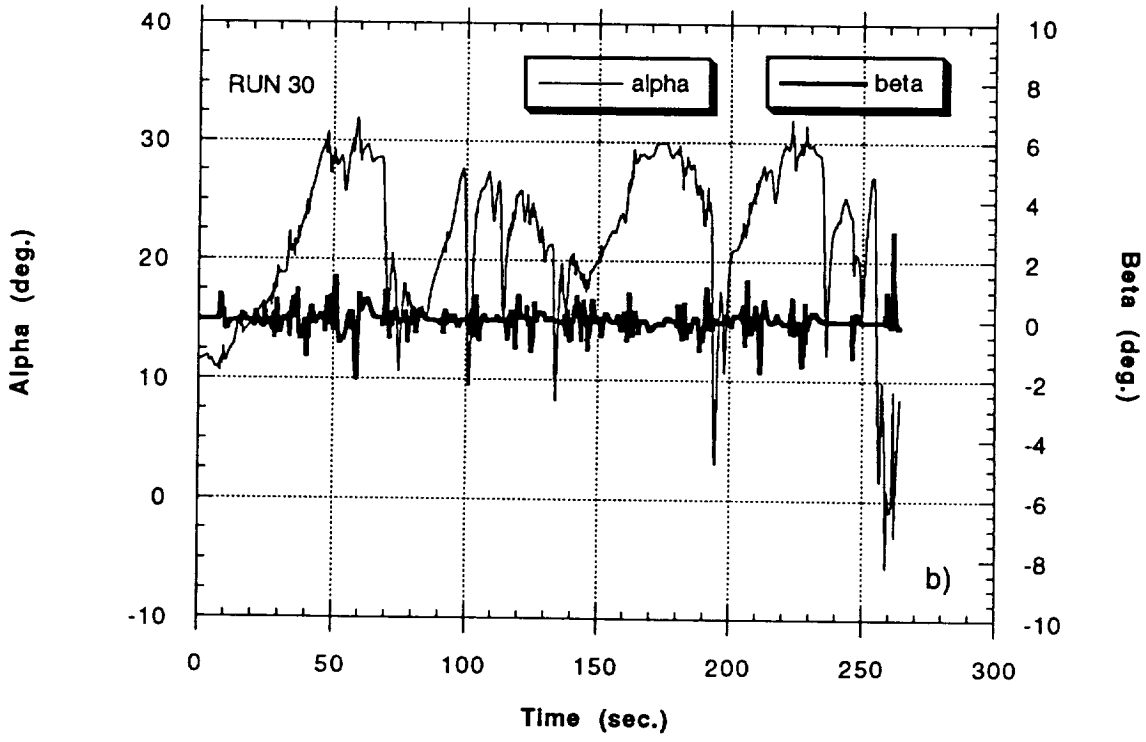

b) Angles of Attack and Sideslip

Figure 48 - Variation in Vehicle Attitude with Time for Example Approach and Landing Task Shown in Fig. 45

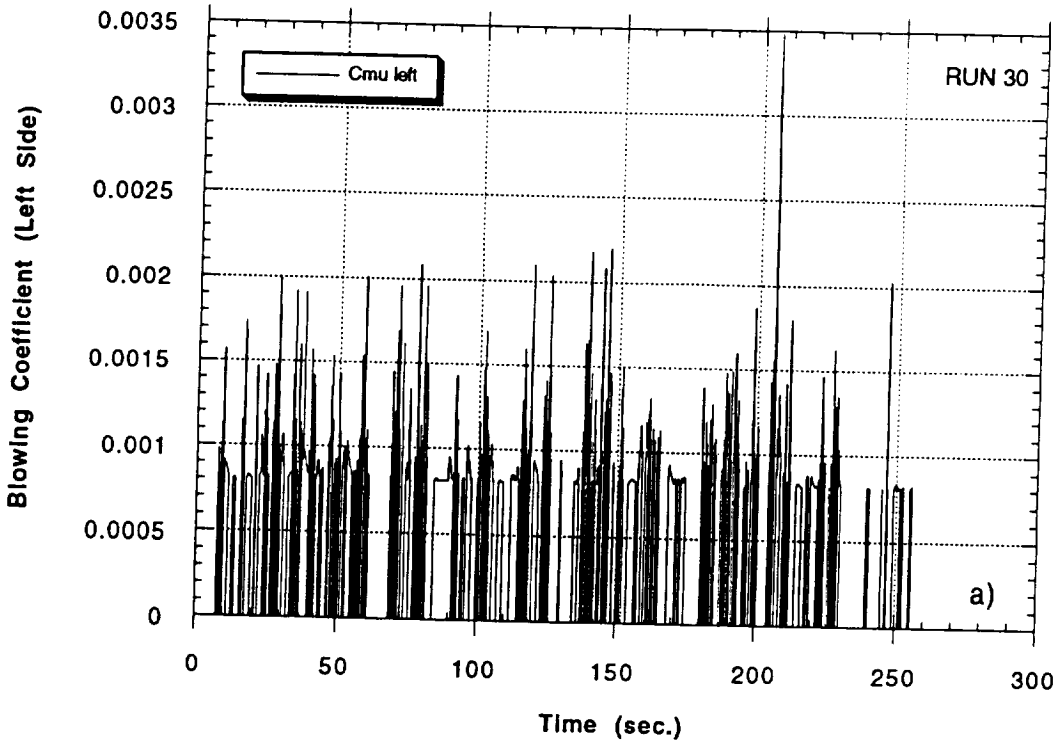

a) Left Nozzle

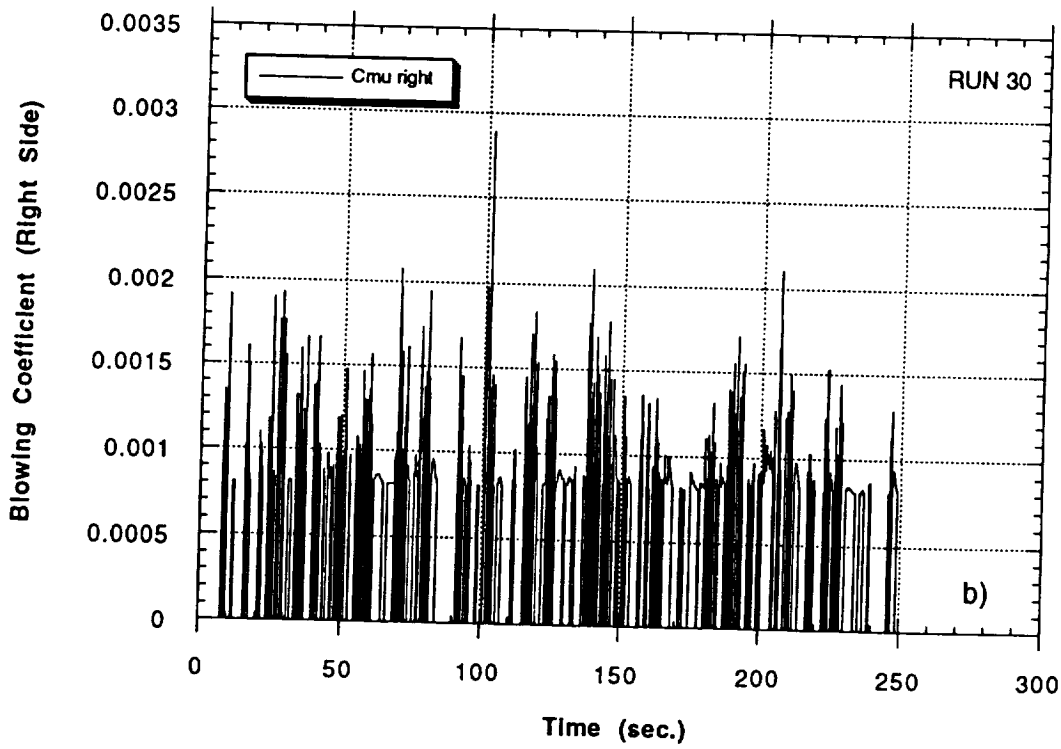

b) Right Nozzle

Figure 49 - Variation in Blowing Momentum Coefficient with Time for Example Approach and Landing Task Shown in Fig. 45

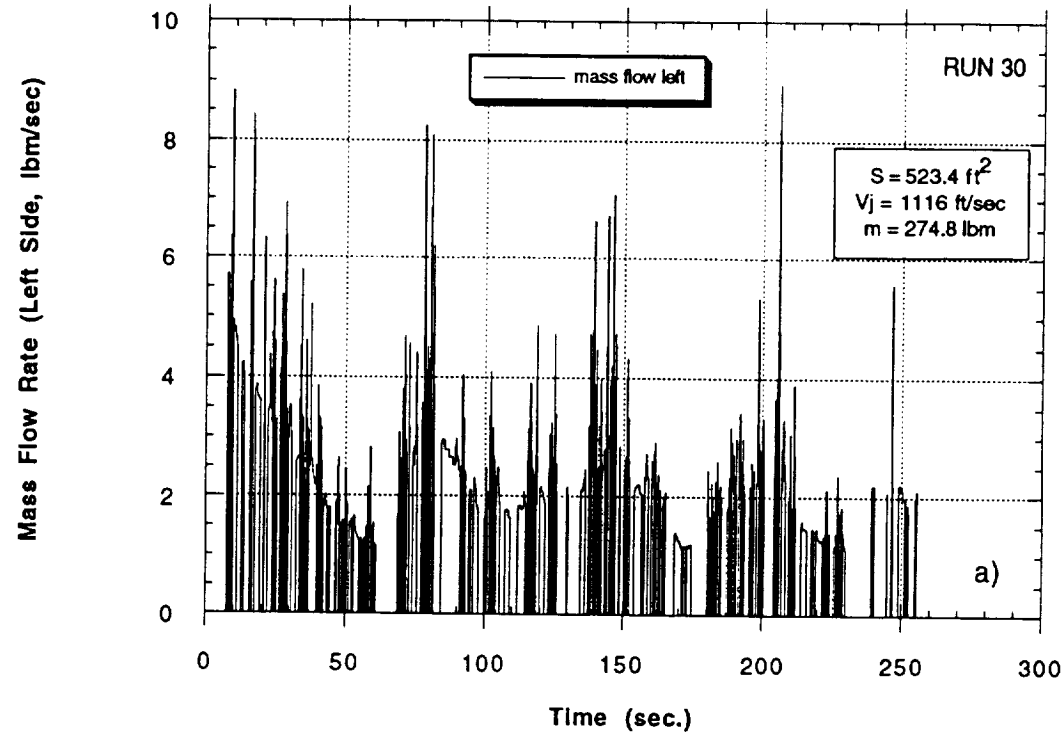

a) Left Nozzle

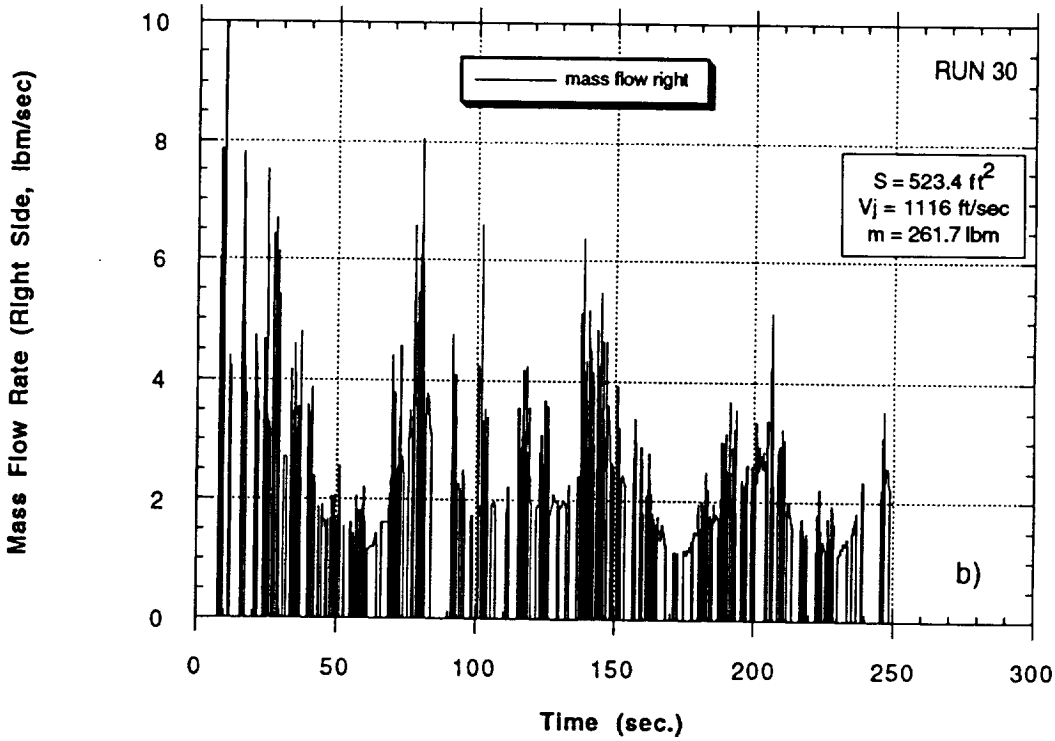

b) Right Nozzle

Figure 50 - Variation in Jet Nozzle Mass Flow Rate with Time for Example Approach and Landing Task Shown in Fig. 45

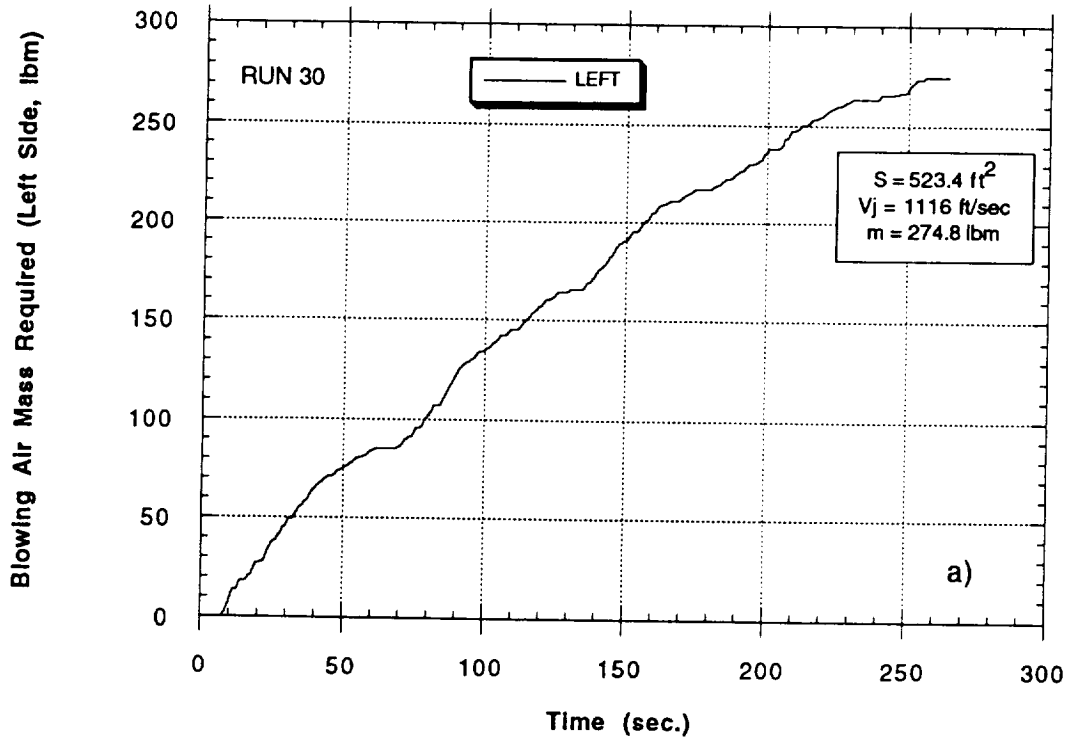

a) Left Nozzle

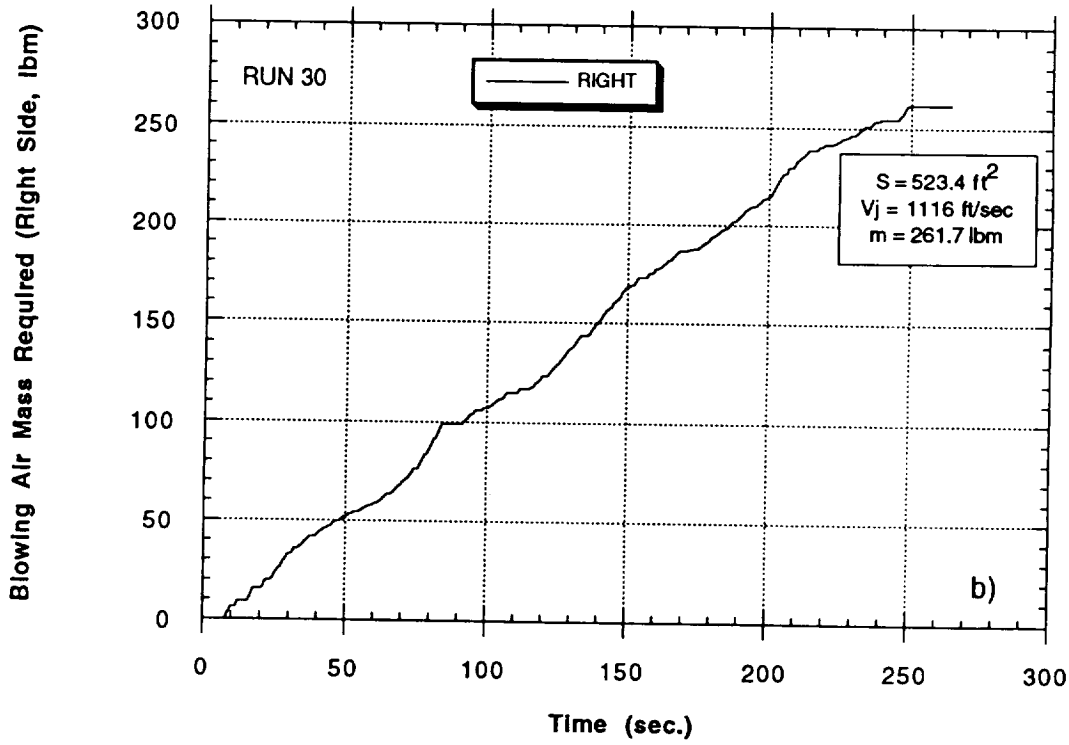

b) Right Nozzle

Figure 51 - Accumulative Total Mass Flow Requirements Integrated over the Total Time for Example Approach and Landing Task Shown in Fig. 45

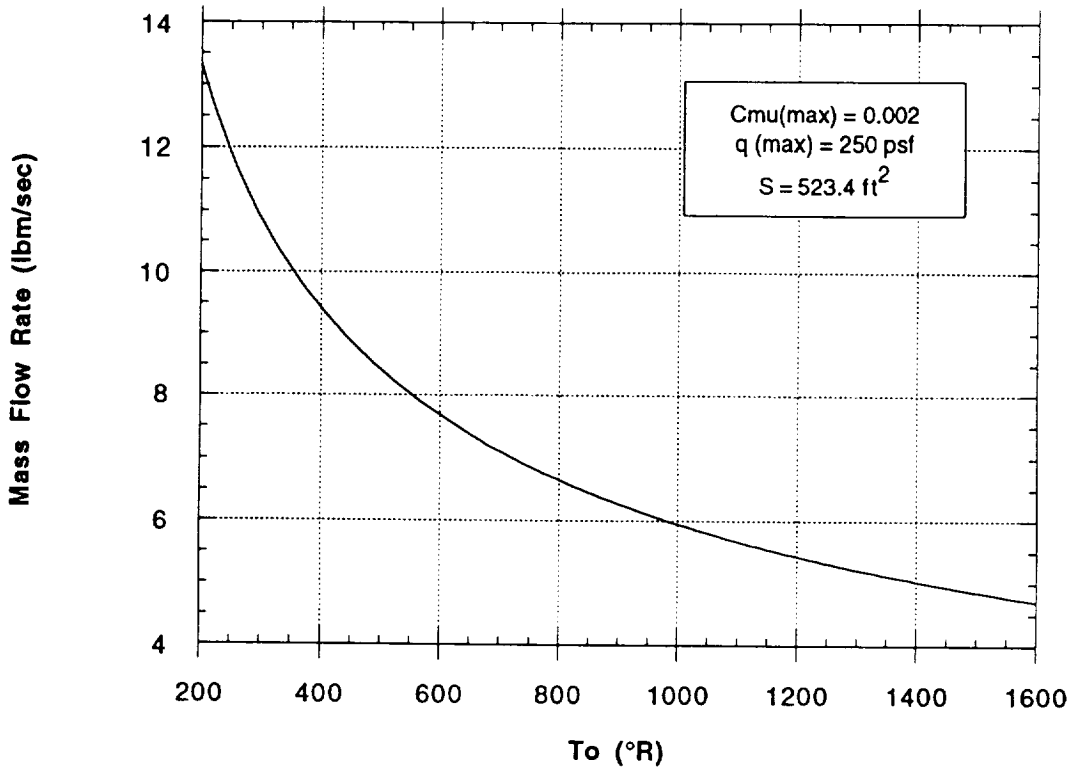

Figure 52 - Mass Flow Variation with Stagnation Temperature of the Air at the Nozzle Exit for the Reference Conditions Shown

REPORT DOCUMENTATION PAGE

Form Approved
OMB No. 0704-0188

1. AGENCY USE ONLY *(Leave blank)*	2. REPORT DATE	3. REPORT TYPE AND DATES COVERED
	September 1993	Contractor Report

4. TITLE AND SUBTITLE
Aerodynamic Control of NASP-Type Vehicles Through Vortex Manipulation, Volume IV: Simulation

5. FUNDING NUMBERS
NAS2-13196

6. AUTHOR(S)
Brooke C. Smith, Carlos Suárez, William M. Porada, and Gerald N. Malcolm

7. PERFORMING ORGANIZATION NAME(S) AND ADDRESS(ES)
Eidetics International, Inc.
3415 Lomita Blvd.
Torrance, CA 90505

8. PERFORMING ORGANIZATION REPORT NUMBER
A-93138

9. SPONSORING/MONITORING AGENCY NAME(S) AND ADDRESS(ES)
National Aeronautics and Space Administration
Washington, DC 20546-0001

10. SPONSORING/MONITORING AGENCY REPORT NUMBER
NASA CR-177626

11. SUPPLEMENTARY NOTES
Point of Contact: Larry Meyn, Ames Research Center, MS 247-2, Moffett Field, CA 94035-1000
(415) 604-5038

12a. DISTRIBUTION/AVAILABILITY STATEMENT
Unclassified-Unlimited
Subject Category – 02

12b. DISTRIBUTION CODE

13. ABSTRACT ***(Maximum 200 words)***

Forebody Vortex Control (FVC) is an emerging technology that has received widespread and concentrated attention by many researchers for application on fighter aircraft to enhance aerodynamic controllability at high angles of attack. This research explores potential application of FVC to a NASP-type configuration. The configuration investigated is characterized by a slender, circular cross-section forebody and a 78° swept delta wing. A man-in-the-loop, six-degress-of-freedom, high-fidelity simulation has been developed that demonstrates the implementation and advantages of pneumatic forebody vortex control. Static wind tunnel tests were used as the basis for the aerodynamic characteristics modeled in the simulation. Dynamic free-to-roll wind tunnel tests were analyzed and the wing rock motion investigated. A non-linear model of the dynamic effects of the bare airframe and the forebody vortex control system were developed that closely represented the observed behavior. Multiple state-of-the-air digital flight control systems were developed that included different utilizations of pneumatic vortex control. These were evaluated through manned simulation. Design parameters for a pneumatic forebody vortex control system were based on data collected regarding the use of blowing and the mass flow required during realistic flight maneuvers.

14. SUBJECT TERMS	15. NUMBER OF PAGES
Generic hypersonic configuration, Forebody vortex control, Wing rock suppression, Experimental/simulation, Aerodynamic control	152
	16. PRICE CODE: A08

17. SECURITY CLASSIFICATION OF REPORT	18. SECURITY CLASSIFICATION OF THIS PAGE	19. SECURITY CLASSIFICATION OF ABSTRACT	20. LIMITATION OF ABSTRACT
Unclassified	Unclassified		